

Investigations on Contact and Non-Contact Based Actuation Studies of Shape Memory Alloy (SMA) Structures and their Life Cycle Behavior

Ph.D. Thesis

By
TAMESHWER NATH



**DISCIPLINE OF MECHANICAL ENGINEERING
INDIAN INSTITUTE OF TECHNOLOGY INDORE**

OCTOBER 2018

Copyright © 2018 by Tameshwer Nath

Email: tameshwer.nath@gmail.com

All rights reserved. No part of this thesis may be reproduced or transmitted, in any form or by any means, electronic or mechanical, including photocopying, microfilming, and recording, or by any information storage or retrieval system, without the prior written permission of the author.

Investigations on Contact and Non-Contact Based Actuation Studies of Shape Memory Alloy (SMA) Structures and their Life Cycle Behavior

A THESIS

Submitted in partial fulfillment of the requirements for the award of the degree

of

DOCTOR OF PHILOSOPHY

By

TAMESHWER NATH



**DISCIPLINE OF MECHANICAL ENGINEERING
INDIAN INSTITUTE OF TECHNOLOGY INDORE**

OCTOBER 2018



INDIAN INSTITUTE OF TECHNOLOGY INDORE

CANDIDATE'S DECLARATION

I hereby certify that the work which is being presented in the thesis entitled **INVESTIGATIONS ON CONTACT AND NON-CONTACT BASED ACTUATION STUDIES OF SHAPE MEMORY ALLOY (SMA) STRUCTURES AND THEIR LIFE CYCLE BEHAVIOR** in the partial fulfilment of the requirements for the award of the degree of **DOCTOR OF PHILOSOPHY** and submitted in the **DISCIPLINE OF MECHANICAL ENGINEERING, INDIAN INSTITUTE OF TECHNOLOGY INDORE**, is an authentic record of my own work carried out during the time period from January 2014 to October 2018 under the supervision of Dr. I.A.Palani, Associate Professor, Discipline of Mechanical Engineering, Indian Institute of Technology Indore, India.

The matter presented in this thesis has not been submitted by me for the award of any other degree of this or any other institute.

Signature of the student with date
(TAMESHWER NATH)

This is to certify that the above statement made by the candidate is correct to the best of my knowledge.

Signature of Thesis Supervisor with date
21/2/2019
(Dr. I.A.PALANI)

TAMESHWER NATH has successfully given his Ph.D. Oral Examination held on **21/02/2019**.

Signature of Chairperson (OEB)
Date: 21-2-19

Signature of External Examiner
Date: 21/2/19

Signature of Thesis Supervisor
Date:

Signature of PSPC Member #1
Date: 21/2/19

Signature of PSPC Member #2
Date: 21/2/19

Signature of Convener, DPGC
Date: 21.2.19

Signature of Head of Discipline
Date: 21/2/2019

PREAMBLE

In this work different actuation media (contact and non-contact) and its impact on NiTi shape memory alloy (SMA), also called smart material, is presented. The functional properties of a Nitinol (NiTi) component can be augmented by changing the energy source. Thermo-mechanical behavior and morphological analysis have been analyzed. Such approaches are comprehensively investigated for various environments, with the actuation medium (Contact: Electrical and Hot water whereas non-contact: Pulsed laser and continuous fiber laser), as the temperature reaches 50-80°C, SMA gets fully compressed for the first few cycles followed by a loss in actuation. The actuation loss is then studied with different characterization methods such as Thermo Gravimetric Analysis (TGA), Scanning Electron Microscopy (SEM) and Energy-dispersive X-ray spectroscopy (EDAX). These studies are required to explain the thermal effect, deterioration, and composition of the impinged surface. Consequently, the present thesis focuses on application point of view and addressed in this thesis for Micro-Electro-Mechanical System (MEMS) devices which are Tripod (for Joule Heating), Heat Engine (for Hot water actuation), Array of Micro-valve (for Pulsed laser actuation) and directional control valve (for continuous fiber laser actuation).

- 1) Life cycle behavior is also investigated for all cases.
- 2) Precise displacement is measured, and Morphological analysis has been done to verify the outcomes.

There is limited published work in the thermomechanical fatigue of SMA, and there is no comprehensive review of this field. A detailed literature review presented in this thesis confirmed the need for significant advancement of the technology. The proposed methodology significantly improves the responsiveness of the complex integrated operations and actuation methodology for decision-making. It is concluded that the proposed approach of actuation will serve as the backbone of any next-generation manufacturing sectors.

Acknowledgment

This thesis is the end of my journey of obtaining my Ph.D. I have not travelled in a vacuum on this journey. This thesis has been kept on track and been seen through to completion with the support and encouragement of numerous people including my well-wishers, my friends, colleagues, and various institutions. At the end of my thesis, I would like to thank all those people who made this thesis possible and an unforgettable experience for me. At the end of my thesis, it is a pleasant task to express my thanks to all those who contributed in many ways to the success of this study and made it an unforgettable experience for me.

*At this moment of accomplishment, first of all, I am also extremely indebted to my guide **Dr. I.A.Palani** This work would not have been possible without his guidance, support and encouragement. Under his guidance, I successfully overcame many difficulties and learned a lot. I can only say a proper thanks to him through my future work. It is to him that I dedicate this work.*

*I take this opportunity to sincerely acknowledge the Ministry of Human Resources and Development (MHRD), Government of India, New Delhi and CSIR for providing financial assistance in the form of Teaching Assistantship as well as Research Associate fellowship respectively which buttressed me to perform my work comfortably. I gratefully acknowledge **Dr. Pradeep Mathur, Director, IIT Indore**, for his understanding, and encouragement which have provided the good and smooth basis for my Ph.D. tenure. My thanks are due to **Dr. Anil Kumar E** for his valuable suggestions and untried help during Experimentation. I am also thankful to **Dr. Durgesh Nandini (Scientist- D, DRDO)** for her constant support and encouragement. I am thankful to **Dr. Reena Disawal, Dr. Shiva S (Assistant Professor: IIT Jammu)** and **Dr. Akash K.(Post Doctoral Researcher: Arizona State University, USA)** for their support during my experimentation in Mechatronics and Instrumentation laboratory. My thanks are due to **Mr. Vishal Dwivedi (Scientist-D, DRDO)**, and **Mr. Abhishek Kumar Upadhyay (Resaerch Scholar: IIT Indore)** for suggestions and inspiration. It's my pleasure to acknowledge **Dr. I.A.Palani** for his constant moral support.*

*I thank my PSPC members, **Dr. Devendra Laxmanrao Deshmukh (Associate Professor-ME)** and **Dr. Amod C. Umairkar (Associate Professor-EE)** for their helpful suggestions and comments during my progress report presentations. I would also like to convey thanks to **DPGC convenor Dr. Shailesh.I. Kundelwal (Assistant Professor-ME)** for his support. I thank to **Dr. Antony Vijesh (Associate Professor-Mathematics Oral Examination Chairman Board, for***

smoothly conducting my Ph.D. Viva-voice. I thank to thesis evaluators who are from India and Outside from India) for giving their valuable comments.

*I cannot forget my Journey in IIT Indore from PACL campus to Simrol Campus via IET, DAVV campus. The road to my Ph.D. started with PACL campus of IIT Indore. I take this opportunity to say heartfelt thanks to **Dr. Bhupesh Kumar Lad (Associate Professor-ME)** and **Dr. I.A.Palani (Associate Professor-ME)** for providing very good training on reliability and building confidence in me to start my work on this topic. I owe gratitude to **Mr. Pradeep Kundu (Research scholar-IIT Delhi)**, **Mrs. Priya Chouhan (Masters student at in Aerospace department at San Jose State University)**, **Dr.Yogesh Madaria** and **Dr. Sunil Pathak (Assistant Professor: Phang Campus, Malaysia University)**, who willingly devoted so much time in giving guidance to me.*

*I expand my thanks to **Dr. Amit Kumar Jain, Dr. Sandeep Gupta, Mr. Amit Kumar Jain, and Mr. Mani Prabu (Thalaiva)** who shared the hostel with me during my stay in IIT Indore and extended brotherly love towards me. I feel highly indebted to **Mr. Rajagopalan** for simply being himself.*

*I would also like to thank some people from the early days of my research tenure. **Mrs. Nandini Patra, Mr. Karthick S., Mr. S. Jaychandran, Mr. Suhel Khan, Km. Ankita Sahu, Mr. Manikandan** for helping me out selflessly.**Mr. Brolin, Mr. Yogeshwaran, Mr. Anand and Mr. Mithun R.**helped were among those who kept me going at the last phase during Ph.D. I am indebted to my many student colleagues for providing a stimulating and fun-filled environment. My thanks go in particular to **Mr. Abhilash Kasliwal, and Mr. Gaurav Raut (IAS: Ministry of communication)**; with whom I started this work and many rounds of discussions on my project with him helped me a lot. I am ever indebted to staff members of the mechanical engineering department, **Deputy Managers Mr. Farhan Babu, Mr. Sachin Laxman Bhirodkar Mr. Ashwin Wagh, Mr. Sandeep Patil, Mr. Kailash Patel,** and. I admire his distinguished helping nature. Academic staff **Mr. Suresh Chandra Thakur (Administrative Officer)** and **Mr. Tapeshe Parihar (Manager)** have helped to too much to process the formalities regarding Ph.D.*

*It's my fortune to gratefully acknowledge the support of some special individuals. Words fail me to express my appreciation to **Mr. Rajiv Gupta (Sr. Engineer: M.P. Vidyut Vitaran Vibhag)** for his support, generous care and the homely feeling at Indore. He was always beside me during the happy and hard moments to push me and motivate me. A journey is easier when you travel together. Interdependence is certainly more valuable than independence. Thank you doesn't seem sufficient but it is said with appreciation and respect to both of them*

*for their support, encouragement, care, understanding and precious friendship. I am much indebted to **Palani sir** for his valuable advice in my work, spending his precious times to read this thesis and gave his valuable suggestions. It is also a pleasure to mention my good friends, Akash, and Shiva for their love, care, support and creating a pleasant atmosphere for me here. I doubt that I will ever be able to convey my appreciation fully, but I owe them my eternal gratitude.*

*Last but not least, I would like to pay high regards to my sisters **Mrs. Pratibha Shukla, Mrs. (Dr.) Durgesh Nandini, and Mrs. Priti** as well as a brother in law's **Mr. Bhupati Kishor Shukla, Mr. Vishal Dwivedi and Mr. Abhishek Kumar Upadhyay** for their sincere encouragement and inspiration throughout my research work and lifting me uphill this phase of life. I owe everything to them. Besides this, several people have knowingly and unknowingly helped me in the successful completion of this project.*

SPECIAL ACKNOWLEDGEMENTS

*I convey my special thanks to a very special person, **my father, Mr. Hridaya Nath Tiwari and my mother Mrs. Vijaya Laxmi Tiwari** for their continued and unfailing love, support and understanding that made the completion of thesis possible. They are always around at times I thought that it is impossible to continue, they helped me a lot to keep things in perspective. I greatly value his contribution and deeply appreciate his belief in me. I appreciate my baby, my little daughter "**Unnati Tiwari**" for abiding my ignorance and the patience she showed during my thesis writing. Words would never say how grateful I am to both of you. I consider myself the luckiest in the world to have such a lovely and caring family (**Especially for Purnima Tiwari**), standing beside me with their love and unconditional support.*

*My heartfelt regard goes to **my father in law, mother in law** for their love and moral support. I thank the Almighty for giving me the strength and patience to work through all these years so that today I can stand proudly with my head held high.*

The Ph.D. degree is the starting of my professional life.

TAMESHWER NATH

Dedicated to my
Parents (Mr.Hridaya Nath Tiwari, Mrs.Vijaya
Laxmi Tiwari),
Wife (Mrs.Purnima Tiwari),
Daughter (Unnati Tiwari)
Mentor (Dr. I.A.Palani)

LIST OF PUBLICATIONS

Patent

1. Palani I.A., Lad B.K., **Nath Tameshwer** and Kundu Pradeep, (2016), "Thermo-mechanical test bench for reliability estimation of Shape memory alloy spring," India, *Application No: 201621007005, Published date:10-11-2017*

Peer Reviewed Journal

1. **Nath, Tameshwer**, Kasliwal, A., Singh R., Kulkarni, K., Raut,G., Kumar, A., Khatri, R., Mittal,S., Palani , I.A.,(2015), "Investigation on the Laser-Based Actuation of Single way Trained SMA sheet and Their Application for the Development of Micro Positioning Stage", *Applied Mechanics and Materials*, 766-767, 427-431, DOI: 10.4028/www.scientific.net/AMM.766-767.427.
2. **Nath, Tameshwer**, Chouhan, Priya, Disawal, Reena, Palani, I.A.,(2017), "Comparative study of electrically and hot water actuated shape memory alloy using developed thermo-mechanical cycle test bench", *Defence Science Journal*, 67(1), 100-107, DOI: 10.14429/DSJ.67.10489 [Impact Factor: 0.50]
3. **Nath, Tameshwer, K.**, Akash., Chouhan, Priya, Lad, B.K.,Palani, I.A., (2018) "Investigation on thermomechanical behavior of SMA spring under the influence of different actuation medium" *Microsystem Technologies (Springer)*, 24(6), 2813–2821, DOI: 10.1007/s00542-017- 3695-z [Impact Factor: 1.581]
4. Kundu, Pradeep, **Nath, Tameshwer**, Palani, I.A.,Lad, B.K.,(2018)"Integrating GLL-Weibull distribution within a Bayesian framework for life prediction of Shape memory alloy spring undergoing Thermo-mechanical fatigue" *Journal of Materials Engineering and Performance, (Springer)*, 27(7), 3655-3666, DOI: 10.1007/s11665-018-3435-2 [Impact Factor: 1.340]
5. Disawal, Reena, **Nath, Tameshwer**, Prakash, Shashi, Palani, I.A., (2018) "Life cycle analysis of Electrically actuated SMA spring using Talbot Interferometry" *Applied Optics (OSA)*, 57(20), 5779-5783, DOI: 10.1364/AO.57.005779 [Impact Factor: 1.791]

6. S. S. Mani Prabu, Mithun R, Muralidharan M. **Nath, Tameshwer**, Brolin A , K. Akash, I.A.Palani., “Thermo-mechanical actuation behavior of shape memory alloy spring using contactless energy transfer irradiated by ytterbium doped continuous fiber laser” Accepted to Smart Materials and Structures, IOP Science, DOI: 10.1088/1361-665X/ab06d8 [Impact Factor : 2.9]

Book Chapters

1. **Nath, Tameshwer**, S. Karthick, Chouhan, Priya, Lad, B.K., Palani, I.A., (2016), “Investigation on Actuation and thermo-Mechanical Behavior of Shape Memory Alloy Spring by comparing On/off and PID Controller for Precise Position Control” *communications in computer and Information science (Springer)*, 627, 95–105, DOI: 10.1007/978-981-10-2845-8_8
2. Chouhan, Priya, **Nath, Tameshwer**, Lad, B.K., Palani, I.A., (2016), "Investigation on actuation and thermo-mechanical behavior of Shape Memory Alloy spring using hot water" *IOP Conference series: material science and engineering*, 149, 1-7, DOI: 10.1088/1757-899X/149/1/012147

Proceedings in International Conferences

1. Verma Akhil, K Anand, Visanth Hari, **Nath Tameshwer**, Palani I.A., "Investigation on hot fluid based actuation of SMA spring and their application for the development for Heat Engine" *AIP Conference Proceedings, 2018 (1)*, 020022, DOI: 10.1063/1.5058259
2. Yogeshwaran S.M., **Nath Tameshwer**, Disawal Reena, Palani I.A., "Design and fabrication of shape memory alloy actuated Stewart platform for automated laser assist micromachining application", ISBN No: 978-93-80689-28-9, 962-965
3. **Nath Tameshwer**, Raut Gaurav Kumar Alok, Khatri Ritesh, Palani I.A., "Investigation on Laser assisted actuation of shape memory alloy based Micro-Valve" DOI: 10.1109/RACE.2015.7097249, Publisher: IEEE, ISBN: 978-81-925974-3-0

4. Singh Himanshu, Juiker Prateek, **Nath Tameshwer**, Palani I.A., Lad B.K., "Failure Diagnosis & Reliability Assessment of NiTi Shape Memory Alloy Spring For Micro- Actuators" DOI: 10.1109/RACE.2015.7097286, Publisher: IEEE, ISBN: 978-81-925974-3-0
5. **Nath Tameshwer**, K Akash., S. Shiva, Babu Farhan, Palani I.A., 'Investigations on The Effect of Laser Actuation And Interaction on Ni-Ti SMA Sheet For The Development Of Micro-Grippers' International Union of Material Research Societies- The IUMRS International Conference in Asia-2014 , held during August 24th-30th, 2014 at Fukoka Japan.
6. Mithun R., **Nath Tameshwer**, S.S. Mani prabu, Palani I.A., "Influence on flow domain parameters on hot water actuation of shape memory alloy spring for barrier gate system" *accepted for AIMTDR 2018, will be held on 13th - 15th December 2018 at Anna University.*

Peer reviewed conference

1. Chouhan Priya, **Nath Tameshwer**, Palani I.A., Lad B. K., "Development of test rig for Laser actuated Shape Memory Alloy (SMA) spring and its life cycle analysis", *Presented on 16th - 18th December 2016 for AIMTDR-2016 at college of Engineering, Pune*".
2. S Karthick, **Nath Tameshwer**, K. Akash, Palani I.A., "Cyber-Physical System Design for Shape Memory Alloy Controller based Intelligent Instrument" *Presented on 23rd - 24th June 2016 for ICAARS 2016 at PSG Tech College of Technology, Coimbatore, India*

TABLE OF CONTENTS

Item	Page No.
CANDIDATE’S DECLARATION	i
PREAMBLE	iii
ACKNOWLEDGMENT	iv
DEDICATION	vii
LIST OF PUBLICATIONS	viii
TABLE OF CONTENTS	xi
LIST OF FIGURES	xvii
LIST OF TABLES	xxv
NOMENCLATURE	xxvi
ACRONYMS	xxviii
Chapter 1: Introduction	1-20
1.1 Shape Memory Alloys (SMA)	2
1.2 Shape Memory Effect and superelasticity	4
1.2.1 One way shape memory effect	5
1.2.2 Two-way shape memory effect	6
1.3 Shape Memory Alloy Actuators	7
1.4 various forms of SMA	7
1.5 Applications based on shape memory properties	8
1.6 Application based on the effects of SMA	10
1.6.1 using shape memory effect	10
1.6.2 using Pseudo-elasticity	11
1.7 Actuation and Thermomechanical Behavior	18
1.8 The need for Thermomechanical behavior and life cycle analysis	19
1.9 Motivation	19
1.10 Research Gaps	20

Chapter 2: Literature Review on Thermo-mechanical and Actuation studies of SMA spring	21-44
2.1 Introduction	21
2.1.1 overview of NiTi	21
2.1.2 The mechanism behind NiTi SMA	24
a) Dislocation slip	24
b) Twinning	25
2.1.3 Equiatomic NiTi	27
2.2 Thermomechanical behavior Life cycle of SMA	29
2.2.1 Joule Heating or Electrical Actuation	29
2.2.2 Hot fluid Actuation	34
2.2.3 Laser Assisted Actuation	41
2.3 Research objectives and approach	43
2.4 Outline of the Thesis	44
Chapter 3: Electrical actuation of SMA spring	45-98
3.1 Introduction	45
3.1.1 Past studies on developed directional control valve (DCV)	45
3.1.2 Fabrication of DCV	47
3.2 Experimental setup for the Thermo-mechanical behavior of the SMA spring	49
3.2.1 Experimentation	51
3.2.2 Actuation analysis	52
3.2.3 Heat Transfer Analysis	62
3.2.3.1 Simulation of Thermomechanical behavior on SMA using COMSOL	63
3.3 Control strategy	67
3.3.1 On-Off controller	67
3.3.1.1 Implementation of controller	68
3.3.2 PID controller	76
3.3.2.1 Mathematical model	77

3.3.3	Comparison of PID controller with on-off controller	77
3.4	Lifecycle analysis	79
3.4.1	Failure Diagnosis Analysis using Morphological analysis	81
3.5	Verification of displacement using Talbot Interferometer	85
3.5.1	Principle	86
3.5.2	Experimental Arrangement	87
3.5.3	Result and discussion	89
3.6	Developed Micro-devices	91
3.6.1	For micro-machining applications	91
3.6.1.1	Stewart platform	91
3.6.1.2	Design and principle work	94
3.6.1.3	Experimentation	94
3.6.1.4	Experimental Result	96
3.7	Summary	97
Chapter 4: Hot water Actuation of SMA spring		99-138
4.1	Introduction	99
4.2	Experimental setup	99
4.3	Mathematical Modeling for hot water actuated SMA spring	101
4.4	Result	102
4.4.1	Thermomechanical behavior	103
4.4.2	Life cycle behavior	104
4.4.3	Characterization Techniques	105
4.4.4	Simulation results of SMA spring	106
4.5	Application: SMA based heat engine	115
4.5.1	Intermediate objectives	117
4.5.2	Components of SMA heat engine	117
4.5.3	Drawbacks in previous heat engine design	118
4.5.4	Modifications in the model	119
4.5.5	comparison of characteristic curves in two models	120
4.5.6	Optimum height from the bottom of bearing axis	121

4.5.7	Heat transfer analysis of heat engine	123
4.5.8	Scaling of the heat engine	124
4.5.9	The efficiency of the developed heat engine	125
4.5.10	Demerits of the developed heat engine	126
4.6	Modified Objectives	126
4.6.1	Components of the Nitinol heat engine	127
4.6.2	Hot water actuated SMA heat engine	127
4.6.3	Experimentation done in the exhaust of the vehicle	131
4.6.4	Keeping the mass constant with change in diameter of the wheel	133
4.6.5	Keeping the constant diameter and changed the mass of the wheel	135
4.7	Comparison of the performance for all three types of the heat engine	137
4.8	Summary	138
Chapter 5: Pulsed Laser Assisted actuation of SMA spring		139-192
5.1	Introduction	139
5.2	Experimental Specifications for laser Actuation	140
5.2.1	Laser Fluence	141
5.2.2	Characterization	142
5.3	Development of Micro-devices	149
5.3.1	Tripod	149
5.3.1.1	Tripod: Using Sheet	149
5.3.1.2	Fabrication	150
5.3.1.3	Experimentation	151
5.3.1.4	Result and discussion	152
5.3.2	Micro-valve	153
5.3.2.1	Micro-valve: using sheet	153
5.3.2.2	Objective	153
5.3.2.3	Fabrication and working	153
5.3.2.4	Experimentation	155
5.3.2.5	Result and discussion	158

5.3.2.6 Characterization	160
5.3.3 Micro-valve array	168
5.3.3.1 Design	169
5.3.3.2 Fabrication	169
5.3.3.3 Result and discussion	170
5.3.3.4 Application of Microvalve Array as a Micromixer	171
5.4 Benefits of using Line beam in place of Spot Beam	172
5.4.1 Preliminary Experimentation	173
5.4.2 Comparison on Point and Line actuation	173
5.4.3 Experimental Set up	176
5.4.4 The framing of the work	178
5.4.5 Result and discussion	180
5.4.5.1 Effect of the cylindrical lens	181
5.4.5.2 Effect of combination Lens	182
5.4.6 Morphological Analysis	186
5.5 The drawback of Pulsed Laser	191
5.6 Summary	192
Chapter 6: Continuous fiber laser assisted actuation of SMA spring	193-226
6.1 Introduction	193
6.2 Details of Experimental Apparatus	194
6.2.1 Procedure of Experimentation	196
6.2.1.1 Experimentation	197
6.2.1.2 Theory of Actuation	198
6.3 Result and discussion	201
6.3.1 Thermomechanical Behavior:	201
6.3.2 Effect of parameters on actuation	208
6.3.3 Mathematical Modelling	210
6.3.4 Simulation	211
6.3.5 Characterization	214
6.3.5.1 Stereo Images	214

6.3.5.2 Scanning Electron Microscope Images	214
6.3.6 Beam Profile	220
6.4 Application	220
6.4.1 Directional control valve: Introduction	220
6.4.1.1 Manually Operated	221
6.4.1.2 Hydraulically operated	221
6.4.1.3 Solenoid Operated	222
6.4.2 Working of a 3/2 Directional Control Valve	222
6.4.2.1 Drawbacks of the current designs of the DCVs	223
6.4.3 Conceptual model Design	223
6.4.3.1 Working	225
6.4.3.2 Actuation of DCV	225
6.5 Summary	226
Chapter 7: Conclusion and Outlook	227-230
7.1 Conclusions	227
7.1.1 Research contributions	227
7.1.2 Utility and industrial implications of Research work	229
7.2 Future scope	230
References	231-245

List of Figures

Fig No	Description	Page No
Fig. 1.1	A different phase of Shape memory alloy	5
Fig. 1.2	The new mixing valve using SMA and biasing coil springs	10
Fig. 1.3	Application of Pseudo-elasticity: a) Antenna, for cellular phone, b) Catheter wire used in the brain, c) Appearance of the guide wire, d) Glasses	12
Fig. 1.4	SMA sheet Applications: a) Micro gripper [26], b)Micro-Pump [27], c) Peristaltic pump	13
Fig. 1.5	SMA spring Applications: a) Tip Articulation mechanism, b) Fiber optic articulator, c) Latch Mechanism, d) Tube type tip articulator, e) Joint Mechanism, f) SMA actuator unit, g) Micro-gripper, h) Biomedical applications [5]	15
Fig. 1.6	SMA wire applications a) Micro-gripper [26] b) Neurosurgical stents c) Orthodontic distracters [25], d) Endodontic file [5]	17
Fig. 1.7	SMA rod applications a) bend condition b) maximum bend condition c) straight condition[30-31], d) in building a structure with exposed-type column base with SMA anchorage [32]	18
Fig. 2.1	Shear modulus vs. temperature considering the chemical and non-chemical contributions [38]	23
Fig. 2.2	Schematic of critical stress vs. temperature for SMAs [39]	24
Fig. 2.3	Schematic of determination of dislocation slip stress in martensite SMA's [41]	25
Fig. 2.4	Schematic of SME in SMAs [43]	26
Fig. 2.5	Partial phase diagram of NiTi from 45% nickel to 59% [50]	28
Fig. 2.6	Wire Tension experimental setup University of Michigan, Department of Aerospace Engineering, (2008)	29
Fig. 2.7	Thermo-mechanical cycling setup, Material Science Division, National Aerospace Lab, Bangalore (2009)	30
Fig. 2.8	Experimental setup for fatigue life cycle analysis of the SMA wire	31
Fig. 2.9	Fatigue cycle simulator for SMA wire using liquid cooling Smart Lab	31
Fig. 2.10	a) Self-Assembled Cycling Machine b) Wire clamping system	32
Fig. 2.11	Thermo-mechanical Characterization of SMA spring Mechanical Engineering Department, University of Rome, Italy (2010)	33
Fig 2.12	Shower faucet with water a) Regulator containing an SMA spring, b) Schematic diagram of regulator	35

Fig. 2.13	Gas flow shielding device with a SMA disk	36
Fig. 2.14	Operating principle of gas flow shielding device	37
Fig 2.15	a)Boiler with SMA hot water safety valve, b) b) Operating principle of hot water safety valves in bath	38
Fig 2.16	a)Hot water safety valves in outlet of bath, b) Operating principle of hot water safety valves in bath	39
Fig 2.17	Bath Tub Adaptors	40
Fig 2.18	Wet SMA actuator design	40
Fig 2.19	Wet SMA actuator array	41
Fig 2.20	Block diagram of actuation methodology	44
Fig. 3.1	Force applied vs extension of the SMA tension spring	46
Fig. 3.2	Design of DCV a) side view, b) front view, c) Top view, d) Isometric view	47
Fig. 3.3	Developed directional control valve (DCV) a) working model, b) Top view	48
Fig.3.4(a)	Line Diagram for SMA actuation for Joule Heating	49
Fig.3.4(b)	Experimental Set up for Joule Heating	50
Fig. 3.5	DSC curve of virgin NiTi spring	51
Fig. 3.6	Displacement vs Time at 2.0 V for different weight a) for 2.5 N, 3.5 N and 4.5 N, b) Temperature vs time plot for 2.5 N, 3.5 N and 4.5 N	54
Fig. 3.7	Hysteresis curve for actuation of SMA at 2.0 V and a) 2.5 N, b) 3.5 N, and c) 4.5 N	55
Fig. 3.8	Hysteresis curve for actuation of SMA at 2.0 V and a) 2.5 N, b) 3.5 N, and c) 4.5 N	56
Fig.3.9	Displacement vs Time at 3.0 V for different weight a) for 2.5 N, 3.5 N and 4.5 N, b) Temperature vs time plot for 2.5 N, 3.5 N and 4.5 N	57
Fig.3.10	Hysteresis curve for actuation of SMA at 3.0 V a) 2.5 N, b) 3.5 N, c) 4.5 N	58
Fig.3.11	Hysteresis curve for five cycles at 3.0 V and a) 2.5 N, b) 3.5 N, and c) 4.5 N	59
Fig 3.12	Displacement vs Time at 4.0 V for different weight a) for 2.5 N, 3.5 N and 4.5 N, b) Temperature vs time plot for 2.5 N, 3.5 N and 4.5 N	59
Fig.3.13	Hysteresis curve for actuation of SMA at 4.0 V a) 2.5 N, b) 3.5 N, c) 4.5 N	60
Fig.3.14	Hysteresis curve for five cycles at 4.0 V and a) 2.5 N, b) 3.5 N, and c) 4.5 N	61
Fig.3.15	Heat loss in cylindrical SMA wire	62

Fig. 3.16	Comparison analysis for actuation of SMA spring for 2.0 V (with experimental and simulation)	64
Fig. 3.17	Simulation of SMA spring under condition of different voltages a) 2.0 V,) 3.0 V, c) 4.0 V	66
Fig. 3.18	The basic principle of the on-off controller	67
Fig. 3.19	Spring loaded with 2.5 N controlled at 10 mm, 15 mm a) Displacement vs. time curve for 2.0 V, 2.5 V and 3.0 V when controlled at 10 mm, b)Temperature vs. time curve for 2.0 V, 2.5 V, and 3.0 V when controlled at 10 mm, c) Displacement vs. time curve for 2.0 V, 2.5 V, and 3.0 V when controlled at 15 mm, d)Temperature vs. time curve for 2.0 V, 2.5 V, and 3.0 V when controlled at 15 mm	70
Fig. 3.20	Spring loaded with 3.5 N controlled at 10 mm and 15 mm, and 20 mm for different voltages a) Displacement vs. Time curve for a controlled position at 10 mm b) Temperature vs. Time curve for a controlled position at 10 mm, c) Displacement vs. Time curve for a controlled position at 15 mm, d) Temperature vs. Time curve for a controlled position at 15 mm, e) Displacement vs. Time curve for a controlled position at 20 mm, f) Temperature vs. Time curve for a controlled position at 20 mm	73
Fig 3.21	Spring loaded with 4.5 N controlled at 10 mm and 15 mm, and 20 mm for different voltages a) Displacement vs. Time curve for a controlled position at 10 mm b) Temperature vs. Time curve for a controlled position at 10 mm, c) Displacement vs. Time curve for a controlled position at 15 mm, d) Temperature vs. Time curve for a controlled position at 15 mm, e) Displacement vs. Time curve for a controlled position at 20 mm, f) Temperature vs. Time curve for a controlled position at 20 mm	76
Fig 3.22	Comparison of spring for on/off (3 V) and PID controller when a) Displacement vs. time curve when spring is loaded with 2.5 N b) Displacement vs. Time curve for loaded with 3.5 N c) Displacement vs. Time curve for loaded with 4.5 N	79
Fig 3.23	The basic principle of Talbot interferometer	80
Fig 3.24	SEM image of the surface of the SMA spring (a) Non-Treated spring (b) deformed spring (c) failed spring	84
Fig 3.25	TGA results in comparison between virgin and failed spring	85
Fig 3.26	The basic principle of Talbot interferometer	86
Fig 3.27	Experimental Arrangement for measurement of	88

	displacement drift	
Fig 3.28	The fringe pattern obtained when the mirror attached to the spring is kept at a) at the focus, b) In focus (1000) cycles, c) In focus (5000) cycles position of the focusing lens	89
Fig 3.29	Displacement drift vs. number of cycles	90
Fig 3.30	Model of Stewart Platform using Mass Spring System	92
Fig 3.31	Kinematic model for the Translational movement	93
Fig 3.32	Kinematic model for the rotational movement	93
Fig 3.33	Stewart Platform a) Design and its nomenclature, b) Fabricated Stewart platform	94
Fig. 3.34	Line diagram of Experimental set up for actuating micro-positioning stage	95
Fig.3.35	Fabrication of Experimental set up for actuation	95
Fig 3.36	Plot between a) Displacement vs time, b) Temperature vs Time and c) Hysteresis curve	96
Fig 3.37	Monitoring of displacement using LDS	97
Fig. 4.1	a) Schematic and b) experimental setup of Hot water actuation	101
Fig. 4.2	Thermomechanical behavior of SMA spring at 2.5 N a) Displacement vs. Time, b) Temperature vs. Time, c) Hysteresis curve	104
Fig. 4.3	Thermo-mechanical analysis of SMA spring till failure for a) 2.5 N, b) 3.5 N and, c) 4.5 N	105
Fig. 4.4	Characterization analysis of hot water actuated SMA spring a) SEM analysis, b) TGA analysis	106
Fig. 4.5	Line diagram for heating of spring	107
Fig. 4.6	Finely meshed geometry	107
Fig.4.7	Flow after a) 5 s, b) 10 s, c) 15 s, d) 20 s, e) 25 s for 65 °C	110
Fig. 4.8	Flow after a) 5 s, b) 10 s, c) 15 s, d) 25 s e) 25 s for 75 °C	112
Fig. 4.9	Flow after a) 5 s, b) 10 s, c) 15 s, d) 25 s e) 25 s for 85 °C	114
Fig. 4.10	Comparative result for simulation at different temperature	114
Fig. 4.11	Time taken vs Temperature graph	115
Fig. 4.12	Moment generated by the force	116
Fig. 4.13	Principle of Actuation	117
Fig. 4.14	SMA Heat Engine model	118
Fig. 4.15	Hub replaced by mild steel bearing holder	119

Fig. 4.16	MS bearing holder replaced by PLA material	120
Fig 4.17	RPM differences between the new and old model	120
Fig 4.18	Optimized design of Heat Engine	121
Fig 4.19	Experimental set up to study optimum height	121
Fig 4.20	RPM vs. Temperature graph	122
Fig 4.21	Line diagram of the rim with springs	125
Fig 4.22	Hot water actuated heat engine	128
Fig 4.23	Cad modeling of different designs of the hub	128
Fig 4.24	The plot for Heights vs. RPM variation	129
Fig 4.25	SMA heat engine a) In front of the exhaust, b) Thermo-graphic images	131
Fig 4.26	variation of the rpm of the SMA engine with the temperature of the exhaust gases	132
Fig 4.27	a) Effect of exhaust gas on SMA wheel, a-ii) Thermal Image of wheel b-i) hub condition before and b-ii) after testing	134
Fig 4.28	RPM vs Temperature variation	134
Fig 4.29	Nitinol based wheel No. 3	135
Fig 4.30	RPM vs Temperature variation	136
Fig 4.31	Variation in power, Torque and angular velocity for a) wheel having diameter = 0.113m and mass = 123g, b) wheel having increased mass of 165 g but same diameter, c) wheel having the same mass but increased the diameter of 295 mm	138
Fig 5.1	a) Setup for actuation of the laser, b) Movement in SMA sheet due to laser power	140
Fig 5.2	Ablation Spots at different fluence levels	142
Fig 5.3	Laser with a fluence of a) Non-Treated SMA, b) 100mJ/cm ² , c) 200mJ/cm ² , d) 300mJ/cm ² , e) 400mJ/cm ² , f) 500mJ/cm ² , g) 600mJ/cm ² , h) 700mJ/cm ²	146
Fig 5.4	The weight percentage of Ni and Ti with varying fluence values	147
Fig 5.5	The atomic percentage of Ni and Ti with varying fluence values	148
Fig 5.6	Comparison of weight percentage of Ni and Ti at different fluence values	149

Fig 5.7	Single way Training of SMA sheets a) Fixture used for training of SMA, b) Ni-Ti sheet trained in omega shape, c) Fabricated Tripod	151
Fig 5.8	Deflection vs. time for actuated SMA NiTi	152
Fig 5.9	Design of Micro valve open and closed assembly	154
Fig 5.10	fabricated micro valve in a) open position, b) open position	155
Fig 5.11	Apparatus used in Training a) Fixture, b) Muffle furnace, c) bent sheet	156
Fig 5.12	a) Laser actuation set up, b) deflection of SMA	157
Fig 5.13	Deflection versus time plot	158
Fig 5.14	SEM image at a) 100 mJ/cm ² , b) 110 mJ/cm ² , c) 120 mJ/cm ² , d) 130 mJ/cm ² ,e) 140 mJ/cm ² and f) 150 mJ/cm ²	162
Fig 5.15	SEM image at a fluence level of a) 70 mJ/cm ² , b) 100 mJ/cm ² ,c) 130 mJ/cm ² ,d) 140 mJ/cm ² and e) 155 mJ/cm ²	165
Fig 5.16	EDX image of SMA sheet	166
Fig 5.17	DSC curve of NiTi sheet	167
Fig 5.18	TGA image of NiTi sheet	167
Fig 5.19	variation of VHN with some training	168
Fig 5.20	Solidworks model showing design for Micro-valve Array	169
Fig 5.21	Fabricated Micro valve array	170
Fig 5.22	Application of Micro valve Array- Micromixer	172
Fig 5.23	Output line gained when passed through Quartz tube with a scale as a reference	174
Fig 5.24	Image captured on a photographic sheet	175
Fig 5.25	Quartz tubes used with varying diameters	175
Fig 5.26	Schematic for laser-based actuation setup	176
Fig 5.27	a) Line-beam generation by using quartz tube b) Displacement calculation using LDS and flapper arrangement	177
Fig 5.28	Lens arrangement used for conversion of point beam into line beam a) only cylindrical lens used, b) cylindrical + convex lens used	179
Fig 5.29	Schematic of the combination of lens arrangement using their focal point	179
Fig 5.30	Microscopic image captured over the photographic sheet	180

Fig 5.31	a) Effect of laser on the photographic sheet, b) Location of LDS in front of the flapper	181
Fig 5.32	Displacement-Time relationship at a) 0.25 W, 100 grams and b) 1.0 W, 100 grams c) 2 W and 200 grams, d) 1 W and 200 grams	184
Fig 5.33	Single Heating-cooling cycle	185
Fig 5.34	Scanning Electron microscopy done at (a) Sample cut out length (10 mm), (b) Original sample, (c) 0.25W, (d) 1.0W, (e) 1.5 W, (f) 2.0W showing depth created due to laser ablation at higher power	188
Fig 5.35	EDX representation showing peaks for particular components	189
Fig 5.36	TGA analysis performed for springs undergoes heating at different laser powers (a) 0.25W, (b) 0.50W, (c) 1.0W	191
Fig 6.1	schematic of laser-assisted actuation and b) on line location of continuous laser assisted actuation	197
Fig 6.2	Schematic diagram for laser actuation of SMA spring	199
Fig 6.3	Actuation of SMA for complete strain recovery	201
Fig 6.4	Actuation of SMA spring at 15 W with varying passes	202
Fig 6.5	Actuation of SMA spring at varying power till full recovery	203
Fig 6.6	Thermo-mechanical behavior of NiTi SMA for its full recovery with a load of 1.5 N, 2.5 N and 3.5 N at a) 15 W, b) 20 W, c) 25 W, d) 30 W, e) 35 W, f) 40 W, g) 45 W, h) 50 W	208
Fig 6.7	The relationship between a) Power and no of passes, b) Power and heating time, c) power and cooling time, d) power and displacement	210
Fig 6.8	a) Simulation study of laser actuated SMA at 15 W, b) thermal behavior for eight passes, c) comparison analysis of temperature for experimental and FLIR camera, d) effect of spot size on heat transfer	213
Fig 6.9	Stereo image of failed spring	214
Fig 6.10	SEM images a) for Non Treated Spring, b) for 5 W, 1.5 N, c) for 5 W, 2.5 N, d) for 5 W, 3.5 N, e) for 10 W, 1.5 N, f) 10 W. 2.5 N, g) 10W, 3.5 N, h) 15 W, 1.5 N, i) 15 W, 2.5 N, j) 15 W, 3.5 N	219
Fig 6.11	Effect of laser on Photographic sheet a) at 0.2 mm (invisible), 2 mm at 2 N b) 5 W, c) 10 W, d) 15W [for 5 passes]	220
Fig 6.12	Schematic of a 3/2 DCV	221
Fig 6.13	(a) Ports A and T are connected when force is not applied (valve un-actuated). (b) Ports A and P are connected when	223

Fig 6.14	force is applied (valve a) Spool position 1 (SMA heated), b) Spool position 1 (SMA cooled)	224
Fig 6.15	a) A working model of Directional Control Valve, b) Top view of Directional Control Valve	225
Fig 6.16	Actuation of DCV	226

List of Tables

Table No.	Description	Page No.
Table 1.1	Shape Memory Material (SMM)[4]	3
Table 1.2	Comparison of properties of Ni-Ti,Cu-Zn-Al and Cu-Al-Ni [8-9]	4
Table 2.1	Different phases of equiatomic NiTi SMA, crystal system, lattice parameters, and interaxial angles [49]	27
Table 3.1	SMA Spring specification	46
Table 3.2	Results from the testing of the SMA tension spring	47
Table 3.3	comparison analysis of different shapes of NiTi SMA	48
Table 3.4	Specification of SMA spring	50
Table 3.5	Heating (H) and cooling (C) at different voltages and weights	54
Table 3.6	Material properties for simulation	65
Table 3.7	Values of Process gain (K) and Time constant (T) for different weights	77
Table 3.8	SMA springs fatigue lifetime data	81
Table 3.9	Displacement drifts of SMA spring using Talbot interferometry after the completion of actuation cycles	89
Table 4.1	Effect on RPM of the wheel for variation in height	122
Table 4.2	Effect of height for RPM of the wheel	129
Table 4.3	Temperature vs. RPM of SMA wheel	131
Table 4.4	Tabulated results obtained from the experiment	134
Table 4.5	RPM of Nitinol wheel and temperature of the exhaust	136
Table 5.1	Fluence values and their corresponding power values	141
Table 5.2	Effect of the laser fluence on the composition of the Nitinol alloy	147
Table 5.3	Deflection at a given power	158
Table 5.4	Orientation at respective deflection	159
Table 5.5	The result of SMA actuation	165
Table 5.6	Output Line and Point heating comparison	174
Table 5.7	Output and input values for both lens arrangements	180
Table 5.8	Results using quartz tubes with a varying diameter	181
Table 5.9	Displacement gain in heating-cooling cycles	182
Table 5.10	EDX analysis after laser interaction	189
Table 6.1	Parameters for Laser actuation of SMA NiTi	204

NOMENCLATURE

Symbol	Unit	Description
σ	$W/m^2 / ^\circ K^4$	Stefan-Boltzmann constant
σ_d		Martensite defoemation or deformed martensite
σ_{slip}	N/mm^2	Critical stress
σ_S	N/mm^2	Twinning start stress
σ_F	N/mm^2	Twinning finish stress
T	$^\circ C/K$	Temperature
∇T	$^\circ C/K$	(Nabla)Temperature Gradient
dT	$^\circ C/K$	Temperature difference
q	W/m^2	Heat flux density
k	$W/m^\circ C$	Thermal Conductivity
h_c	$W/(m^2K)$	Heat Transfer coefficient or convection coefficient
A	mm^2	Surface Area
V	m/s	the velocity of the fluid
P	N/mm^2	pressure
ρ	$Kg m^{-3}$	Density of fluid
I		Identity matrix
F	N	External Force
C_p	J/K	Heat Capacity at constant pressure
C		Specific heat of water
T_∞	$^\circ C/K$	Hot water Temperature
C_b	mm	The diameter of the bearing holder
D	mm	The wire diameter of SMA spring
D	mm	Coil diameter of SMA spring
D_r	mm	The diameter of the steel rim
L	mm	Length of a spring
N		Number of coils
N_s		Number of springs attached in the wheel
Cl	mm	Clearance between each hole in bearing holder
I_c	A	the current flowing in the circuit.
M	kg	mass of water in the container
V	volt	voltage
N		number of LEDs connected in series
P	W	Laser power
d	mm	Laser spot diameter
V	mm/sec	Scan velocity
r	m^3/s	Flow rate
R	Ω	Resistance
$\frac{d\xi(T)}{dt}$		the rate of conversion of martensite into austenite
ΔH		change in energy associated with phase transformation
e		Error signal
L_c		collimating lens
L_d		de collimating lens

MO

microscopic objective

ACRONYMS

S.No.	Acronyms	Expansion
1	SMA	Shape Memory Alloys
2	SMM	Shape Memory Materials
3	SME	Shape Memory Effect
4	PE or SE	Pseudo Elasticity or Superelasticity
5	MEMS	Micro Electro Mechanical Systems
6	OWSME	One Way Shape Memory Effect
7	TWSME	Two Way Shape Memory Effect
8	NITINOL	Nickel-Titanium Naval Ordnance Laboratory
9	M _s	Martensite Start
10	M _f	Martensite Finish
11	A _s	Austenite Start
12	A _f	Austenite Finish
13	M _d	Martensite Deformation
14	M _T	Martensitic Transformation
15	CG	Centre of Gravity
16	SCPI	Standard Commands for Programmable Instruments
17	TTL	Transistor–transistor logic
18	PV	Process variable
19	SP	Set point
20	PPS	Programmable power supply
21	LDS	Laser displacement sensor
22	DAS or DAQ	Data acquisition system
23	Nd-YAG	Neodeum doped Yittrium Aluminium Garnet
24	DCV	Directional control valve
25	FEA	Finite Element Analysis
26	BS	Beam Splitter
27	SEM	Scanning Electron Microscopy
28	EDS	Electron Dispersive Spectroscopy
29	VHN	Vicker’s Hardness Number
30	XRD	X-Ray Diffraction
31	DSC	Differential Scanning Calorimetry
32	TGA	Thermo Gravimetric Analysis
33	HT	Heating Time
34	CT	Cooling Time

Chapter 1

Introduction

In this introductory chapter, the background of shape memory alloys, motivation, and methodologies of the current research are presented to highlight the importance. The summary of the chapter is presented to provide a brief overview.

Manufacturing, over the years, has evolved through three revolutions brought out by the impact of mechanization, electricity, and information technology [1]. The next change in manufacturing has its roots in intelligence. There has been a continuing trend in technology towards ever-smaller scales for mechanical, optical as well as electro-mechanical devices. Actuators, which are the driving mechanism and usually the moving part of these devices, must, therefore, undergo similar miniaturization in design and construction. These actuators are mainly electrical, hydraulic, pneumatic, etc. Some factors, such as power consumption, work density; costs and space constraints gain increased importance in the selection of suitable technologies. However, conventional actuators, including electric motors, pneumatic and hydraulic actuators, suffer a large reduction in power that they can deliver as they are scaled down in size and weight. These constraints have led to the emergence and development of novel actuator technologies such as piezoelectric actuators, electrostatics, magnetostrictive materials and shape memory alloys (SMAs).

SMAs are generally considered a type of ‘smart’ materials due to actuation functions, temperature sensing, electrical or structural functions and so enable compact and multifunctional features. SMAs are easily adapted to miniaturization in design with their noise free, smooth and lifelike motions eliminating the need for power transmission elements [2]. These include micro-robotics, surgical devices, and micro-electromechanical (MEMS) applications. As SMA manufacturing techniques improve and design objectives become more severe, they will find increasing use in almost all engineering domains. Among all the presently known actuation principles, SMA show one of the highest work

densities at 10^7 Jm^{-3} , which is a factor of 25 times higher than the work density of electric motors [3]. Currently, there are very few actuator technologies that can match the energy densities of SMA.

This chapter will provide a brief description of SMA, followed by their benefits and drawbacks regarding actuator applications. The motivations and need for this research behind in this thesis will be established. Moreover, the thesis work will try to underline the opportunities and the room for new ideas to enlarge the range of SMA applications. Finally, this chapter will conclude with a summary.

1.1 Shape Memory Alloys:

The SMA can memorize and recover its original shape after it has been deformed by heating over its transformation temperature. This unique effect of returning to an original geometry after a large inelastic deformation (near 10%) is known as the Shape Memory Effect (SME).

In 1932, the Swedish physicist Arne Olander discovered an interesting phenomenon when working with an alloy of gold (Au) and cadmium (Cd). In 1961, a group of U. S. Naval Ordnance Laboratory researchers led by William Beuhler made a significant discovery in the field of SME and SMA [4-5]. The SME had been found as early as 1932, and until 1971 it was believed to be common to all alloys that undergo thermoelastic martensitic transformations [6]. SMA exhibit a similar coupled effect between temperature and mechanical deformation.

Table.1.1: Shape Memory Material (SMM)[4]

S.No	Alloy	Composition	Transformation temperature (A_s) °C	Hysteresis (°C)
1.	Ag-Cd	44-49% Cd	-190 to 50	15
2.	Au-Cd	46.5-50% Cd	30 to 100	15
3.	Cu-Al-Ni	14-14.5 weight % Al and 3-4.5 weight % Ni	-140 to 100	35
4.	Cu-Sn	15 at% Sn	-120 to 30	10
5.	Cu-Zn	38.5-41.5 wt.% Zn	-180 to -10	
6.	Cu-Zn-X (X = Si, Sn, Al)	Small weight % X	-180 to 200	
7.	Ni-Al	36-38 weight % Al	-180 to 100	10
8.	NiTi	46.2-51 % Ti	-50 to 110	30
9.	NiTi-X (X =Pd or Pt)	50 at % Ni+X	-200 to 700	100
10.	NiTi-Cu	15 at % Cu	-150 to 100	50
11.	NiTi-Nb	15 at % Nb	-200 to 50	125
12.	NiTi-Au	50 at % Ni+Au	20 to 610	
13.	Ti-Pd-X (X = Cr or Fe)	50 at % Pd+X	0 to 600	50
14.	Mn-Cu	5-35 at % Cu	-250 to 180	25
15.	Fe-Mn-Si	32wt%Mn, 6wt%Si	-200 to 150	
16.	Fe-Pd	30 at % Pd	50	100
17.	Fe-Pt	25 at % Pt	-130	4

The properties of NiTi, Cu-Zn-Al and Cu-Al-Ni alloys are reasonably different, as tabulated in Table 1.2, due to their different microstructure. The NiTi alloys have much higher strength, more considerable recoverable strain, high power to weight ratio, excellent corrosion resistance (comparable to series 300 stainless steel), less expensive, easier to work with high biocompatibility and most importantly higher reliability than Cu-Zn-Al. They are the standard choice for use in space and several other engineering applications [7].

Table1.2: Comparison of properties of NiTi,Cu-Zn-Al and Cu-Al-Ni [8-9]

Properties	NiTi	Cu-Zn-Al	Cu-Al-Ni
Melting temperature (°C)	1300	950-1020	1000-1050
Transformation range (°C)	-200~110	<120	<200
Hysteresis (°C)	30-50	15-25	15-20
Recovery Strain (%)	8.5%	4	4
Recovery stress	500 Mpa	200Mpa	150 Mpa
Number of cycles	10 ⁵	10 ²	10 ²
Corrosion resistance	Excellent	Problematic	Better
Machinability	Poor	Fair	Fair

1.2 Shape Memory Effect and Super-elasticity:

SMA's can easily change their shape from one form to the other when initiated either by stress or warmth. These are called 'temperature induced phase transformation' and 'stress-induced phase transformation,' due to a change in temperature or stress respectively. On application of stress, these materials can deform plastically. When these materials are subjected to appropriate thermal or stress conditions, they will return back to their memorized shape. They can sustain a large amount of strain without any stable deformation [11]. The strains can be recovered upon either by changing the temperature or the load. A reversible, solid-state phase transformation, known as 'martensitic transformation,' is the main driving force behind SMA's.

The super-elasticity (SE), while dependent upon the same physical processes, is demonstrated by the alloy's ability to recover a very high deformation without the application of heat. The difference between the two processes is dependent upon the surrounding temperature and applied stress. Both SE and the SME may be exhibited by the same material yet under different conditions.

The SME is favored over super-elasticity for actuator applications since it is desirable to actively control the strain recovery. The change that occurs within the SMA crystalline structure during the SME is not thermodynamically reversible. In other words, there is energy dissipation due to internal friction and the creation of structural defects. As a result, a temperature hysteresis occurs. [11]

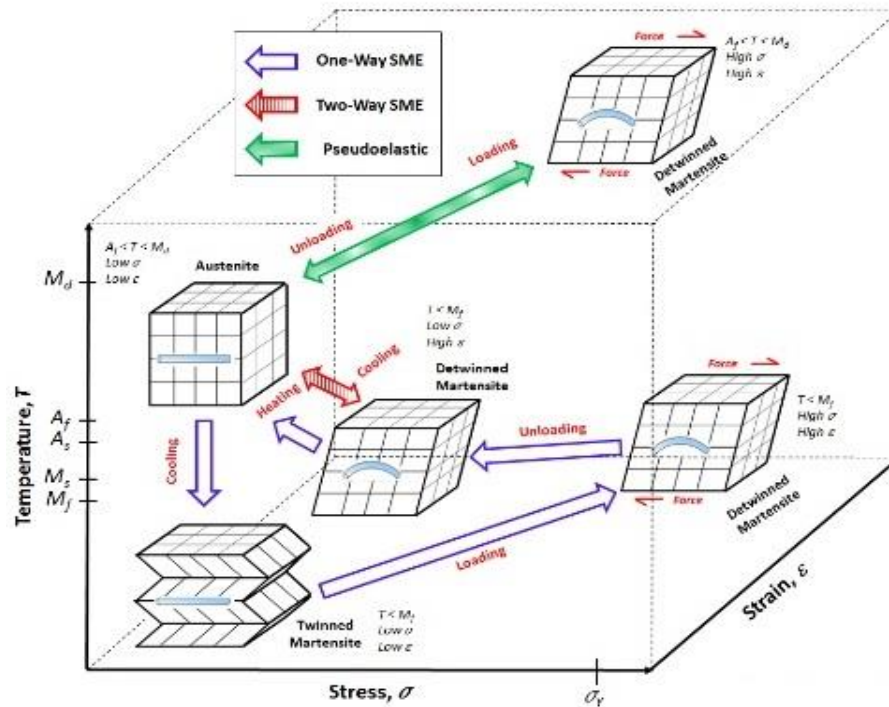


Fig 1.1: Different phase of SMA's [10]

If the material is deformed at a high temperature, on the other hand, large deformations can be recovered by simply removing the applied load (mechanical recovery), known as SE.

SME is of two types:

1.2.1 One-way shape memory effect (OWSME): At low temperature, an SMA material can be plastically deformed. This deformation involves the movement of highly mobile boundaries (twin boundaries, martensite/martensite interfaces). Upon heating, SMA material reaches the Austenite phase with the initial orientation, and so the specimen reverts to its original shape. While cooling, no additional shape change takes place; this effect is called “OWSME”. The one-way

effect can be repeatedly induced by deforming SMA in the martensitic state. Initially, in an SMA material displaying one-way SME, there is no movement on heating. The shape change starts at Austenite start temperature (A_s) and get completed in a small temperature range (e.g., 10 to 30 K). A_s the temperature of NiTi SMAs can be significantly tuned by suitable selection of the chemical composition of the alloy and dopants [12].

1.2.2 Two-way shape memory effect (TWSME): SMAs with a TWSME, "remember" both a high-temperature shape (austenite) and a low-temperature shape (martensite). Though TWSMAs can switch from their low-temperature shape to their high-temperature shape; their recoverable strain is usually about half of their corresponding one-way SMAs. To produce a two-way effect, it is necessary to induce a special mechanical/thermal treatment in an SMA. One method to produce a two-way effect is based on a severe deformation in the martensitic state. In addition to this, there are still some other methods to produce a TWSME. They are (1) SME training, (2) stress-induced martensite training, (3) combined training, (4) forces of inactive surface layers, etc. [13]

During heating, the specimen will move towards its original shape, and the high-temperature shape gets formed. On cooling again, the pre-existing martensite plates will accommodate the stress field of the induced dislocation structure and preferred martensite variants forms, which give rise to the formation of low-temperature shape. Thus, by temperature cycling, one gets the two-way effect. This method of the production of the two-way effect can be used for training in the NiTi alloys since it displays high ductility.

Researchers began to propose SMA devices to perform dynamic tasks; thus, they began to play the role of actuators [14-15]. Many alloys displaying the SME have been found (see Table.1), and considerable effort is still being made to discover new materials. Of these alloys, however, only two alloy systems¹, Cu-Zn-Al and NiTi, and their combinations with minute quantities of other elements are present of commercial importance. Other alloys are not suitable for industrial

manufacturing either because the constituent elements are too expensive or because they cannot be used unless they are in the form of single crystals [14].

1. Fe based alloys are only used as fasteners and in some other, very simple applications, due to their low price.

1.3 Shape Memory Alloy Actuators:

The use of SMA for actuation represents a technological opportunity for development of innovative thermostatic and electro-mechanical actuators. SMA's can be used in the actuator applications, depending on whether their SME is either one-way or two ways. Although two-way SMA can act in both directions, the associated transformation strain is generally half of that of one-way SMA. An alternate approach is to put two one-way SMA actuators, one against the other, to generate two-way mechanical performance as well. It can be achieved by heating one SMA actuator to get forward motion and another SMA actuator in the reverse direction. The advantage of the one-way actuator is higher motion and higher force than that of the two-way actuator [17]. At the same time, the two-way actuator is simpler, compact and contains less number of elements. The SMA actuators function in three modes as mentioned below (section 1.2).

1.4 Various forms of SMA:

a) Sheet: Generally, bulk SMAs exhibit large strokes and high actuation forces, and at the same time, they suffer from the poor response. However, thin film SMAs provide a larger energy density, higher frequency response and longer life time at the microscopic level. NiTi sheets are the most appropriate material for micro-actuation mechanisms because of their extensive energy density, displacement, work output per unit volume and improved frequency response. At this level, smaller mass and a larger surface to volume ratio enable a significant increase in the heat transfer and low power requirements. Hence, large stresses and strains can be realized. SMA springs are preferred over sheet due to some particular application [16].

b) Spring: Strokes of spring can be increased at the expense of recovery force via heat treatment to form compressed springs in their heat-activated, austenitic state. For that required parameters include wire diameter, spring diameter, transition temperature, number of active turns, bias force and direct current magnitude [17-18].

c) Wires: Regarding fatigue performance, SMA wires were reported to be better than SMA springs, where the recovery force and strain of SMA springs decreased by 30% after 1000 cycles and by 60% after 10,000 cycles [19]. NiTi wire can be changed into the required shape, i.e. spring (helical, torsion), bar, etc. Two NiTi alloy is difficult to join, i.e. weld, both to itself and other materials. Laser welding NiTi to itself is a relatively routine process. More recently, strong joints between NiTi wires and stainless steel wires have been made using nickel filler.

d) Rods: It is also an excellent form of NiTi alloy. NiTi Belleville washers with rod show good potential to form the basis for a Nitinol damping device [20] All these advantages make these NiTi SMA (sheet, spring, wire, rod) a very promising actuator material for micro-device applications such as micro-valves, micro-grippers, micro-mixer, micro-mirror, micro-pumps, micro-cage, micro-robotic, micro-sensors, micro-switch, micro-petitioners and such other applications [21].

1.5 Applications based on shape memory properties:

The nature of shape memory recovery and transformation has been selectively explored for commercial applications. The categorizations fall into the following broad groupings:

There are four commonly used types of applications

a) Free Recovery: These are applications based on the ability of the material to deform in its martensitic state and recover its original shape when heated to temperatures above the transformation temperature thereby recovering the deformation strain. These applications employ thermoelasticity, and notable

applications are in space antenna, eyeglass frames (special eyeglasses which recover deformation in hot water), blood clot filter, self-expanding stents, and atrial septal defect occlusion device used for sealing the hole in heart walls [30]

b) Constrained Recovery: This application employs thermo elastic property, but unlike the free recovery, this application is based on partial recovery. The extent of recovery of the shape memory element is not complete but rather restricted to a particular configuration/dimension, which leads to the build-up of stresses. The stress generated is the key property of interest in the use of these materials. This means when the deformed martensite is heated to austenite the recovery to the pre-deformed shape is halted after a certain percentage recovery and full recovery is not obtained. The predetermined dimension to be attained in a particular application is specified, and the shape memory element is forced to halt its recovery to meet the desired specification. This is used in fastener and couplings (tubes and pipes) for aerospace, marine and orthopedic applications [2].

c) Actuators: This application is based on the thermo elastic property of shape memory alloy. The material acts as a functional element or component of a larger system. The shape memory element senses a situation and acts in accordance to it depending on the system requirement. The SMA element undergoes activation and deactivation of mechanical work in addition to its thermo elastic property when in use. A fire alarm is an example where this can be applied; the activation of the austenite phase would bring about the turning off electrical systems and subsequent fire control measures. Fire safety valves, deep fat fryer, temperature fuses are other relevant applications [3].

d) Super-elasticity: Super-elasticity is the shape memory property that has been most explored for commercial use. Its application is guided by the ability of SMAs to sustain large elastic strains at specific temperatures during use. The storage of a large amount of energy when stress is applied accompanied by constant unloading of this stress is the basis for applications employing this

property [5]. This is seen in eyeglass frames, brassieres underwires, medical tools cellular phone antenna, and orthodontic corrections.

1.6 Application based on the effects of SMA:

1.6.1 Using shape memory effect: The type of applications may be summarised as follows:

a) Coupling: Couplings are the first most successful applications of SMAs, which were developed by Raychem Corp. To hydraulic systems of F-14 Jet Fighters. Electric connectors for IC developed by the same company belong to the same category (Fig 1.2).

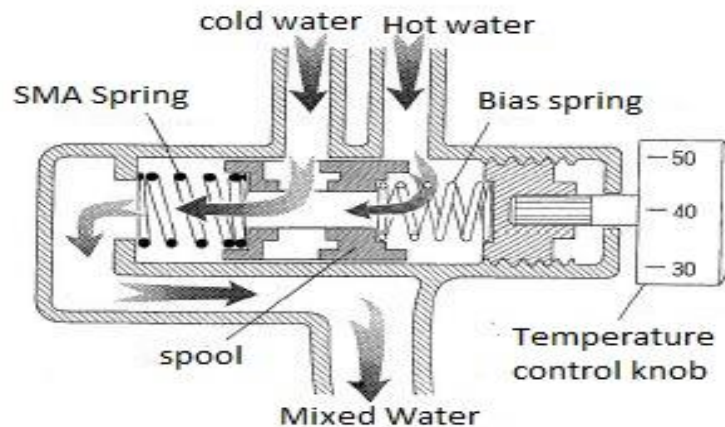


Fig 1.2: The new mixing valve using SMA and biasing coil springs [32]

b) Smart materials: In the previous example, used SMA was as an actuator as well as a sensor. Thus it is also called smart (intelligent) material. The possession of the dual function leads to the miniaturization of actuators, and thin films are expected from this point of view, Another type of smart materials are composites of NiTi SMAs with polymer or metal matrix [22]. The NiTi wires embedded in polymers may be used for vibration control of space vehicles since the elastic constants can be changed widely by changing the temperature in the transformation temperature range The NiTi wires embedded in Al matrix may be used to strengthen Al matrix by the same mechanism of pre-stressed concrete [23].

1.6.2 Using Pseudo-elasticity: Super-elasticity, which is a non-linear pseudo-elasticity as much as 7-8%, was also successfully applied in various fields such as orthodontic, brassieres for women, antennas for cellular phones. Since the super-elastic wire is quite flexible and is not subject to damage. One most important application is to guidewires for catheters in medical use. A catheter, which is a tube made of plastics, is a standard tool for diagnosing the circulatory system by injecting a contrast medium into vessels or for medical treatment by dilating a lumen of the blood vessel at the site of the obstruction [24]. To introduce the catheter in a required place of the vessel in the brain, heart, liver, etc., a guide wire is necessary (Fig. 1.3).



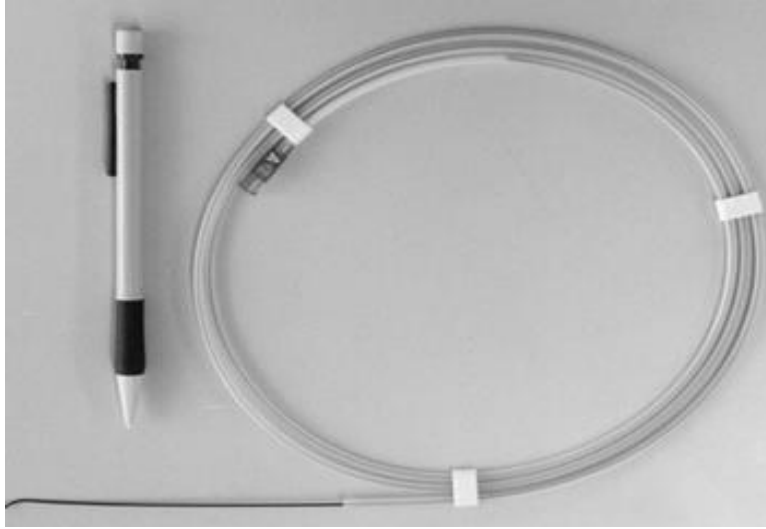


Fig 1.3: Application of Pseudo-elasticity: a) Antenna, for cellular phone, b) Catheter wire used in the brain, c) Appearance of the guide wire, d) Glasses [25]

Various shapes are required by an application such as

a) Sheets: The stress generated by SMA, when the shape recovery is constrained during heating from to, is exploited for fracture treatment by using orthopedic staples [25] or plates. Fig 1.4 shows its application in Micro-gripper and micro pump. Application of NiTi sheets are given below:

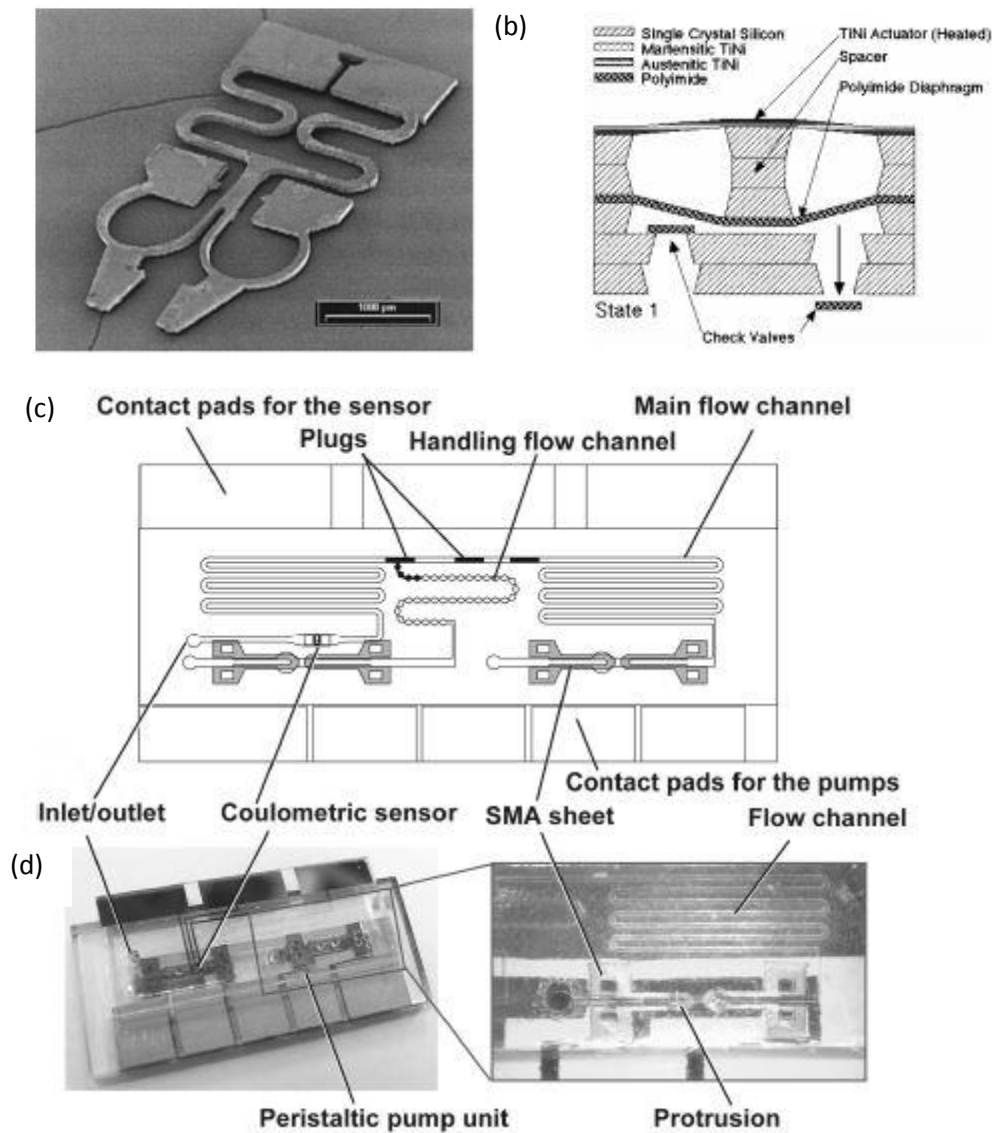
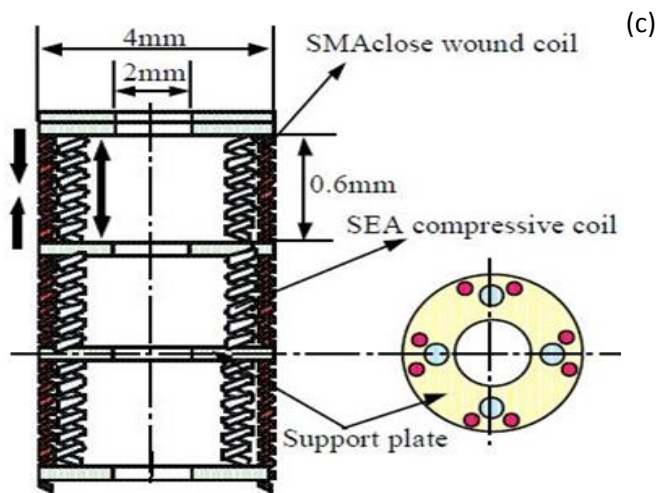
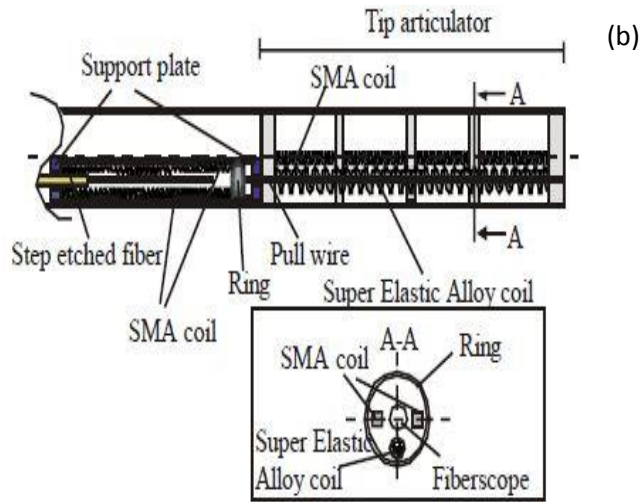
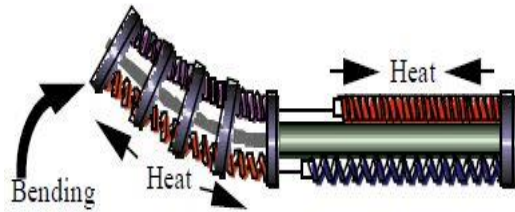
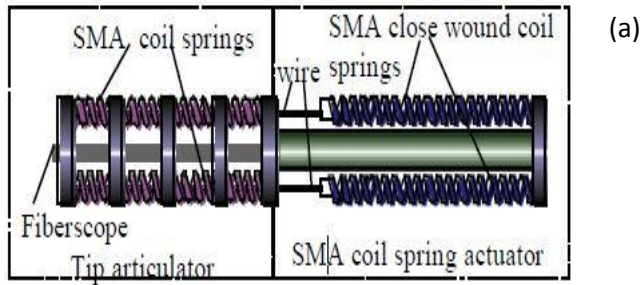
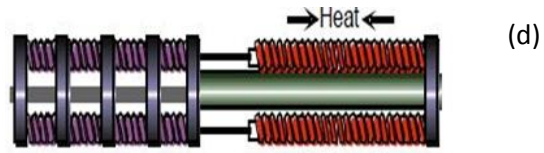


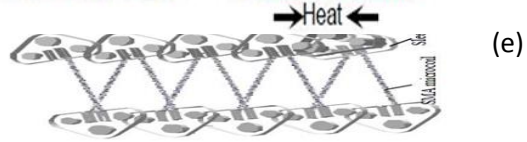
Fig.1.4: SMA sheet Applications: a) Micro gripper [26], b)Micro-Pump [27], c) Peristaltic pump [28]

b) Springs: Most of the proposed actuator designs are based on an SMA spring as the active element, where large macroscopic displacements can be generated out of a relatively small microscopic strain. Example: a) Tip Articulation mechanism, b) Fibre optic articulator, c) Latch Mechanism, d) Tube type tip articulator, e) Joint Mechanism, f) SMA actuator unit, g) Micro-gripper, h) Biomedical applications (Fig 1.5) [26-28].

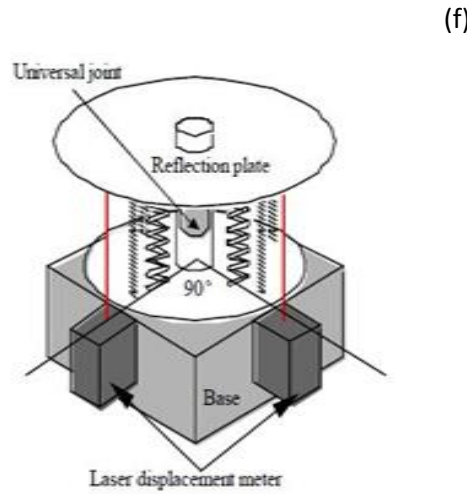




(d)

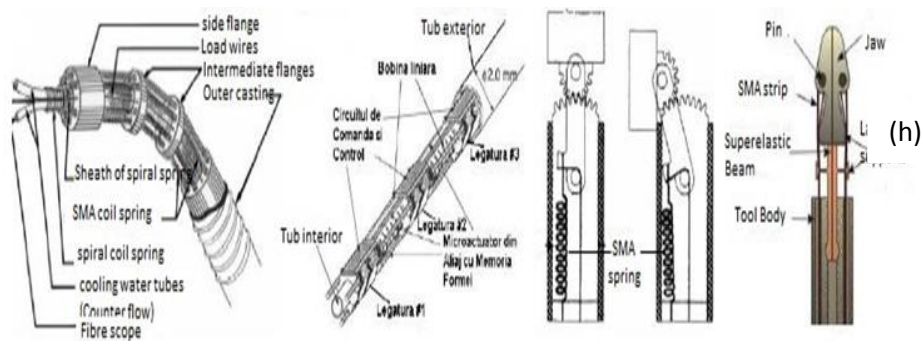
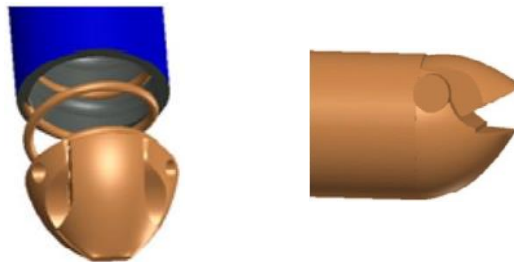


(e)



(f)

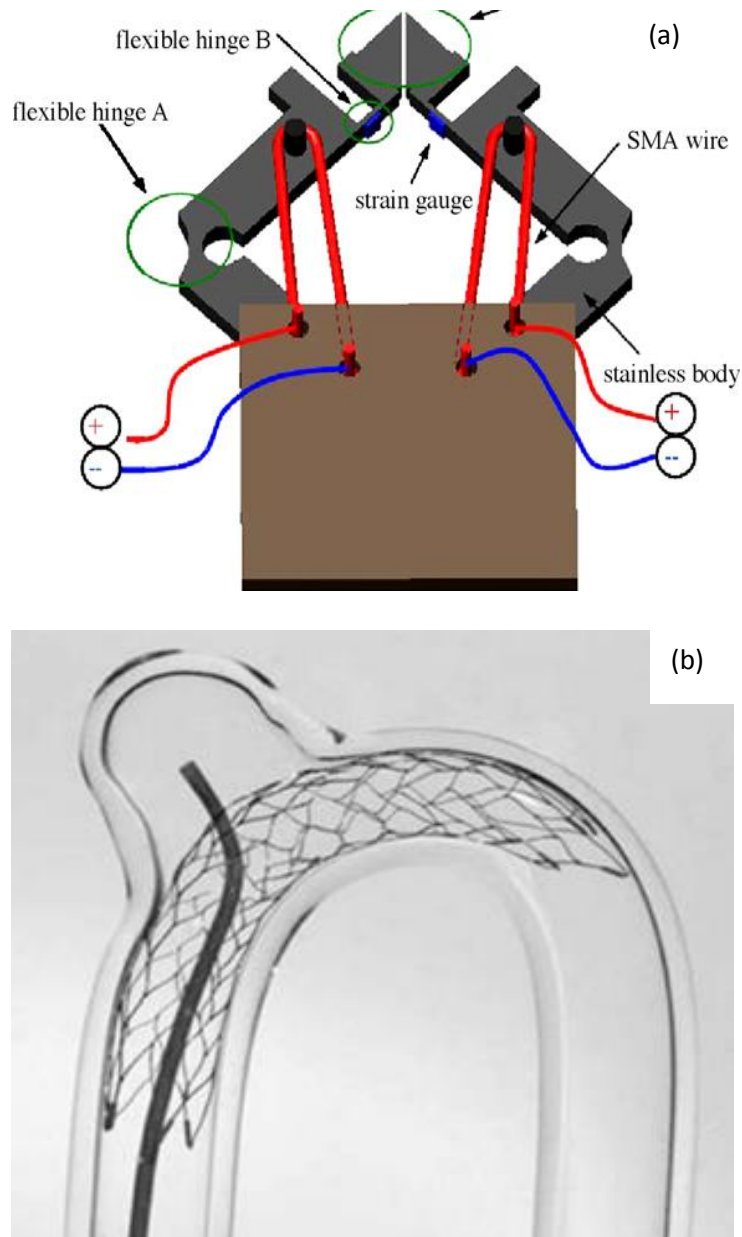
(g)



(h)

Fig.1.5: SMA spring Applications: a) Tip Articulation mechanism, b) Fibre optic articulator, c) Latch Mechanism, d) Tube type tip articulator, e) Joint Mechanism, f) SMA actuator unit, g) Micro-gripper, h) Biomedical applications [5]

c) **Wires:** NiTi wires, which are in the austenitic phase at the temperature of the buccal cavity, have been successfully used for years in fixed orthodontic treatment with multibrackets. NiTi alloys in the neurosurgical field [26] are used for producing three types of devices: (1) coils, (2) stents and (3) micro-guidewires. Applications of SMA wires are given below (Fig. 1.6)



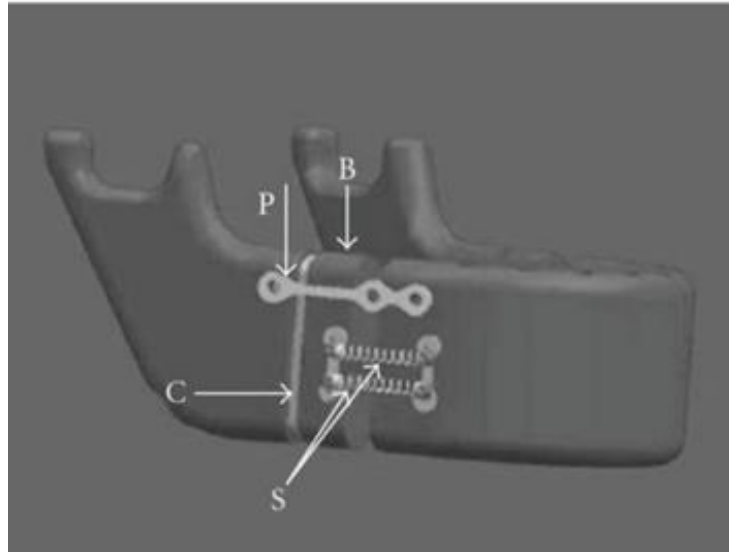


Fig 1.6: SMA wire applications a) Micro-gripper [26] b) Neurosurgical stents c) Orthodontic distracters [25], d) Endodontic file [5]

d) Rods: NiTi rods are also inserted in devices for correcting scoliosis [30-31]. One of the applications of SMA helical springs is a seismic retrofit of buildings (Fig 1.7) [32].

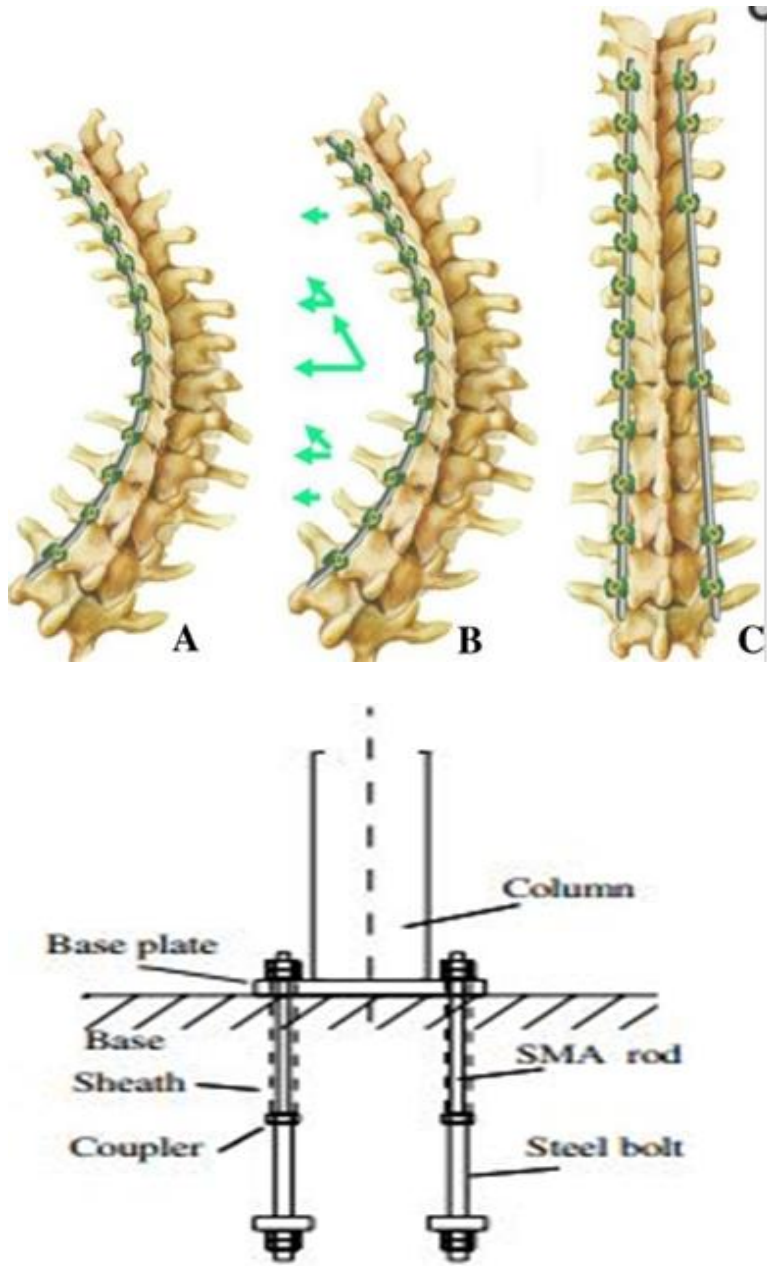


Fig 1.7: SMA rod applications a) bend condition b) maximum bend condition c) straight condition[30-31], d) in building a structure with exposed-type column base with SMA anchorage [32]

1.7 Actuation and Thermomechanical Behavior:

Meaning of actuation is to put into motion by required energy. Some methods have been proposed to reduce the parameters which will help to actuate SMA

such as deactivation time, including forced convection [33], and lagging the SMA with a conductive material in order to manipulate the heat transfer rate.

Based on previous literature, actuation methodologies can be categorised into two types: contact and non-contact. Consequently, SMA actuation is typically asymmetric, with a relatively fast actuation time and a slow de-actuation time. Actuation will lead to thermo-mechanical behavior because of heating and cooling.

1.8 The Need for Thermomechanical Behavior and Life cycle analysis:

Investigation of thermo-mechanical responses are required for the SMA structures, which are subjected to mechanical and thermal cyclic loading. This thermo-mechanical response will lead to investigate its life cycle also. As demanded by the functional architecture, the various environment is required to actuate SMA viz. contact and non-contact.

The thermo-mechanical response is due to the elongation of SMA. SMA actuators typically undergo thermally activated transformation cycles during operation. In most applications, such actuators are employed to overcome a bias force, which could be constant or variable during the course of actuation. Under such conditions, it becomes necessary to understand the thermomechanical transformation fatigue behavior under different applied stress condition. If the thermo-mechanical behavior is estimated in the iterated manner, then it will give life cycle of SMA element.

1.9 Motivation:

Thermo-mechanical behavior in SMA occurs when it is stressed under mechanical cyclic loading. During that process, energy transfer may occur as heat accompanying the deformation. Thermo-mechanical behavior concerning the

coupling of thermal and mechanical effects is evolved. On deformation at low-stress levels, the elastic strain is dominant.

Plenty of applications equipped with SMAs are available but limited work has been reported for the measurement of its thermo-mechanical behavior, and no work is addressed for actuation study under different environment. Thermo-mechanical behavior will lead to its life cycle also. After multiple cycles, it will fail and would not perform its function correctly. Therefore it is required to know the life cycle for predicting its useful life. Above work motivated us to do the thermo-mechanical behavior and life cycle testing of NiTi alloy under different actuation medium. The motivation increased to probe into the development of application in order to improve the quality of the micro-devices.

1.10 Research Gaps:

Shape memory alloys are used in various fields because of the unique properties they possess. Literature review shows some gaps over which work is done here. Listed below are some of the common challenges faced by most of the researchers.

- a)** There are no detail reports on contact based actuation including the electrical and hot water based actuation
- b)** There are very limited reports on non-contact based actuation, particularly laser-based actuation which are of high demand
- c)** Lack of thermomechanical behavior and life cycle analysis of shape memory alloy structures at different actuation conditions are not well explored.
- d)** There is no detailed analysis on morphologies of contact and non-contact based actuation.

Chapter 2

Literature Review on Thermo-mechanical and Actuation Studies of Shape Memory Alloys

To distinctly highlight the contribution of this work and its position in the available work, a systematic review of the literature with emphasis on thermo-mechanical set up for all cases, and their application in MEMS is carried out. Further, the present status of actuation strategies utilized for SMA is discussed in detail. In the end, findings from the literature review and narrow research objectives, approach, and outline of the thesis is presented.

2.1 Introduction:

In this chapter, background information, as well as the state-of-the-art of NiTi SMA research, is presented. This section elaborates the findings from literature reviews of SMA and the effect of the composition by varying its constituent for materials point of view. Section 2.2 provides an overview of past work on SMA's regarding experimental setups design related various methods of actuation for development of test bed. The literature review places more emphasis on research of NiTi SMA Actuators for finding out its thermo-mechanical behavior, rather than the non-actuator applications. The dominance of actuators in the multidisciplinary applications made them an inevitable ingredient of notable innovations. However, the technological progress eventually thrusts the demand of an actuator that is entirely devoted to work specific application.

2.1.1 Overview of NiTi: Since SME was observed in the early 1950s, the engineering importance of SMAs has not been well recognized till the equiatomic NiTi alloys (Nitinol), in 1963 as reported earlier [34]. "Nitinol" derives its name from its chemical components and its finders: Ni (Nickel) + Ti (Titanium) + NOL (Naval Ordinance Lab). During the last three decades, binary NiTi alloys are being intensively investigated to cater functional applications. Recently, NiTi based SMAs are the most commercial SMAs because of their unique shape-memory performance, ease of processing, pseudo-elasticity and have the required mechanical properties [34]. The

unique characteristics of SMA actuators such as one-way shape memory, two-way shape memory, and pseudo elasticity make them suitable for specific applications. The response of SMA actuator depends upon (1) applied bias force, (2) type of sensor used for feedback, (3) way the heat is applied and removed, and (4) parameters used for obtaining the feedback, i.e., strain, resistance, temperature or the actuation force [21-22]. Also, the alloy exhibits excellent corrosion resistance and is also bio-compatible in nature. The NiTi, inter-metallic compound is extraordinary because it has moderate solubility range for the excess of nickel or titanium, as well as with other metallic elements. This solubility allows, alloying possibility with many other elements, to modify both the mechanical and phase transformation properties. These materials have exhibited some exciting application potentials in micro-electro-mechanical systems (MEMS), medical implants, intelligent materials, and structural systems, either in the monolithic form or with combination of other materials. More detailed information about NiTi SMA basic properties is available. A NiTi (nickel-titanium) wire actuator with a diameter of 1 mm, which is a typical SMA actuator, can produce large forces sufficient to lift a mass of 15 kg. NiTi wire can apply a force of 10.6 N. If the wire is 10 cm long it would weigh 11.4 mg and could contract 0.8 cm. Thus, the actuator can lift an object 94,000 times its own weight nearly 1 cm [5]. Particular SMA is chosen in this thesis is Nitinol, due to its commercial availability and unique features. In the present work, it is used in various forms, i.e. sheet, spring, wire, rod, etc.

The SMA transformation can be explained based on thermodynamic testing since it is driven either by the stress or the temperature. The heat interaction between the SMA sample and the surroundings, at a specific temperature, decides the shifting of phase. Differential Scanning Calorimetry (DSC) evaluates the phase transformation temperature. A thermodynamic analysis provides an insight into SMA's unique features such as hysteresis, super-elasticity, one-way effect, two-way effect, etc [35]. Gases can be generally liquefied by a suitable application of pressure or stress.

Similarly, a phase transition from the parent phase to martensite can be induced by the application of a stress. The thermodynamic analysis explains thermal and mechanical effects on the SME. Thermodynamics is an excellent

tool to perform calculations on the thermal implications of the stress-induced phase transition. It also explains the reversibility of the phase transition in certain SMAs and highlights energy contributions that control the hysteresis phenomenon [36].

Gibbs theory of thermodynamic stability helps to explain the phase transition, when an alloy system is considered to be under equilibrium condition. Gibbs theory is suitable only for equilibrium condition. A martensitic transformation can be considered to be a succession of several equilibrium states [37]. The martensitic transformation is a solid state transformation. The thermodynamic analysis based on internal variables (latent heat of the phase transformation, enthalpy and entropy) can be applied for a single crystal of SMA. The classical Clausius-Clayperon equation can be derived as it relates to stress and temperature. The analysis can be conducted for a single crystal of SMA because it facilitates the investigation of the SMA specimen as a thermodynamic system with only one component.

The complete martensitic transformation cycle of SMA is characterized by the following temperatures: a) Austenite Start (A_s), b) Austenite Finish (A_f), c) Martensite Start (M_s), d) Martensite Finish (M_f). As shown in Fig2.1 the heating process of NiTi, evolves into austenite when the temperature reaches (A_s) and completes the transformation process when it reaches A_f . While the cooling process, martensite at (M_s) and finishes at M_f . The difference between the transition temperatures is called hysteresis.

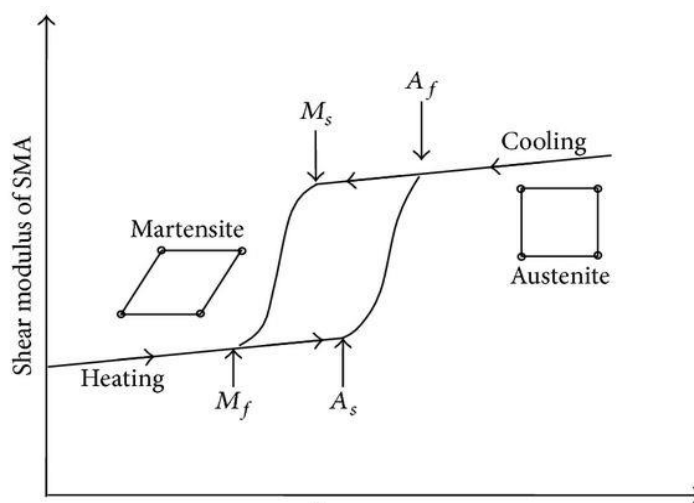


Fig 2.1: Shear modulus vs. temperature considering the chemical and non-chemical contributions [38]

This property is important and requires careful consideration during SMA material selection for targeted technical applications; e.g., a small hysteresis is required for fast actuation applications (such as MEMSs and robotics), larger hysteresis is required to retain the predefined shape within a large temperature range (such as in deployable structures and pipe joining) [38]. These characteristic temperatures are in the order of $M_f < M_s < A_s < A_f$. The mentioned above relation is temperature induced stress.

Martensitic transformations can also be stress induced it occurs at constant temperature, moderately above the austenite finish temperature leading to superelasticity to form stress-induced transformation. Temperature-induced transformations involve the deformation at low-temperature phase (martensite phase).

2.1.2 Mechanism behind NiTi SMA: Behind the shape memory effect, two important mechanisms play an important role in that which are: Slip and twinning. It results in affecting their pseudo-elasticity and shape memory performance.

a) Dislocation slip: A similar stress vs. temperature correlation is experimentally observed [39] for determination of dislocation slip stress in austenite SMAs (Fig 2.2). The critical stress for martensitic transformation increases with temperature above A_f and the critical stress for dislocation slip of austenite decreases with temperature.

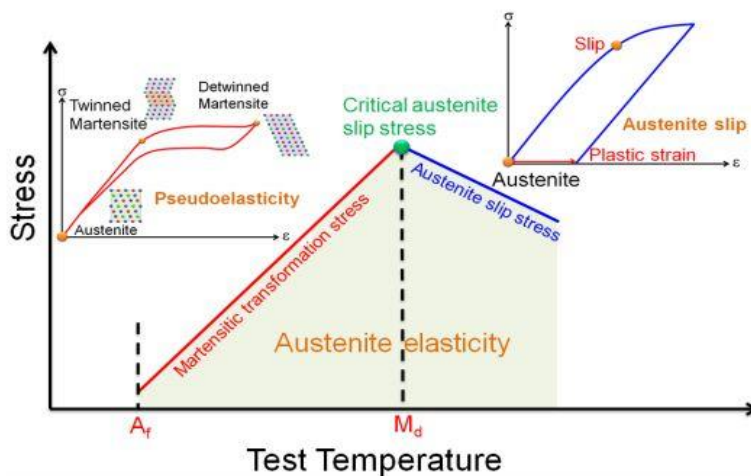


Fig 2.2 Schematic of critical stress vs. temperature for SMAs. [39]

- The critical stress represents the stress-induced martensitic transformation below temperature M_d (red straight line) and the dislocation slip of the austenite phase above M_d (blue straight line). A_f is the austenite finish temperature, and the M_d is the temperature above which the martensite cannot form under deformation [40]

When these two values cross at the deformation temperature M_d , the stress-induced martensitic transformation is no longer possible, but only the dislocation slip of austenite (Fig 2.3). The critical austenite slip stress at M_d is considered as the experimental data for austenite slip [41].

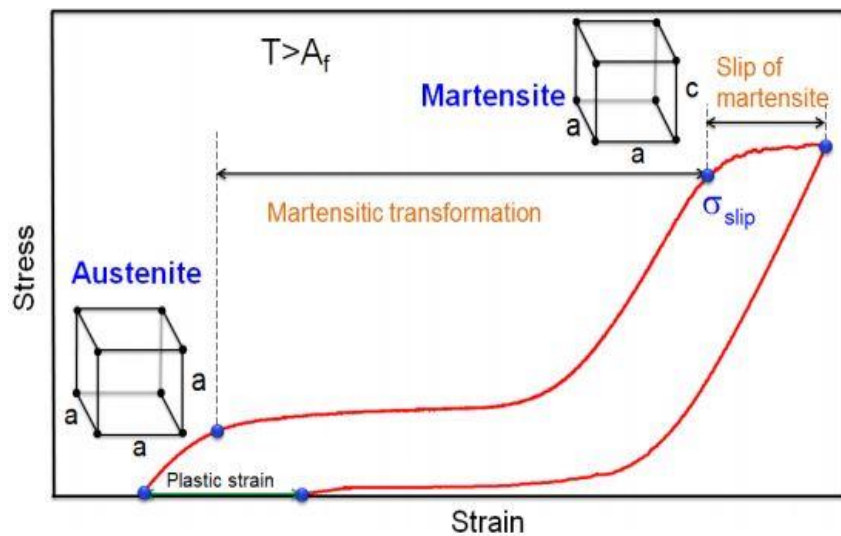


Fig 2.3 Schematic of determination of dislocation slip stress in martensite SMA's [41]

Temperature above austenite finish temperature A_f , the material is fully austenitic. After elastic deformation of the austenite, a stress-induced martensitic transformation occurs. When the critical stress, σ_{slip} , for martensite yield is reached, slip of oriented martensite is observed. Upon unloading, the martensitic single crystal undergoes elastic deformation followed by pseudo-elastic behavior and reverse martensite to austenite transformation occurs.

b) Twinning: Twinning in SMAs is of paramount importance, which exists in two main characteristics of SMAs. A schematic of the SME is shown in Fig 2.4. In the first case, when the alloy in the austenitic state is cooled below the martensite finish temperature with no external stress, the internally twinned martensite is formed. If the twinned martensite is subsequently deformed, the

twin variants that are oriented favourably to the external stress grow in expense of others. The growth of the twin is a process of advancement of twin interfaces and requires overcoming an energy barrier called the 'unstable twin fault energy'. Upon further deformation, the internally twinned martensite detwins completely into a single martensite crystal. After unloading, the twinning-induced deformation remains. If the material is heated over the austenite finish temperature, then martensite to austenite transformation occurs and the material reverts back to austenite. Hence, the heating and cooling changes can make the material behave as an actuator, which is called 'shape memory effect (SME) [42-44].

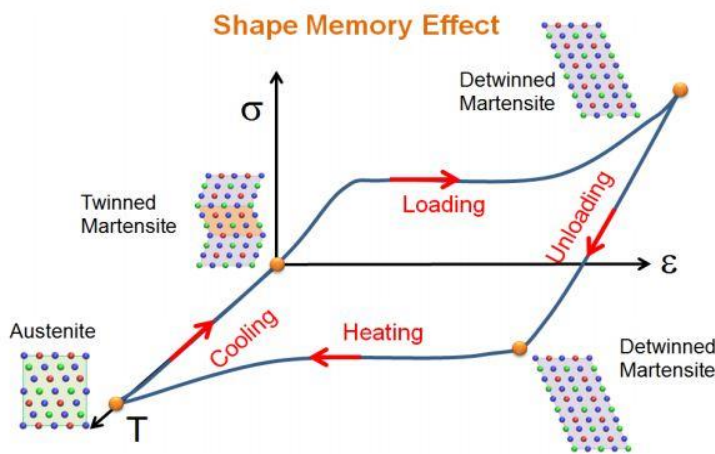


Fig 2.4 Schematic of SME in SMAs [43]

Therefore, the phenomenon of twinning or de-twinning either during shape memory or during pseudo-elasticity relies on the atomic movements in the martensitic crystal. It influences the recoverability, the transformation stress levels, hence both the SME/PE response. For shape memory, the martensite is deformed first and then heated to the austenitic phase for full recovery. Martensite undergoes twinning during deformation at relatively low stress levels. If slip occurs during martensite deformation, this would curtail full recoverability. On the other hand, during pseudo-elasticity, austenite transformation to martensite takes place upon loading [45]. If slip resistance is low, then austenite and martensite domains can deform plastically inhibiting full recoverability upon unloading. Despite the significant importance of twinning in SMAs, there has been no attempt to develop models to predict

their twinning mechanism. Thus, a fundamental understanding of twin nucleation is essential to capture the mechanical response of SMAs.

2.1.3 Equiatomic NiTi: Thermo-mechanical cycling was carried out to study the change of functional properties of the material in using condition (shape memory fatigue or functional fatigue). Near equiatomic NiTi alloys are the most promising SMA in terms of practical applicability. In this alloys, shape memory effect and super-elasticity are due to thermo-elastic martensitic transformation from parent austenite phase with B2 structure to the monoclinic (M) or rhombohedral (R) martensitic phase transformation. [46]. Phase diagrams are very important in studying different alloy systems, composition and temperature dependent phases, and control of the microstructure [47]. Physical properties of materials are strongly correlated with compositions and phases. Equiatomic NiTi (50 atomic% Ni, 50 atomic% Ti) SMA is an ordered intermetallic compound [48]. Fig 2.3 shows the determination of dislocation slip stress in martensite SMAs. At the temperature above austenite finish temperature A_f , the material is fully austenitic. After elastic deformation of the austenite, a stress-induced martensitic transformation occurs. When the critical stress, σ_{slip} , for martensite yield is reached, slip of oriented martensite is observed. Upon unloading, the martensitic single crystal undergoes elastic deformation followed by Pseudo-elastic behavior and reverse martensite to austenite transformation occurs.

Table 2.1 Different phases of equiatomic NiTi SMA, crystal system, lattice parameters, and interaxial angles [49]

NiTi	Crystal System	Lattice Parameters	Interaxial angles
Austenite	B2, ordered BCC	$a = b = c$	$\alpha = \beta = \gamma$
Martensite (M)	Monoclinic	$a \neq b \neq c$	$\alpha = \gamma \neq \beta$
Martensite (R)	Rhombohedra	$a = b = c$	$\alpha = \beta = \gamma \neq 90^\circ$

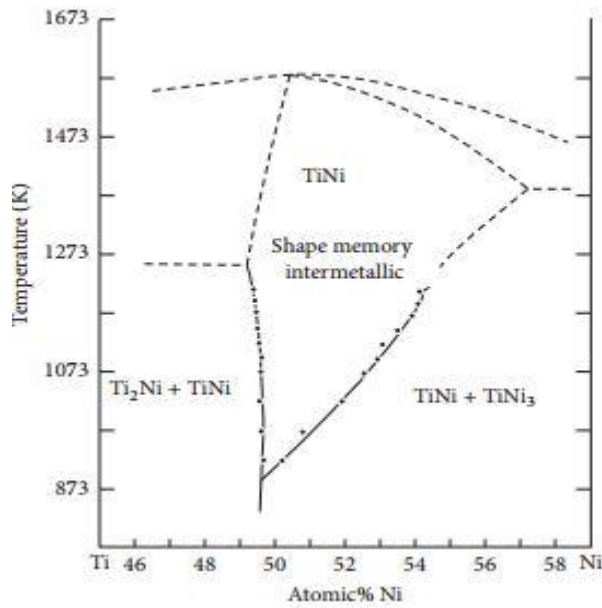


Fig 2.5: Partial phase diagram of NiTi from 45% nickel to 59% [50]

Partial phase diagram of NiTi system is given in Fig 2.5 [50]. B2 phase region is known to be very narrow at temperature below 923 K. It is generally accepted that B2 phase region is only between 50 and 50.5 atomic% nickel. If nickel content is higher than 50.5 atomic%, then the alloy will decompose during cooling below 973 K to Ti-Ni and TiNi₃. Ti₃Ni₄ and Ti₂Ni₃ are intermediate phases formed during transformation. The central part of Fig 2.4 where NiTi transforms to monoclinic B19' martensitic phase is important. For the titanium rich side, equilibrium phase is Ti₂Ni and TiNi. Table 2.1 shows different phases of equiatomic NiTi SMA, crystal system, lattice parameters, and inter axial angles [49]. If NiTi alloy is constrained to shape change upon phase transformation, then 700 MPa stresses can be generated, which are too much as compared to shape memory polymers where the amount of stress is much smaller. Due to the possibility of large recoverable strain of about 8% without force generation and 700 MPa stress without recoverable strain, there is a high possibility to use NiTi SMA for the design of components with different strain outputs and different amounts of external work output [50].

2.2 Thermomechanical behavior and Life cycle of SMA:

SMA can undergo a large number of repeated thermal mechanical actuation cycles [51-58]. Existing work on fatigue of SMAs predominantly focuses on high cycle, and low cycle fatigue performed using cyclic mechanical loading either to constant stress [59-60] or a constant strain amplitude [61-63]. Under mechanical cycling to a constant strain amplitude of 10–11% (inducing complete transformation), NiTi has shown a fatigue life of 10^3 – 10^4 cycles under electric actuation. As the constant strain amplitude is decreased from 10%, the fatigue life of the SMA increases and for strain amplitudes less than 1%, the fatigue life exceeds 10^7 cycles [64-66]. Other parameters influencing the fatigue behavior of SMAs have found to be: stress amplitude [66-68], complete or partial transformation [70], alloy composition [71-72], heat treatment [73-74], the environment of testing [75] and surface finish of specimens [76]. Experimental setups for all actuation mediums have been reviewed:

2.2.1 Joule Heating or Electrical Actuation: The thermo-electric behavior of SMA sheet/spring/wire were presented. When the Sheet/spring/wire was electrically heated above its transformation temperature by the current, a large mechanical force is exerted due to transformation in its phases.

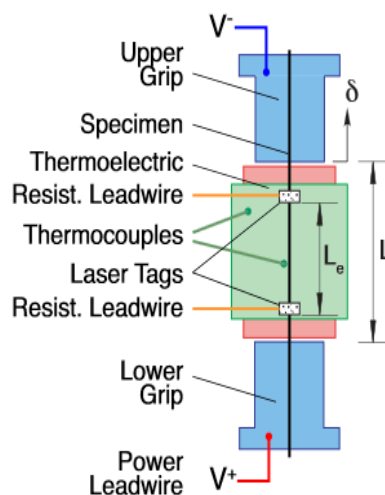


Fig 2.6 Wire Tension experimental setup University of Michigan, Department of Aerospace Engineering, (2008) [77]

Few research groups have developed test rig for specific applications. Fig 2.6 shows the SMA wire tension experimental setup to investigate the thermo-mechanical behavior of the conditioned SMA wire [77]. The SMA wire was clamped to a 100 N load cell. The heating cycle was obtained using an electrical resistive heating and natural convection was used for cooling to generate thermo-mechanical cycle. The thermo-mechanical behavior was imaged using a low power laser. The major limitations of this setup are 1) restricted to wire 2) variable load cannot applied.

Fig 2.7 shows setup to investigate the thermo-mechanical cycle on SMA wire, the thermo-mechanical cycling has been performed through the transformation range under a constant or fluctuation load [78].

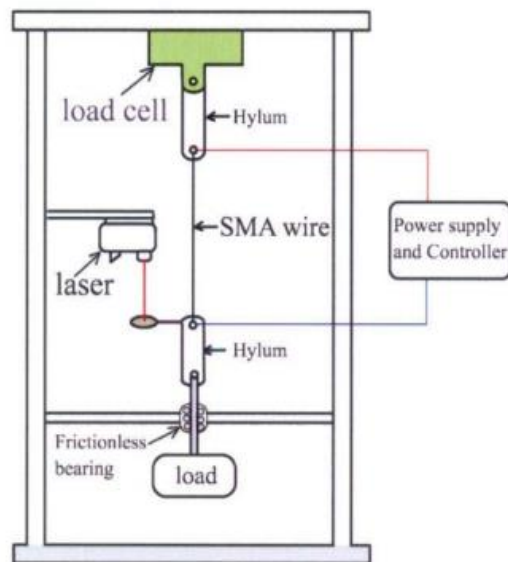


Fig 2.7. Thermo-mechanical cycling setup, Material Science Division, National Aerospace Lab, Bangalore (2009) [78]

The cycles were performed by resistive heating and forced cooling. The Displacement of the wire during thermo mechanical cycle was monitored using non-contact laser device which has a resolution of 10 μ m. The recovery strain (RS) and the remnant deformation (RD) were recorded continuously throughout the experiment. However monitoring the true strain is limited with laser displacement sensor.

Fig 2.8 shows the set up developed to investigate the fatigue in SMA wired. The wire is attached to a rigid clamp [79]. The lower end of the SMA wire is

constrained which is heated through an electrical resistance and the fan maintains a constant air flow across the wire. The equipment has compatibility to apply constant stress, constant strain, constant stress with limited maximum strain and linear stress-strain cycle. However, the system is limited to measure the engineering strain, and there is no provision to acquire the data for every cycle. In the previous setup, forced convection was applied through cooling fan.

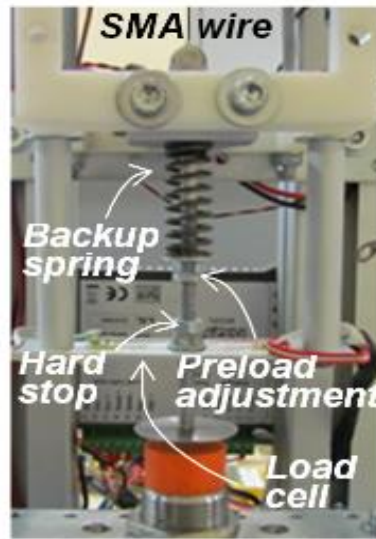


Fig 2.8: Experimental setup for fatigue life cycle analysis of the SMA wire [79]

In the setup shown in Fig 2.9, the forced convection is adopted by passing a chilled fluid, thus inducing a martensite transformation in the system and the wire is actuated through electrical biasing [80].

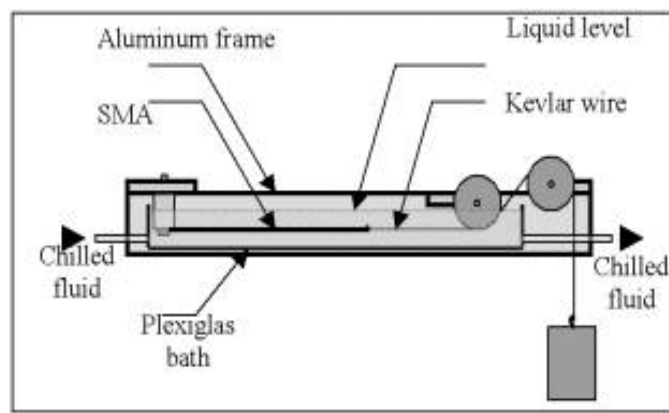


Fig 2.9: Fatigue cycle simulator for SMA wire using liquid cooling Smart Lab [80]

In the given set up an experimental-numerical approach is used to study the thermo-mechanical behavior of NiTi wire for defining what parameters are the most important in actuator designing [80- 81]. Tests were carried out heating, by an electrical current, a wire having a diameter of 150 μ m, under constant stresses of 200 MPa. Data concerning strain, applied current and voltage are acquired during the tests by PC while wire temperature is recorded by thermographic system. Experimental tests were carried out heating the wire by electrical power and current, voltage, strain and wire temperature were acquired simultaneously [81].

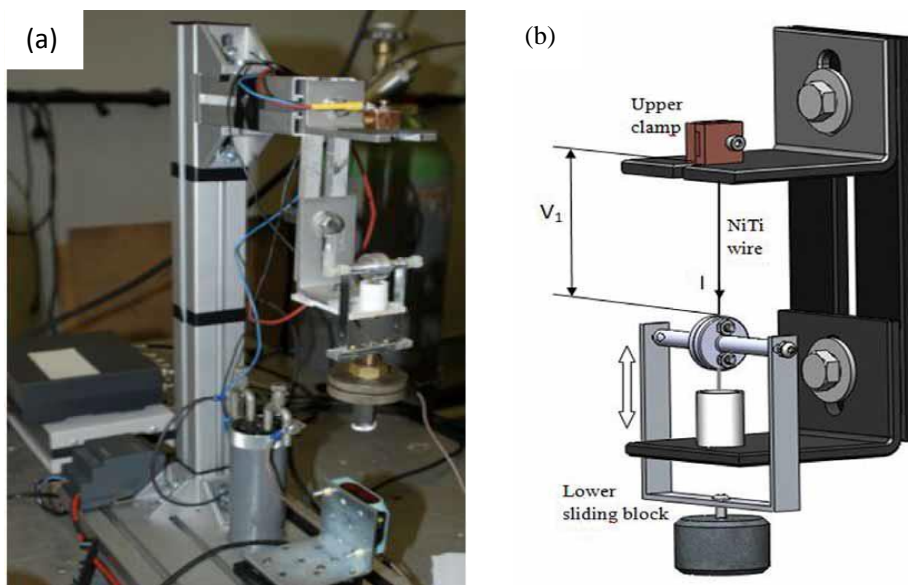


Fig. 2.10: a) Self-Assembled Cycling Machine b) Wire clamping system [81]

To evaluate the cycling behavior of SMA wires in a range of 20-200 μ m in diameter, as well as the fatigue resistance of the material and its functional characteristics, a self-assembly system was designed and realized (Fig 2.10 a). The wire was vertically arranged and was constrained to the system structure through an upper clamp and to induce constant stress into the material, an axial weight was coupled to a lower vertical sliding block, directly hanged by the NiTi wire (Fig 2.10 b) [81].

Fig 2.11 shows a basic setup to investigate the thermo-mechanical behavior of the SMA spring. The actuation is performed by electrical resistive heating, followed by natural cooling cycles in a fully automatic manner [82].

The system consists of a relay circuit actuated by a Transistor-transistor logic (TTL) signal coming from a function generator. A metallic base with a ceramic guide fixed inside has been adopted for the characterization of the cyclic experiments of the spring. However the major limitation in this setup is the lack of online monitoring and the experiments are performed for the complete elongation of the springs and cannot be opted for small displacement.

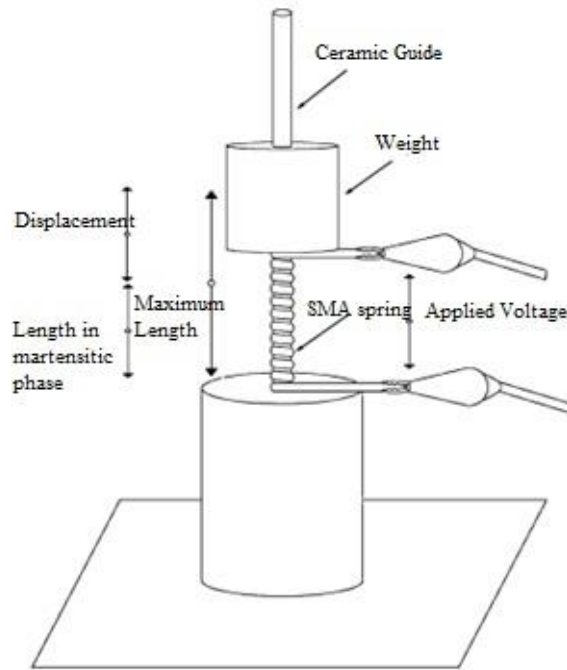


Fig 2.11. Thermo-mechanical Characterization of SMA spring Mechanical Engineering Department, University of Rome, Italy (2010) [82]

Furthermore, the work reported on SMA reliability or life estimation is scarce. The work done by previous researcher group show the degradation of the SMA material properties with thermo-mechanical cycling and found to be unstable. In each of the work during cycling strain or/and stress responses were measured and it was observed that with the number of cycles SMA behavior was unstable. During initial cycles, the rate of increase in the plastic deformation was found to be very high in comparison of at higher cycles.

The all reported work does not define any cause and effect relationship to represent the spring failure. The rate of increase or decrease in the strain or stress value is the effect produced because of various causes such as voltage, the external load applied and stiffness. The reported work just showed how the effect behaves with the life of the spring. However, for the same effect the

different life of the SMA material can be obtained, and consequently, it depends on the causes of the spring failure. Also, [82] defined the relationship between the strain and the life of the spring by plotting all the failure data on a log plot. The relationship was totally deterministic, but real life data always associated with some uncertainty and have some probabilistic distribution because for same strain or stress value SMAs can have a different life.

One another attempt made by [83-84] to calculate the life of the SMA wire. Resistivity based mathematical model is developed to calculate the remaining useful life of the SMA wire. Reduction in the life of the wire is observed with increase in the difference between the minimum and maximum resistivity after attaining the austenite transformation. However the developed mathematical model depends only on a single parameter, i.e., resistivity. However, there are always some additional parameters on which the health of the component is dependent, i.e., operating and environmental conditions. As a component operating in the harsher environment will fail early in comparison of component operating in the milder environment. Therefore additional parameters should be included in the model to get the accurate life prediction. Most of the test rigs are limited to investigate the behavior of the SMA wire; very fewer reports on SMA springs are available. For precise measurement of displacement, the interferometer is also investigated. On the usage of Michelson's interferometer with continuous monitoring of true strain for every cycle can be monitored, which is discussed in chapter 3.

2.2.2 Hot Fluid Actuation: The application of SMAs in a hot water supply system is described in this section. A faucet with a water temperature regulator is one of the most important applications of SMA. The combination of an SMA spring that expands or contracts automatically by water temperature and a bias spring operated by a water temperature control knob manually can achieve a comfortable water temperature by the precise adjustment of the hot and cold water mixture. Other applications such as bathtub adaptors for adding water and for holding water temperature are also described.

a) Shower faucet with water temperature regulator: A water temperature regulator for a shower faucet is one of the most well-known applications of SMAs. Fig 2.12 (a) shows an example of a regulator containing an SMA

spring and the schematic illustration is shown in Fig. 2.12 (b). The regulator is composed of the following elements: (1) hot water and cold water inlets, (2) a shape memory spring and a bias spring which is made of stainless steel, (3) a flow control regulator valve for hot water and cold water and (4) a knob for temperature adjustment.

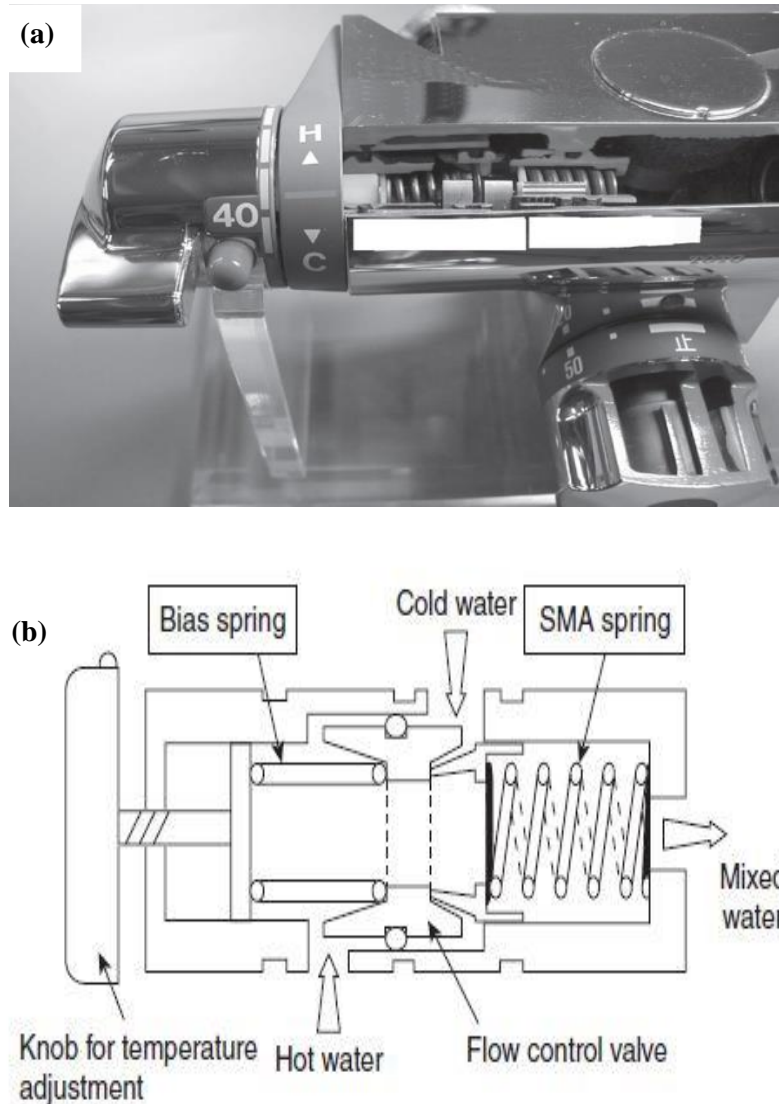


Fig. 2.12: Shower faucet with water a) Regulator containing an SMA spring, b) Schematic diagram of regulator [85]

When the outlet water temperature is higher than the set temperature, the SMA spring expands due to the reverse transformation so that the inlet valve for hot water closes and the inlet valve for cold water opens. As a result, the temperature of the mixed water decreases. On the other hand, when the outlet

water temperature is lower than the set temperature, the SMA spring shrinks to open the valve for hot water and to close the valve for cold water, resulting in an increase in the outlet water temperature. The middle of the R-phase transformation temperature and the reverse transformation temperature of the SMA spring is about 40 °C and then the spring moves to control water flow in proportion to the difference between the set temperature and the outlet water temperature. The SMA spring and bias spring are set out so that they work in opposition other than in the regulator. If the temperature becomes 50 °C, the balancing position shifts to point B. The bias force increases and then force is applied to the flow control valve to move exact distance, resulting in the decrease of the mixed water temperature. When the set temperature is changed to 50 °C, the bias spring is compressed and also the bias force increases, resulting in the stroke moving to particular displacement which corresponds to the amount of adjustment of the knob. As a result, the balancing position moves to required distance [85].

b) Gas flow shielding device: There is a potential for gas leakage due to melting of the gas meter when fire occurs because the gas meter and joining parts are made of die-cast aluminum. This concern for gas leakage has led to the development of a gas flow shielding device operated by a thermal sensor that uses a SMA to cut the gas flow.



Fig 2.13: Gas flow shielding device with a SMA disk [85]

As shown in Fig.2.13, a thin circular SMA disk, which is bent at room temperature, is set in the gas flow path. If fire occurs, the atmosphere temperature rises above 70–80 °C and the SMA disk becomes flat. There is a ring under the valve to fix the SMA disk in the gas flow path. A rod axis is installed at the upper side of the bent SMA disk as shown in Fig 2.14 in order to smooth the flow of gas during ordinary use. [85]

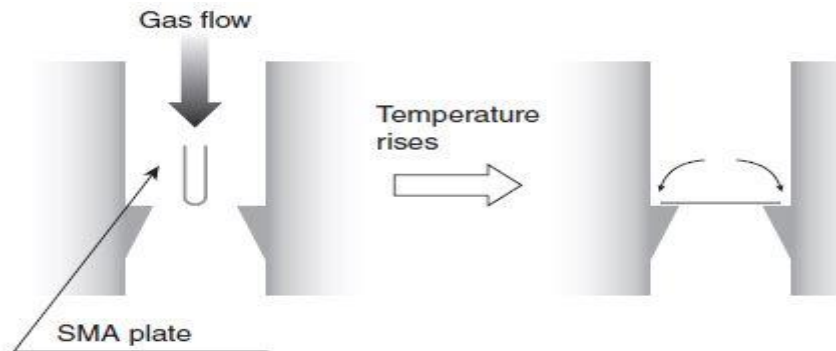


Fig 2.14: Operating principle of gas flow shielding device [85]

c) **Bathtub adaptors:** SMA springs are also equipped in hot water safety valves for shower faucets and a bathtub adaptor for maintaining water temperature. The hot water safety valve for the shower faucet for preventing scalding is set at the connecting part to the boiler as shown in Fig 2.15 (a). Fig 2.15 (b) illustrates the operating mechanism of the thermal protection valve by the combination of the SMA and biased spring.

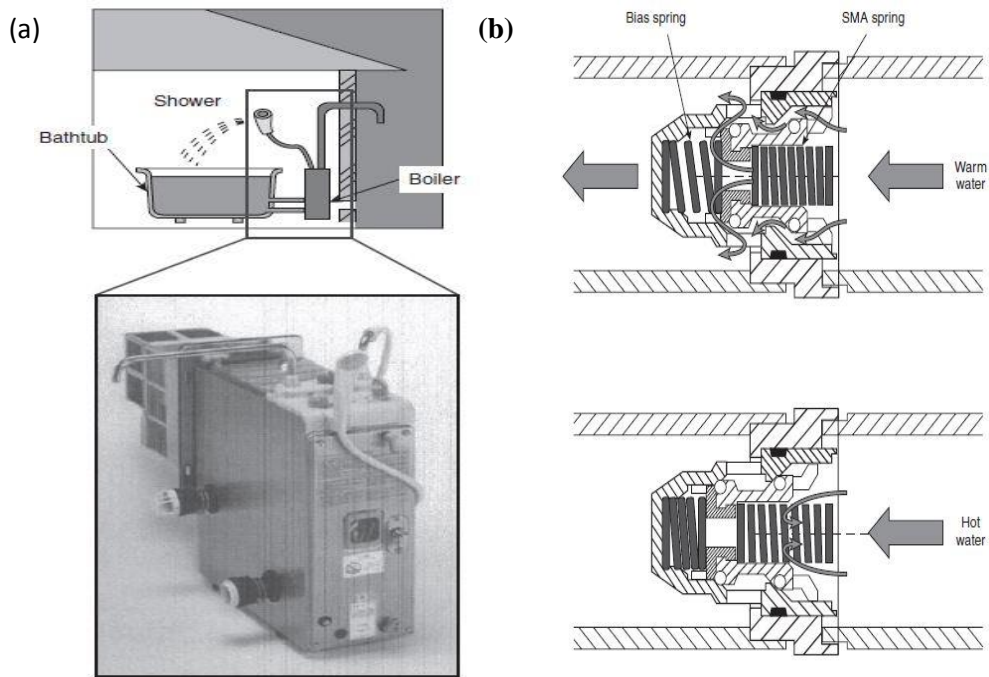


Fig 2.15 a) Boiler with SMA hot water safety valve b) Operating principle of hot water safety valves in bath [85]

When hot water flows through a SMA spring, the SMA spring expands to close the valve because the recovery force overcomes the bias spring force. The SMA springs are also applied to bathtub adaptors for adding hot water safely. Two hot water safety valves are set in the outlet of the bath as shown in Figs. 2.16 (a) and (b). The reverse transformation of the SMA spring is about 70 °C so that the SMA springs contract to close the valves when the hot water is higher than 70 °C. Both SMA valves cut hot water when the bathtub is not filled enough. On the other hand, only the upper spring operates if the bath is filled with hot water because the lower valve is cooled by water in the bath. This means hot water can be added safely in the bathtub. Another example is the cut-off valve for circulation of hot water in the tub. The valve is set in the outlet of the boiler and prevents the circulation of hot water in order to hold water temperature in the bath as shown in Figs. 2.17 and 2.18 [85].

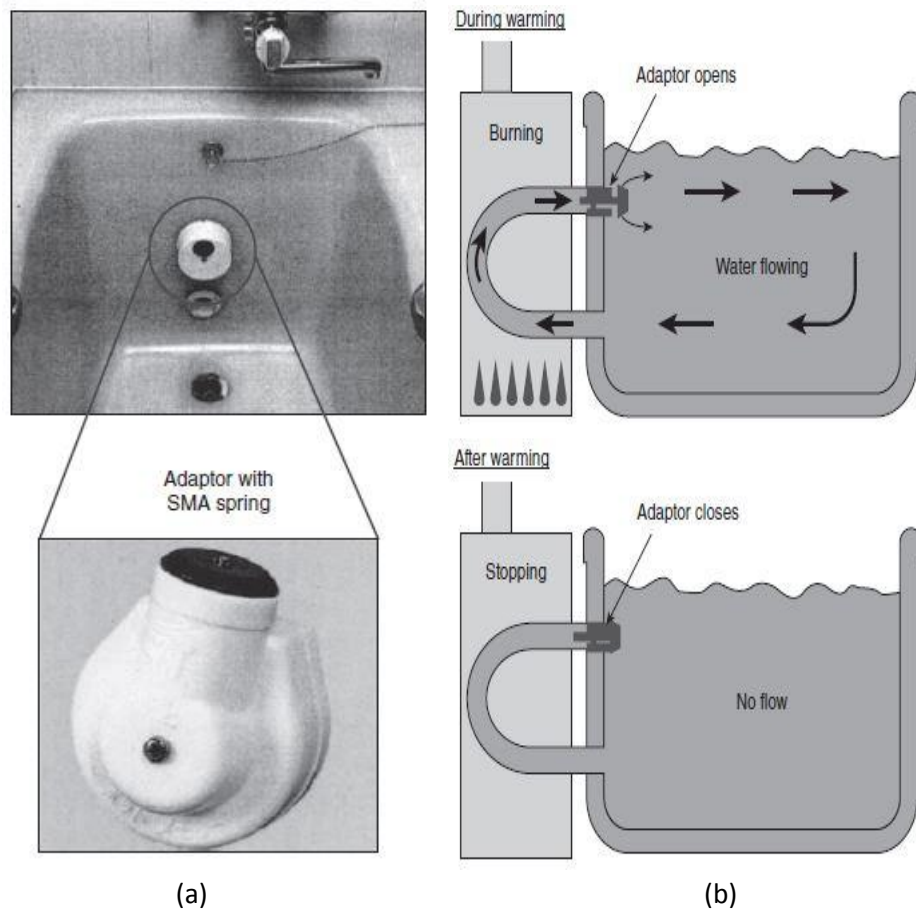


Fig 2.16 a) Hot water safety valves in outlet of bath, b) Operating principle of hot water safety valves in bath [85]

All applications which are mentioned above are of hot water-actuated, but there is no any experimental set up to describe SMAs reliability, so one novel set up is designed for evaluating SMAs reliability, and its application is also fabricated, which is discussed in chapter 4.

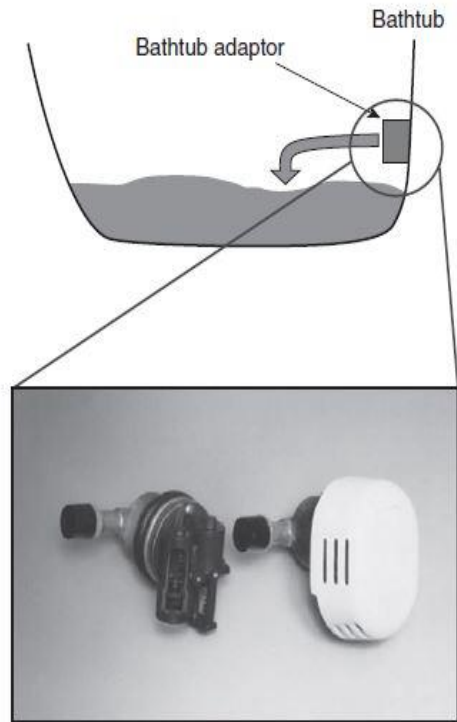


Fig. 2.17: Bath Tub Adaptors [85]

Authors Studied a wet SMA actuator consists of SMA wire enveloped in fluid that is contained within a compliant tube [86-87]. This compliance allows for the actuator to expand and contract with minimal spring resistance.

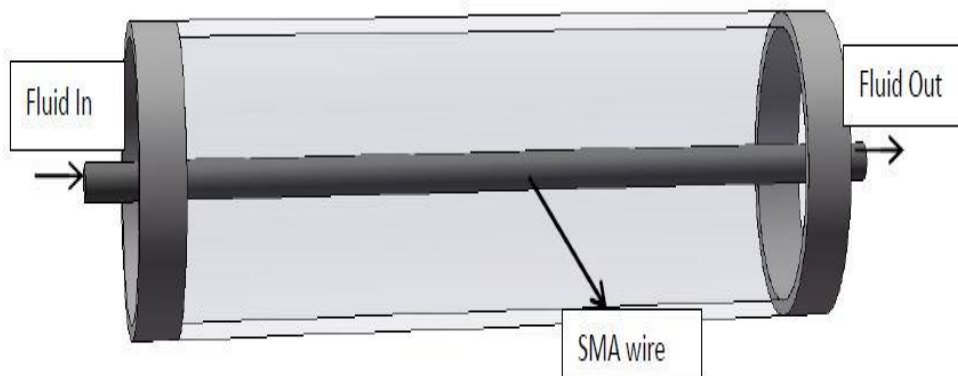


Fig. 2.18: Wet SMA actuator design [86]

The fluid inlet of the actuator is connected to a terminal that is supplied with hot or cold fluids, and the outlet is connected to a terminal that dumps the used fluid into a lower pressure reservoir (Fig 2.18). Entire wet SMA actuator arrays have been used to control hand and finger movement and could be used to control other high degree-of-freedom mechanisms as well.

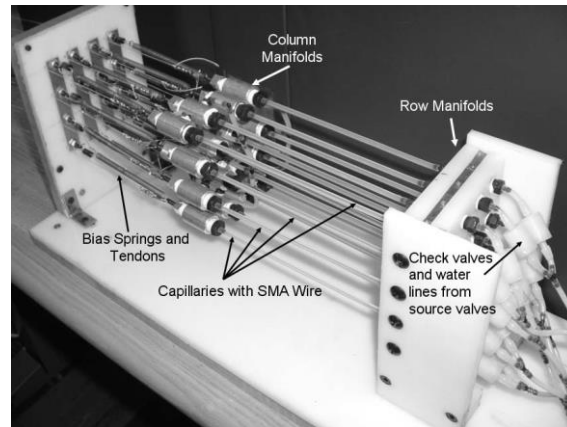


Fig. 2.19: Wet SMA actuator array [87]

The initial prototype contains a 4x4 array of 16 actuators controlled by ten solenoid valves, where 25% of the actuators can be activated at any one time (Fig 2.19). Since only a subset of the actuators can be activated at any time, various methods of scheduling the resources (i.e., valves) are investigated [88], as well as various ways to define the error or difference between the desired and actual states of the array.

2.2.3 Laser Assisted Actuation: The super-elasticity and shape memory properties of NiTi alloy make it a potential material for new biomedical applications. Laser surface treatment is used to improve the corrosion resistance of NiTi SMA Plates. Potentio-dynamic tests in physiological Hank's solution show that the laser treatment performed in air improved all corrosion parameters [89]. The surface is homogenized, and a Scanning Electron Microscopy SEM observation indicates a decrease of corrosion pit size and numbers. First, Castleman and Motzkin [90] widely studied Nitinol biocompatibility and found that titanium could be considered as a physiologically stable material, while nickel is involved in the allergic process and toxicity if present in high amount. The mechanical properties of NiTi

SMA components are sensitive to thermal influence during laser machining. Thermal effects, associated with the use of a laser beam as a source of heat during laser machining, are one of the most important and studied aspects, because they are strongly able to affect the quality of the obtained result. These effects can be amplified when temperature sensitive materials, such as SMAs, are processed using laser technology [91]. Several authors proposed an optimization of the cut edge quality regarding kerf geometry, spatter, HAZ extent, and roughness using Nd: YAG laser [91]. This laser is significantly appreciated because of its obvious advantages, such as high beam quality, good focus-ability, high productivity, and reliability. Laser machining is the most exploited fabrication process used to shaped micro SMA elements [92-97]. Nd: YAG lasers are widely used in micromachining, including the manufacturing of vascular stents [98]. Yung et al. [96] described the Nd: YAG laser cutting of thin NiTi sheets (thickness: 350 μm) for MEMS applications. Unfortunately, this technology produces some surface defects (oxides and melted materials) that compromise the final functional properties of the SMA active element. There are many methods to weld, machine and cut the NiTi. Fibre laser cutting is emerging as a competitive process with higher beam quality, reliability and process efficiency. To evaluate the cutting quality between pulsed Nd: YAG lasers and fibre lasers, comparative experiments were conducted by Ahmed et al. [97] and Meng et al. [99]. In previous work, fibre laser is used for Machining of SMA, but for getting thermo-mechanical behavior, no set up is available. For this, Pulsed Nd—YAG laser interaction on NiTi is discussed in chapter 5 and continuous Fibre laser interaction on NiTi is elaborated in chapter 6.

The phase transition is associated with heat emission (or absorption during a reverse loading). Since the phase transformation is induced either by temperature or stress, so the local temperature will change accordingly [100]. NiTi is preferred for thermo-mechanical treatment due to its high sensitiveness to variations [101]. For the thermo-mechanical cyclic deformation of NiTi SMAs, many experimental observations and constitutive models were performed and constructed in the last decades, respectively, as reviewed by Kang et al., [102] and Lagoudas et al., [103] and more recently in Refs. [104-111]. The state-of-art of thermo-mechanical cyclic deformation of NiTi SMAs

can be referred to the reviewed papers mentioned above and the referred literature there.

Thermo-mechanical behavior and life cycle analysis of SMA is required to know the fatigue limit of the used form of shape sheet, spring, wire or rod. Various applications of SMA are summarised in the upcoming section.

2.3 Research Objectives and Approach:

SMA actuators have generally been considered to be slow, inaccurate and difficult to control continuously. The approach that will be adopted for conducting this research will include performing a literature search to provide a summary control technique that has been suggested for SMA's especially NiTi. The primary objective of this study is to provide various mediums of actuation of SMA and investigate control methods that are more effective than those currently available.

Specifically, intentions are on:

- 1.** Design and development of experimental set up for electrically actuated SMA sheet/spring and implementation of control strategies with its practical application with its characterization. Different Interferometer technique is also implemented for precise positioning of SMA's.
- 2.** Design and development of experimental set up for hot water actuated SMA spring with its practical application with its characterization. Comparative analysis is also done for Hot water actuation as well as Joule heating.
- 3.** Development of experimental set up for laser (continuous fibre) assisted actuation of SMA spring with its practical application with its characterization.
- 4.** Development of test bed for pulsed laser assisted actuation and its comparison with the previous one.

This research will include studying control techniques that lend themselves to open as well as closed-loop control of SMA's. Included chapters are focussed on the design and development of micro-systems.

Actuation methodologies which are used in this thesis are given as a block diagram in Fig 2.20:

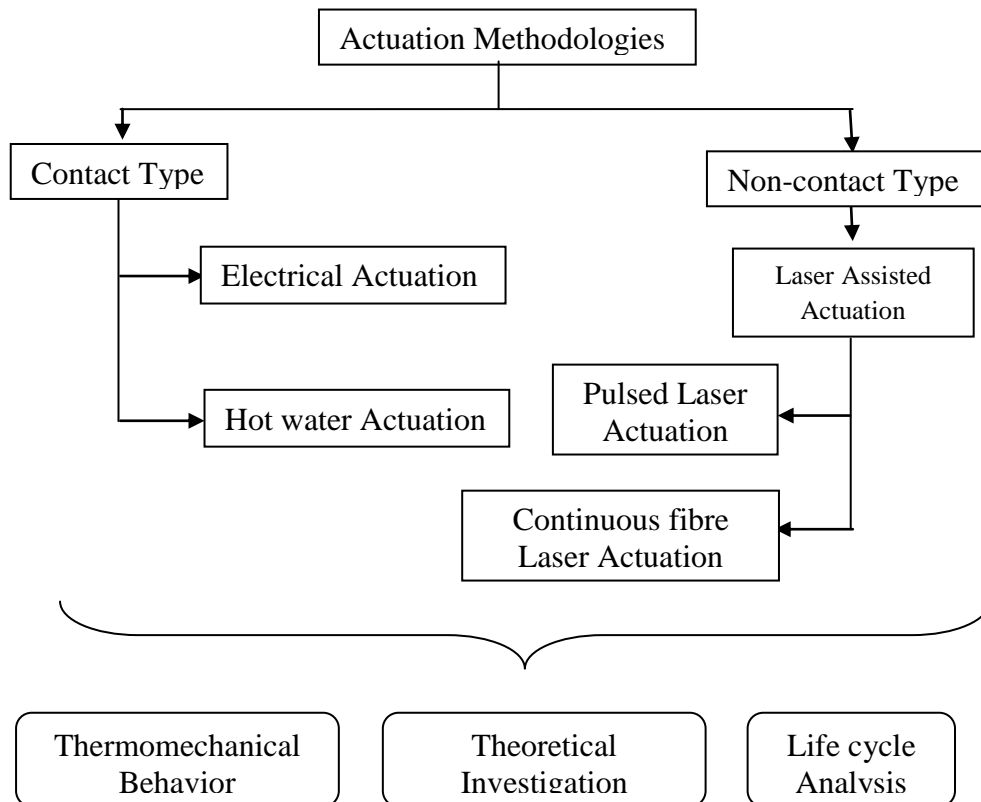


Fig. 2.20: Flow chart of actuation approach

2.4 Outline of the Thesis:

This dissertation is organized in the following manner:

- Chapter 1 concludes with the outlines of the intended contributions of this study.
- Reviews for thermo-mechanical behavior and life cycle analysis with applications are summarised in chapter 2.
- In chapter 3, actuation study of SMA through Joule heating is investigated, and the application has been developed.
- Hot water actuation of SMA has been explored with its relevant application.
- Non-contact actuation studies have been performed to explore the SMA actuation in chapter 5 (Pulsed laser actuation of SMA) and 6 (continuous laser based SMA actuation).
- Chapter 7 gives the conclusion of the current research work and the scope of future work.

Chapter 3

Electrical Actuation of SMA spring

This chapter discusses the development and comprehensive investigations of the thermo-mechanical behavior of electrically actuated shape memory alloy (SMA) spring. Control strategies, i.e., on-off controller, PID controller is implemented for precise control of displacement which is verified through Talbot interferometry and compared with laser displacement sensor measurement. Micro-device such as Stewart platform is developed and analyzed. Further, characterization analysis is performed to investigate the material properties in detail. Further, Theoretical and heat transfer analysis is performed to correlate the results.

3.1 Introduction:

There have been several discussions over the past few decades as to whether SMAs can respond rapidly. As discussed in the literature review from chapter 2, researchers have chosen NiTi in various forms due to its unique properties such as shape memory effect, super-elasticity, high damping capacity, high kinetic output, noise-less operation largest actuation force among actuators [112-113]. In this chapter, a novel experimental set up has been fabricated for life cycle estimation of SMA through electrical actuation.

The hysteresis response of NiTi is highly dependent on the applied load and temperature. Life cycle estimation of SMA can be done by using heating and cooling, in which Joule heating plays an important role to actuate SMA, for cooling natural convection and radiation is the best option. SMA material is actuated via Joule heating and proposed for a different application which is discussed below. Parameters which have varied during experimentation are voltage, load, and displacement.

3.1.1. Past studies on developed directional control valve: In the past, a novel directional control valve (DCV) using SMA springs was used to reduce the draw [121]. In this DCV, SMA spring is used to reduce the drawbacks present in other designs with lever-spring operated DCV automation where the frequency of operation is limited.

Table 3.1: SMA Spring specification

Parameters	Value
Coil Diameter (D)	3.5 mm
Wire diameter (d)	1.5 mm
Number of Turns (n)	20
Length of spring (l)	$n*d = 30$ mm (compressed)

For its development, it was required to know the stiffness of NiTi SMA. Therefore the stiffness of NiTi spring is measured initially.

• **Procedure to measure Stiffness:** Displacement of the spring was measured using digital vernier caliper by varying the load applied in the steps of 0.5N each starting from 1.0 N to 3.5 N which was limited by the capacity of the spring.

It was observed that the plot between force vs. extension was not linear for the entire range of forces utilized. Since the properties of SMA vary in high degrees as compared to any steel alloy, this non-linearity was highly expected, Further, when the curve was broken into linear segments, equation for the each of them found to have some constant term as shown in Fig 3.1, which is the unique property of all tension springs known as “prestressing”.

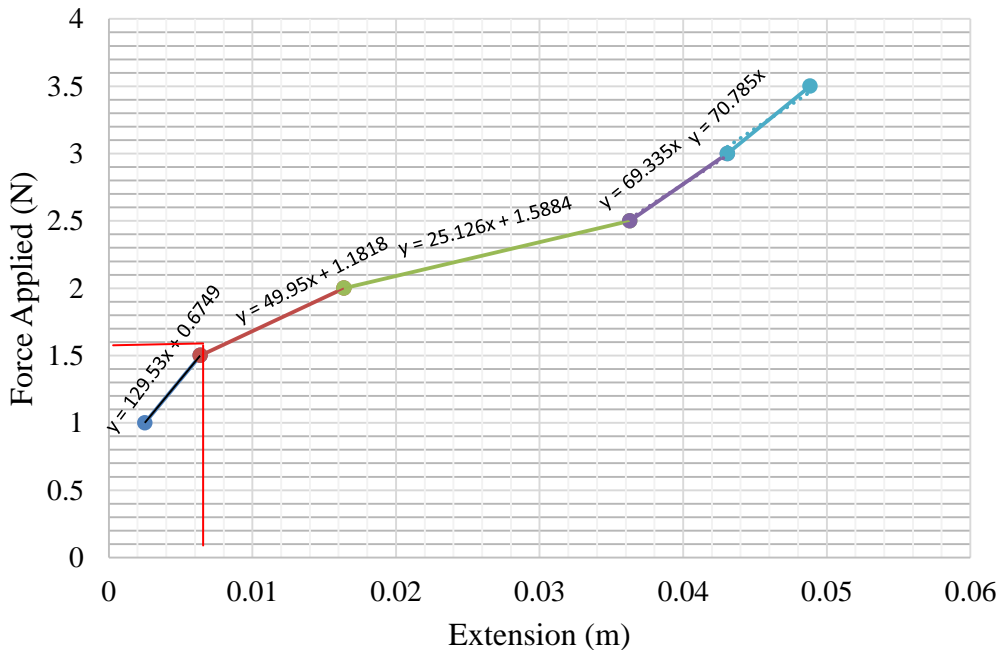


Fig. 3.1: Force applied vs extension of the SMA tension spring

Therefore from these results, the spring constant (spring stiffness) values for different loads were obtained along with the pre-stress values which are mentioned in Table 3.2.

Table 3.2: Results from the testing of the SMA tension spring

Force Range (N)	Spring stiffness (N/m)	Pre-stress value (N)
1.0-1.5	129.53	0.6749
1.5-2.0	49.95	1.1818
2.0-2.5	25.13	1.5884
2.5-3.0	69.34	0
3.0-3.5	70.79	0

3.1.2 Fabrication of DCV: SMA spring stiffness of 344.43 N/m was used to fabricate directional control valve. DCV which was designed through Pro-Engineer software according to given dimensions in Fig 3.2.

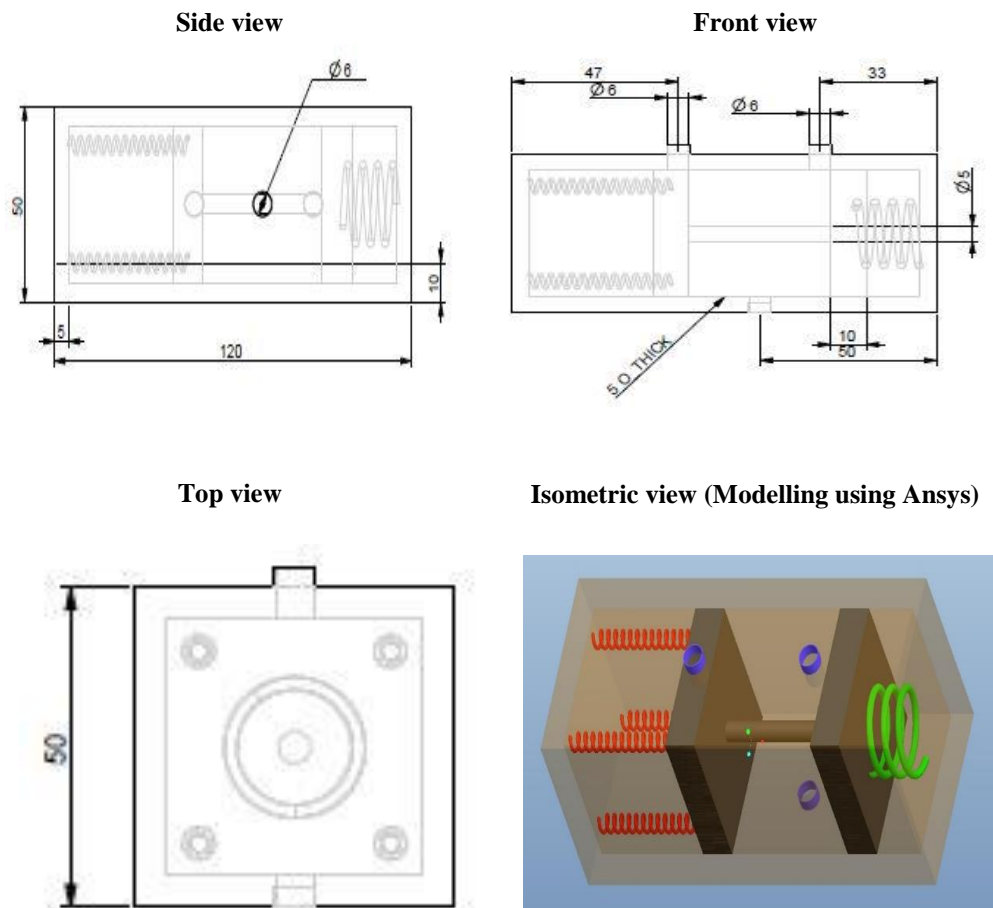


Fig. 3.2: Design of DCV a) side view, b) front view, c) Top view, d) Isometric view

To check its thermomechanical behavior an experimental set up was fabricated. Identical set up was utilized for the life cycle of SMA spring. Fig 3.3 depicts the working model of DCV.

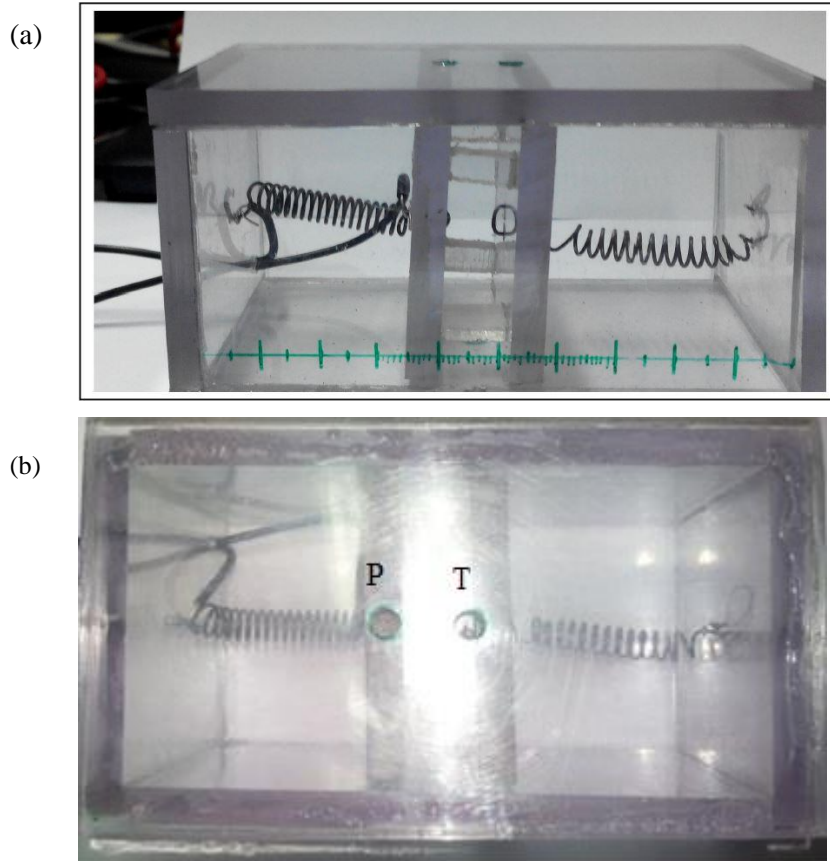


Fig. 3.3: Developed directional control valve (DCV) a) working model, b) Top view

According to the literature [5], comparative analysis is given, and spring was preferred than the other shapes 5 which are mentioned in Table 3.3.

Table 3.3: comparison analysis of different shapes of NiTi SMA

Property	wire	sheet	Tension spring
Actuation (Relative displacement)	Very Small	Moderate	Adjustable
Restoring force required	Low	Very High	Very Low
Implementation in the design	Easy	Difficult	Easy

3.2 Experimental setup for the Thermo-mechanical behavior of the SMA spring:

A test bench has been developed for investigating the thermo mechanical behavior through Joule heating. The life cycle analysis requires actuation through heating and cooling of the SMA actuator over some cycles until the failure was observed. It was further verified through characterization techniques. The spring has undergone thermomechanical fatigue, and it was observed that the springs failed to return to its original shape with an increase in cycles due to inelastic deformation.

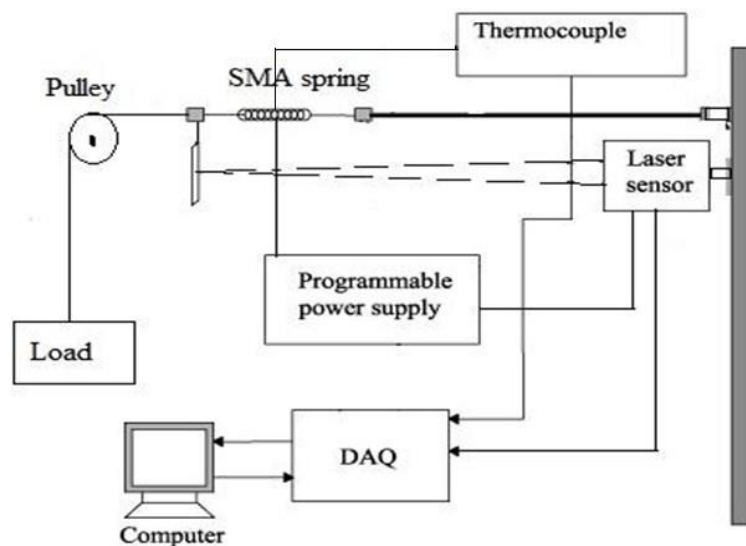


Fig 3.4 (a): Line Diagram for SMA actuation for Joule Heating

SMA fatigue behavior is generally characterized in three different ways [98]. First, fatigue by fracture due to stress or strain cycling at a constant temperature. Second, change in physical, mechanical and memory properties due to pure thermal cycling through the transformation region. Third, change in physical, mechanical, and memory properties are due to a combination of thermal cycling through the transformation region with constant stress or strain loading.

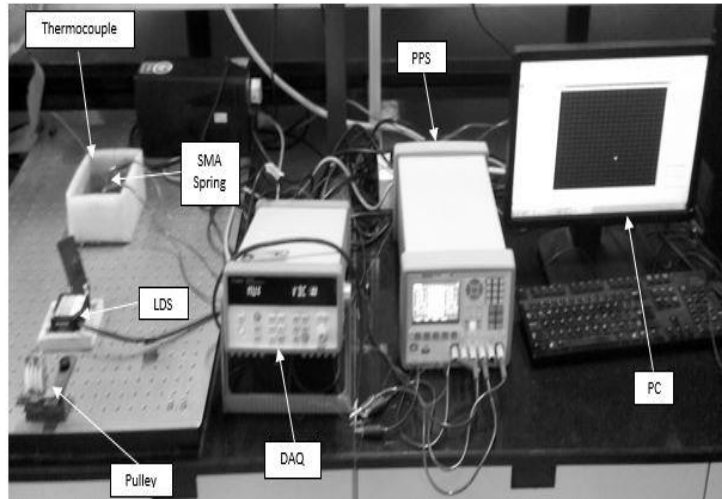


Fig 3.4 (b): Experimental Set up for Joule Heating

In most of the mechanical applications, the third kind of fatigue behavior is common, and the same is considered here. For that, an experimental set up was designed and developed to carry out the data from the starting point to till failure. Fig 3.4 (a) and 3.4 (b) represents the schematic overview and photographs of the experimental setup. Components used in developed set up are:

i) SMA spring: Due to the spring action, one-way trained SMA springs are widely used as micro-actuators. Therefore, this setup incorporated spring as an SMA component. Specification of SMA springs is given below:

Table 3.4: Specification of SMA spring

wire dia. (mm)	Mean diameter of the coil (mm)	No. of turns	Solid length (mm)	Actuation Temperature (°C)
0.77	5.69	18	13.86	70-80

DSC analysis of SMA NiTi spring (Equiatomic) is shown in fig 3.5

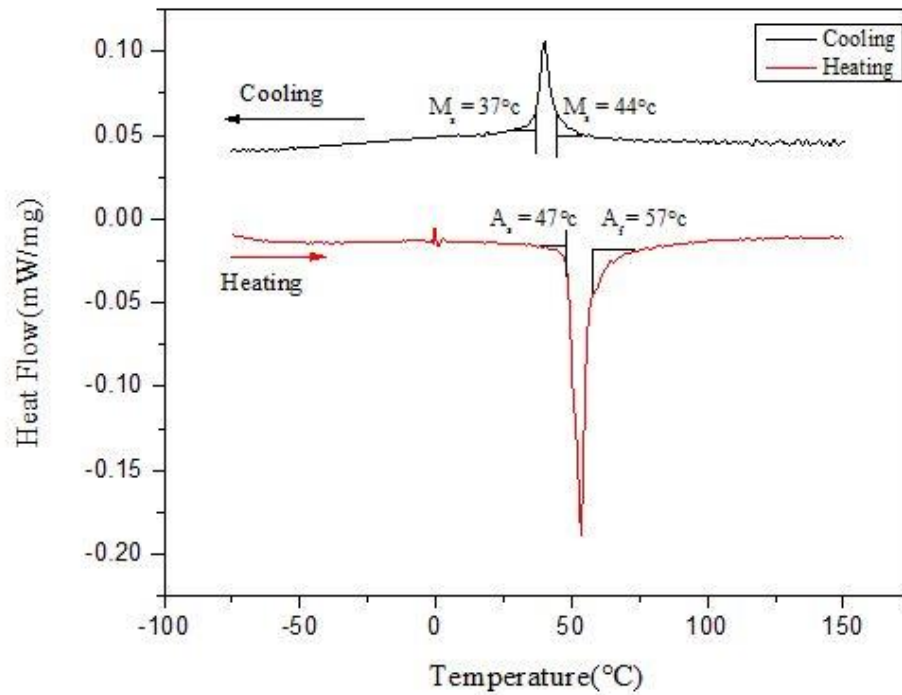


Fig 3.5: DSC curve of virgin NiTi spring

ii) Load: External force was needed to keep the spring extended as the spring was trained to contract upon actuation. Different weights are used experimentation.

iv) Programmable power supply (PPS): Thermomechanical cycles of the spring's required specific power which was obtained using a PPS (Model: RIGOL: DP1308A).

v) Laser Displacement Sensor (LDS): As the study involved micro-actuation, LDS was chosen over other displacement measuring devices which gave the resolution of $2.5\mu\text{m}$. (Panasonic HLG108-A-C5). Measurement and center distance for this LDS was 85 ± 20 mm whereas beam diameter was 0.75×1.25 mm.

vi) Thermocouple: K-type thermocouple was used to record the temperature of the spring over the actuation cycles. K-type provided stable calibration in the actuation range (-200°C to $+1350^\circ\text{C}$).

vii) Data Acquisition System (DAS): Measurements provided by LDS were recorded using a DAS and were directly saved into a computer for further study (Agilent 34970A). The Keysight 34970A data acquisition/data logger switch consists of a three-slot mainframe with a built-in 6 1/2 digit digital multimeter. Each channel can be configured independently to measure one of

11 different functions without the added cost or hassles of signal-conditioning accessories.

3.2.1 Experimentation: The set up used an LDS, K- type thermocouple; PPS; external weight applied to the spring with the help of a pulley and SMA spring. The NiTi SMA spring was procured to investigate the life characteristics of the spring. The specification of the spring used for the current case study is given in Table 3.4. It was one way trained and spring contracts upon actuation, i.e., application of voltage. The external load has been applied to keep the spring in the extended position. The specific energy required for the phase transformation of the spring is supplied through PPS. PPS also helps in controlling the heating and cooling cycles of the springs.

At the beginning of the experiment; weight is applied to the spring and keep the spring in extended position. After applying a voltage V_c to the spring through PPS; spring recover its original length against the gravity by lifting the weights. After recovery; voltage has been cut off and allows the spring to cool at room temperature. During cooling, the external weight applied to the spring force to spring back to the deformed shape. Some iteration has been performed to calculate the time for heating and cooling of the SMA spring. The heating and cooling phase of the spring is named as actuation. The combined actuation for one cycle is required for measuring the life cycle of spring. The reduction in elongation over the number of cycles is the representation of the failure. The elongation of the spring was measured with the help of the LDS. K- Type thermocouple was attached to measure the temperature during actuation and release of the spring.

The designed experimental set up has the following advantages for life cycle analysis which is elaborated in section 3.5.

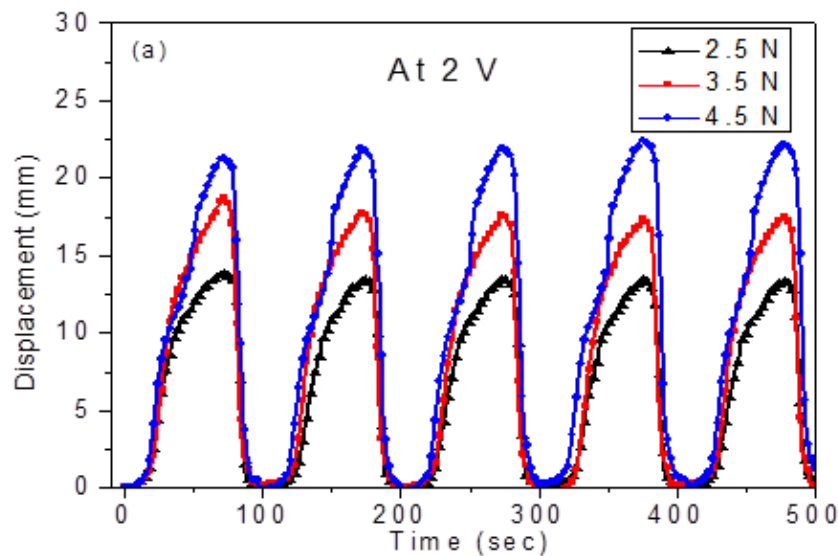
- a) The voltage can be supplied to the spring from 0 V to 6 V. So, accelerated life analysis can be made through supplying different voltages to the spring.
- b) The mechanical load applied to the spring can be varying from 0 N to 20 N. By considering mechanical load as a stress factor for the spring failure an accelerated life analysis can be done.

c) Spring of different stiffness parameter can be used for the analysis. Consequently, the model can be developed by considering stiffness as a stress factor.

d) Stimulus (i.e., voltage) and weight can be applied in steps for accelerated step for life cycle analysis.

3.2.2 Actuation Analysis: Experiments were performed with the springs having similar mechanical properties using different voltage waveforms. During each experiment, the displacement and temperature data of the spring was recorded for every 200th milli-seconds for the entire operating life of the spring.

Thermo-mechanical behavior is investigated at three different weights i.e., 2.5 N, 3.5 N and 4.5 N and with three different voltage 2.0 V, 3.0 V and 4.0 V. Its corresponding temperature is measured with K- type thermocouple which is in the range of 30°C - 60°C. At 2.5 N weights, displacement is 15.10 mm with its temperature 54.49°C which increased up to 18.32 mm at 3.5 N with 58.69°C. Maximum displacement is achieved which is 21.25 mm at 4.5 N with 58.93°C. In order for getting constant displacement for each cycle, the value was optimized and tabulated below (Table: 3.5)



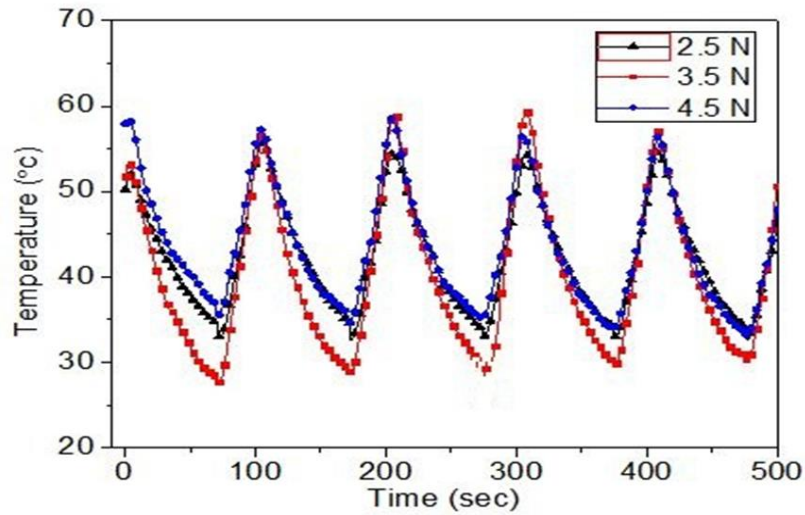
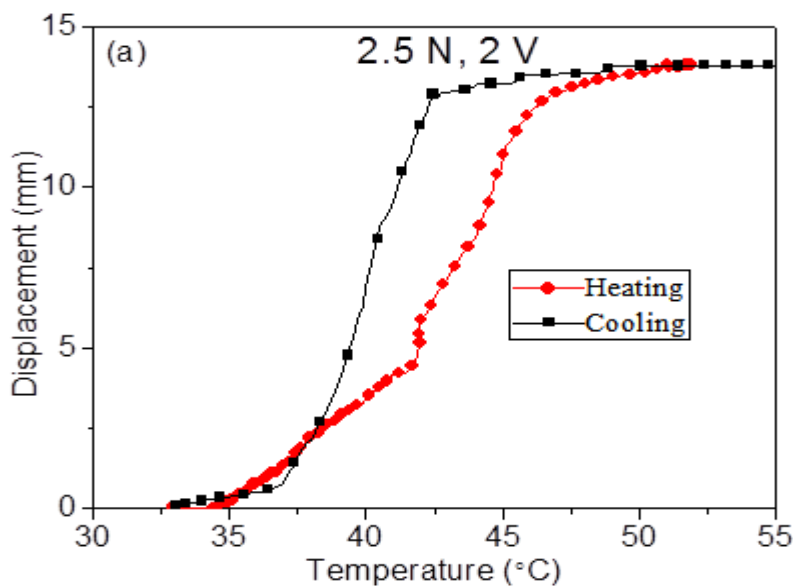


Fig 3.6: Displacement vs Time at 2.0 V for different weight a) for 2.5 N, 3.5 N and 4.5 N, b) Temperature vs time plot for 2.5 N, 3.5 N and 4.5 N,

For the same cycle, the hysteresis curve is plotted for various mentioned weight, i.e. 2.5 N, 3.5 N and 4.5 N (Fig 3.7 a, b and c).

Table 3.5: Heating (H) and cooling (C) at different voltages and weights

Parameters	Voltages					
	2V		3V		4V	
Weights						
2.5 N	H-30 s	C-70 s	H-28 s	C-69 s	H-20 s	C-63 s
3.5 N	H-32 s	C-72 s	H-24 s	C-65 s	H-18 s	C-80 s
4.5 N	H-34 s	C-74 s	H-30 s	C-58 s	H-14 s	C-82 s
Displacement	At 2.5 N	15.10 mm	At 3.5 N	18.32 mm	At 4.5 N	21.25mm



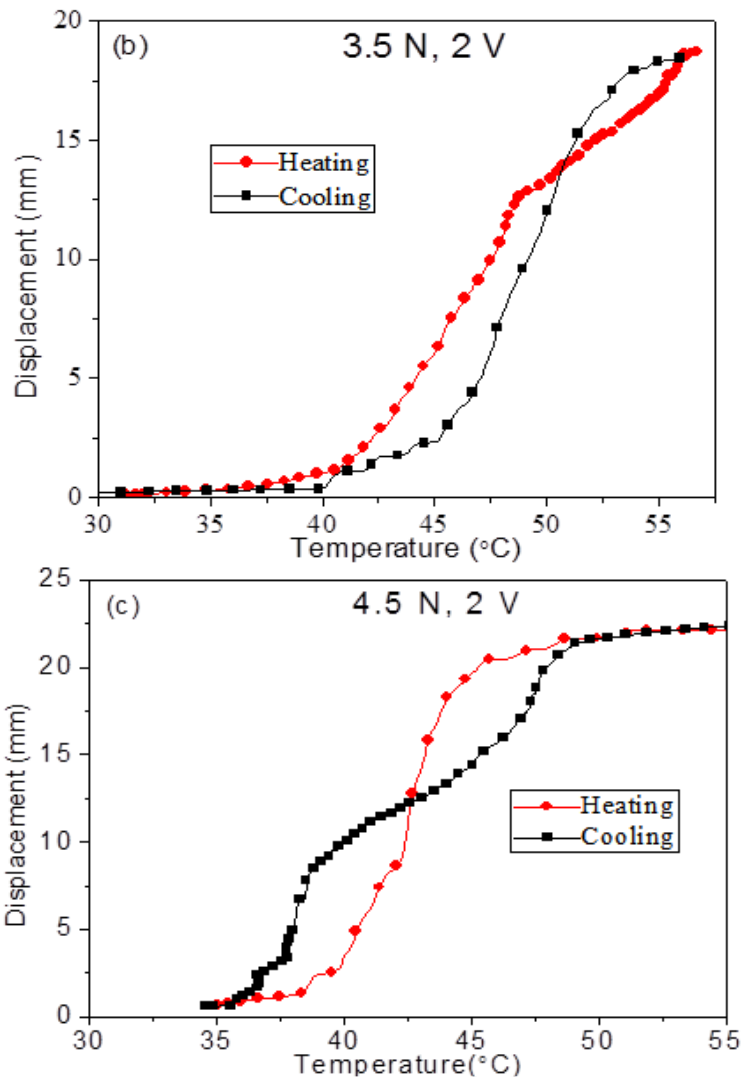
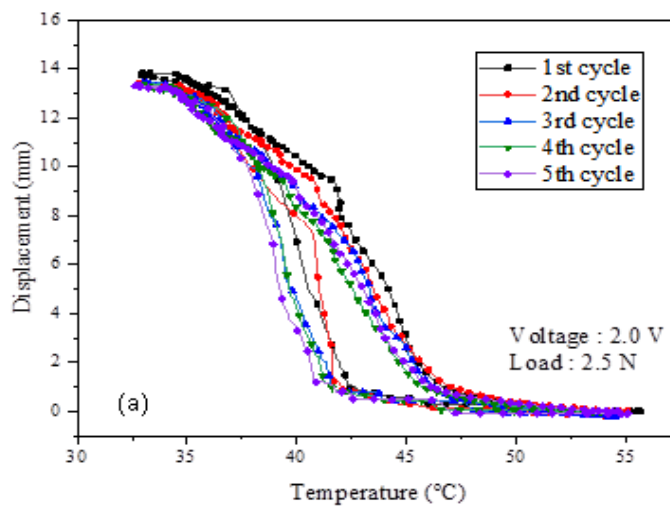


Fig. 3.7: Hysteresis curve for actuation of SMA at 2.0 V and a) 2.5 N, b) 3.5 N, and c) 4.5 N



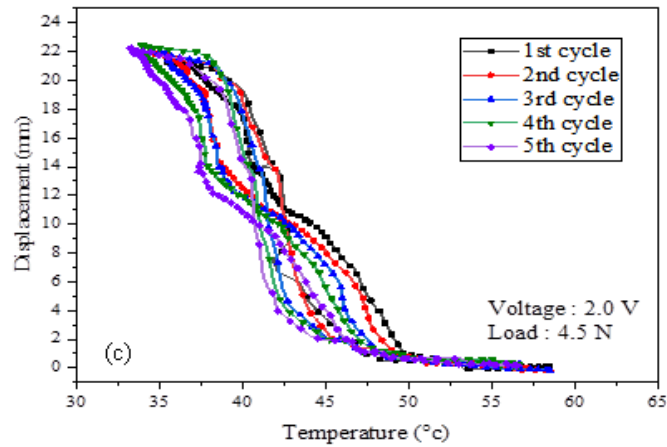
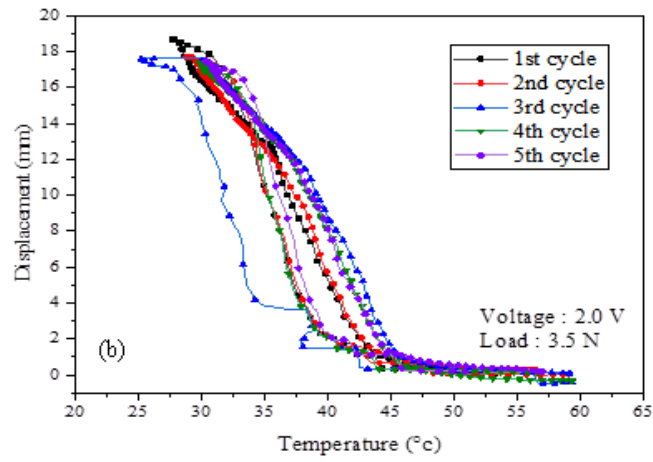
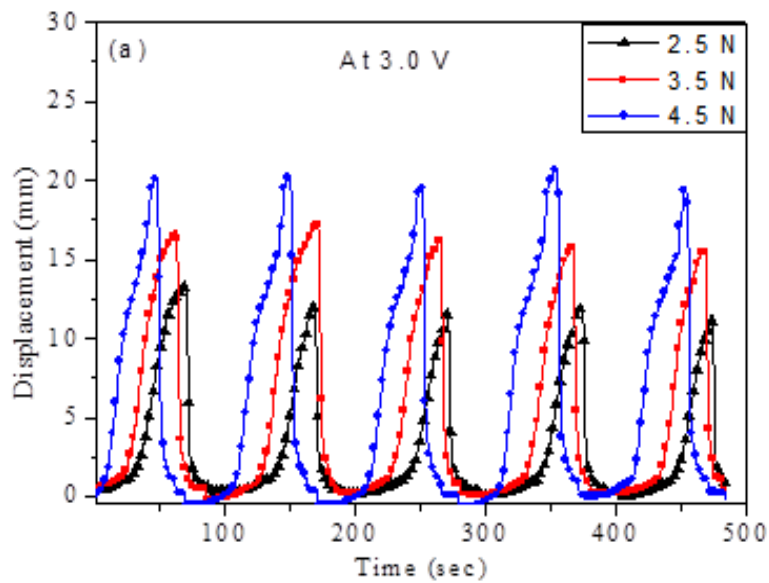


Fig. 3.8: Hysteresis curve for actuation of SMA at 2.0 V and a) 2.5 N, b) 3.5 N, and c) 4.5 N

Hysteresis curves for five cycles at different load (2.5 N, 3.5 N and 4.5 N) with 2.0 V is plotted in Fig 3.8. Since the spring was used in test bench so it can be in a reversed manner also.



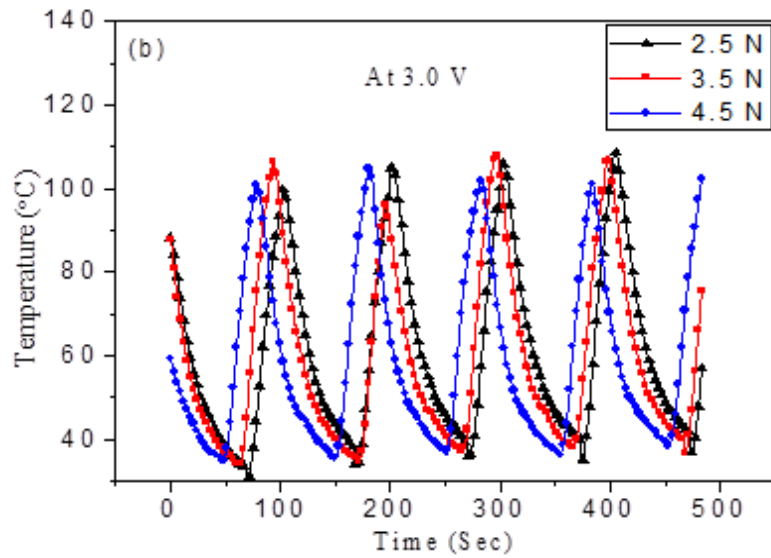
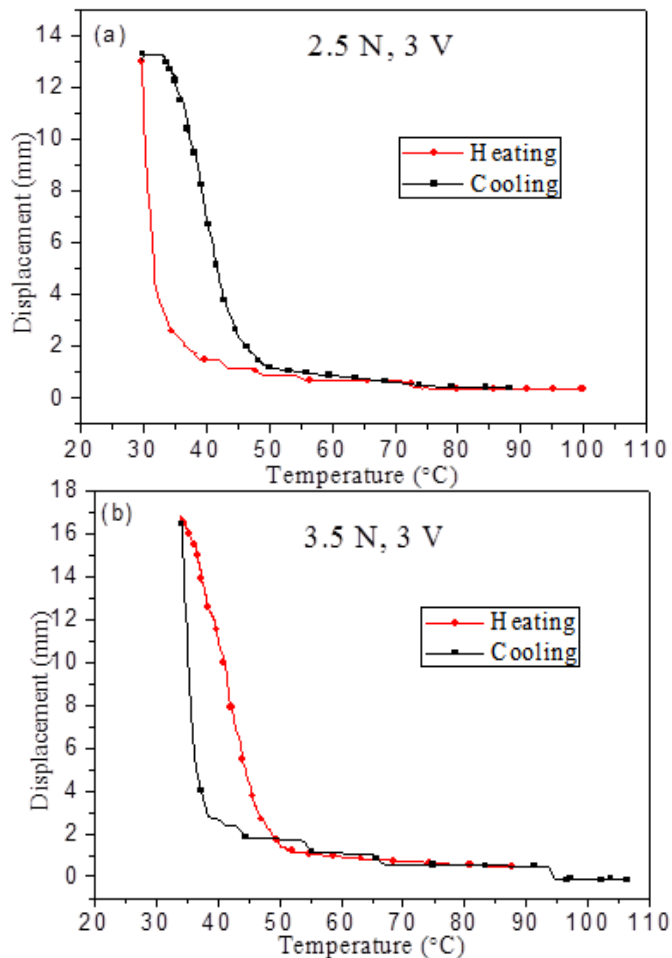


Fig. 3.9 Displacement vs Time at 3.0 V for different weight a) for 2.5 N, 3.5 N and 4.5 N, b) Temperature vs time plot for 2.5 N, 3.5 N and 4.5 N

Similarly, the thermomechanical behavior of SMA (displacement vs. time) is plotted in Fig 3.9 when spring was loaded at 2.5 N, 3.5 N and 4.5 N and applied with 3.0 V. For the same cycle temperature vs. time graph is plotted. Actuation behavior for the single cycle is plotted in Fig 3.10.



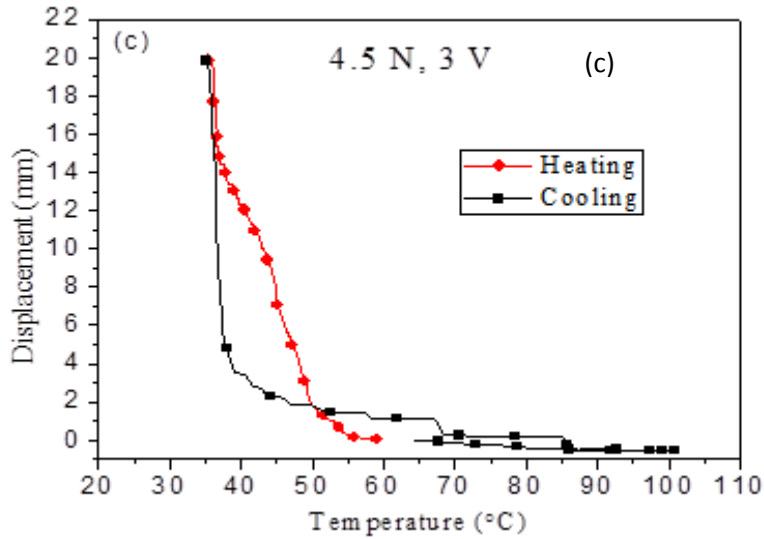
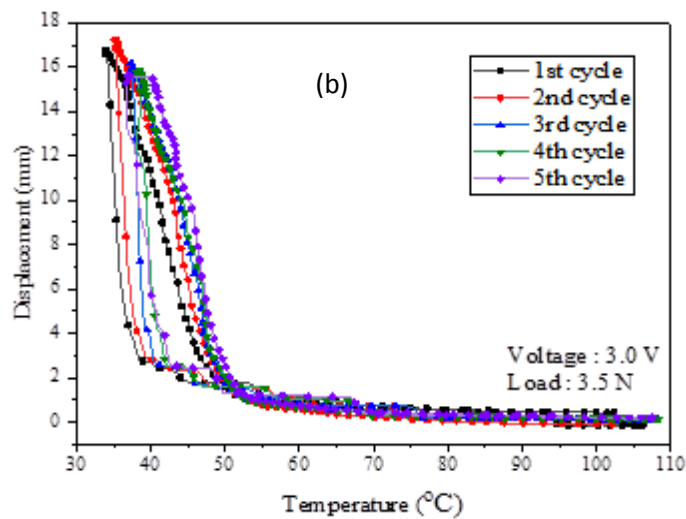
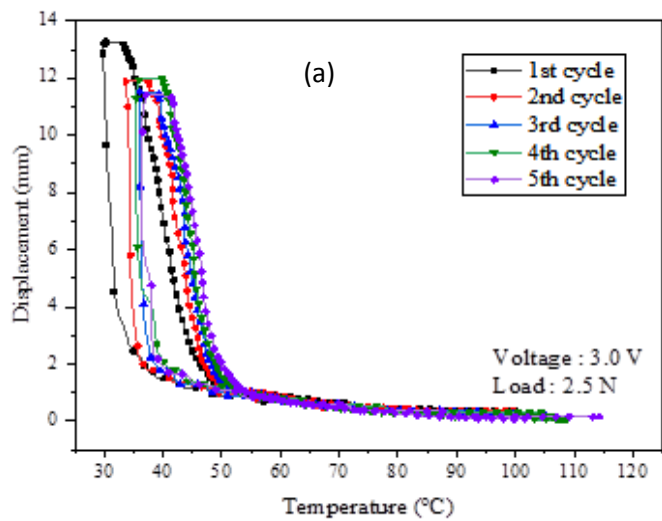


Fig 3.10: Hysteresis curve for actuation of SMA at 3.0 V a) 2.5 N, b) 3.5 N, c) 4.5 N

Hysteresis curves for five cycles are also shown below in Fig.3.15, at 3.0 V for the same loading condition.



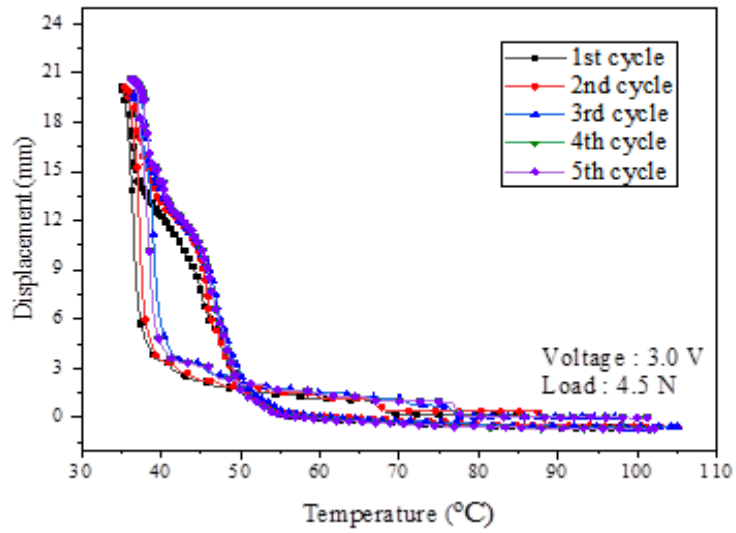


Fig. 3.11: Hysteresis curve for five cycles at 3.0 V and a) 2.5 N, b) 3.5 N, and c) 4.5 N

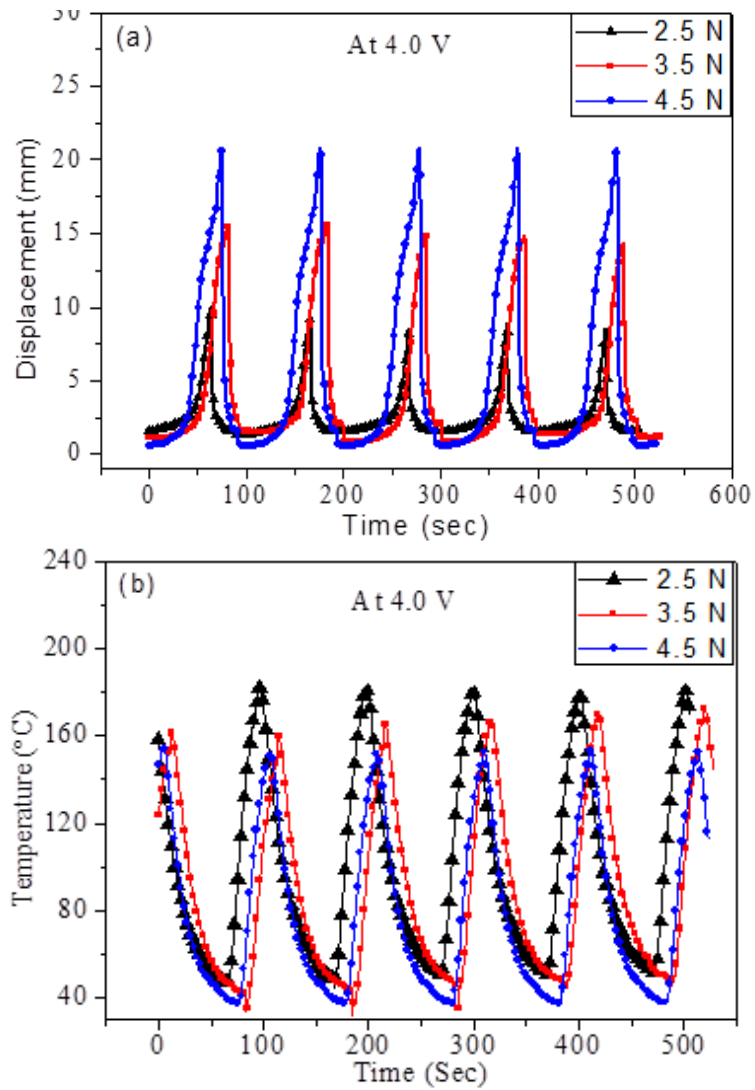


Fig 3.12: Displacement vs Time at 4.0 V for different weight a) for 2.5 N, 3.5 N and 4.5 N, b) Temperature vs time plot for 2.5 N, 3.5 N and 4.5 N

When Spring was actuated with 4.0 V, and at the same loading condition, the range for displacement was 10-15 mm. The same process was repeated by five times whose thermomechanical behavior and hysteresis curve is graphed in Fig 3.14.

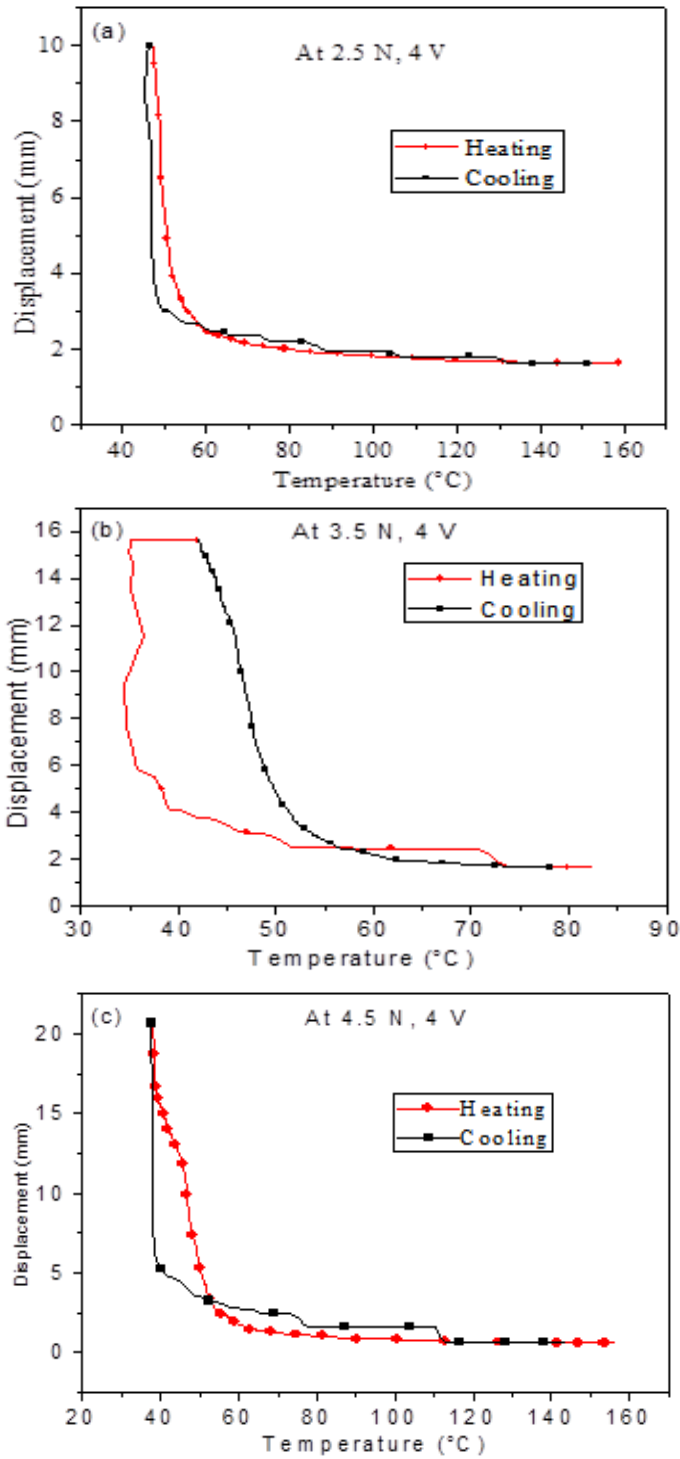


Fig 3.13 Hysteresis curve for actuation of SMA at 4.0 V a) 2.5 N, b) 3.5 N, c) 4.5 N

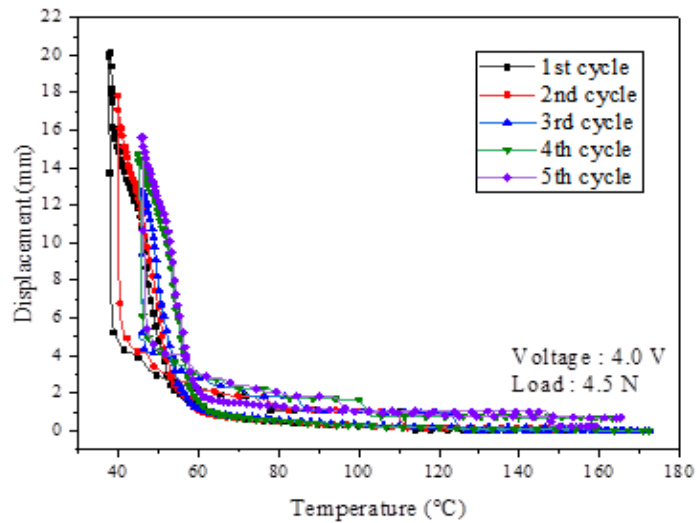
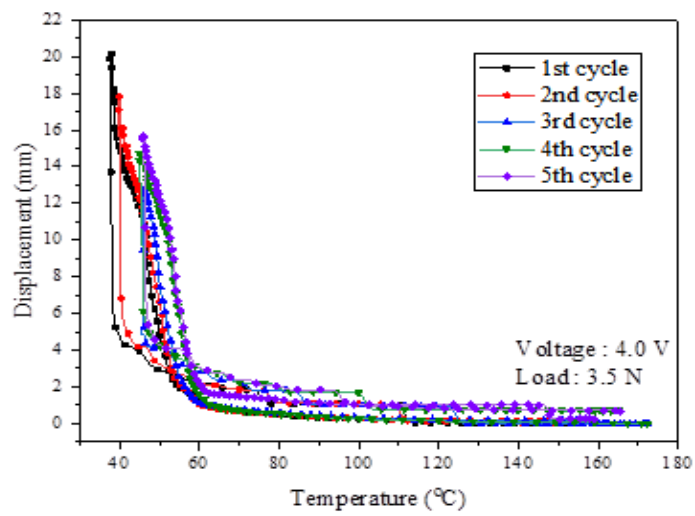
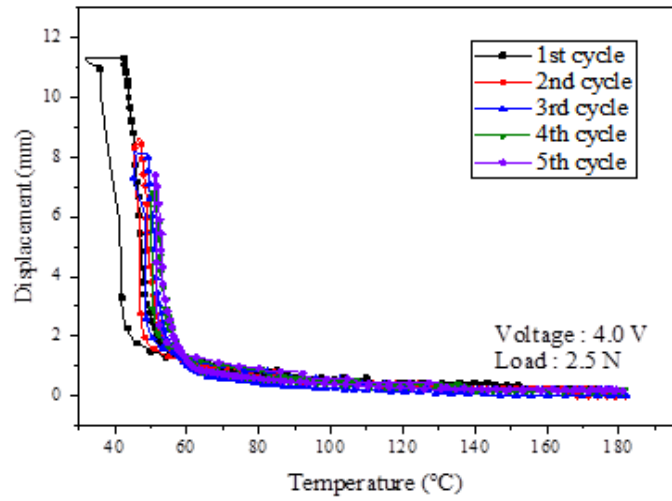


Fig. 3.14: Hysteresis curve for five cycles at 4.0 V and a) 2.5 N, b) 3.5 N, and c) 4.5 N

In all hysteresis curves, it can be easily seen that they are intersecting each other at a particular point. In Fig 3.7 point of intersection is 12.74 mm due to its phase transition. While heating it was not visible but when cooling started at that time, austenite came to the martensite phase and crossed the curve, resulting intersection. The plot for displacement and Time, Temperature and time, and hysteresis curves are shown in Figs 3.7- 3.15.

3.2.3 Heat Transfer Analysis: Knowing the heat transfer of the joule heated SMA spring places a vital role in determining its application. For that Heat balanced equation can be written as:

$$\frac{V^2}{R} = Q_{cond} + Q_{conv.} + Q_{rad.} + mC \frac{dT}{dt} \dots \dots \dots Eq 3.1$$

Here m is the mass of the spring, V is the potential difference applied, R is the electrical resistance of the spring, C is the specific heat, T is the surface temperature of the spring and t is the time as observed from the experiment. Pictorial representation is in Fig 3.15.

Shu et al. [114] proved that for long wires, the temperature distribution is uniform along the length of wire and cross sections except for the two ends, so we neglect $Q_{conduction}$. It seems valid to avoid this term since heat loss due to conduction

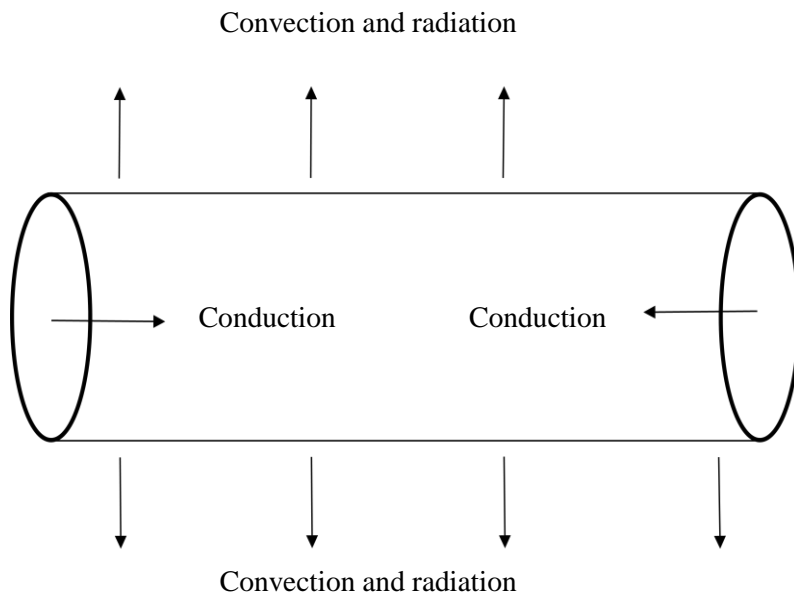


Fig 3.15: Heat loss in cylindrical SMA wire

would be negligible in the alloy due to its metallic properties which added with small radius of the wire leads to small Biot's number (Bi). Hence $Q_{rad.}$ can be neglected due to its less value.

Heat transfer coefficient was calculated for heating in air, calculated by Hossein Talebi and Hossein Golestanian [115]:

$$h(T) = -4.034 \times 10^{-7}T^4 + 0.0001654T^3 - 0.2586T^2 + 2.07T + 41.96$$

T (°C) and h (W.m². °C⁻¹)

We can call that heat required for phase transformation as $Q_{phase\ transformation}$.

To determine the value of $Q_{phase\ transformation}$ we need to discuss about $\xi(T)$ i.e. Martensite fraction relation. Liang, and Rogers [116] proposed a model for $\xi(T)$.

$$Q_{phase\ transformation} = m\Delta H \frac{d\xi(T)}{dt} \dots \dots \dots Eq\ 3.2$$

Here ΔH is change in energy associated with phase transformation. $\frac{d\xi(T)}{dt}$ is the rate of conversion of martensite into austenite.

So considering all these factors in account, the final equation becomes:

$$\frac{V^2}{R} = h(T)A(T - T_{surr}) + mC \frac{dT}{dt} + m\Delta H \frac{d\xi(T)}{dt} \dots \dots \dots Eq\ 3.3$$

V is the potential difference applied, R is the electrical resistance of the wire, h is the heat transfer coefficient, A surface area of the spring, T is the temperature of the spring, T_{surr} – surrounding's temperature, m is mass of the spring, S is the specific heat of the SMA.

3.2.3.1 Simulation of Thermomechanical behavior on SMA using COMSOL:

It is simulated using comsol software also, which is shown in Fig. 3.17. It was necessary to test the model for the thermo-mechanical behavior of SMA spring. The most critical component of the assembly was obviously the SMA

tension spring, and thus it was simulated for all the voltages. The load is only playing important role for extension of spring and temperature is responsible for actuation of the spring. The followings are the result of the simulation performed under a different voltage applied to simulate the electrical actuation effect in the Shape memory spring. The following analysis is the result in which spring is attached with clipper of the power supply and heat is transferred uniformly. Spring is actuated by 2.0 V when it was loaded with 2.5 N then temperature profile was compared as per heat transfer analysis.

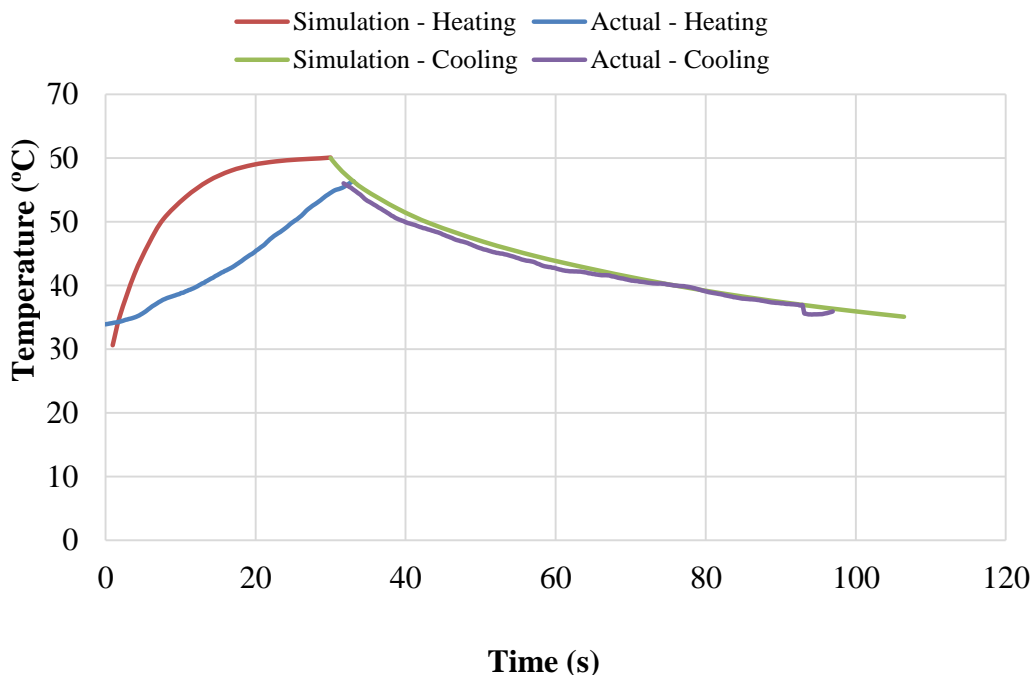


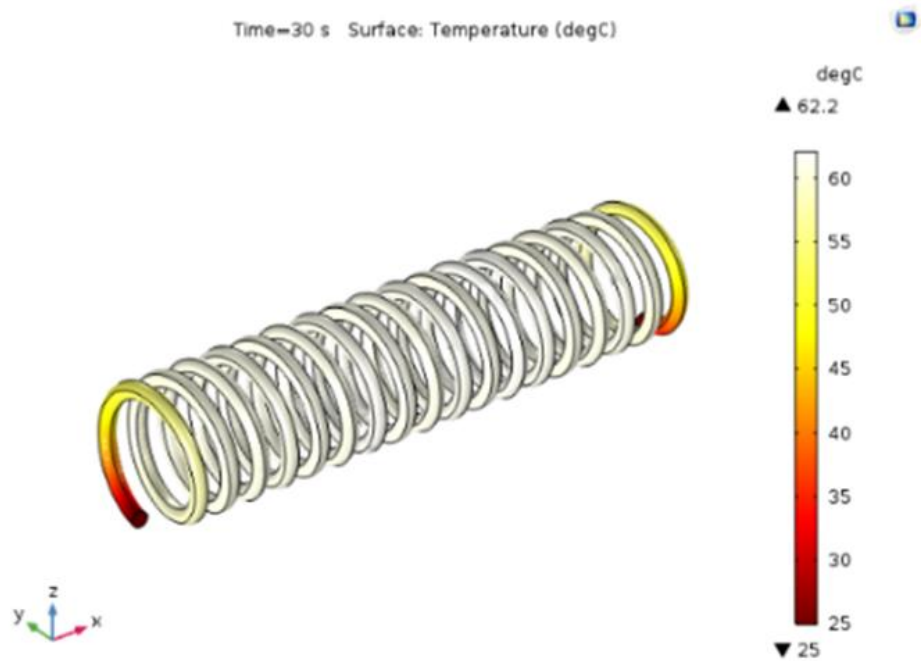
Fig 3.16: Comparison analysis for actuation of SMA spring for 2.0 V (with experimental and simulation)

Fig 3.16 shows the comparison analysis of simulation. Since temperature is important parameter for heat transfer. Behavior of spring is continuously affected due to its voltage value.

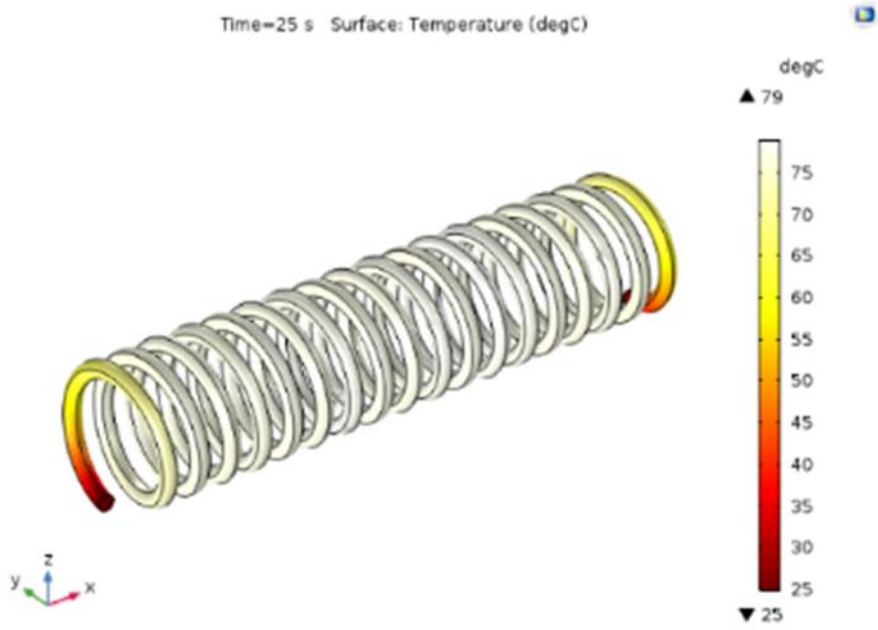
Table 3.6 shows the required properties for simulation:

Table 3.6: Material properties for simulation

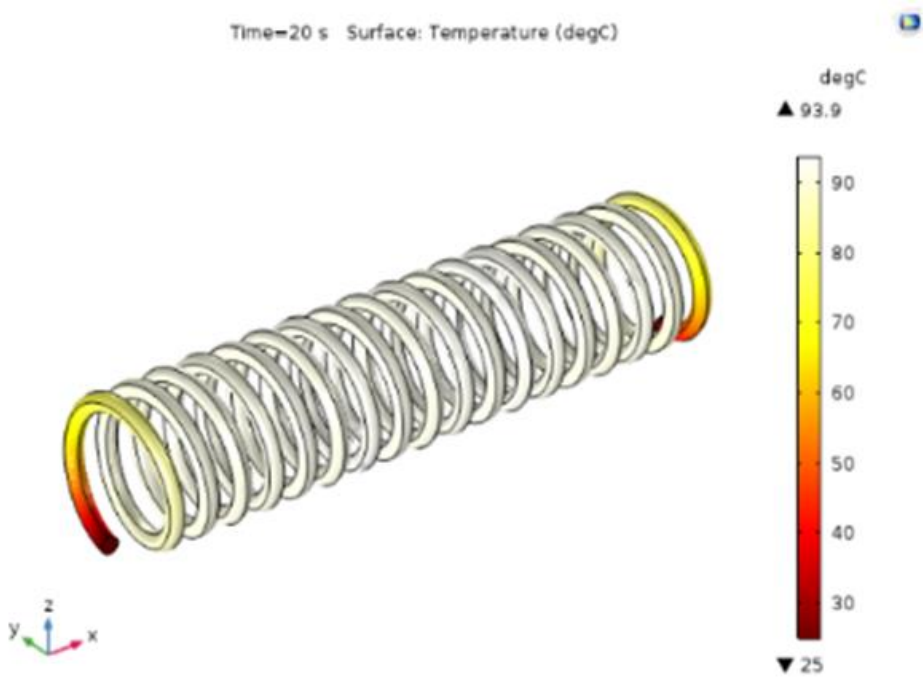
Material Properties	Values (Unit)
Density	6450 (Kg/m ³)
Heat capacity at constant pressure	550 (J/Kg-K)
Thermal conductivity (Austenite)	18 (W/m-k)
Thermal conductivity (Martensite)	5 (W/m-k)
Electrical conductivity	6e5 (S/m)
Relative Permittivity	0.9
Terminal	Voltage
Heat Transfer Coefficient	90-120 (W/m ² .K)
Ambient Temperature	25 (°C)



(a)



(b)



(c)

Fig 3.17: Simulation of SMA spring under condition of different voltages a) 2.0 V,) 3.0 V, c) 4.0 V

Note: The boundary condition of this process is the same as the previous one, but the above was performed for various cycles. Since the potential difference between the two ends of the heating contact becomes zero at the center, the highest temperature is witnessed at that point itself. The red portion shows the most vulnerable section as both ends is attached with a clipper. When 2.0 voltage is applied then one cycle completed in 30 s for that temperature was exceeding from 25 to 60 °C, whereas for 3.0 V, one cycle is completed in 25 s for the temperature requirement of 25 to 75 °C. For 4.0 V, one cycle is completed in 20 s for the temperature requirement of 25 to 80 °C

3.3 Control Strategy: In this experimental set up two types of controllers were used to control the displacement precisely i.e.on-off controller, and proportional-integral-derivative (PID) controllers.

3.3.1. On-Off controller: On-Off control is the easiest form of feedback control. An on-off controller is simplest type of feedback control. An on-off controller simply drives the manipulated variable from fully closed to fully open depending on the position of the controlled variable relative to the set point. Although on-off is a very cheap form of control. It is rarely used in process control applications because of the oscillation it causes in the controlled and manipulated variables. In a connected process, these oscillations would be propagated right through the system.

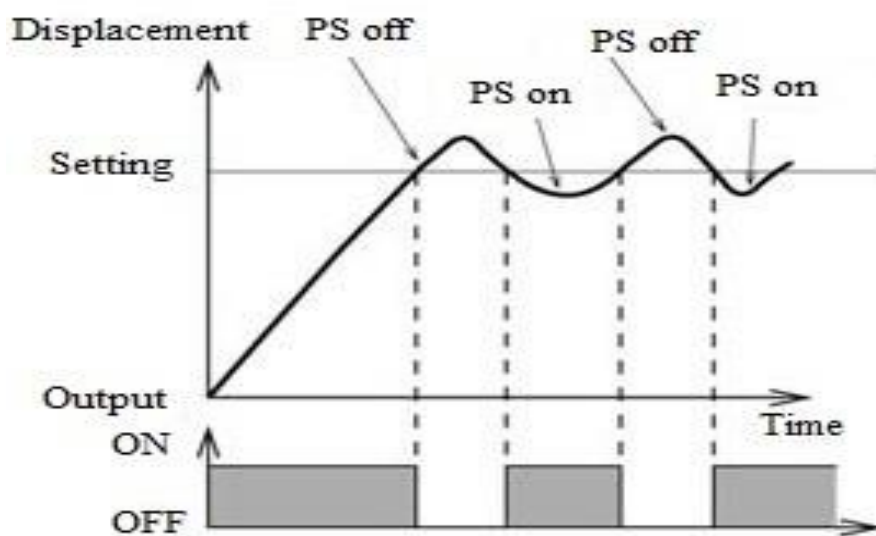


Fig. 3.18: Basic principle of on-off controller

On-off control is like operating a switch. This type of displacement controller will turn on the power supply (PS) when the process variable is below the set point (SP) and turn it off when the process variable (PV) is above the set point. These controllers normally include a delay, hysteresis and or a cycle time to reduce the cycling or "hunting" when the process variable is close to the set point (Fig 3.18).

If it has too much power. On/off controller will struggle to provide exact displacement control because the heating element (SMA) will store and deliver too much heat before the displacement reached the "off" points shown in Fig 3.20. Since displacement is controlled, so it was stable at a particular position. Hence overshoot can be seen in the temperature profile.

The difference between desired output and current output is actuating error signal (e) that depends on the sign of e for control signal i.e.

$$U(t) = U_1 e(t) < 0 \text{ at on condition} \\ = U_2 e(t) > 0 \text{ at off condition}$$

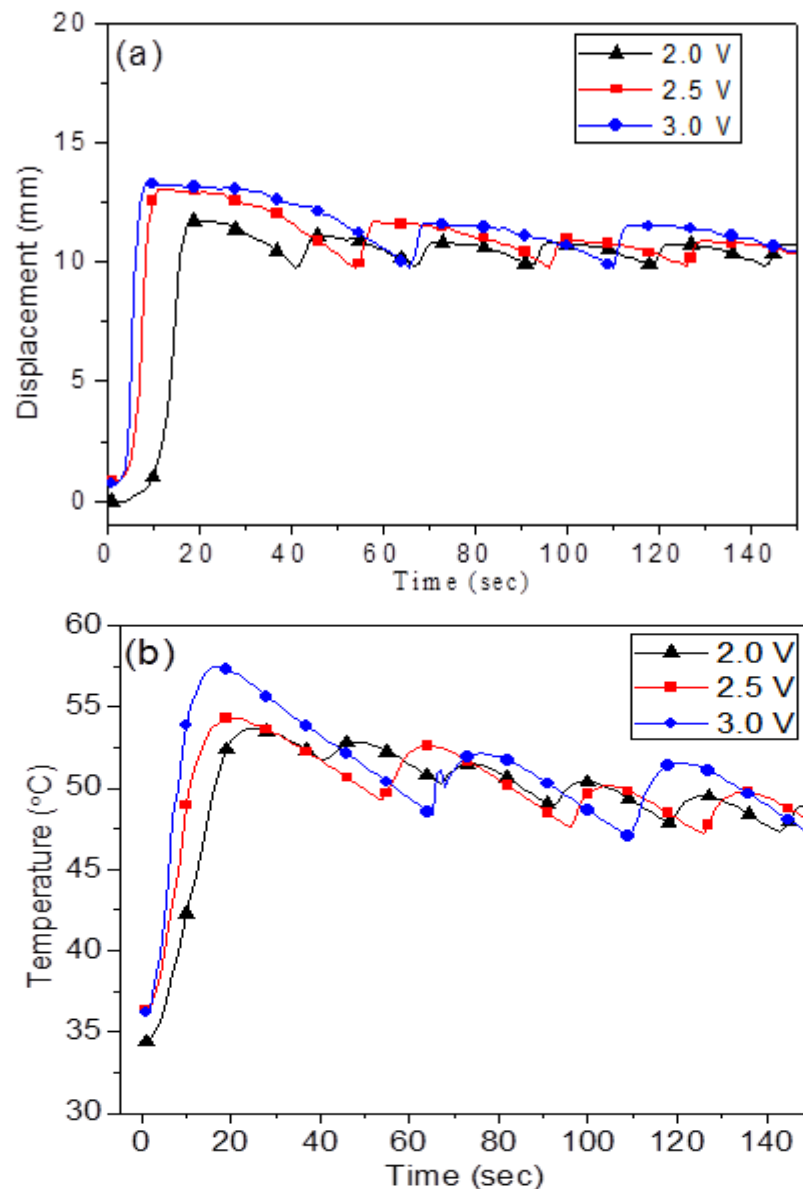
In the current scenario, to control the position of SMA spring U_1 was set to 0V and U_2 was varied as 2.0 V, 2.5V, and 3.0 V.

Note: *It should be noted that, even though the spring is compressing, the scales have to be multiplied with a common factor to have a zero reference and a positive scale for better understanding. It was observed that, while the spring was compressed during actuation, the values change from negative to zero. After changing the values to positive scale, the reading indicates the control position at 10 mm, 15 mm and 20 mm which was observed as -10 mm, -5 mm and 0 mm.*

3.3.1.1. Implementation of the controller: In place of the simple power supply, the programmable power supply is used to control the SMA displacement according to requirement. Parameters are optimized for different displacement. The timing for actuation of SMA is optimized, as mentioned in Table 3.3, as it was required to know that how much elongation can be achieved at a particular voltage and weight. On displacement basis, SMA is

controlled. SMA displacement is controlled at 10 mm, 15 mm and 20 mm for 2.0 V, 2.5 V and 3.0 V with the weight of 2.5 N, 3.5 N and 4.5 N.

Fig 3.19 (a) and 3.19 (c) shows controlled position of spring at 10 mm and 15 mm for 2.5 N and its corresponding time versus temperature graph is represented in Fig 3.19 (b) and Fig 3.19 (d). The experiments were conducted with three different voltages of 2.0 V, 2.5 V and 3.0 V. Only two control positions were selected as the spring returned to its original position. It can be observed from Fig 3.19 (a) that, at 2.0 V a maximum displacement of 12 mm within 9 s was detected, and the spring attained its controlled limit within 28s. Further, it returned to the control position in 44 s. The precise control was achieved at a cycle time of 42 s.



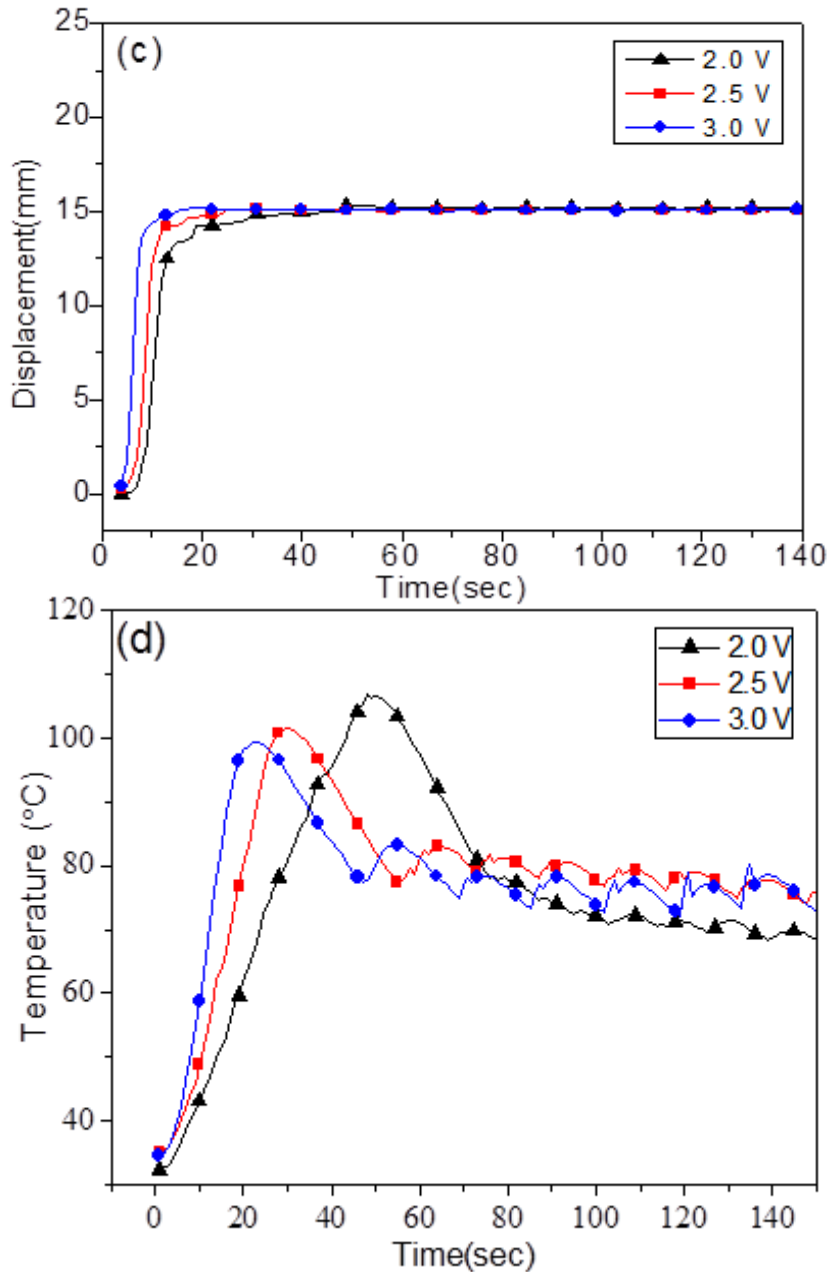
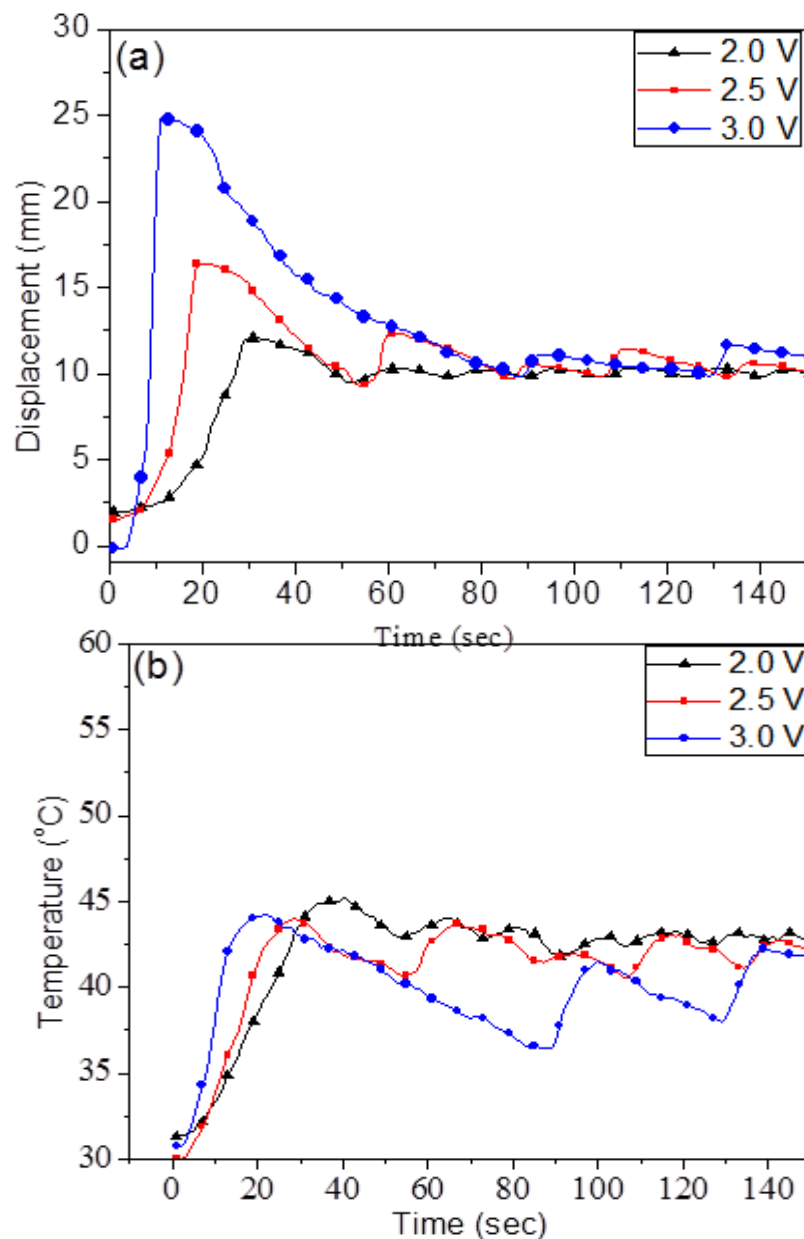


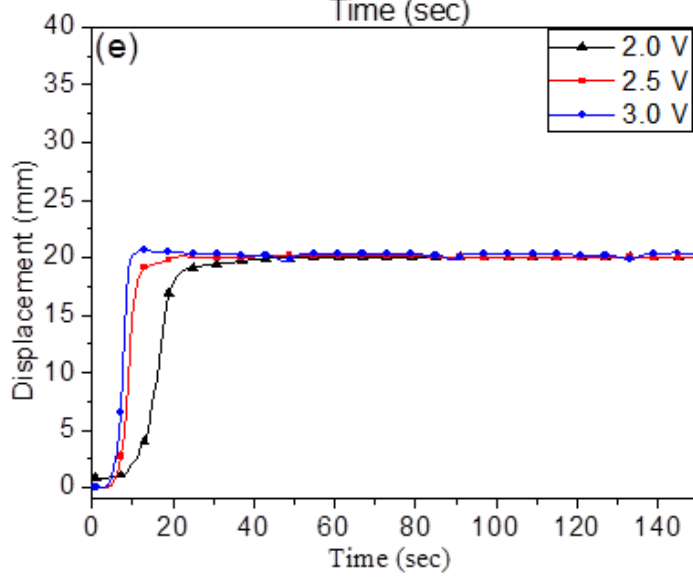
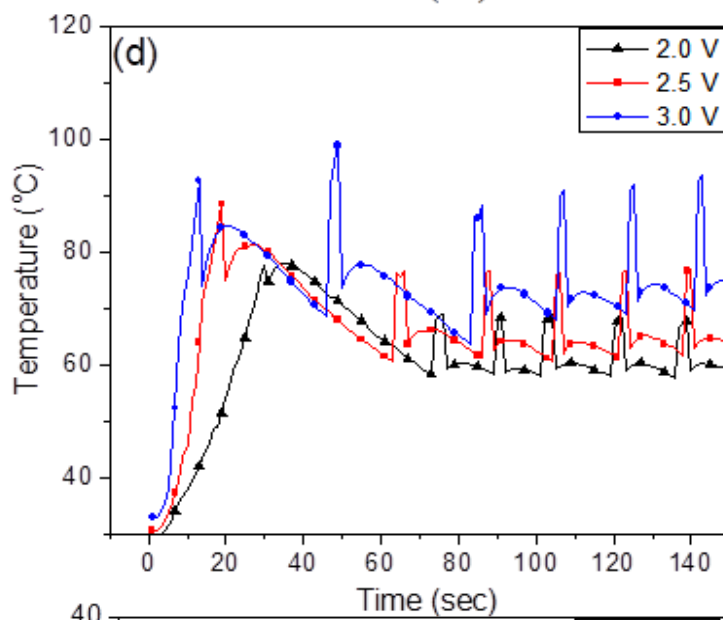
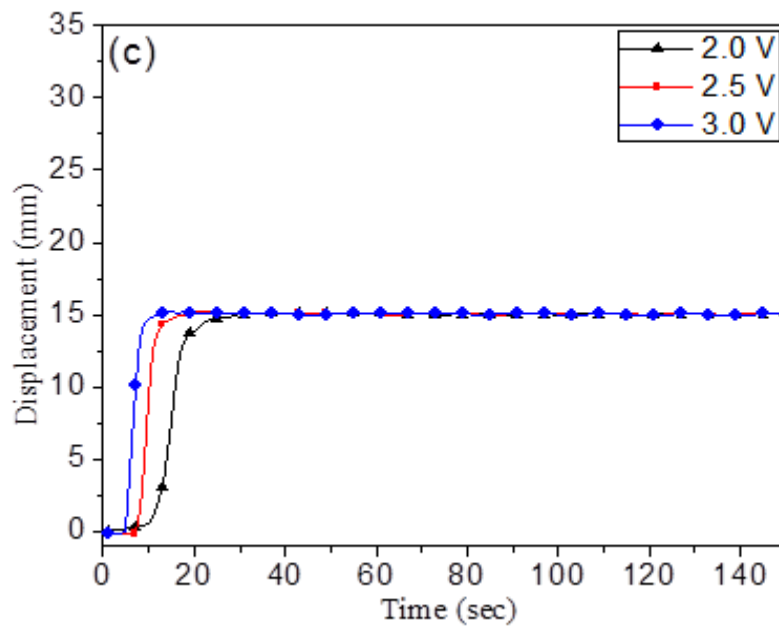
Fig 3.19: Spring loaded with 2.5 N controlled at 10 mm, 15 mm a) Displacement vs. time curve for 2.0 V, 2.5 V and 3.0 V when controlled at 10 mm, b) Temperature vs. time curve for 2.0 V, 2.5 V and 3.0 V when controlled at 10 mm, c) Displacement vs. time curve for 2.0 V, 2.5 V and 3.0 V when controlled at 15 mm, d) Temperature vs. time curve for 2.0 V, 2.5 V and 3.0 V when controlled at 15 mm

At 3.0 V, maximum displacement was 10 mm and it took approximately 67s to reach the control position. In Fig 3.19 (c), spring is loaded with 2.5 N, and controlled at 15 mm, working under different voltages. All voltages are able to control the spring at 15 mm after 50 s from the beginning. The temperature profile for 10 mm control was varying from 45°C-60°C, and it increased

drastically for 15 mm, where it reached 100°C but gradually reduced after the first cycle. It was evident that, at 2.5 N, 15 mm control was reliable with on/off controller.

At higher loads, one more control position was possible when the maximum elongation achieved. In Fig 3.20 (a) displacement versus time at 2.0 V is shown, where the displacement increased drastically. It reached 14 mm and then gradually reduced to 10 mm whereas at application of 2.5 V, displacement was 14.5 mm and it was not stabilized properly at 10 mm. There were fluctuations in displacement and temperature as the voltage was increased to 3.0 V. At 3.0 V, maximum displacement was 25 mm then it returned to 9.5 mm.





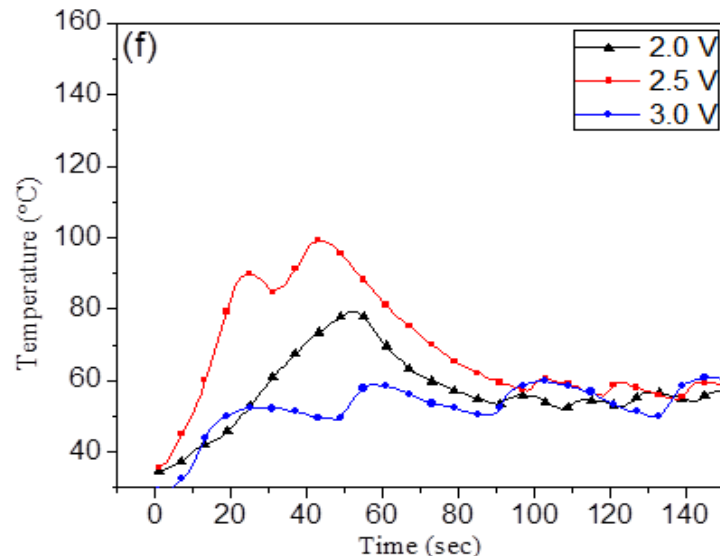
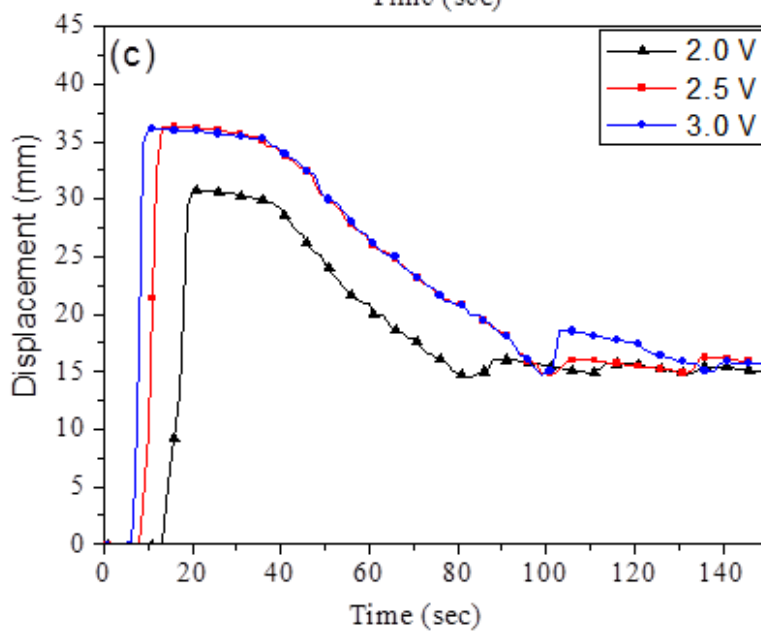
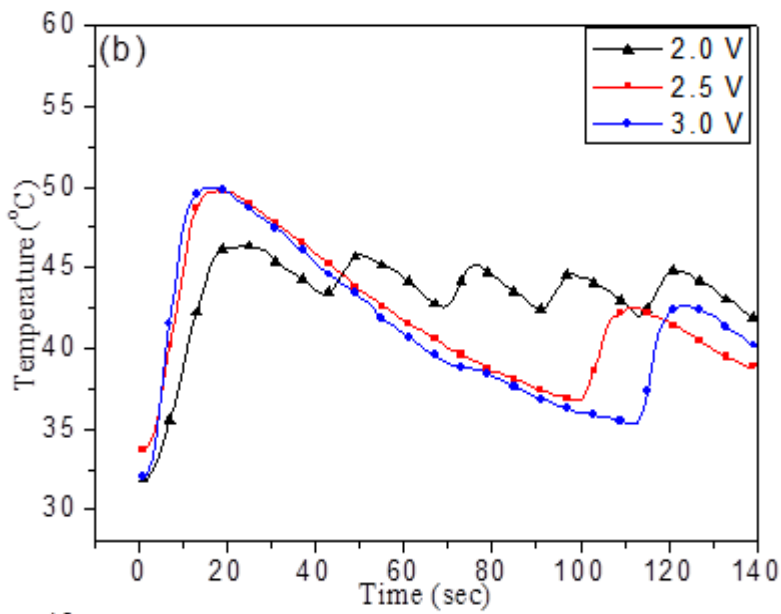
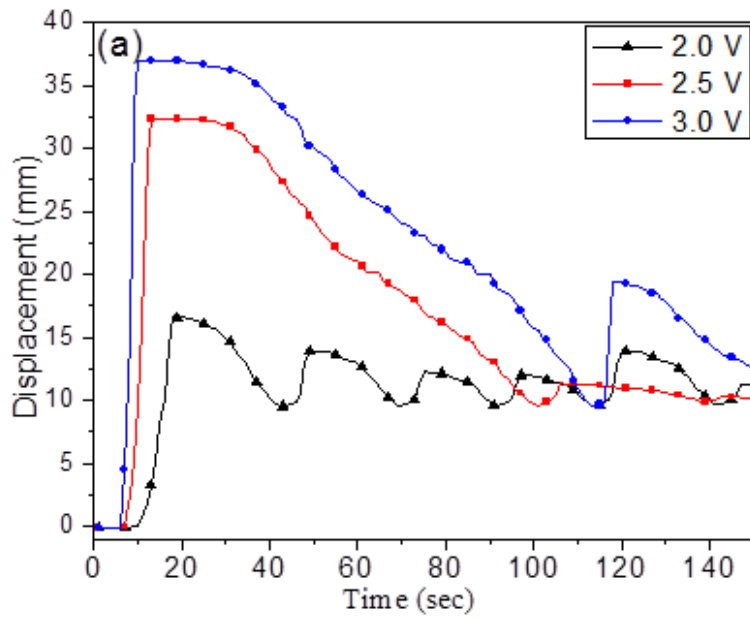
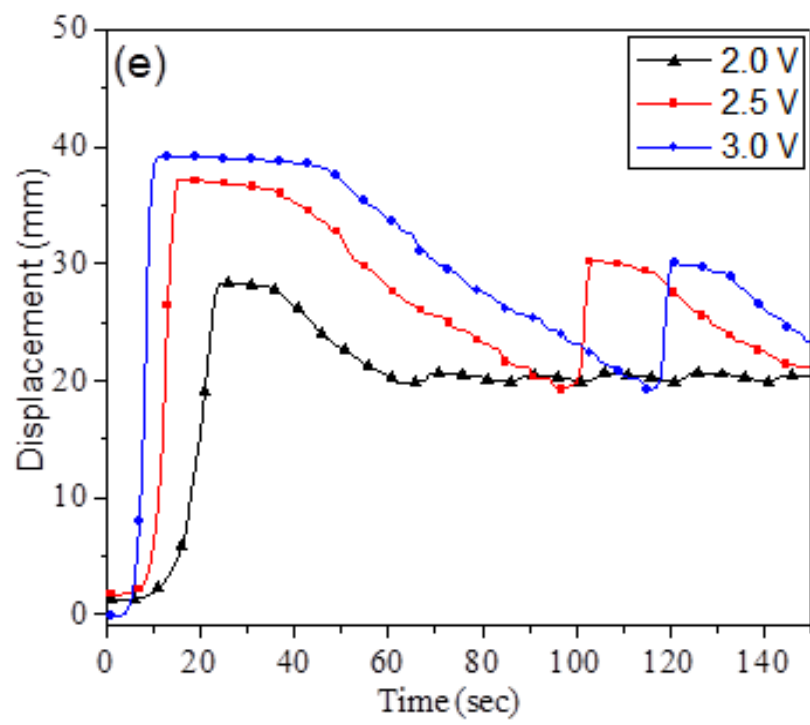
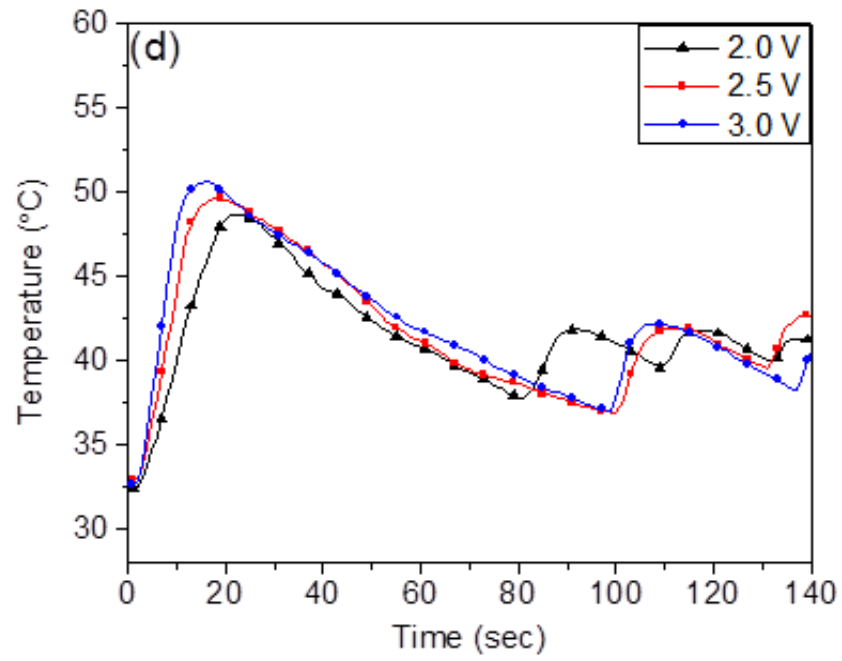


Fig. 3.20: Spring loaded with 3.5 N controlled at 10 mm and 15 mm, and 20 mm for different voltages a) Displacement vs Time curve for controlled position at 10 mm b) Temperature vs Time curve for controlled position at 10 mm, c) Displacement vs Time curve for controlled position at 15 mm, d) Temperature vs Time curve for controlled position at 15 mm, e) Displacement vs Time curve for controlled position at 20 mm, f) Temperature vs Time curve for controlled position at 20 mm

mm is achieved at every voltages after 25 s, for that 60°C - 70°C is required as depicted in Fig. 3.21 (d). In Fig 3.20 (e) shows displacement versus time at a voltage of 2.0 V, 2.5 V, and 3.0 V. when spring is controlled at 20 mm with 3.5 N loads, It was observed that displacement is not precisely controlled as observed in the previous study at 15 mm. Fig. 3.20 (f) shows that temperature is also fluctuating at that time. Therefore, 15 mm was precisely controlled for the 3.5 N loads with different voltages. Further increasing the load showed that the control was better as witnessed at 15 mm. However, the temperature of the spring fluctuated.

The load was increased from 3.5 N to 4.5 N, and three control positions were selected. The time vs. displacement graphs is shown in Fig 3.21 (a, c, e). Its corresponding temperature profile is plotted in Fig. 3.21 (b, d, and f). Since displacement depends on-increment or decrement of voltage fluctuation was observed as seen in Fig 3.21(a), when the control position was 10 mm. The maximum displacement was 15 mm, 32 mm and 37 mm for 2.0 V, 2.5 V, and 3.0 V respectively. In the Fig, 3.21, it can be seen that at controlling time for 10 mm distance of all the voltages were increasing, i.e. 20 s, 80 s and 100 s. However, control is not proper due to fluctuations.





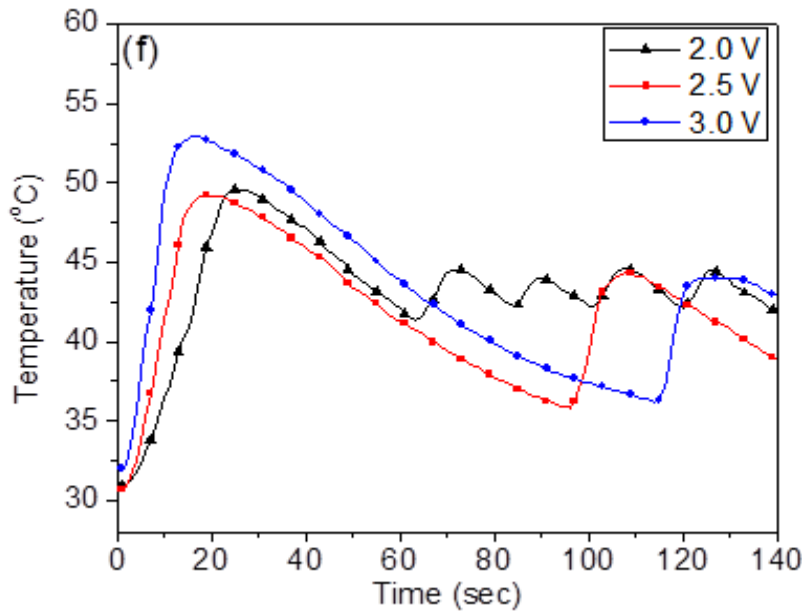


Fig. 3.21: Spring loaded with 4.5 N controlled at 10 mm and 15 mm, and 20 mm for different voltages a) Displacement vs Time curve for controlled position at 10 mm b) Temperature vs Time curve for controlled position at 10 mm, c) Displacement vs Time curve for controlled position at 15 mm, d) Temperature vs Time curve for controlled position at 15 mm, e) Displacement vs Time curve for controlled position at 20 mm, f) Temperature vs Time curve for controlled position at 20 mm

When controlling position was 15 mm and 20 mm, as shown in Fig 3.23 (c) Temperature for all these cases was varying between 40-50 °C due to difficulty in control.

3.3.2 PID Controller: The equation used for control using PID controller is -

$$U(t) = K_p \cdot e(t) + K_i \left(\int_0^t e(t) \right) + K_d \cdot \frac{d(et)}{dt} \dots \dots \dots \text{Eq 3.4}$$

In these equations, K_p is the proportional tuning constant, K_i is the integral tuning constant, K_d is the derivative tuning constant, T_i is the integral time, T_d is the derivative time and error $e(t)$ is the difference between the setpoint $r(t)$ and the process variable $c(t)$ at time t . The process of determining the parameters for PID controller K_p , T_i and T_d to achieve high and consistent performance specifications is known as controller tuning. In the design of a PID controller, these controller parameters must be optimally selected in such a way that the closed loop system has to give desired response [102]. Moreover, the operation of the parameter determination must be performed as fast as possible for a given process.

3.3.2.1 Mathematical Model: A first-order linear transfer function was chosen to model the SMA spring. A step input of 2.0 V was provided to the SMA spring for obtaining the transfer function where the response time and temperature was recorded. The analytical expression for this transfer function is:

$$G(s) = K / (T_1S + 1) \dots \dots \dots \text{Eq. 3.5}$$

Where K is process gain and T₁ is time constant for process

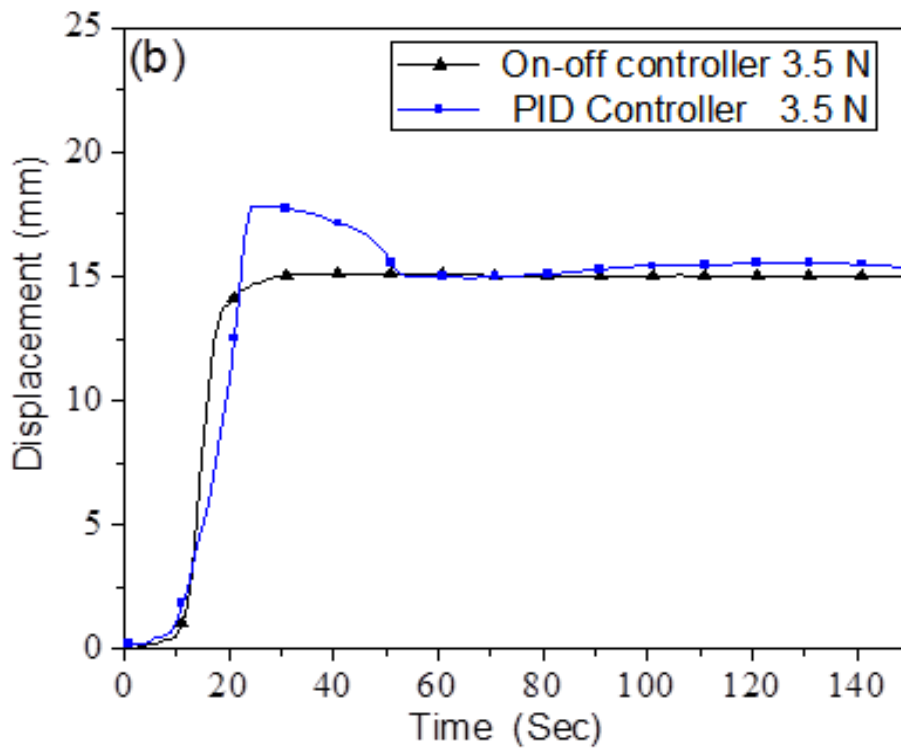
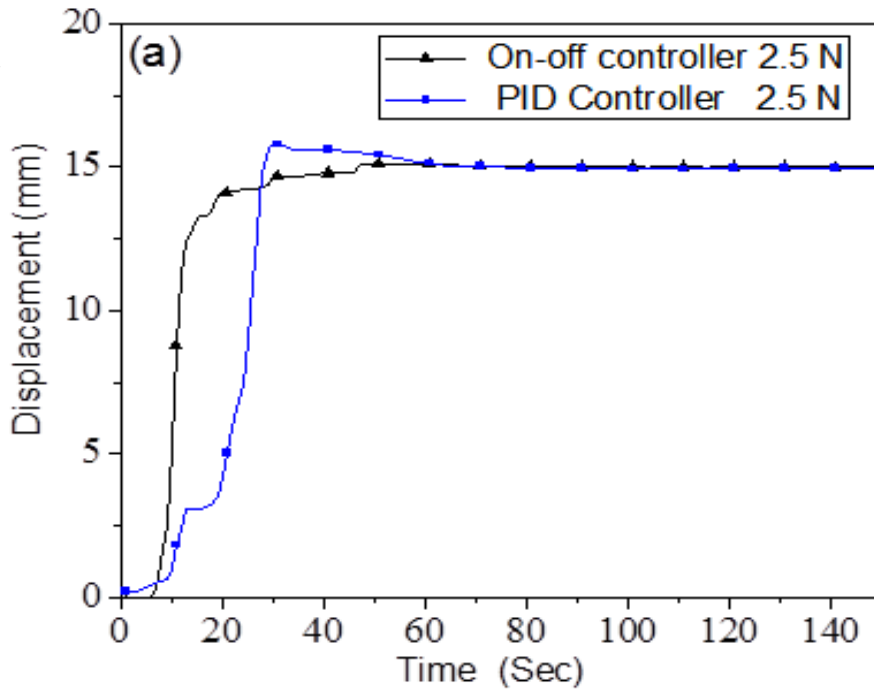
The transfer function of the given SMA spring system was incorporated in MATLAB using the system identification tool. It is to be noted that the transfer functions will change in a different physical setup, where different loads are used as the response behavior will vary.

Hence the values of the constants, fitting the transfer function equation of the system are compiled in Table-3.7.

Table-3.7: Values of Process gain (K) and Time constant (T) for different weights

Weight(N)	K	T ₁
2.5	10.059	1965.5
3.5	10.609	1783.5
4.5	11.16	1602

3.3.3 Comparison of PID controller with the on-off controller: In this section, a comparative study was done for on/off the controller and PID controller when spring was loaded with different weights. The finest control achieved with on/off the controller and the corresponding voltage value was taken as input for the PID controller for comparison. Fig.3.22 (a, b, c) shows 15 mm controlled position at different loads 2.5 N, 3.5 N, 4.5 N



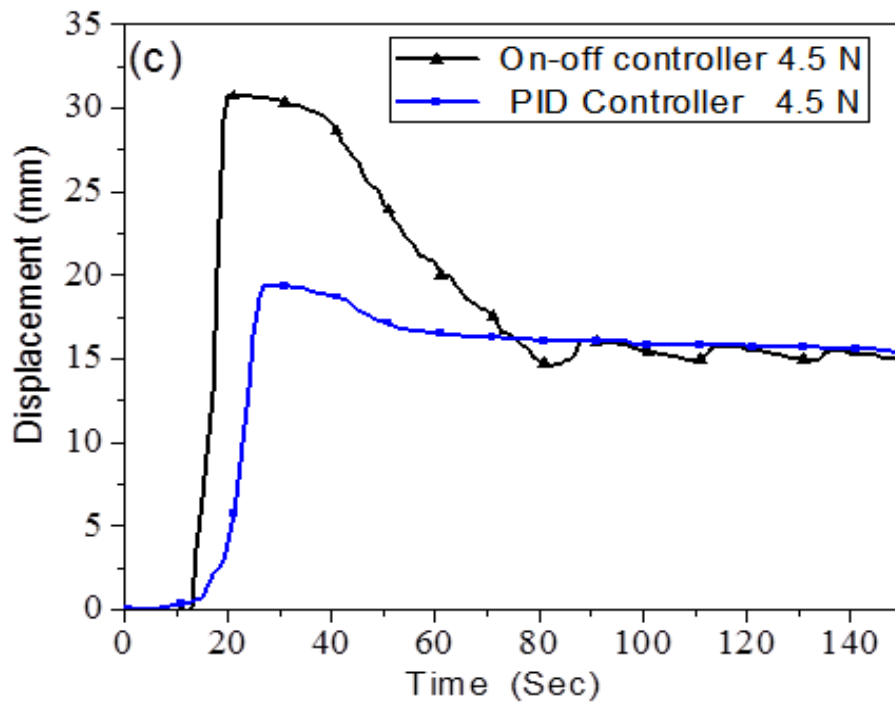


Fig 3.22: Comparison of spring for on/off (3 V) and PID controller when a) Displacement vs time curve when spring is loaded with 2.5 N b) Displacement vs Time curve for loaded with 3.5 N c) Displacement vs Time curve for loaded with 4.5 N

When controlling distance was 15 mm with 2.5 N loading conditions as shown in Fig 3.22 (a) with on/off controller and PID controller, both implementation gives precise control, however at lower loads PID controller needed certain time to gain its control over the spring, which was not in the case with on/off controller. As the load was increased to 3.5 N, the time required increased as seen in Fig 3.22 (b) and it required approximately 32 s for PID controller to gain control. With a higher load of 4.5 N, the overshoot was less with PID controller, and it was much more suitable than on/off the as fluctuations were high and the cyclic behavior as observed Fig 3.22 (c).

3.4 Life Cycle Analysis:

In this study, experiments were performed at three different voltage waveforms of 2.0 V, 3.0 V, and 4.0 V and at an external load of 3.5 N. The spring was assumed to fail when the elongation reaches to 0.1 mm (i.e., critical elongation = 0.1 mm). Ten spring's run to failure experiment was performed at each voltage, i.e., 30 experiments.

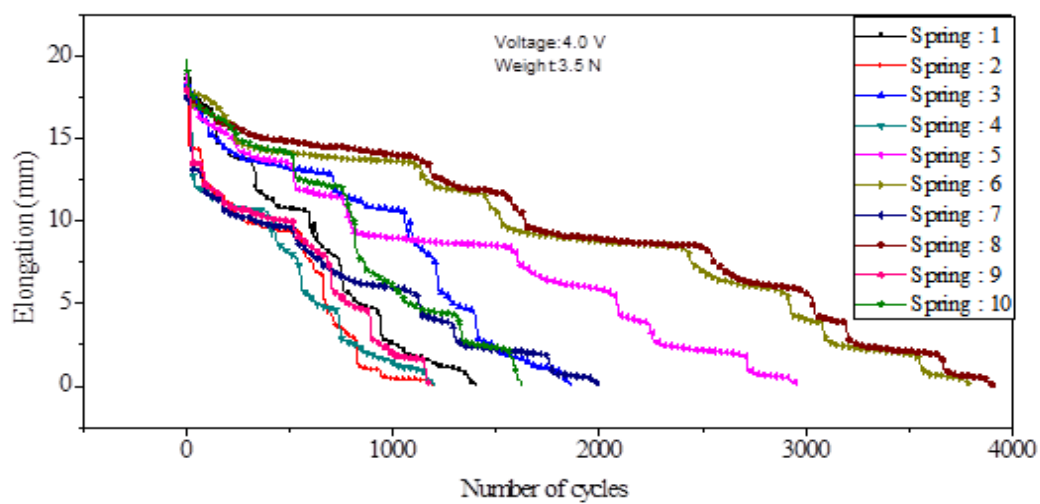
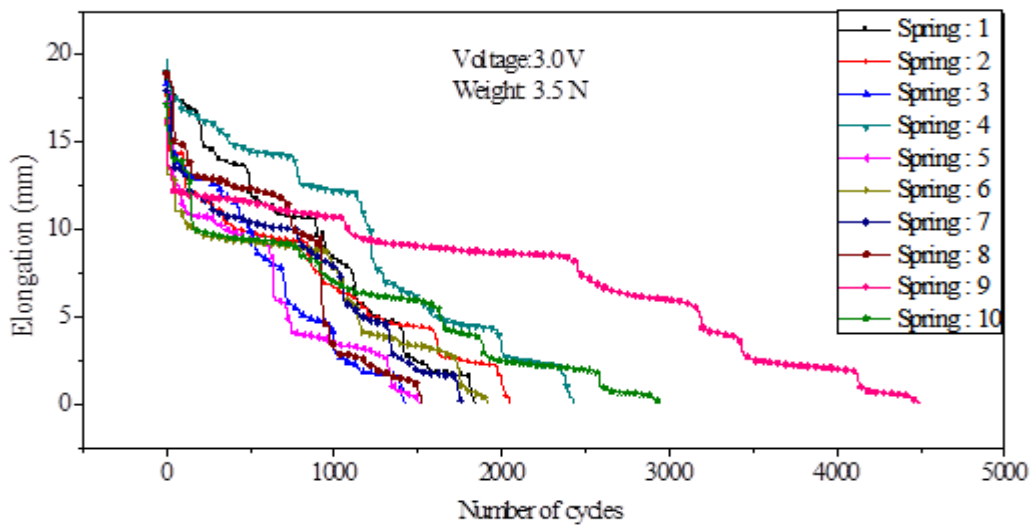
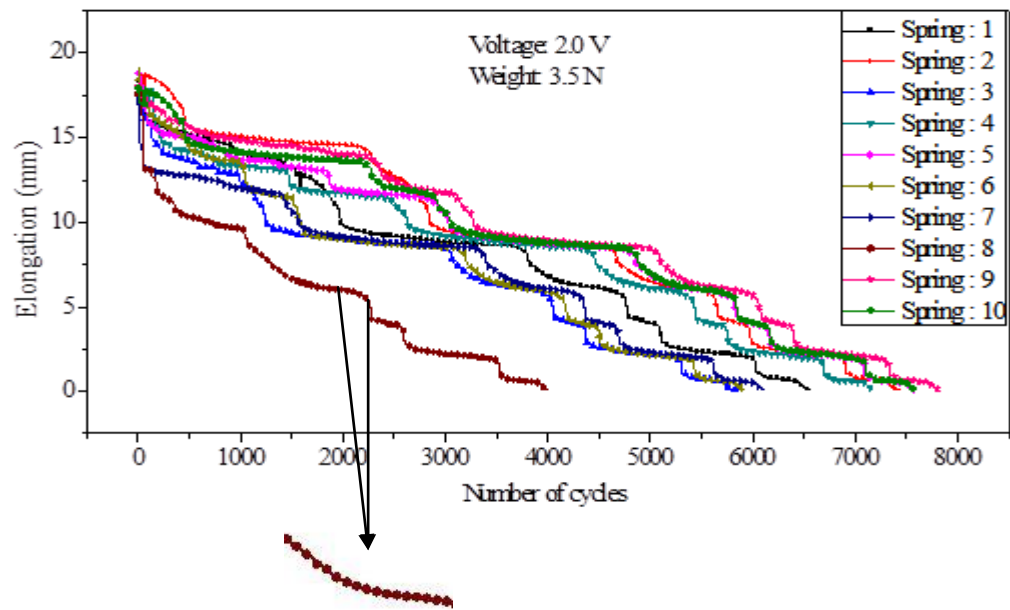


Fig 3.23: Plot showing reduction in elongation with number of cycles

Table 3.8 SMA springs fatigue lifetime data

Spring ID	1	2	3	4	5	6	7	8	9	10
TTF (for 2.0 V)	6560	7432	5824	7168	7564	5912	6100	3996	7808	7584
TTF(for 3.0 V)	1839	2049	1422	2427	1503	1917	1761	1524	4488	2943
TTF (for 4.0 V)	1398	1192	1860	1198	2956	3792	2000	3904	1174	1618

From figs 3.23 of each experimental condition; it was observed that recovery stress or strain in spring is continuously changing with some cycles and this behavior gets stabilize only after some number of cycles. The time to failure obtained for each spring is shown in Table 3.8.

3.4.1 Failure Diagnosis using Morphological analysis: The cause of the spring failure is degradation in mechanical properties; the same is investigated using Scanning Electron Microscopy (SEM) and Thermogravimetric Analysis (TGA). SEM is generally used to carry out the surface morphology of the object. TGA monitors the mass of a substance due to gas release or absorption as a function of temperature as the specimen subjected in a controlled atmosphere.

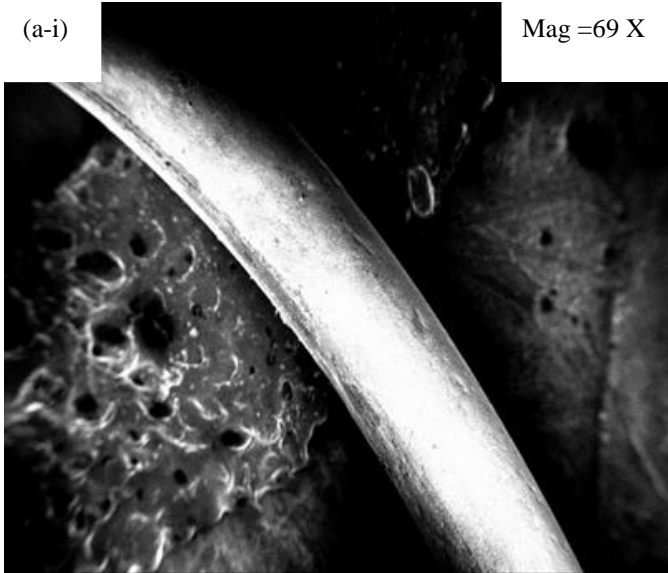
Three different analyses have been carried out here: virgin spring (i.e., run for zero number of cycles), deformed spring (i.e., run for 100 number of cycles) and failed spring (i.e., run till failure). Fig 3.24 shows the obtained image using SEM for all three cases.

From Fig 3.24 (a), uniform surface morphology throughout the length of the virgin spring is observed and with cycles of operation spring is lead to cross the elastic deformation (Fig 3.24 (b) and Fig 3.24 (c)). It means with aging, the material is not able to retain residual strain in it and results in the generation of pores with some cycles. These pores are generally formed during the application of the stimulus. SMA is generally at higher temperature and oxygen is entrapped into it and which ultimately makes the material brittle and leads to failure of the spring. The same phenomenon has been investigated using TGA analysis.

So, from TGA and SEM it can be concluded that failed spring has the higher oxygen entrapment which results in retardation in actuation of the SMA spring.

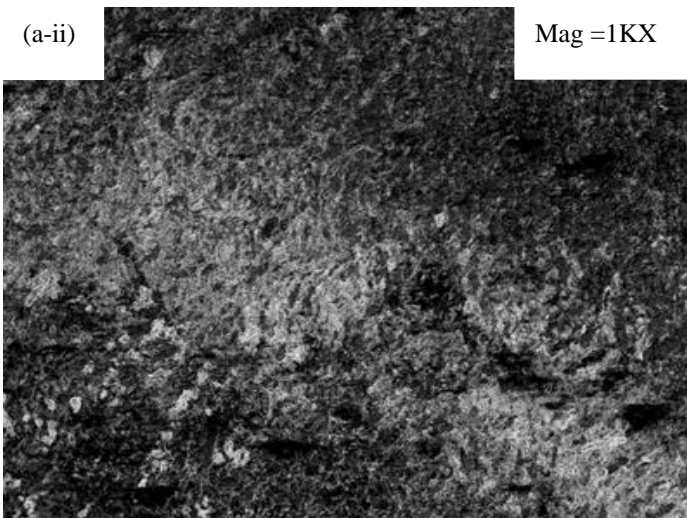
(a-i)

Mag =69 X



(a-ii)

Mag =1KX



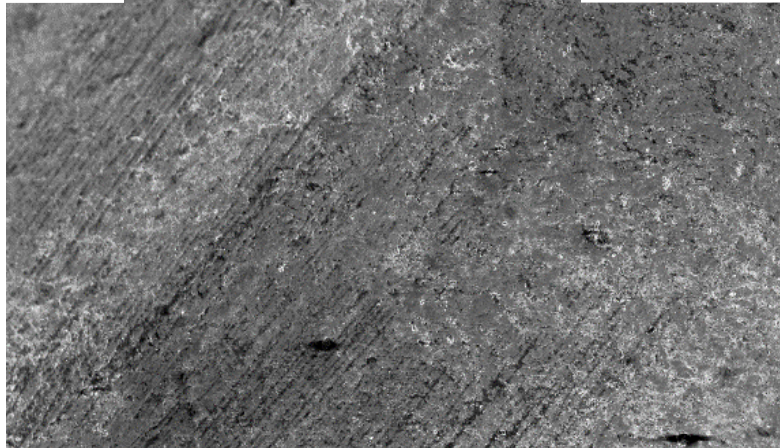
(b-i)

Mag =69 X



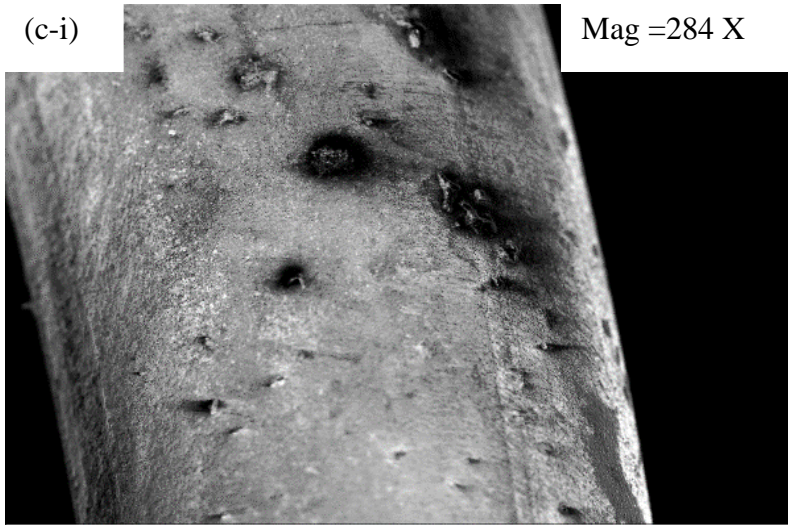
(b-ii)

Mag =1KX



(c-i)

Mag =284 X



(c-ii)

Mag =1KX

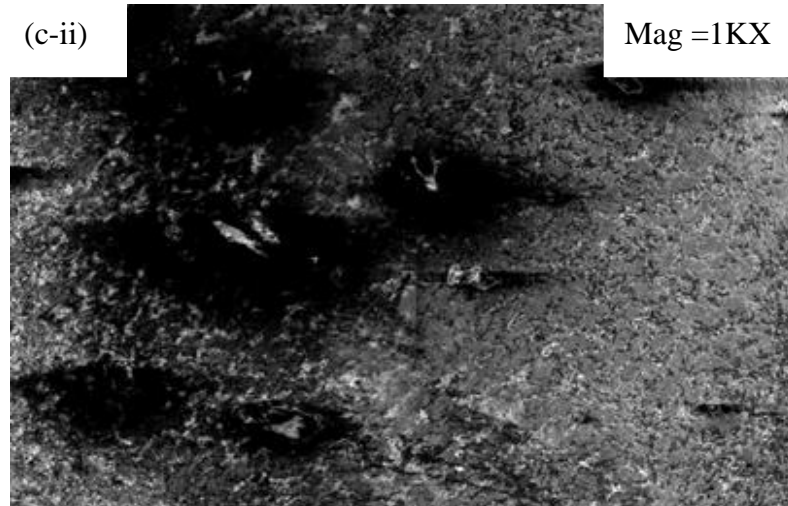


Fig. 3.24: SEM image of the surface of the SMA spring (a) Non-Treated spring (b) deformed spring (c) failed spring

The TGA plot (Fig 3.25) shows the percent mass as a function of sample temperature. During analysis, the samples are put inside the furnace in an inert atmosphere. All samples were heated to 300° C from room temperature with a heating rate of 10° C/ minute. From TGA plot, it can be seen that the failed spring loses the material concentration with the temperature which indicates the accelerated melting in comparison of Non-Treated spring. Because in failed spring, oxygen gets entrapped inside the alloy, which ultimately leads to break the bond between Ni and Ti and material gets removed at high temperature during TGA from failed spring.

Furthermore, Ti is responsible for the oxidation formation inside the alloy; because Ti has the great affinity to react with the oxygen as a comparison to Ni. Also, from the periodic table, as we go across a period, the nuclear charge will increase; whereas the energy level will stay the same in the same period. It means there is a stronger and stronger attraction for the electrons for the metal which is farther in the periodic table as compared to the nearest metal. Thus, it is more and more difficult to lose electrons and consequently the reactivity of the metal decreases as we go from left to right across the periodic table.

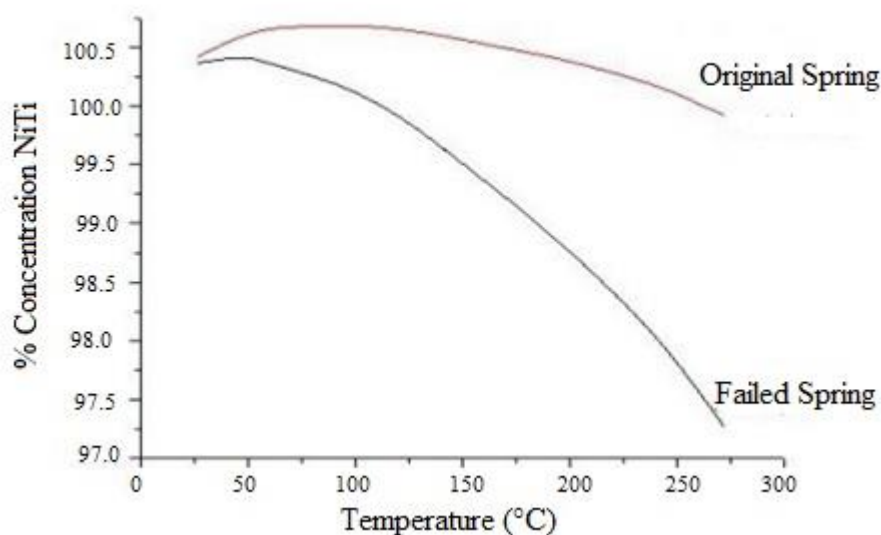


Fig 3.25 : TGA results comparison between virgin and failed spring

As Ti has atomic number 22 and Ni has atomic number 28, it means based on the reason explained in above paragraph Ti is more reactive than Ni.

Consequently, Ti has great affinity to react with the oxygen and generally forms TiO_2 or TiO_4 .

3.5 Verification of displacement using Talbot Interferometer:

Various methods are available for the displacement measurement and life cycle analysis of the SMA spring based on inductance, resistance, load change, etc. Aguiar et al. [117] reported the displacement measurement using resistive displacement transducer. Costanza et al. [118] described a method in which a metallic base with a ceramic guide fixed inside has been adopted for the characterization and cyclic experiments of the springs. Ikuta et al. [119] developed a displacement control system for SMA spring actuators using resistance for estimating the displacement. The author described good position-control characteristics over a broad range of strain. After that, many researchers have used resistance feedback control in different applications. [120]

Interferometric techniques are accurate, precise and provide the highest sensitivity [121]. With the recent developments in the area of optoelectronic detection and storage, it is easy to process the data in real time. Interferometric techniques depend on measuring the phase change when the light passes through the specimen. This phase change is a function of the measurement variable. However, these techniques are sensitive to environmental perturbations too. To overcome this limitation, the use of shearing interferometers in measurements has been proposed. The shearing interferometers are common path interferometers, and hence the effects of environmental perturbations cancel out.

Talbot interferometer is one among several commonly used shearing interferometers. It uses diffraction grating as the shearing element. Talbot interferometry is stable, inexpensive and compact with a simple design. It is widely used in many engineering applications [122-126]. In these interferometers, the test and reference wavefronts are sheared and made to interfere with each other. The experimental arrangement is arranged such that when the spring is in the unloaded condition, the mirror attached to it is located at the at-focus position of the lens. As the spring is displaced because of the applied load, the position of the mirror relative to the lens varies. The

defocusing errors generated because of the displacement is analyzed using the double grating configuration. The orientation of the moiré fringe formed is proportional to the displacement

3.5.1 Principle: Fig 3.26 shows the schematic of Talbot interferometry. When a grating with period ‘p’ is illuminated by a collimated coherent beam, the Fresnel diffraction pattern generate its self-image without a lens, at a distance,

$$Z_T = \frac{mp^2}{\lambda} \dots \dots \dots \text{Eq 3.6}$$

Where ‘m’ is an integer, ‘p’ is the pitch of gratings and ‘λ’ is the wavelength of light.

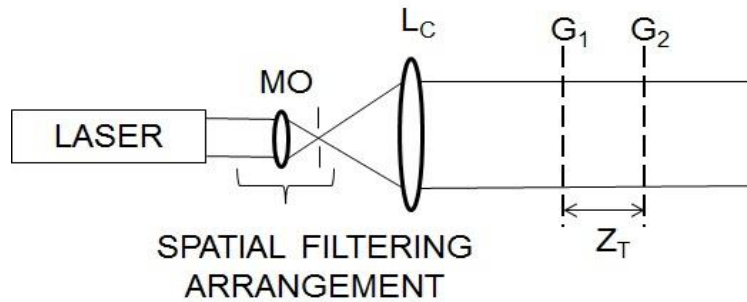


Fig 3.26: Basic principle of Talbot interferometer

The self-image is called Talbot image, and the distance between the grating and its self-image is called Talbot length. Previously, Prakash e. al. reported the collimation testing using double-grating shearing interferometry [127]. In the reference, authors reported the correlation between the defocusing of the lens and angle of orientation of moiré fringes, and report high accuracy (0.1%) in the determination of defocusing distance using the principle. The principle has been extended for the measurement of displacement drift of the SMA spring. The relationship between the defocusing distance (Δd) and the angle of orientation of fringes (∅) is given by,

$$\Delta d = \frac{2 \tan \emptyset \cdot \tan \left(\frac{\emptyset}{2} \right) \cdot d^2}{Z_T} \dots \dots \dots \text{Eq 3.7}$$

where,

∅ is the angle of orientation of fringes,

θ is the angle between two gratings,

L is the focal length of lens L_D

and Z_T is the Talbot distance

In this case, the defocusing distance relates to the displacement drift of the SMA spring. Fig. 3.26 shows the schematic of the experimental arrangement for determining the displacement of the SMA spring using Talbot interferometry. It is explained in detail in the next Section.

3.5.2 Experimental Arrangement: The experiment for the life cycle analysis of SMA spring is performed in two stages. In the first stage, the five different SMA springs are electrically actuated for 1000, 2000, 3000, 4000 and 5000 cycles with the actuation mechanism consisting of data acquisition system (Model: Agilent 34970A) and programmable power supply (PPS) (Model: Rigol DP 1308A). In the stage, the displacement drift of SMA spring is measured using Talbot interferometry. After going through the repeated cycles, there occurs deterioration in the SMA property, and the spring loses its ability to return back to its un-stretched condition fully on the application of the actuation potential. Because of this, there induces a drift in the displacement value measured. To measure displacement drift of the springs, Talbot interferometer has been used. The schematic of the experimental setup is shown in Fig 3.27. The light from 15 mW He-Ne laser having wavelength 6328 nm is passed through the microscopic objective (MO) of 60X and the pinhole of size 5 μm to get uniform illumination. The light is then allowed to fall on collimating lens L_C of 250 mm focal length. The collimated light is then passed through the 50-50 beam splitter (BS).

The directly transmitted beam after passing through the focusing lens L_D is incident onto the plane mirror, kept at the focal plane of the L_D . One end of the SMA spring is fixed, and the other end is attached to a 1N load. From the spring a lightweight mirror is also attached. Initially, the mirror is so positioned that it is exactly at the 'at-focus' position when the spring is in unloaded condition. The back-reflected light from the M is reflected by the beam splitter BS and is incident on the set of two Ronchi gratings G_1 and G_2 of period 2lines/mm placed at the Talbot distance. It forms the fringe pattern at

the charged coupled device (CCD) plane. CCD has 1392×1040 pixels with each pixel sized $4.65 \times 4.65 \text{ mm}^2$.

After application of a load of 1.0 N on the pulley, the spring gets elongated, and the mirror moves to the in-focus position of the lens. On application of power supply of 2.0 V and 2.0 A the spring is actuated which results in the position corresponding to the un-stretched position of the spring. Initially before stretching original spring is used; the un-stretched position is set as ‘at focus’ position and this position is treated as a reference for other springs. The process is repeated for the springs actuated for 1000 to 5000

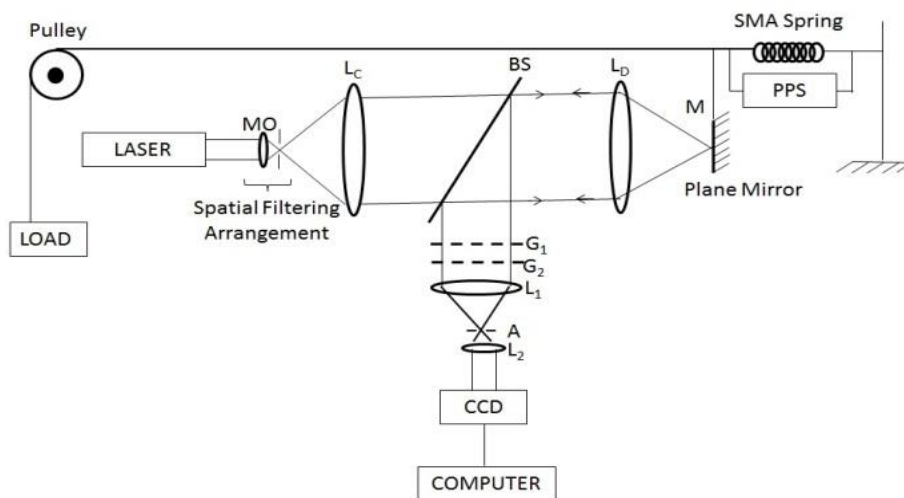


Fig 3.27: Experimental Arrangement for measurement of displacement drift

cycles. But, on application of power supply, the spring does not return to its original un-stretched position due to the displacement drift, and hence the oriented fringes are obtained. Hence, the difference between the at-focus position and in-focus position of the mirror equals the displacement drift of the SMA spring.

3.5.3 Result and discussion: The experiment was performed with five different springs to measure the displacement drift using Talbot interferometry. Initially, the original un-stretched spring is attached to the mirror, it is set at a ‘at-focus’ position of the defocusing lens and hence the horizontal fringes are obtained at CCD plane as shown in Fig. 3.28 (a). This setting is considered as a reference for further observations. In next step, the SMA spring actuated for 1000 cycle is used in place of original un-stretched SMA spring and loaded with 1.0 N load. On application of power supply, the spring gets actuated, but did not return to its reference position due to

deterioration of SMA property and mirror moves towards ‘in-focus’ position of the lens L_D , hence fringes oriented as shown in Fig 3.28 (b) are obtained. The procedure is repeated for four other SMA springs. Fig. 3.28 (c) shows the fringe pattern obtained when the SMA spring actuated for 5000 cycle is used.

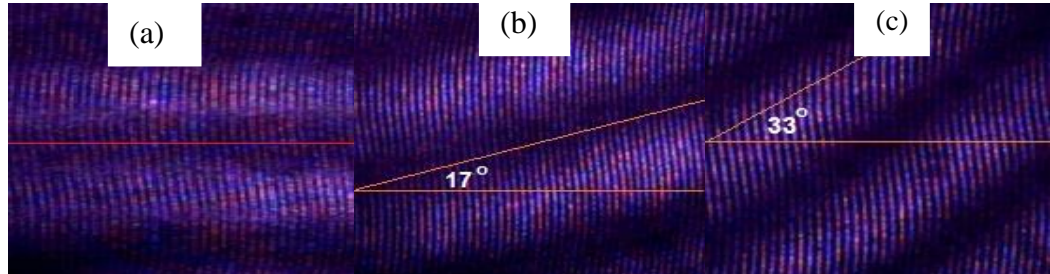


Fig 3.28: Fringe pattern obtained when the mirror attached to the spring is kept at a) at focus, b) In focus (1000) cycles, c) In focus (5000) cycles position of the focusing lens

The angle of orientation of fringes is a function of displacement drift. It is observed from Fig. 3.28 (b) and 3.28 (c) that the inclination angle of fringes increases as the number of cycles increases. Fig 3.29 shows the plot of displacement drift with respect to number of cycles. It is observed that the displacement drift increases as the number of cycle increases. It also shows that the spring gets deteriorated after multiple uses which indicate the setting in fatigue inside the springs. As in any other measurement system, measurements are affected by errors.

Table 3.9: Displacement drifts of SMA spring using Talbot interferometry after the completion of actuation cycles

Sr. No.	Number of cycles	Angle orientation of fringes (Degree)	Displacement drift (mm)
1	1	0	0
2	1000	17	0.875
3	2000	24	1.275
4	3000	27	1.459
5	4000	31	1.720
6	5000	33	1.859

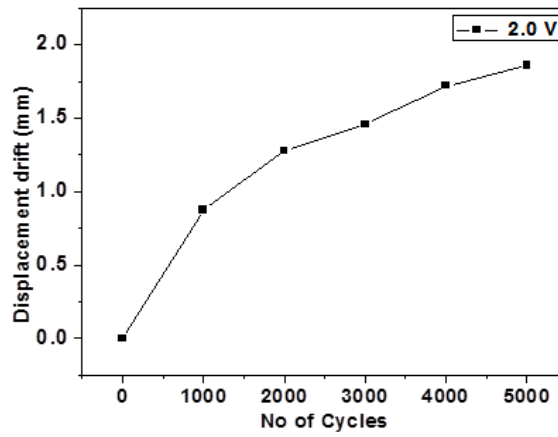


Fig.3.29: Displacement drift vs number of cycles

A brief discussion on the sources of errors looks pertinent. The errors are introduced due to finite imperfections/tolerances in mechanical components; aberration of lenses etc. There are errors due to source instabilities and detector nonlinearities also. The error in positioning and integrating mirror and gratings to the interferometer system is also there [128]. Distortions of the mirror can also degrade the fringe contrast in the interferometer and cause measurement errors. The mirror used has a local flatness of $\lambda/10$ yielding maximum error of 63 nm due to surface imperfections (manufacture's specification). The mirror misalignment does affect the measurement accuracy. To check the mirror alignment due care has been taken by setting and matching the direction of light reflected from the mirror to the optic axis in the interferometry system.

3.6 Developed Micro-Devices:

Miniaturized mechanical and electro-mechanical elements come in the category of Micro-Electro-Mechanical Systems, or MEMS, (i.e., devices and structures) that are made using the techniques of micro-fabrication. The critical physical dimensions of MEMS devices can vary from well below 1.0 μm on the lower end of the dimensional spectrum, all the way to several millimeters. Likewise, the types of MEMS devices can vary from relatively simple structures having no moving elements, to extremely complex electromechanical systems with multiple moving elements under the control of integrated microelectronics. Some microdevices are developed using sheet and spring whose fabrication and experimentation is described in detail:

3.6.1 For Micromachining Applications:

3.6.1.1 Stewart Platform: The most novel mechanism used for flight simulators and position maintaining is Stewart platform or parallel manipulator. It is a classic example of a mechanical design that is used for positioning and orientating the platform concerning a fixed base. The main application is to fulfill the requirement of high load carrying and precise positioning capability. Most of them available are actuated with hydraulics and pneumatics whose drawback is the control of the position. The same platform can be used for the position control in other applications. Traditional actuators such as electric motors, hydraulic pump, and pneumatic necessitate the use of large and heavy supported and are usually very noisy. Electric motors are bulky, revolve at very high revolution in which reduction gear is required to produce needed torque [129]. In recent decades, the parallel mechanisms have become attractive because they exhibit advantages in the manufacturing accuracy and speed. This plays an important role in developing the micro-scale positioning platform. Researchers have investigated several positioning platforms based on a parallel mechanism and emphasized the advantages of a parallel mechanism in the precision positioning field [130]. Authors have designed and conducted experiment on the stiffness of a platform consisting of several flexure hinges [131]. Authors have reviewed a parallel manipulator platform based on the Stewart–platform [132]. Various arrangements for Stewart platform have been studied to understand the behavior of platform. In this work developed Stewart platform is explained and experimentation of SMA spring performance was carried out to find important data such as speed of contraction, the minimum and maximum weight that can be lifted and operating conditions. Fabrication and construction process of the platform using SMA spring actuators was based on analysis of the experimental results. In the upcoming sections design, fabrication, experimentation and control strategy is discussed in detail.

The conventional Stewart platform developed through hydraulic actuators [133], pneumatic actuators [134] and servo motor [135]. The hydraulic actuators are large in size which can exert large force and fluid leakage is a major drawback. The maintenance cost of hydraulic system is higher. The

pneumatic actuators are faster and clean. It is limited with generating constant speed to control movement of bodies and has low accuracy. It is difficult to perform at slow speed. Servo motor technology provides great variety of advantages over other conventional actuators. It can provide better accuracy and repeatability. However the cost of this is high.

SMA based Stewart platform reported so far is involve complicated design, and provide very limited displacement [136-138]. This limits the development of miniature Stewart platform. There are only few studies reported on the development and performance analysis of SMA based miniature Stewart platform. In this work, SMA spring based smart Stewart platform design is proposed which can replace the conventional actuators. The proposed design has simple mechanical structure and light weight when compared to conventional actuator based Stewart platform. The proposed design has three Degrees of freedom (DOFs), two of which enable the Stewart platform to rotate in x- and y-axis while the third DOF is responsible of moving the platform in z-axis. The construction of this device involves a platform, a base platform, and four limbs with identical dimensions. Each limb consists of a bias spring and an SMA actuator. The SMA actuator and bias spring placed coaxially to perform the 3 DOF motion. Developed Stewart Platform has been taken after Kinematic analysis (Fig.3.30), which is explained below:

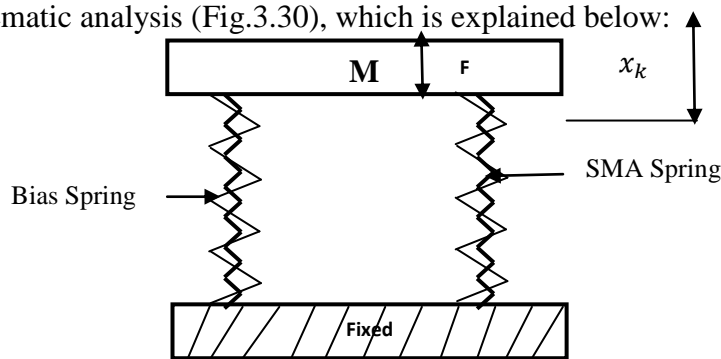


Fig.3.30: Model of Stewart Platform using Mass Spring System

Assumption: The system is Undamped

b = 0, The second order ODE is

$$F = m\ddot{x} + b\dot{x} + kx$$

Where, F = overall force, M = mass of the platform, x= displacement

$$F_k = (-x_k * K_{SMA}) + (-x_k * K_{Bias})$$

Where,

F_k =force exerted by the springs (Both SMA spring and Bias spring)

K_{SMA}, K_{Bias} =Spring constant

$$K_{SMA} = K_{s1} + K_{s2} + K_{s3} + K_{s4}$$

$$K_{Bias} = K_{B1} + K_{B2} + K_{B3} + K_{B4}$$

$$m\ddot{x} = \sum F = -F_K + F$$

$$m\ddot{x} = ((-x_k * K_{SMA}) + (-x_k * K_{Bias})) + F$$

- **Kinematic Model:** The proposed Stewart platform consists of 3 degrees of Freedom (DOF). One translation in z direction and two rotational x in and y directions.

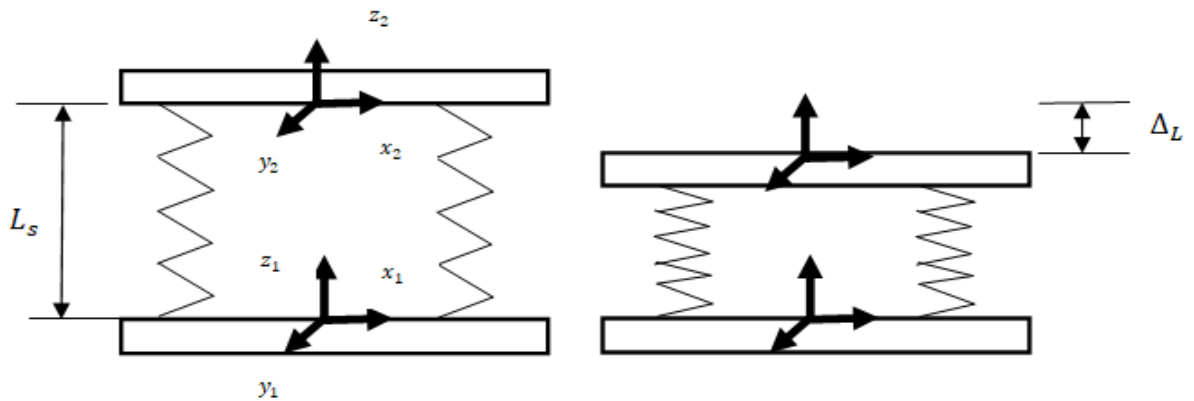


Fig.3.31 Kinematic model for the Translational movement

Translation with respect to z axis

$$z = L_s - \Delta_L$$

Where, z=translational displacement with respect to z axis

L_s = Length of the spring

Δ_L =Change in the length of the spring

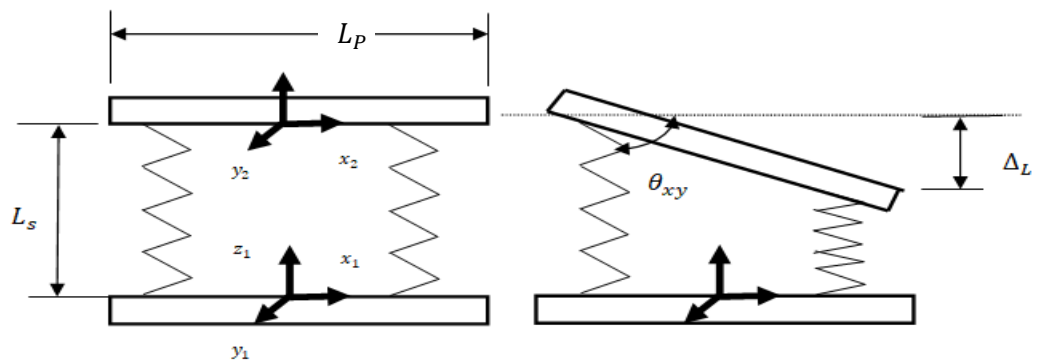


Fig. 3.32 Kinematic model for the rotational movement

Rotational with respect to in x and y axis

$$\theta_x = \sin^{-1}(\Delta_L/L_P)$$

$$\theta_y = \sin^{-1}(\Delta_L/L_P)$$

Where,

L_P = Length of the platform

θ_x = Rotation angle with respect to x axis

θ_y = Rotation angle with respect to y axis

3.6.1.2 Design and principle work: The design of the Stewart platform is developed in a mini scale of 50*50*8 mm³ and attain three degrees of freedom with rotation on x and y-axis with 4 mm and prismatic in z-axis with 3 mm. The platform consists of four similar SMA and four biased springs coaxially. The resolution of the system is estimated to be around 0.2 mm, and accuracy is up to 0.5 mm. The springs are hinged at both ends of the platforms. One side of the platform is fixed like a cantilever beam. The platform is designed in a CAD model with hooks for mounting the springs and converted to stereolithography format for 3D printing (Fig 3.33). The bottom platform is hinged with the table, and SMA springs are mounted first into the designed hooks. Biased springs are installed coaxially with SMA springs and wires are commonly grounded, and the positive supply pins are connected to separate relays for the control for actuation for its actuation.

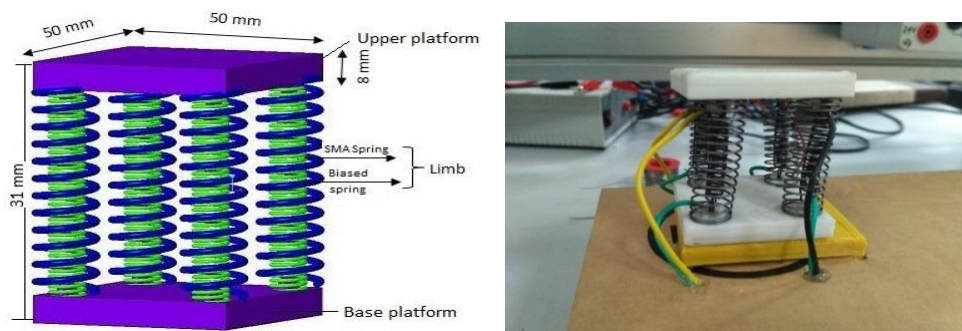


Fig 3.33: Stewart Platform a) Design and its nomenclature, b) Fabricated Stewart platform

3.6.1.3 Experimentation: Fig. 3.34 shows the experimental setup with its components and connections. They work in a synergic way for the desired output. The serial communication between Arduino, DAQ and PPS is done. The signal for actuation is synced for all the devices. The control of relay through Arduino to the SMA spring is switched by the GUI interface in the Lab-view Program.

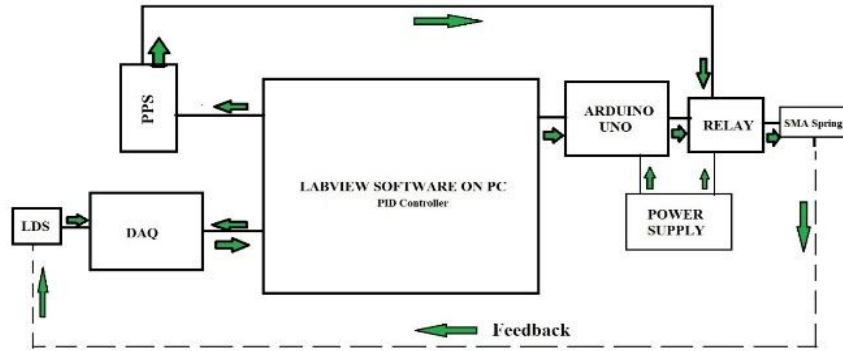


Fig 3.34: Line diagram of Experimental set up for actuating micro-positioning stage

The LDS gets the feedback, and the data is simultaneously recorded in 200 ms time interval. The power supply is attached to the relay and Arduino because they cannot be operated in the same potential for actuating the spring. The selection of springs to be actuated using the Arduino. The centralized system which is an integrated computer with a graphical user interface (GUI) which the Atmel 328p in Arduino, PPS, and DAS are connected.

The master command is from the GUI and the components connected acts like a slave. All the communication is done through a serial communication cable with different Baud rates. The actuation command is given from graphical user interface for the Arduino, PPS, and DAQ at the same time. The Laser displacement sensor (LDS) is connected to the DAQ for feedback.

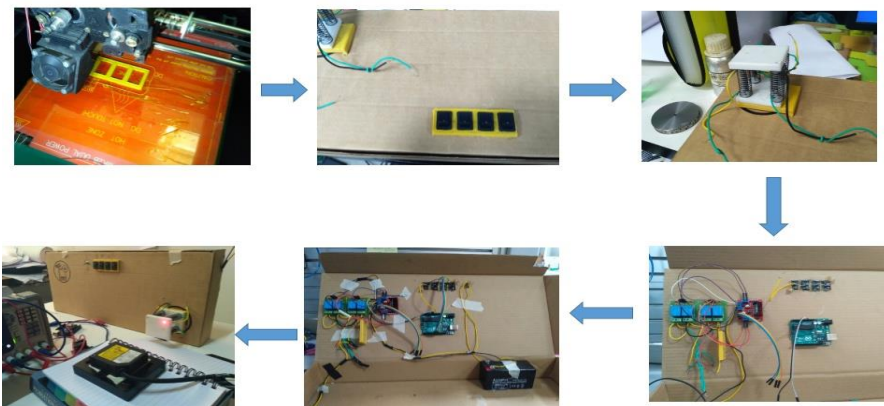


Fig 3.35: Fabrication of Experimental set up for actuation

The GUI will supply analog signal for the PPS for the current parameter control. The maximum output range from the PPS will be 3.0 V and 1.3 A for the actuation. It is sufficient to Joule heat the spring for actuation.

Fig 3.35 shows the steps for fabrication of set up. The on-off controller is embedded with GUI for the control of current. The actuation tilt and movement of the platform due to the degree of freedom. The biased spring which acts as a load for making the SMA back to the position after the heat dissipation in natural cooling.

3.6.1.4 Experimental Result: To apply SMA spring actuator repeatable behavior is very important. The application mentioned above are driven by electric current and controlled LDS feedback. To measure the thermal cyclic behavior of SMA wire actuators it is required to heat the SMA spring many times while measuring the response. A thermal cycling test bench was developed for continuously monitoring the various parameters. Requirement for actuation of single SMA spring is 3.0 V and 1.3 Ampere. Experimentation is done for multiple cycles out of which only 5 cycles have been presented. Displacement and temperature corresponding to time plot have been shown in Fig 3.36 (a) and (b). Maximum 3 mm displacement is achieved for SMA spring after implementing on-off controller. Hysteresis curve for first cycle is shown in Fig. 3.36 (c).

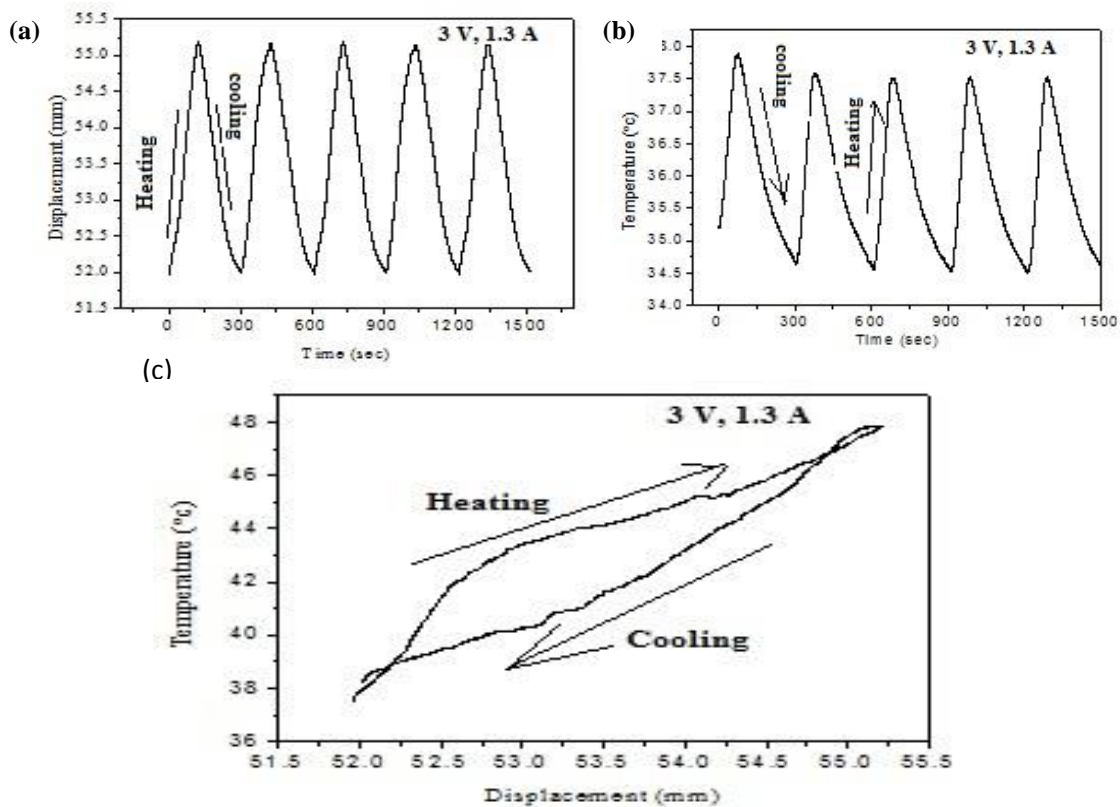


Fig 3.36: Plot between a) Displacement vs time, b) Temperature vs Time and c) Hysteresis curve

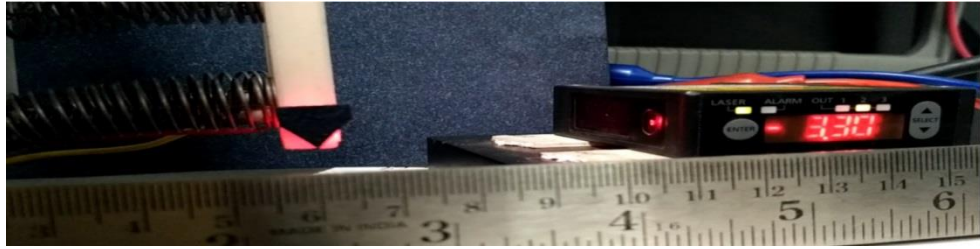


Fig.3.37: Monitoring of displacement using LDS

When one SMA is activated (within 120 s), the opposite SMA that is already in a high temperature produces a larger resistive force. Thus to reach to the same negative deflection as the previous case the passive spring should cool off reasonably. The cooling time, however, is longer, and it takes about 180 s which is almost three times longer than heating. The variation of the module's displacement when an external load is applied demonstrates the flexibility and low stiffness of the module. This property may be very useful in the application of the module in stages. The platform uses 12 A for actuating the springs at the same time, but for control constraints, the platform is given only 5 A for all four springs. The average response time of the system is less than 3 s for different temperature environment. One leg at the time is actuated for higher displacement in a particular direction and two for a controlled direction with a limit. The combination of legs actuated in a sequence makes them to move in the desired path. The on-off controller is implemented because the system is highly nonlinear, so to reduce the errors in the open loop system the closed-loop control system takes the role to rectify it.

3.7. Summary: This chapter can summarize in few points:

- A comprehensive study has been done with varying parameters such as load (2.5N, 3.5N and 4.5N), voltage (2.0V, 3.0 V and 4.0 V) and positions (10 mm, 15 mm, 20 mm) to understand the thermo-mechanical behavior of NiTi SMA Spring.
- The transformation temperature was found to be in the region of 25°C – 80°C, as observed from the hysteresis plots. on/off controller was primarily employed for experiments.

- It was observed, the control was better at lower loads such as 2.5 N and 3.5 N with position control at 15 mm. Temperature of the spring was drastically increasing when the control was better.
- Another position control was not vastly precise with fluctuations at regular intervals. The results was compared with PID controller, where it was further demonstrated that on/off controller was advantageous than PID controller.
- Therefore a position control up to a maximum 5 mm can be realized with the help of on/off the controller. However with higher loads or larger elongation of the spring, requires PID controller to have precise control.
- On the application point of view stewart platform (using NiTi spring) has been fabricated and analysed. Life cycle analysis is also investigated through Talbot interferometry technique
- Heat transfer analysis is also done and it is compared with its experimental results.
- All the above said results are verified through morphological analysis.

Chapter 4

Hot Water Actuation of SMA spring

Chapter 2 identified that the review of hot water actuated systems entirely includes literature. Thus, on that basis, this chapter intends to develop experimental set up for actuation of shape memory alloy (SMA) spring using hot water. Moreover, a comprehensive performance investigation has been carried out to analyze the robustness and implications of developing a heat engine. It is verified through characterization technique and simulations.

4.1 Introduction:

The section explains the optimal design and analysis of hot water actuated SMA spring. Smart materials exhibit unique properties that make them a preferred choice for industrial applications in many branches of engineering. The beneficial properties of a NiTi piece can be improved by altering the energy source. With hot water actuation, as the temperature reaches 70°-90°C, spring gets fully compressed for the first few cycles followed by a loss in actuation. The actuation loss is then studied with different characterization methods such as Thermo Gravimetric Analysis (TGA) and Scanning Electron Microscopy (SEM). With SEM results, it can be strongly recommended that the energy source is sufficient for actuation (not affecting too much the structure). Results observed from TGA shows high oxygen content at a lower temperature, suggest the need for conducting experiments in an inert atmosphere. In addition to this, the application of hot water actuation is some micro-devices such as a micro valve for drug delivery application, and heat engine is also explored.

4.2 Experimental set up:

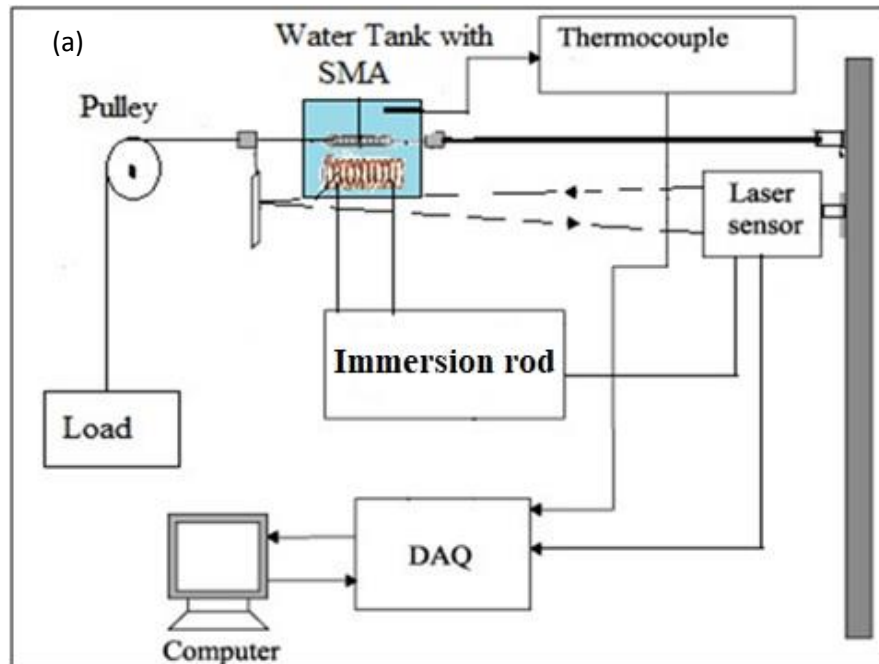
The test setup is developed to perform experiments based on the medium used. It comprises of an actuation unit and a displacement sensing unit with a load pulley arrangement. Nitinol spring which is equiatomic is used with specifications

as described in Table 3.1. Heating-cooling cycle is defined based on the time when steady state is achieved.

NiTi SMA Spring which is equiatomic is actuated using hot water. An immersion rod is used to heat the water kept in the container (Fig 4.1) which in turn supply thermal energy to the spring. The temperature imparted to the spring with this thermal energy when reaches the transformation limit, in turn, actuates the spring. However, the actuation was not linear indeed drastic. Spring is held fixed at one end and at the other end load is applied.

Data from LDS is measured voltage with the help of a data acquisition system, and then the reading can be seen on the system. To generate a displacement, hot water is poured in the container and then cooling is done through natural convection.

- During heating, the martensite changes to austenite; the length of the spring reduces, and the mass moves upward.
- During cooling, the austenite changes to martensite; the length of the spring increases and the mass moves downward.



The heat transfer in fluids, either free or forced convection, is governed by Newton's law of cooling.

$$q = h_c A dT \dots \dots \dots Eq. 4.2$$

where ' h_c ' is the heat transfer coefficient, ' A ' is the surface area and ' dT ' is the temperature difference between the surface and fluid. The motion of fluid through or over the domain is considered to be a laminar flow. The laminar flow is governed by the Navier Stokes equations and continuity equation.

Navier Stokes equation stands for the conservation of momentum, where the inertial force is equal to the summation of the pressure, viscous and the external force applied to the fluid [139]. For a time-dependent problem, the Navier Stokes equation is given by

$$\rho \frac{\partial v}{\partial t} + \rho (v \cdot \nabla) \cdot v = \nabla \cdot [-p \cdot I + \mu (\nabla \cdot v + (\nabla \cdot v)^T) - \frac{2}{3} \mu (\nabla \cdot v) \cdot I] + F \dots \dots Eq. 4.3$$

where ' v ' is the velocity of the fluid, ' p ' is the pressure applied to the fluid, ' ρ ' is the density of the fluid, ' I ' is the identity matrix, ' F ' is the external force and ' μ ' is the dynamic viscosity of the fluid.

The continuity equation represents the conservation of mass

$$\frac{\partial \rho}{\partial t} + \nabla \cdot (\rho v) = 0 \dots \dots \dots Eq. 4.4$$

In conjugate heat transfer, the heat lost due to the conduction compensates the heat gained due to the convection. Thus for a time-dependent conjugate heat transfer, the governing equation is given by,

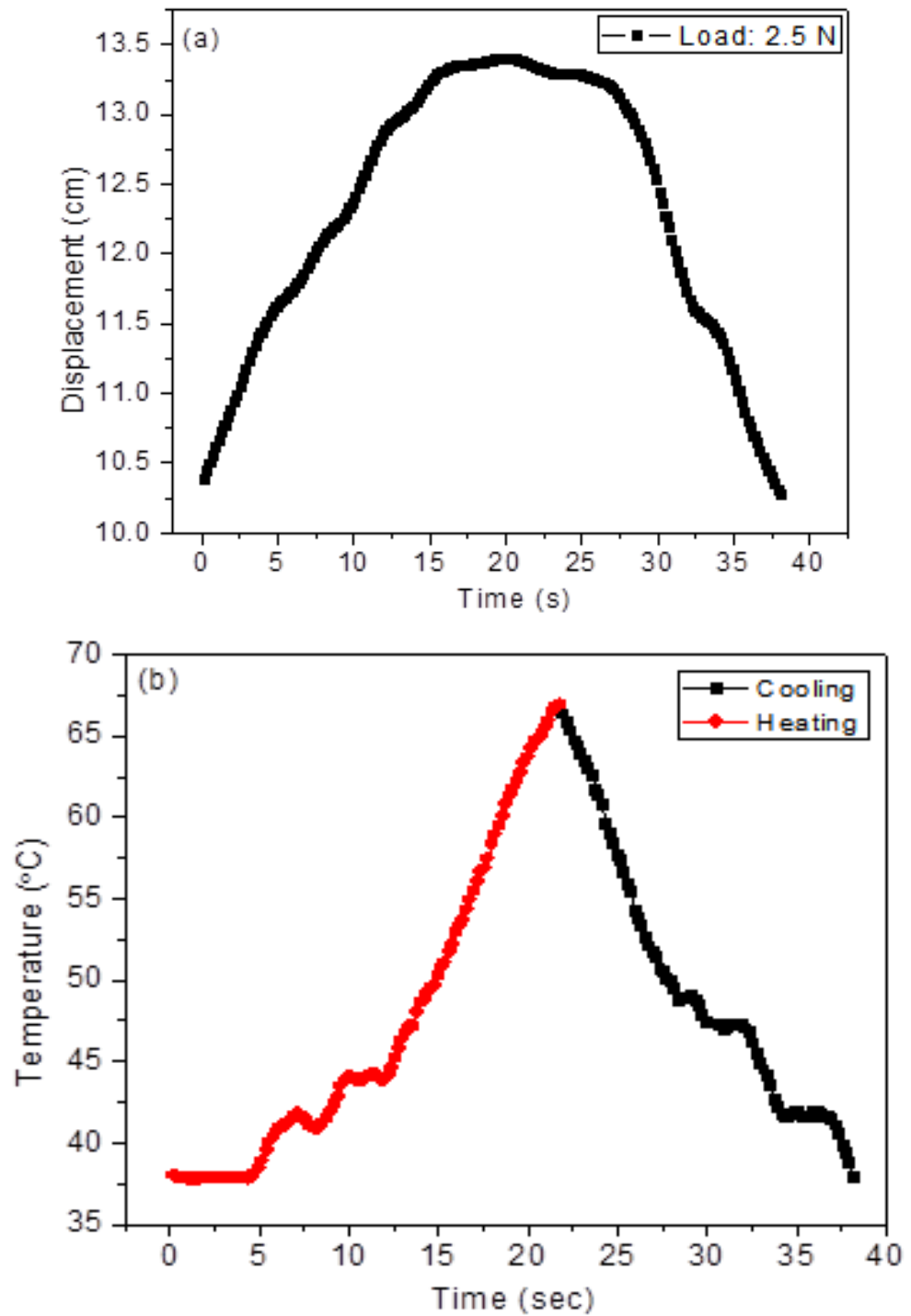
$$\rho C_p \frac{\partial T}{\partial t} + \rho C_p u \cdot \nabla T + \nabla \cdot q = Q \dots \dots \dots Eq 4.5$$

Where ' C_p ' is the heat capacity at constant pressure.

4.4 Result: This section is sub categorized into the following subsections which are given below.

4.4.1 Thermo-mechanical behavior: Fig 4.2 (a) shows displacement versus time graph when spring is loaded with 4.5 N. Heating time (25 s) is less compared to cooling time (20 minutes). The graph shows the hysteresis nature, i.e. dynamic lag between input and output stage. As the temperature reached 83°C, a

deflection of 4.3 mm can be seen from Fig. 4.2 (c). Data from LDS is measured in terms of voltage with the help of a DAS and reading is transferred to the system. For the same cycle temperature versus time curve Fig 4.2 (b) is plotted, fluctuations while gaining the temperature can be seen which may be due to release/absorption of latent heat and heat transfer with the ambient condition [156]



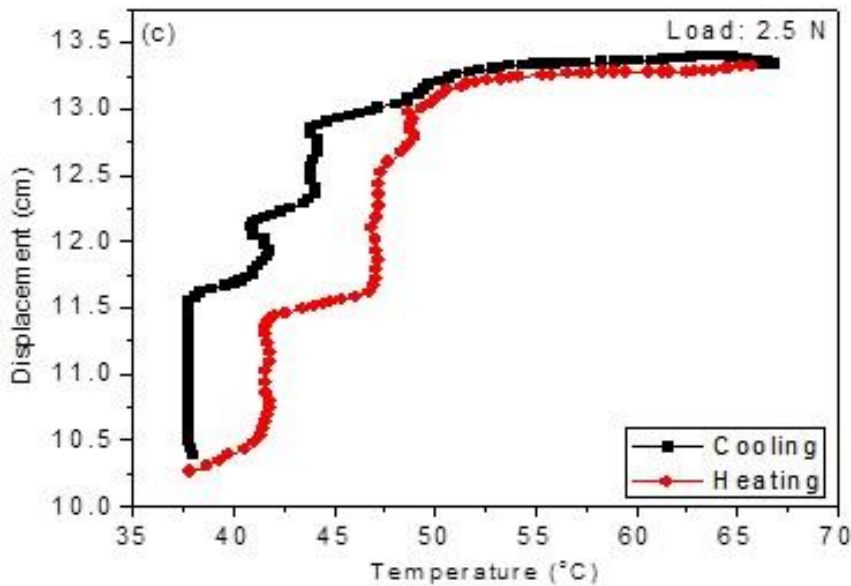
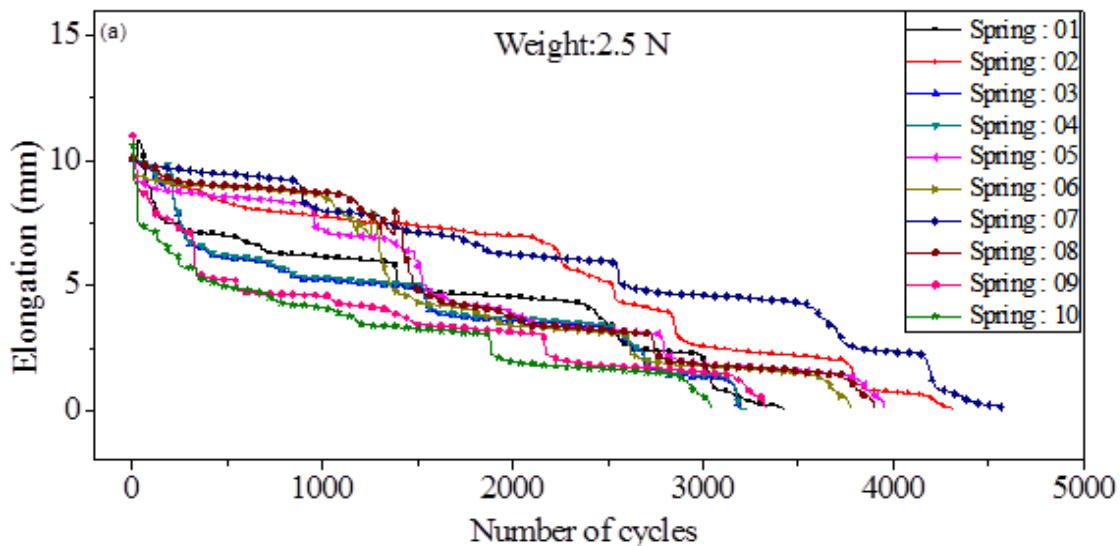


Fig 4.2: Thermomechanical behavior of SMA spring at 2.5 N a) Displacement vs Time, b) Temperature vs Time, c) Hysteresis curve

The transformation range for the one cycle (heating and cooling) is approximate 40°C -90 °C. Hot water actuation is gained when the temperature is reached stated above, and then cooling happens through natural /forced convection.

4.4.2: Life cycle analysis: It has been reported till its failure at different loading condition also, which shows the life of SMA spring.



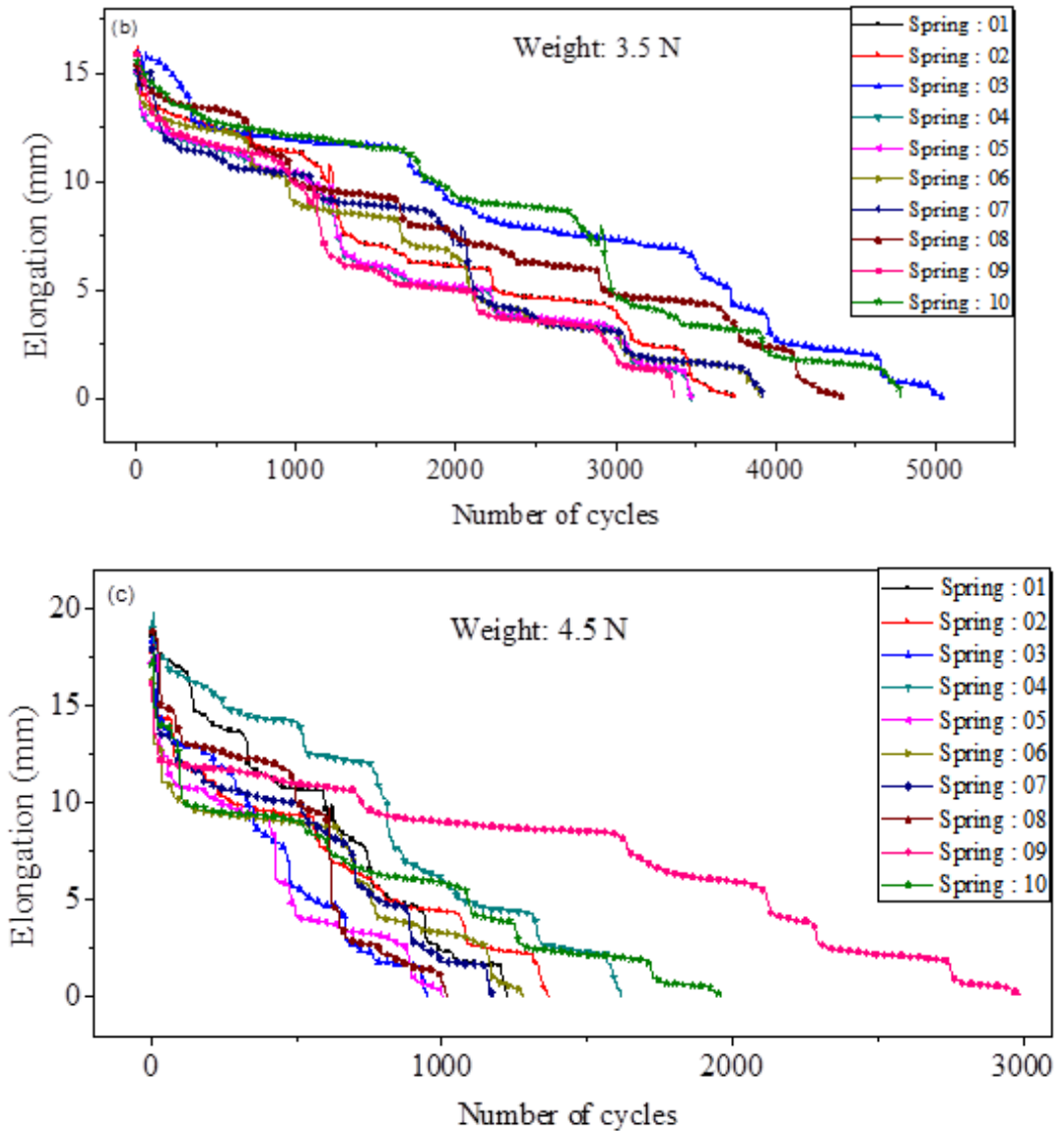


Fig 4.3: Thermo-mechanical analysis of SMA spring till failure for a) 2.5 N, b) 3.5 N and, c) 4.5 N

4.4.3 Characterization Techniques: SEM was performed over samples which are subjected to five cycles of heating-cooling. Fig 4.4 shows scanning electron microscopy images hot water activation. A hot water actuated sample is more dense morphology than electrical actuated samples (discussed in the previous chapter) in which structure shows elongated grains where the black part is for titanium and that grey is nickel. Nickel content is more than Titanium content though elongated grains results in an increase in strength and hardness, but it is

also observed that the alloy becomes more brittle and more liable to fracture due to this actuation.

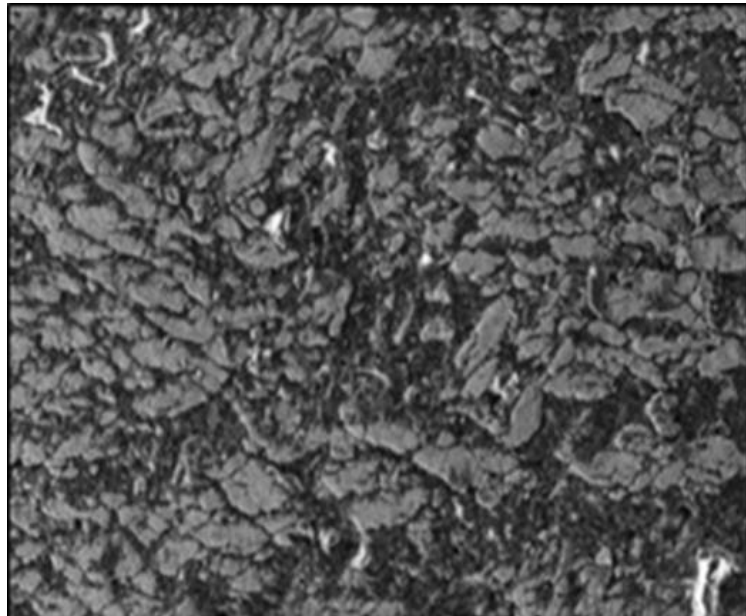


Fig 4.4 SEM analysis of hot water actuated SMA spring

Upon cooling the Ni-Ti becomes weaker and the spring easily deforms the actuator while it closes tightly in the structure [140]. The loss or gain of material can be because of decomposition or oxidation. [141].

Here hot water media for SMA has been proposed. It has been found that actuation gained by hot water is good enough to use in practical applications. It is capable of actuating the spring once the temperature reached transformation limit. Hot water can be used at places where we cannot go for electrical connections, as it makes the setup clumsy. Applications can be heat engine for thermal power plant where waste hot water will be used for recovery. The present study could represent the vital observations and results when actuated with Hot water.

4.4.4 Simulation results of SMA spring: COMSOL Multi-physics, a finite element tool for analysis and simulation of various engineering problems especially coupled physics, is used to analyze the parametric study of heat transfer in the hot water actuation. The conjugate heat transfer equation is incorporated into it using a multi-physics interface between the general heat transfer and the

laminar flow. COMSOL, in a conjugate heat transfer problem, enforces continuity of temperature at the fluid-structure interfaces. The spring is defined as the solid domain, over which the water flows.

Boundary condition: Room temperature is 25°C

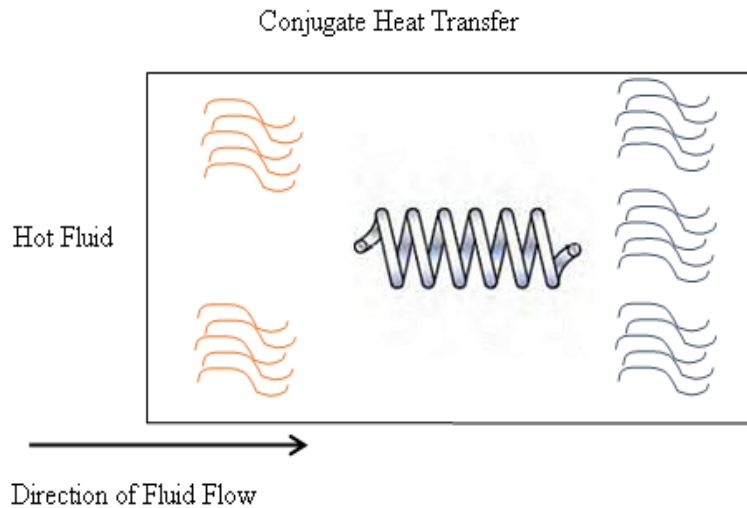


Fig 4.5 Line diagram for heating of spring

So an enclosure of the container is created as a fluid domain. The user size for the spring and the "fine" mesh size for the enclosure was done. Fig 4.6 shows the finely meshed geometry. The inlet and the outlet of the flow were determined. The velocity and temperature, at which the water enters the fluid domain are initialized.

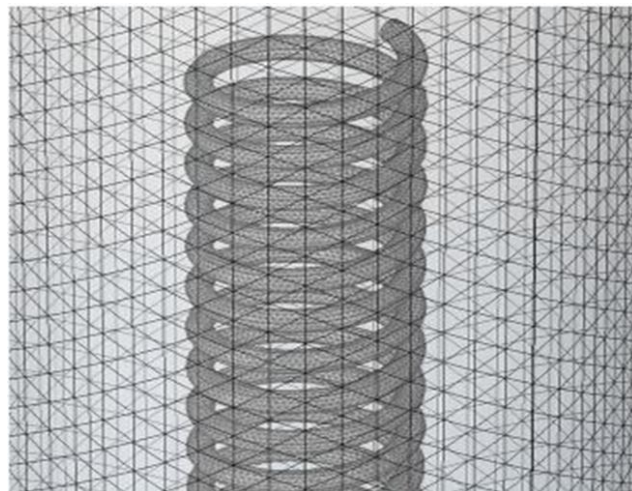
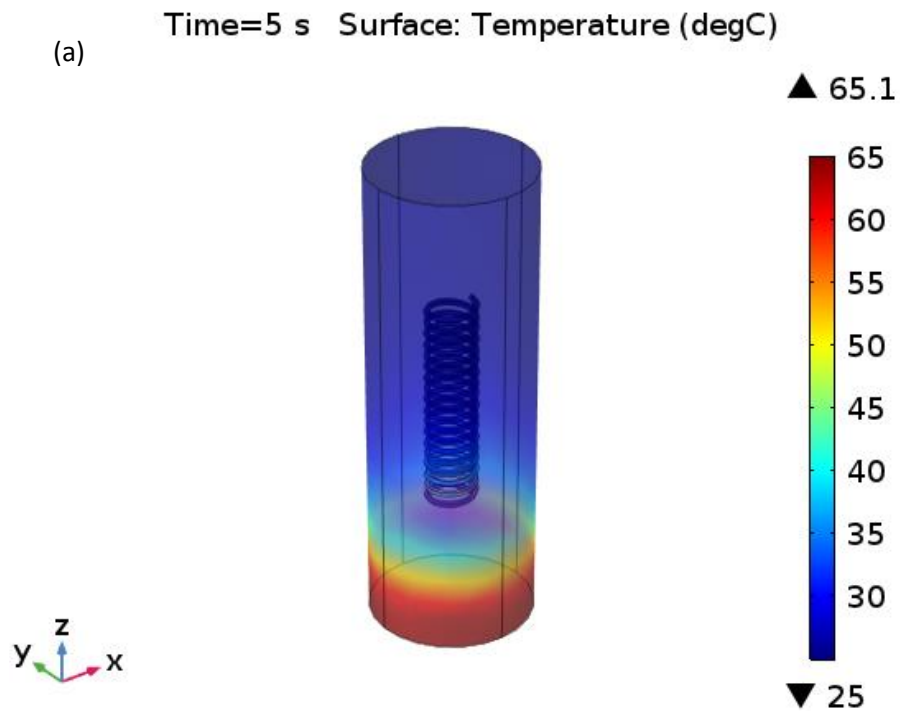


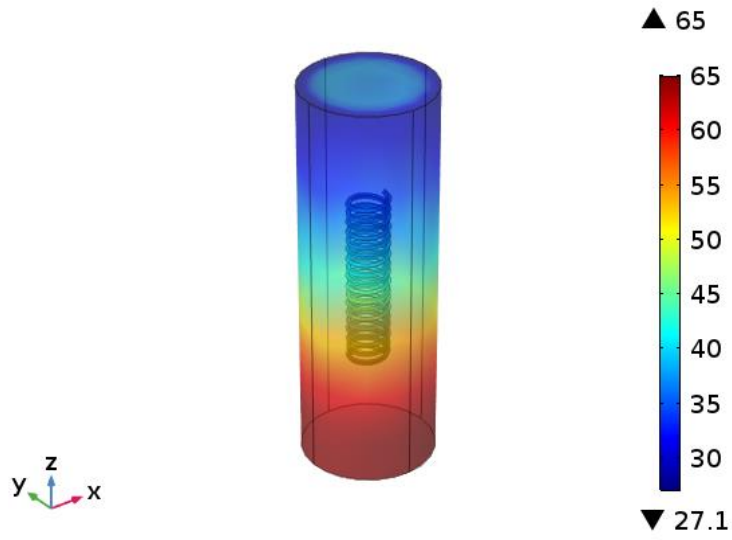
Fig 4.6 Fine meshed geometry

The analysis is done based on the mathematical modeling and assumptions (There is no loss while transferring heat from hot water to spring) considered in this study. Time-dependent analysis of this conjugate heat transfer problem is considered as the temperature of the spring varies with the time of flow of water, into the container. Fig 4.7 shows the temperature change of the spring over the time as the water rises inside the container. After 25 s, the whole spring reaches an average probe temperature of 75°C. These results are satisfactory with the experimental results.

Even though the time taken for the actuation (25 s) is less than the time taken for cooling (1200 s), this approach cannot be used in a real-time application. Hence, to optimize the parameters, a parametric sweep for the inlet temperature of the water (65°C, 75° C, 85°C) and the velocity of water flow (5mm/s, 7 mm/s) is done.

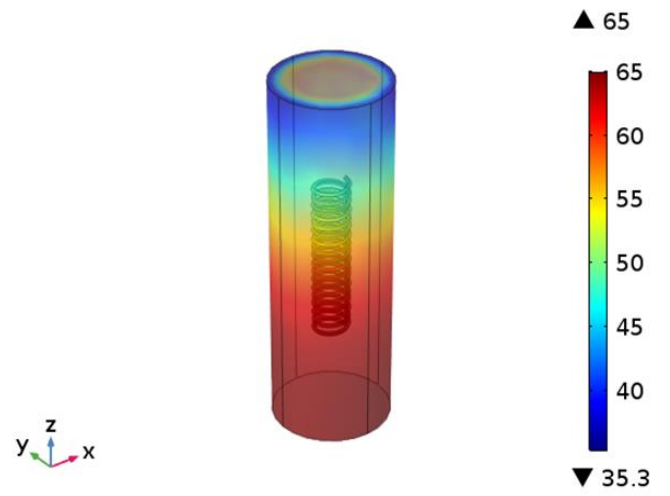


(b) Time=10 s Surface: Temperature (degC)



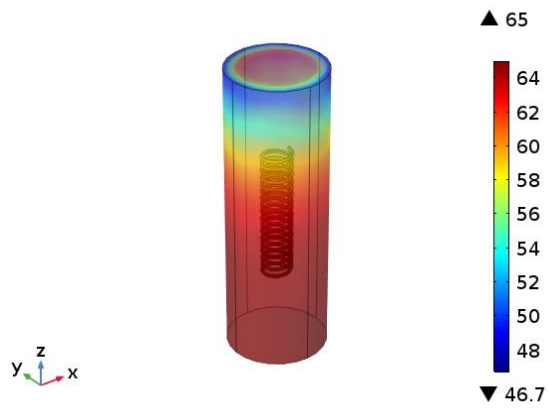
Time=15 s Surface: Temperature (degC)

(c)



Time=20 s Surface: Temperature (degC)

(d)



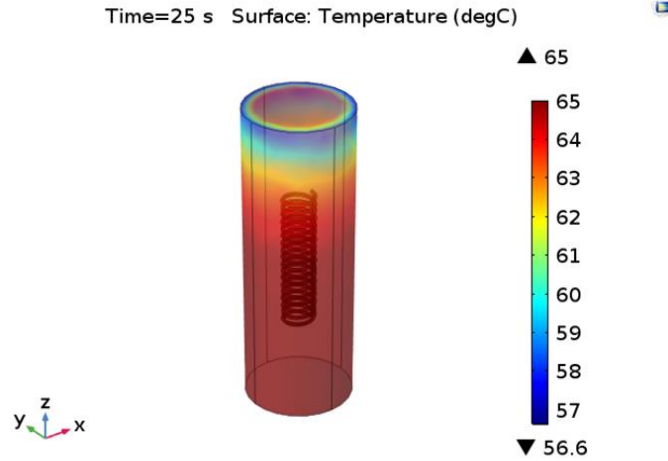
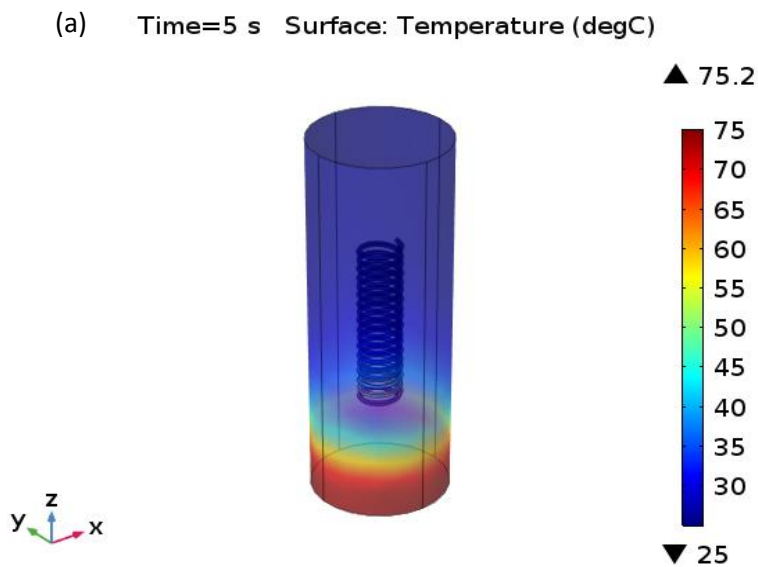
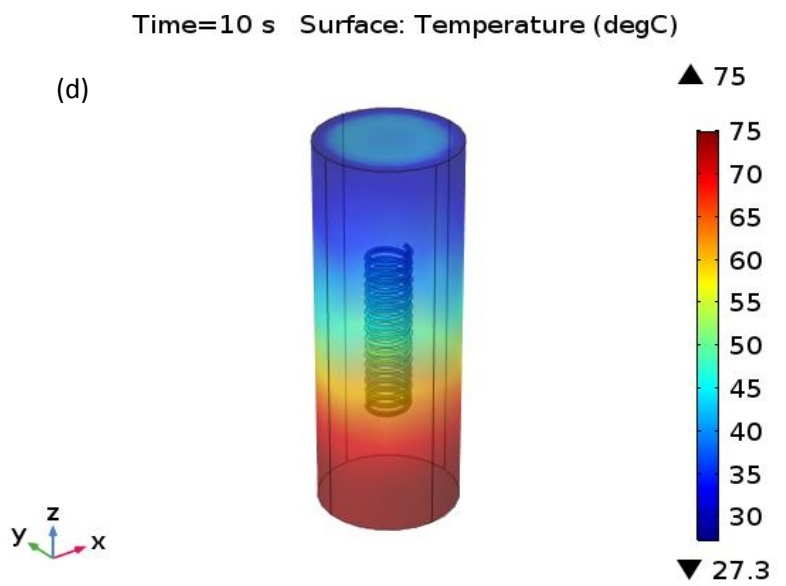
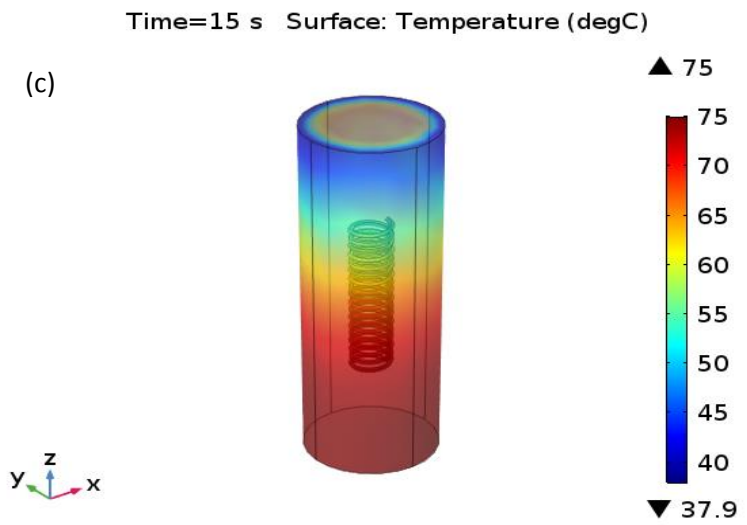
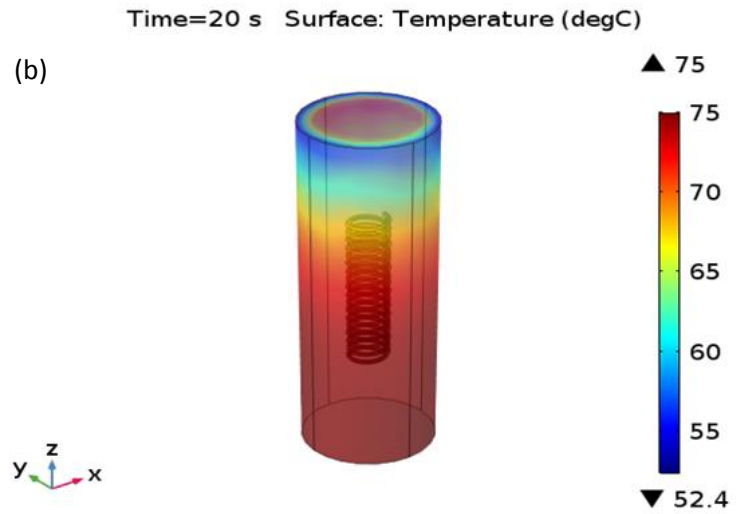


Fig 4.7 Flow after a) 5 s, b) 10 s, c) 15 s, d) 20 s, e) 25 s for 65°C

When the inlet water temperature was increased from 65°C to 75°C, the time taken by the spring to reach 65°C was reduced from 25 s to 13 s. When the flow velocity was increased to 7 mm/s, the time required to reach 65°C were 16s, 9s, and 7s for an inlet temperature of 65°C, 75°C, and 85°C respectively (Fig 4.8). Fig 4.9 shows the effect of temperature on spring when it is increased from 65°C to 75°C.





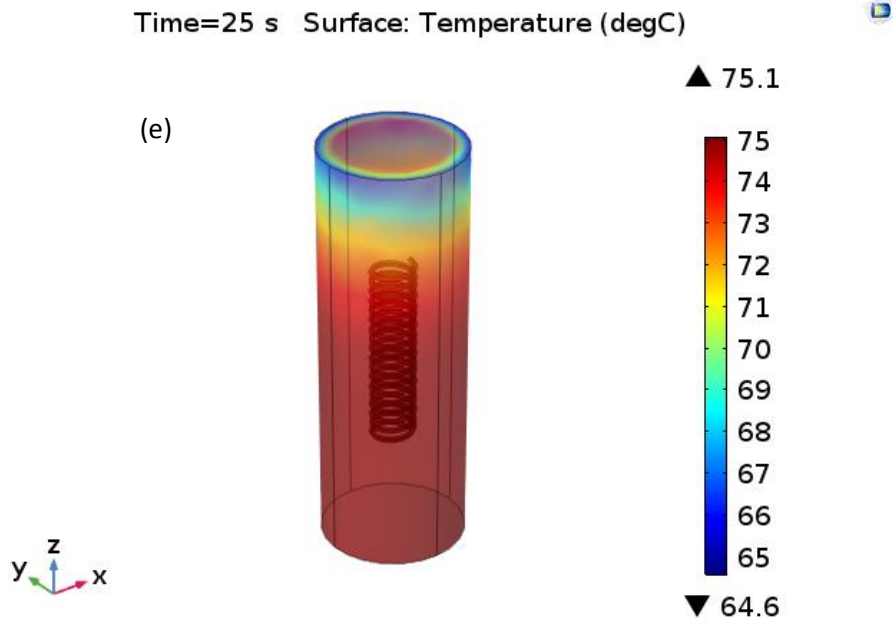
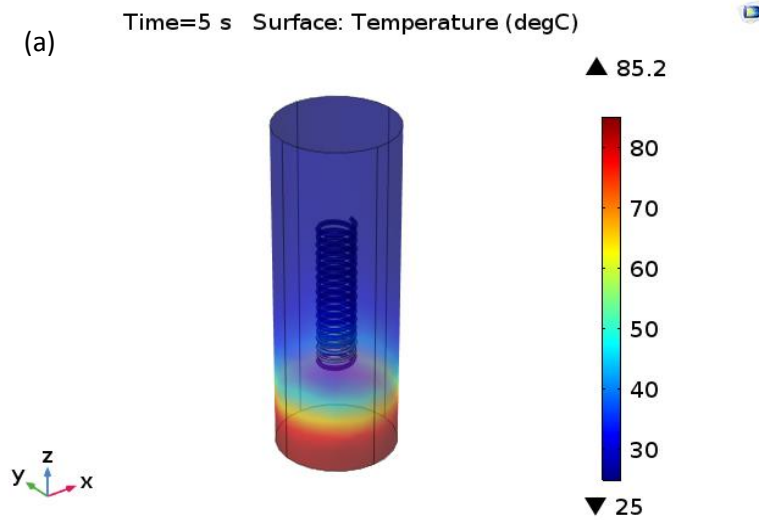
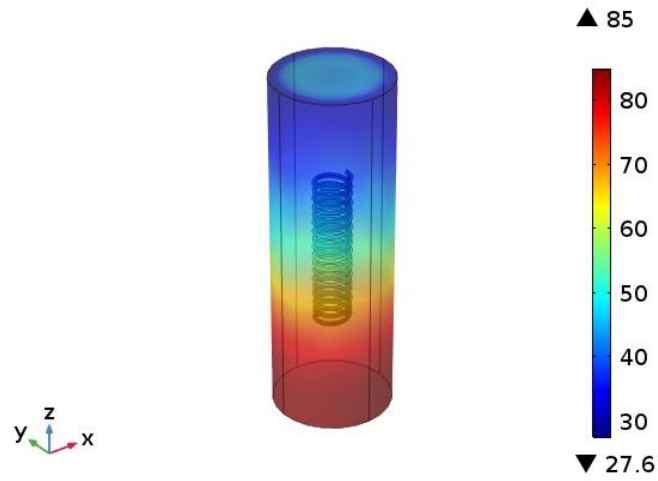


Fig 4.8 Flow after a) 5 s, b) 10 s, c) 15 s, d) 20 s, e) 25 s for 75°C

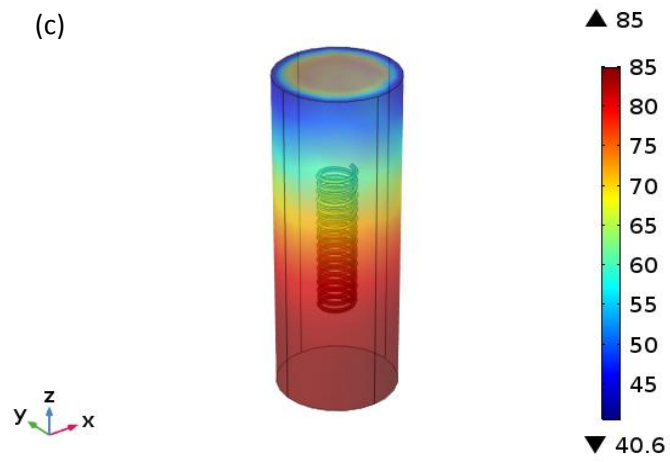
Further increasing the temperature of the water to 85°C, the time gets reduced to 11 s. Fig 4.9 shows the temperature profile when it increases from 75°C to 85°C.



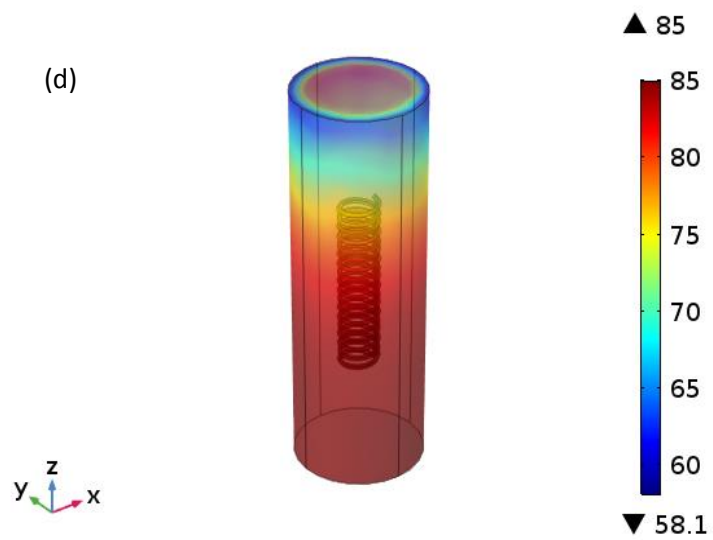
Time=10 s Surface: Temperature (degC)



Time=15 s Surface: Temperature (degC)



Time=20 s Surface: Temperature (degC)



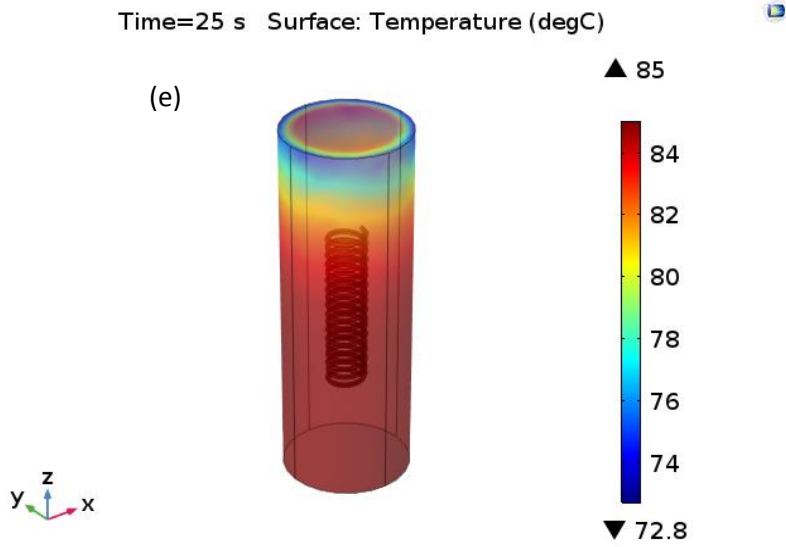


Fig 4.9 Flow after a) 5 s, b) 10 s, c) 15 s, d) 20 s, e) 25 s for 85°C

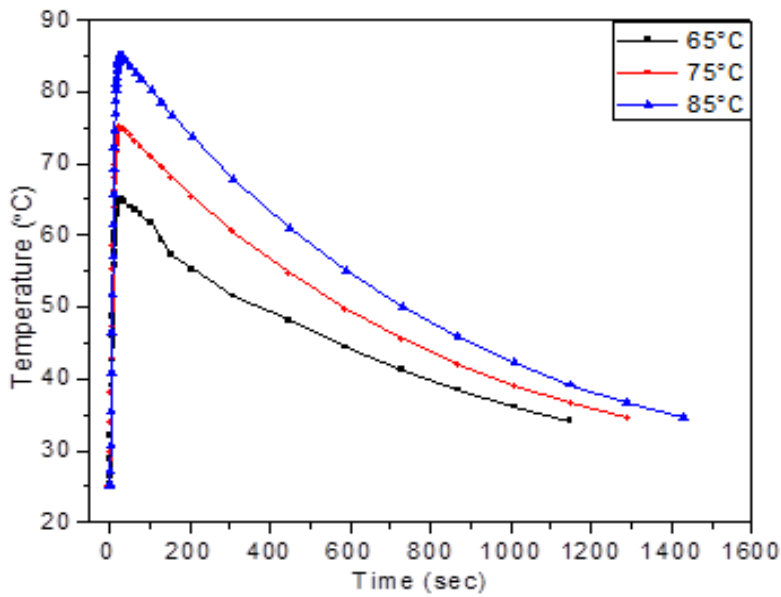


Fig 4.10: Comparative result for simulation at different temperature

It is clear from Fig 4.10 that actuation at 65, 75 and 85 heating time are 20 seconds only but for cooling 20 minutes are required

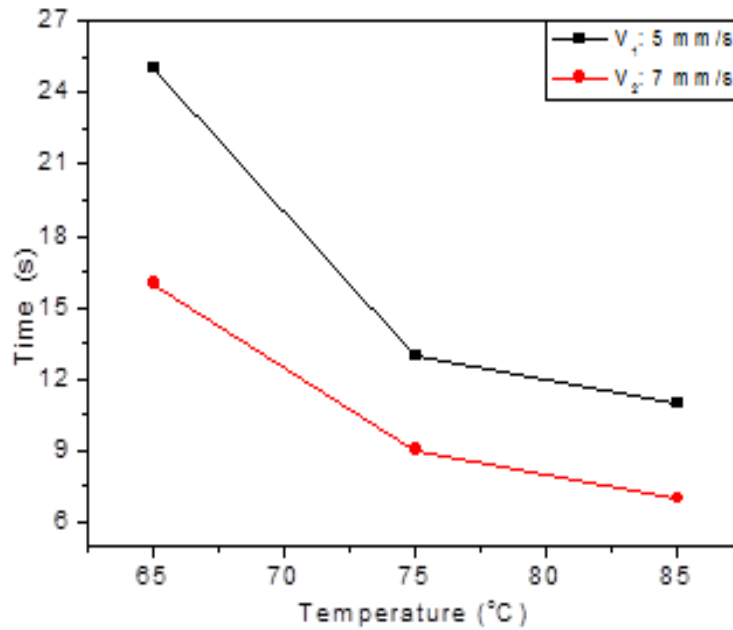


Fig 4.11: Time taken vs Temperature graph

SMA spring starts to actuate slowly at 65⁰C itself. Hence, it is taken as the reference data for a water flow velocity of 5 mm/s. If velocity increases from 5 mm/s to 7 mm/s then for the same temperature actuation is fast according to Fig 4.11.

4.5 Application: SMA Heat Engine

Shape-memory alloy heat engine is a device which converts waste heat into useful work [142-143]. In our work, It was tried to develop a simple device for achieving waste heat recovery from different systems for improving their efficiency. A prototype is constructed for experimentation to optimize its design for obtaining an improved design with better actuation capabilities.

- **The principle of Actuation:** The principle of actuation of SMA Heat engine is that when a force is acted at a distance from the hinge point, a moment is generated. If in place of hinge a bearing is used an act of rotation is generated.

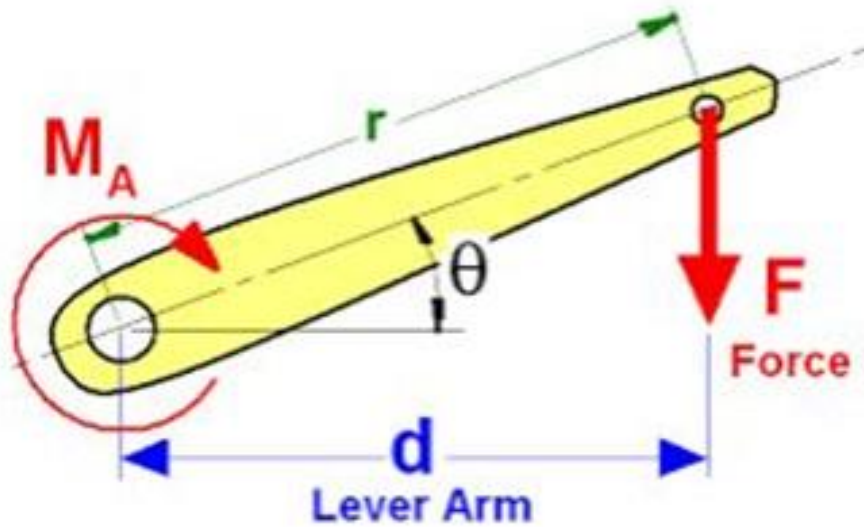


Fig 4.12 Moment generated by force

In the present work, the above-stated principle is utilized for achieving the purpose of actuation. SMA springs are connected radially to steel rim, another side of spring is connected to the hub (containing bearing). Initially, when springs are equally stretched, Centre of gravity (CG) is at the geometric center of the rim. When lower springs come in contact with hot water they get compressed, rim CG shifts from Hinge point (It can either shift to left or right). Due to this shifting of CG about hinge point moment or torque is produced which causes rotation. This phenomenon is explained in the Fig 4.13. In the diagram, springs are shown in the form of straight lines.

The rotation of wheel can occur in any direction depending on the direction of movement of CG from its position. Consider the case, in which CG shifts in the right direction from its center position, a clockwise moment is generated in this case causing rotation of the wheel in a clockwise direction and vice versa.

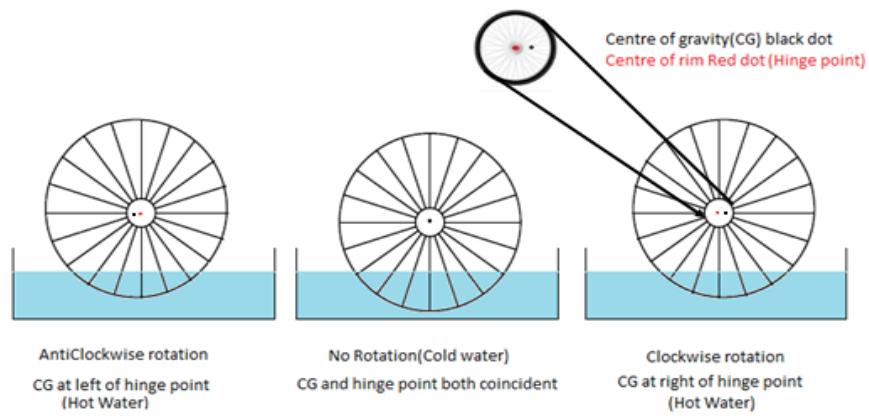


Fig 4.13 Principle of Actuation

4.5.1 Intermediate Objective

- i) To search for methods using shape memory alloy for conversion of waste heat into mechanical work.
- ii) To develop a 3-d drawing of setup to be fabricated.
- iii) To fabricate experimental setup for study of actuation.
- iv) To optimize the size of the developed setup for obtaining better actuation.
- v) To optimize operating parameters for obtaining the best possible power.
- vi) To select the best design of heat engine for further analysis.
- vii) Device Application :
 - Identifying other possible applications of the device(Eg: Power plant, Waste heat recovery in an automobile)
 - Fabricating the prototype.
 - Performing experiments with the fabricated part.
- viii) To develop small 3-d printed model to study actuation from exhaust gases for automobile applications.
- ix) To perform experiments on 3-d printed model to predict behavior under practical condition.

4.5.2 Components of SMA Heat Engine: Following are some of the main components of Heat engine prototype (Fig 4.14) A stainless steel rim whose diameter was 280 mm with the hub (diameter: 25 mm), equipped ball bearing was

used for connecting SMA springs radially provides stiffness to model. Mild steel stand was fabricated to hold the hub and to provide height for mounting the wheel. NiTi springs were used for actuation of Heat engine model. A heater is used to maintain the temperature of hot water. Color coated sheet container: A container is used for heating water. Although, SMA Heat engine is developed with a viewpoint of waste heat recovery from different systems. Input energy is consumed for heating water because of non-availability of the waste heat source.



Fig 4.14 SMA Heat Engine model

4.5.3 Drawbacks in previous Heat Engine design: As stated above prototype of SMA heat Engine was fabricated for experimentation to reach an optimum model. While performing experiments in the prototype following were the observations:

- 1.** Springs were connected in an inclined manner with the wheel hub. The reason for using inclined springs was the fact that CG shifts more when springs are inclined to the axis.
- 2.** During experimentation of prototype wobbling of Steel rim was observed about a transverse axis.
- 3.** Steel hub is used, and actuation of ball bearing occurs due to SMA Springs around the hub, the high moment of inertia of hub was opposing the motion of rim.

4. Due to the Higher weight of hub and bearing, high initial torque is required for the motion of rim.

All these problems were rectified in a modified prototype of a Heat engine which is explained in the next section.

4.5.4. Modifications in the model: Following modifications were incorporated in the previous model for its improvement:

Hub containing bearing replaced by shaft containing mild steel bearing holder: In the prototype developed, wobbling of steel rim was a major problem. To rectify the problem hub is replaced by bearing holder. When initially hub was used, springs were inclined to the axis. Due to inclined nature of springs wobbling of wheel was prominent. Thus springs are connected radially in the new design. In the Fig 4.15 mild steel bearing holder is shown, the bearing is attached at the center of bearing holder.

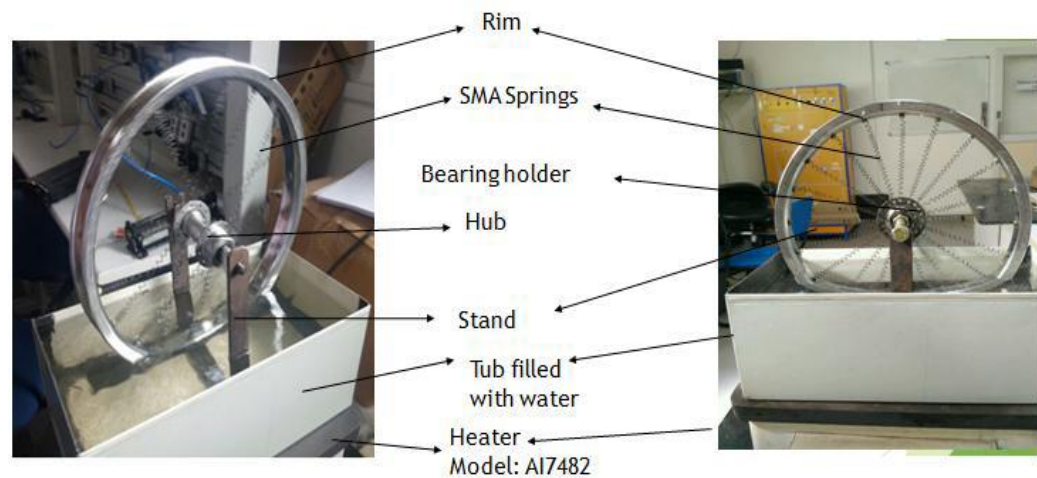


Fig 4.15 Hub replaced by mild steel bearing holder

To reduce weight mild steel bearing holder is further replaced by Poly Lactic Acid (PLA) material: When mild steel bearing holder is used weight of high-density material offers resistance in motion of steel rim, to reduce weight 3-d printed bearing holder is used of polylactic acid material. The polylactic acid bearing holder is manufactured using 3-d printing technique and is modeled in

CATIA Software. It has advantages over Mild steel bearing holder that it is easy to manufacture a product with low weight.



Fig 4.16 MS bearing holder replaced by PLA material

The Poly Lactic Acid (PLA) bearing holder used (Fig 4.16) offers relatively lesser resistance in the motion of rim as compared to mild steel, which is further analyzed by comparing rpm values in later part of this work.

4.5.5 comparison of characteristic curves in two models: After performing modifications as stated in the previous section. A comparative study was performed to analyze improvement in the design of Heat Engine. Rotations per minute calculations with temperature analysis showed improvement in actuation behavior of the proposed Heat engine. Fig 4.17 shows a graph of RPM vs. Temperature in two cases.

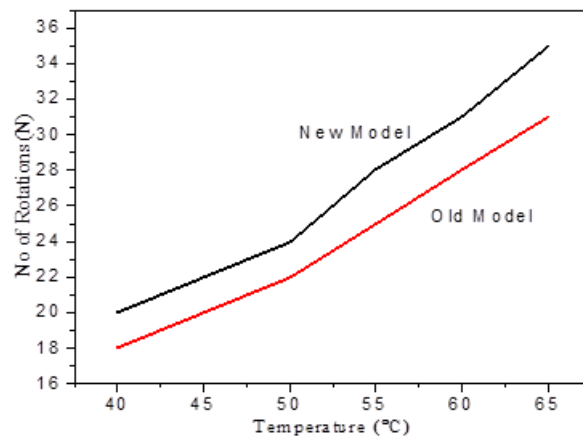


Fig 4.17 RPM differences between new and old model

4.5.6 Optimum height from bottom of bearing axis: Fig 4.18 shows the optimized design of SMA Heat engine prototype after incorporation of different modifications for better actuation. In all previous experiments height of axis of bearing from the bottom surface of the container was 22 cm.



Fig 4.18: Optimized design of Heat Engine

The height determines the number of springs coming in contact with hot water thus experiment were performed at different heights to achieve an optimum height of axis. Experiments were performed at different height, above and below the mean height.



Fig 4.19: Experimental set up to study optimum height

Graph 4.20 is plotted at three different heights showing the optimum height of axis.

Table 4.1 : Effect on RPM of wheel for variation in height

S.No	The temperature of the Hot water	Rotation per minute (RPM) with variation in center height		
		H ₁ = 22	H ₂ = 19	H ₃ = 21
1	80	45	43	48
2	70	40	37	43
3	60	36	33	40
4	50	32	30	35

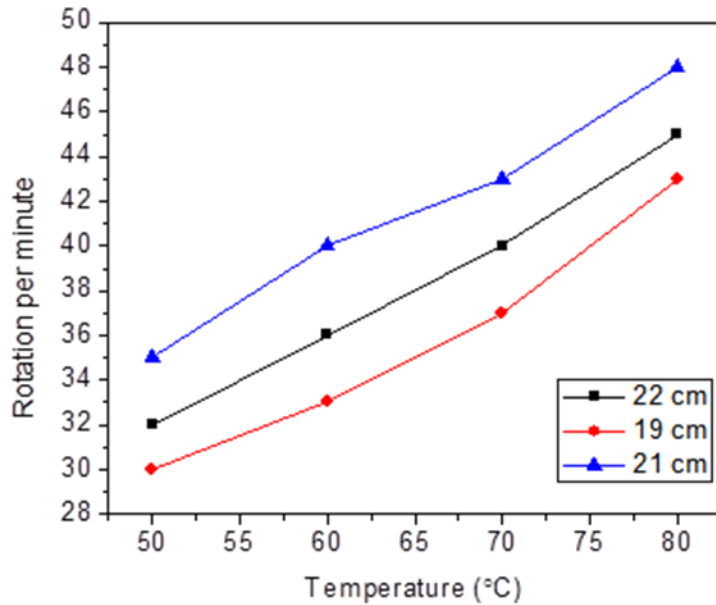


Fig 4.20: RPM vs Temperature graph

Observations from the above experiment:

1. Initially, all experiments were performed with a center height of 22 cm.

2. As height is decreased, power is increased up to a particular optimum height.
3. Best results were obtained at the height of 21 cm.
4. When height is reduced below 21cm, RPM of the wheel is reduced.
5. Increased resistance due to the viscosity of water is the reason for reduced RPM.

Besides hot water actuation, the developed heat engine also possesses the potential for actuation by hot exhaust gases from the automobile. Although actuation from hot gases is tested at its preliminary stage, results are positive, and we can look forward to the implementation of the engine in this area also for utilization of energy produced.

The actuation of a heat engine is due to Shape memory behavior of NiTi material; the material possesses this behavior due to temperature gradient provided to by hot water (or any source as the case be). Thus it is essential to study heat transfer in NiTi and to check the of actuation for the long better performance of a heat engine

Different equations of heat transfer can be applied to NiTi for developing a model for heat transfer. Further results can be verified from simulations. In the next chapter, we will discuss the heat transfer aspects of the heat engine and try to analyze the cyclic behavior of SMA springs.

4.5.7 Heat transfer analysis of Heat Engine: Heat transfer analysis in hot water actuation is performed to understand how heat is being transferred to improve the actuation for obtaining better performance. Since the spring is fully immersed in hot water and heat transfer is taking place from Hot water to spring.

Assume SMA wire is considered as a cylinder. Parameters related to SMA spring are:

d = wire diameter (mm)

h_c = convection coefficient, $W/m^2 / ^\circ K$

T = starting temperature, $^\circ K$

T_{∞} = Hot water temperature, °K

σ = Stefan-Boltzmann constant, $W/m^2 / ^{\circ}K^4$

$$m * c * \frac{dT}{dt} = -\pi dl * h (T - T_{\infty}) - \pi dl * e * \sigma (T^4 - T_{\infty}^4)$$

$$\frac{dT}{dt} * \rho * c * l * \frac{\pi d^2}{4} = -\pi dl * h (T - T_{\infty}) - \pi dl * e * \sigma (T^4 - T_{\infty}^4)$$

$$\frac{dT}{dt} * \rho * c * \frac{\pi d^2}{4} = -\pi d * h (T - T_{\infty}) - \pi d * e * \sigma (T^4 - T_{\infty}^4)$$

$$\frac{dT}{dt} = \frac{-\pi dh (T - T_{\infty}) - \pi de \sigma (T - T_{\infty}^4)}{\rho * c * \frac{\pi d^2}{4}} \dots \dots \dots Eq. 4.6$$

Following are predictions based on heat transfer analysis;

- Thin spring is expected to give better actuation as compared to thick wired spring.
- Length of wire is not having any effect on actuation.
- The result concluded are very important in the sense that it gives us the idea that this small prototype of the heat engine can give same performance even with long wire spring when the large model is required for more power generation.

4.5.8: Scaling of heat engine: Heat engine discussed in present work can be enlarged for obtaining better actuation. Some springs can be increased for reduced depending on the requirement of actuation. More the number of springs attached to the rim, more are the springs which are in contact with hot water, hence better is actuation obtained.

Some springs connected to the rim is related to the size of rim and wire diameter of spring. An equation stating the relation is derived in the present section.

Consider the following parameters in the Heat engine model with springs arranged perfectly radial manner.

D_r = Diameter of the steel rim, C_b = Diameter of bearing holder, cl = Clearance given between each hole in bearing holder, l = Length of a spring, d = Wire

diameter of spring, n = number of coils in spring, N_s = Number of springs attached in wheel

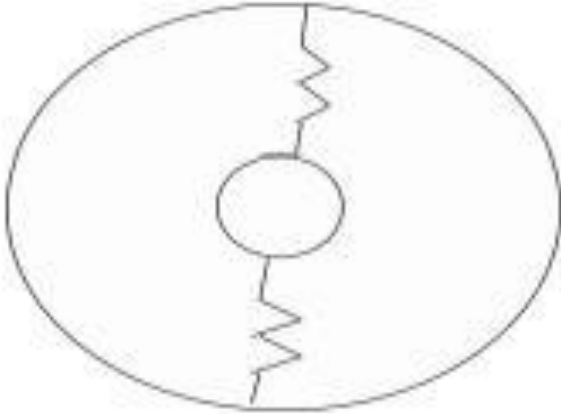


Fig 4.21 Line diagram of rim with springs

$$D = C + 2 * l$$

Where l = length of SMA spring

$$D = C + 2 * (\pi dn)$$

Consider small bearing holder attached in centre,

Let's clearance (distance provided to avoid overlapping) is cl :

$$\pi C = N_s (d + cl)$$

$$C = \frac{N_s(d + cl)}{\pi}$$

Putting the value of C in equation (ii):

$$D = \frac{N_s(d+cl)}{\pi} + 2 * (\pi dn) \dots \dots \dots Eq. 4.7$$

So number of springs attached to wheel the can be find out.

The relation derived above is very important for heat engine design. More the number of springs attached to the rim more will spring which are coming in contact with hot water thus better will be actuation obtained.

4.5.9 Efficiency of Developed heat engine: Although the application of SMA heat engine is in waste heat recovery. Waste energy is always beneficial for

improving the net output of the system. The derivation of efficiency expression for SMA heat engine is presented in this section.

Let m = mass of water in the container, C = Specific heat of water, dT = Temperature difference produced due to heating., t = Time required for heating,

$$\text{Output} = n * \text{current}(I) * \text{Voltage (V)}$$

Where,

I = current flowing in circuit, V = voltage across DC motor, n = number of LEDs connected in series,

$$\text{Output} = n * I * V = 100 * 10 \text{ mA} * 5 \text{ V} = 0.5 \text{ W}$$

Input = Average rate of heat Input =

$$\frac{m * c * \Delta T}{t} = \frac{1 * 4200 * 30}{7200} = 11.4 \text{ W}$$

$$\text{Efficiency in \%} = \frac{0.5}{11.4} * 100 = 4.30\%$$

4.5.10 Demerits of developed heat engine: Weight of the wheel was very much high.

- Higher initial torque by the springs is required.
- Wobbling was a problem hence the rotations generated was very low.
- Power generated was also very much less.
- There was no such arrangement to get power directly from the shaft because in between the hub and springs, a bearing was connected and thus the shaft was not rotating.

Due to these drawbacks, one more nitinol-based heat engine was developed and analyzed. To investigate it following details were required:

4.6 Modified Objectives: The intermediate objectives are as follows.

- The intermediate objective is to check the influence of hot water heated by an electric tank on the Nitinol wheel.
- To investigate the parameters to increase the rotations as well as power and there by efficiency.

- To check the influence of the hot exhaust gases on the wheel and on its rotations.
- To check the design parameters and its influence on the rotations, power, and efficiency.
- To check the performance with the gear and pinion arrangement and measuring the output with the help of a dynamo.
- To check the performance of the nitinol wheel with the permanent magnetic generator.
- To fabricate the pulley set up with its foundation.
- To check the efficiency of the heat engine by making a cardboard chamber.

4.6.1 Components of the Nitinol heat engine.

Following are some of the main components of heat engine prototype:

An aluminum wheel (Thickness: 3 mm; lighter the wheel, more will be the rotations) was used for connecting SMA springs radially of diameter 295 mm and mass 123 grams. A polylactic acid hub (ID: 10 mm, OD: 70 mm) made from 3d printing machine was used and, for testing in the exhaust gas of an automobile. A mild steel stand to support the shaft of the setup at three different heights was made by CNC milling. Nitinol springs were used for actuation of heat engine model. A heater is used to maintain the temperature of hot water.

4.6.2 Hot water actuated SMA heat engine: To improve the performance of the heat engine, aluminum which is a lightweight material is used to make a wheel and springs are connected as spokes in a radial manner which is then connected with a hub. In order to rotate, the shaft is directly connected to the hub instead of the shaft is connected to the bearing directly then hub. The wheel and shaft are made of aluminum (Fig 4.22). The diameter of the shaft is 10 mm, and the mass of the shaft is 62.7 grams.

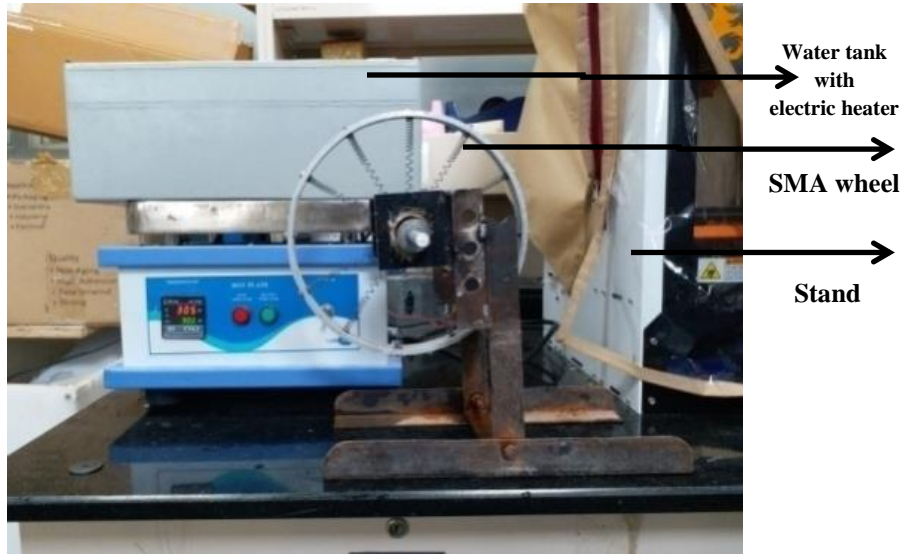


Fig 4.22: Hot water actuated heat engine

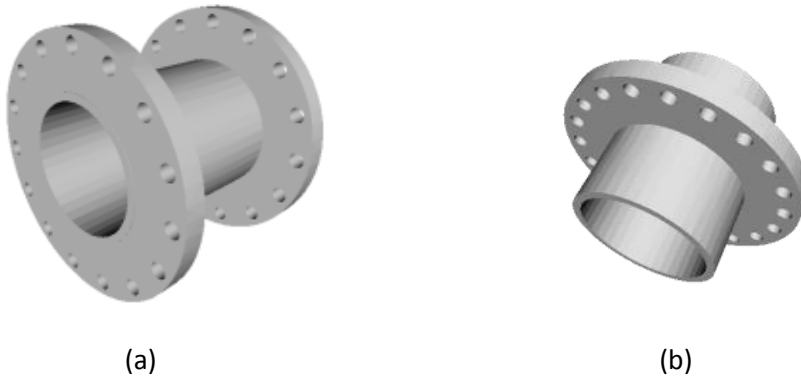


Fig 4.23: Cad modelling of different designs of the hub

The SMA wheel is tested with two different hub designs. Design 4.23 (a) has the facility to use more springs, but there is more wobbling in the wheel with this design in comparison with 4.23 (b). Hence for the complete testing, the hub 4.23 (b) is used.

The setup is kept in a water tank which is being heated by an electric heater. Some part of the lower springs has contact with the heated water. When lower springs comes in contact with the heated hot water they get compressed, wheel CG shifts from Hinge point (It can either shift to left or right). Due to this

shifting of CG about hinge point moment or torque is produced which causes rotation.

Table 4.2: Effect of height for RPM of wheel

S.No	Height (cm.)	RPM
1	16	46
2	19	57
3	20.5	50
4	22	41

The table given comprises the variation of heights of the axis of the shaft from the bottom of the hot water tank with the rotations per minute of the wheel.

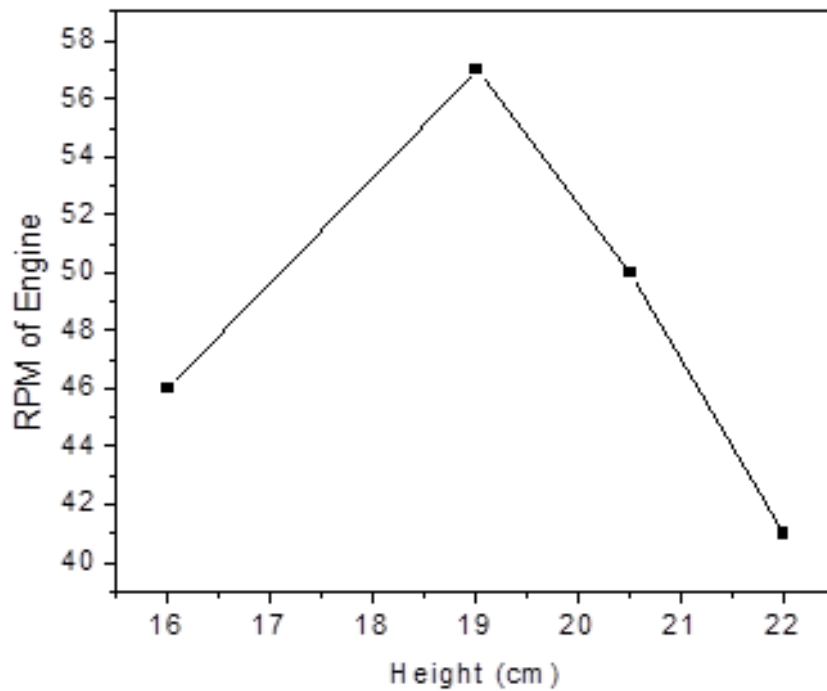


Fig 4.24: Plot for Heights vs RPM variation

The above plot shows the variation of height vs. revolution. First, the rpm increases up to a 57 rpm, the reason for this is that viscous forces acting on the springs becomes lesser as the height is increased and reaches up to optimum height. Then it starts to decrease with more increase in height because of the heat transfer from water to the spring becomes less.

4.6.2.1 Calculations:

$$\text{Power} = \frac{2IIN}{60}$$

Where N= number of revolutions per minute, T= torque, Torque= $I\alpha$, I= moment of inertia

α = angular acceleration

$$\text{Moment of inertia } I = 0.5 M (R^2 + r^2)$$

Angular acceleration α = angular velocity/time

$$R = 0.113\text{m}; r = 0.104; M = 0.129 \text{ kgs}$$

$$\text{After substitution, } I = 1.959 \times 10^{-3} \text{ Kg m}^2$$

$$\text{Angular velocity} = 2\pi N/60 = 2 \times 3.14 \times 57/60 = 1.9457 \text{ rad/s}$$

$$\text{Angular acceleration} = 5.96/0.5 = 8.37 \text{ rad/s}^2.$$

$$\text{Torque} = 1.9457 \times 10^{-3} \times 8.37 = 0.01252 \text{ N-m.}$$

$$\text{Power} = 2 \times 3.14 \times 100 \times 0.01252/60 = 137 \text{ mW.}$$

$$\text{Maximum Torque} = 0.01252 \text{ N-m.}$$

$$\text{Maximum Power} = 137 \text{ mW}$$

Now the same heat engine is then tested in exhaust gases of the vehicle.

4.6.3 Experimentation done in the exhaust of the vehicle: Here the hot exhaust gasses are made to fall on the wheel. Through the vehicle (Fig 4.25 a). The same wheel of dia 205 mm is used here. However, the wheel is now more lighter mass is 129 grams in a comparison to the previous case. The ambient temperature 27°C (with the help of the thermal camera: Fig 4.25 b).

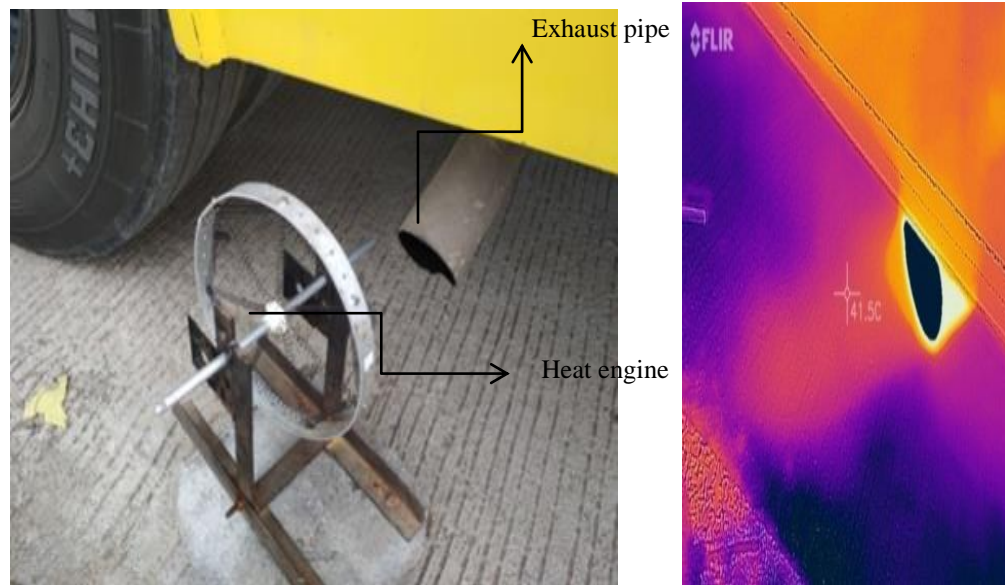


Fig 4.25 : SMA heat engine a) In front of the exhaust, b) Thermo-graphic images

Table 4.3 : Temperature vs RPM of SMA wheel

Temperature of exhaust gases in°C	RPM of Engine	RPM of SMA wheel
45	500	0
66	800	2
80	1500	35
100	1800	70
145	2000	79
160	2000	85

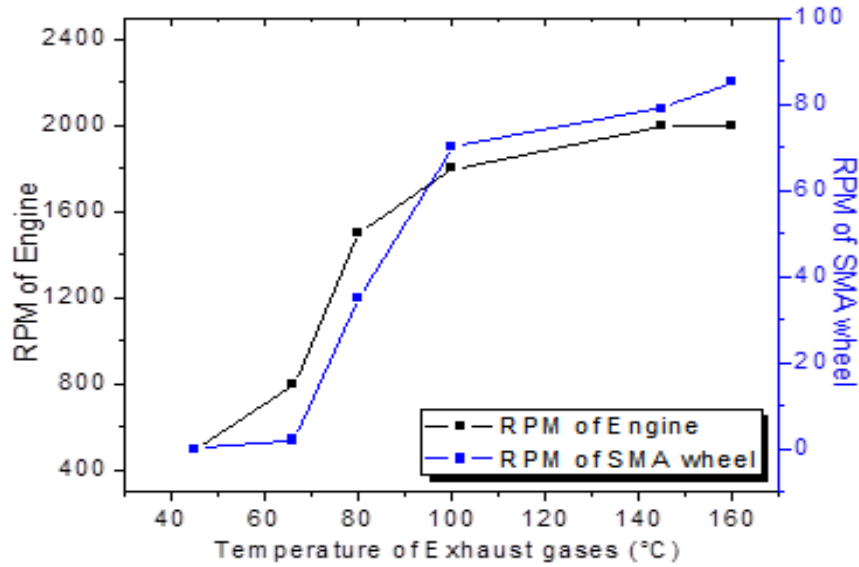


Fig 4.26: variation of the rpm of the SMA engine with the temperature of the exhaust gases

4.6.3.1 Calculation:

$R=0.113\text{m}$; $r=0.104\text{m}$; $M=0.1229\text{ kgs}$

After substitution, $I= 1.449 \times 10^{-3}\text{ Kg m}^2$.

Angular velocity = $2\pi N/60 = 2 \times 3.14 \times 87/60 = 9.10\text{ rad/s}$

Angular acceleration = $9.10/0.5 = 18.21\text{rad/s}^2$

Torque = $1.449 \times 10^{-3} \times 18.21 = 0.0263\text{ N-m}$

Power = $2 \times 3.14 \times 87 \times 0.0263/60 = 239\text{mW}$

Maximum torque = 0.0263N-m .

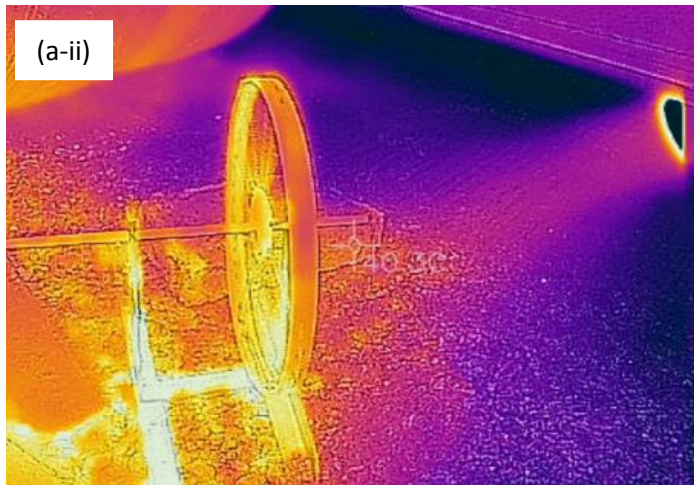
Maximum power = 23 mW .

4.6.4 Keeping the mass constant and change in diameter of the wheel: Now, the diameter of the wheel is increased to 295 mm but keeping the mass constant and then the wheel is tested in the exhaust gas. The temperature of the exhaust gas is increased by giving the accelerator of the bus. The rpm of the engine is now increased to maximum RPM of 145.

(a-i)



(a-ii)



b-i)

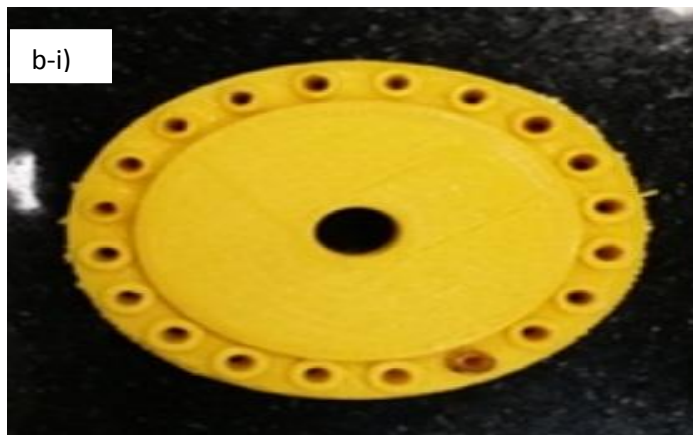




Fig 4.27: a) Effect of exhaust gas on SMA wheel, a-ii) Thermal Image of wheel b-i) hub condition before and b-ii) after testing

Table 4.4: Tabulated results obtained from the experiment

The temperature of exhaust gases in (°C)	RPM of the engine	RPM of SMA wheel
40	500	0
62.4	800	1
87	1500	23
145	1800	120
160	2000	145

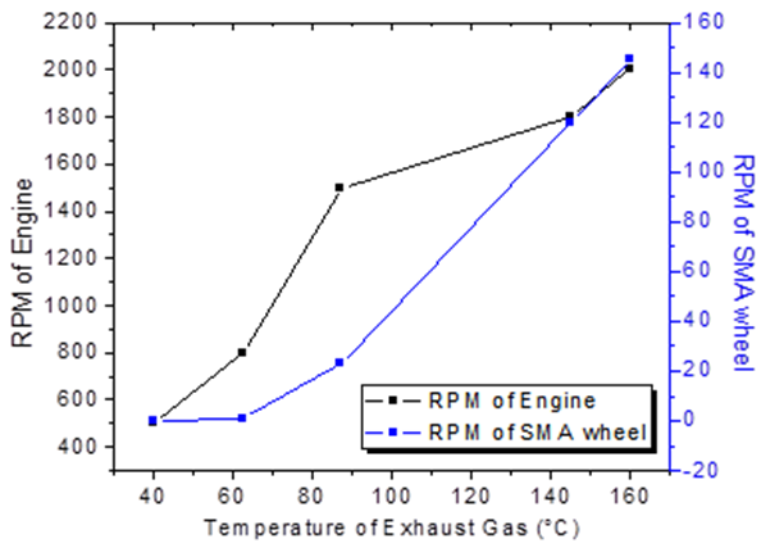


Fig 4.28: RPM vs Temperature variation

4.6.4.1 Calculations

$R=0.145\text{m}$; $r=0.148$; $M=0.1229\text{ kgs}$

After substitution, $I= 2.6379*10^{-3}\text{ Kg m}^2$.

Angular velocity = $2\pi N/60= 2*3.14*145/60= 15.17\text{ rad/s}$

Angular acceleration = $4.19/0.5= 30.34\text{ rad/s}^2$

Torque = $1.4959*10^{-3} * 30.34 =0.08003\text{ N-m}$

Power= $2*3.14*145* 0.08003/60 = 1514\text{mW}$

Maximum torque= 0.08003 n-m .

Maximum power = 1.514W .

4.6.5 Keeping the constant diameter and changed the mass of the wheel:

Here, now the diameter is kept constant as 208 mm but the mass is changed to 165 grams, and then the wheel is tested. Due to the increase in inertia as a result of increase in the mass of the wheel the rotations is decreased. The maximum power and torque are calculated.



Fig 4.29: Nitinol based wheel No. 3

Table 4.5 : RPM of Nitinol wheel and temperature of exhaust

The temperature of exhaust gases in °C	RPM of the engine	RPM of SMA wheel
42	500	0
70	800	15
85	1500	40
120	1800	66
150	2000	79

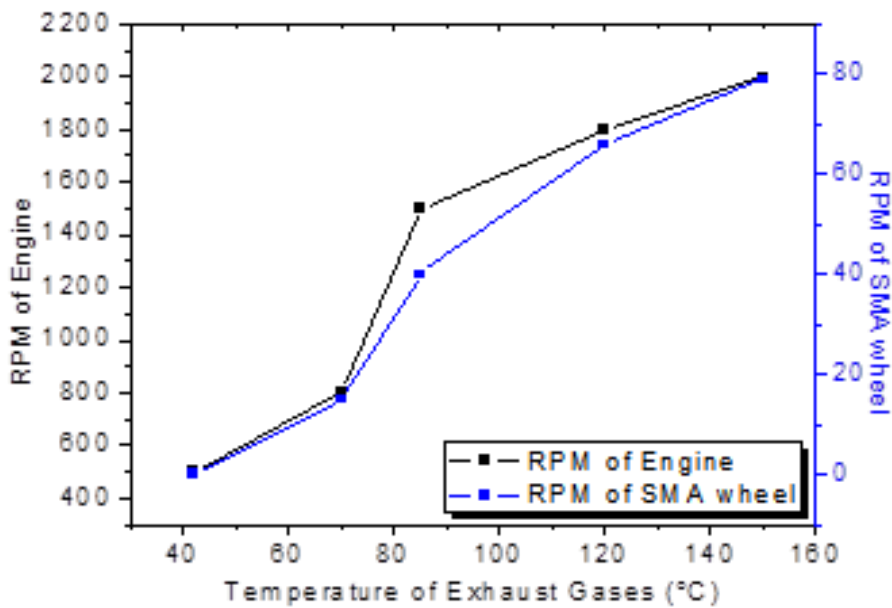


Fig 4.30: RPM vs Temperature variation

4.6.5.1 Calculation.

$R=0.113\text{m}$; $r=0.104$; $M=0.165\text{ kgs}$

After substitution, $I= 1.9457 \cdot 10^{-3}\text{ Kg m}^2$.

Angular velocity = $2\pi N/60 = 2 \cdot 3.14 \cdot 79/60 = 8.26\text{ rad/s}$

Angular acceleration = $8.26/0.5 = 16.53\text{ rad/s}^2$

Torque = $1.9457 \cdot 10^{-3} \cdot 16.53 = 0.0321\text{ N-m}$

$$\text{Power} = 2 \times 3.14 \times 79 \times 0.0321 / 60 = 265 \text{mW}$$

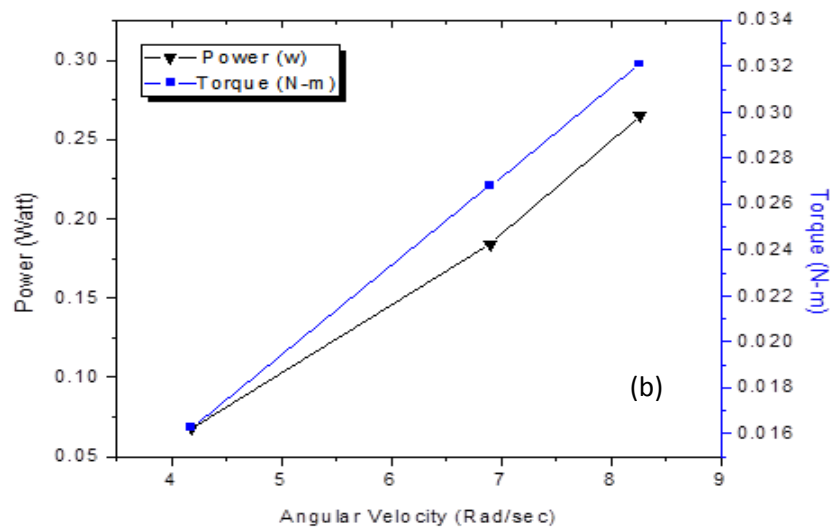
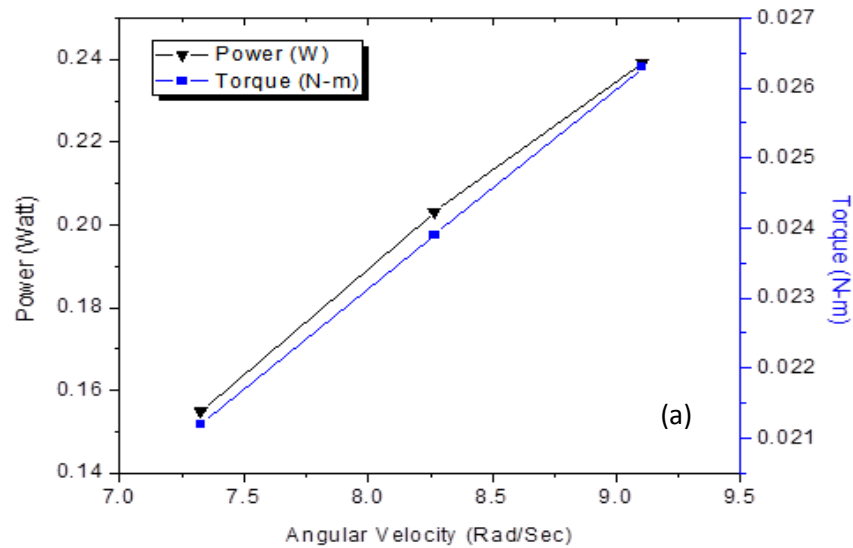
Maximum RPM = 79

Maximum Torque = 0.0321 Nm

Maximum Power = 265 mW

4.7 Comparison of the performance for all three types of heat engine

It can be seen that the power and torque obtained from the wheel having 0.295 m diameter and 0.165 kg mass is high, and hence the design is chosen as optimum. In Fig 4.31 a, maximum 0.24 W power is required to achieve 9.2 rad/s with generated torque of 0.0261 N-m.



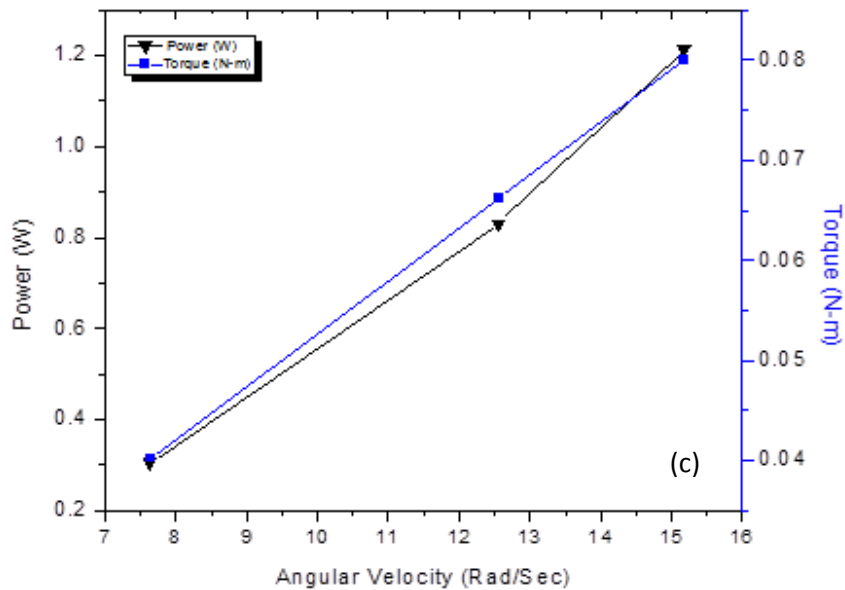


Fig 4.31: Variation in power, Torque and angular velocity for a) wheel having diameter = 0.113m and mass = 123g, b) wheel having increased mass of 165 g but same diameter, c) wheel having same mass but increased diameter of 295 mm

4.8 Summary:

In this summary, research contributions related to hot water actuation is outlined:

- The purpose of this work was to present the actuation behavior of SMA spring using the hot fluid medium.
- In light of the past work it has been attempted in this area, it seems unlikely that the earlier inventions could be scaled up to the point where they have practical utility.
- For application point of view, one heat engine is designed and developed which is beneficial for the thermal power plant. By using waste heat, springs were actuated, and it will be used for energy harvesting also.
- Actuation of SMA heat engine is done by using hot gases also.
- Three nitinol heat engines of different parameters are fabricated and analyzed with its comparison.

Chapter 5

Pulsed Laser Assisted Actuation of SMA's

In this chapter, a novel approach is developed to handle the actuation of shape memory alloy (SMA) using a pulsed laser, which will be significant for remote actuation. Thermo-mechanical behavior is investigated at various laser parameters; Array of Micro valve is developed for drug delivery application, and the device properties are verified through various characterization techniques.

5.1 Introduction

The idea of actuating the SMA through a laser came from [147], where the author used a focused laser beam to achieve large amplitude and localized controlled actuation in a microstructure made of ferromagnetic SMA. Various researches have been done on actuation of SMA which is discussed in Chapter 2. Limited work is done using a laser as actuation, and specific gaps were found over which work is done in this project.

Their stable power output and high power density have made pulsed Nd: YAG lasers ideal for industrial applications. Several key parameters are used to control the pulsed Nd: YAG laser process. These parameters include pulse width, peak power, frequency, travel speed and defocus distance. The advantage of laser-assisted actuation is the ability to attain high energy densities and hence to produce maximum penetration in the workpiece. This is achieved when the light is focused to a minimum waist diameter or focus spot size at the zero defocus distance [148]

SMA's are used in various fields because of the unique properties they possess. Literature review shows some gaps over which work is done here. Listed below are some of the common challenges faced by most of the researchers. Electrical connections near micro-actuator make the setup clumsy: Electrical wiring for

supplying electricity to the SMA uses much space near the actuators and makes the whole setup cumbersome.

Focused spot laser is used: Firstly, spot laser is used for actuation of SMA NiTi sheet.

5.2 Experimental Specifications for laser Actuation

For laser actuation study, the trained SMA sheets were mounted on stand. To investigate the laser actuation Nd:YAG Laser (Model: INDI- HG-10S) with second harmonic frequency of 532 nm was used with 10Hz frequency. For actuation, an optimum laser fluence and spot diameter were determined by studying behavior of SMA sheet for various fluence and spot diameter

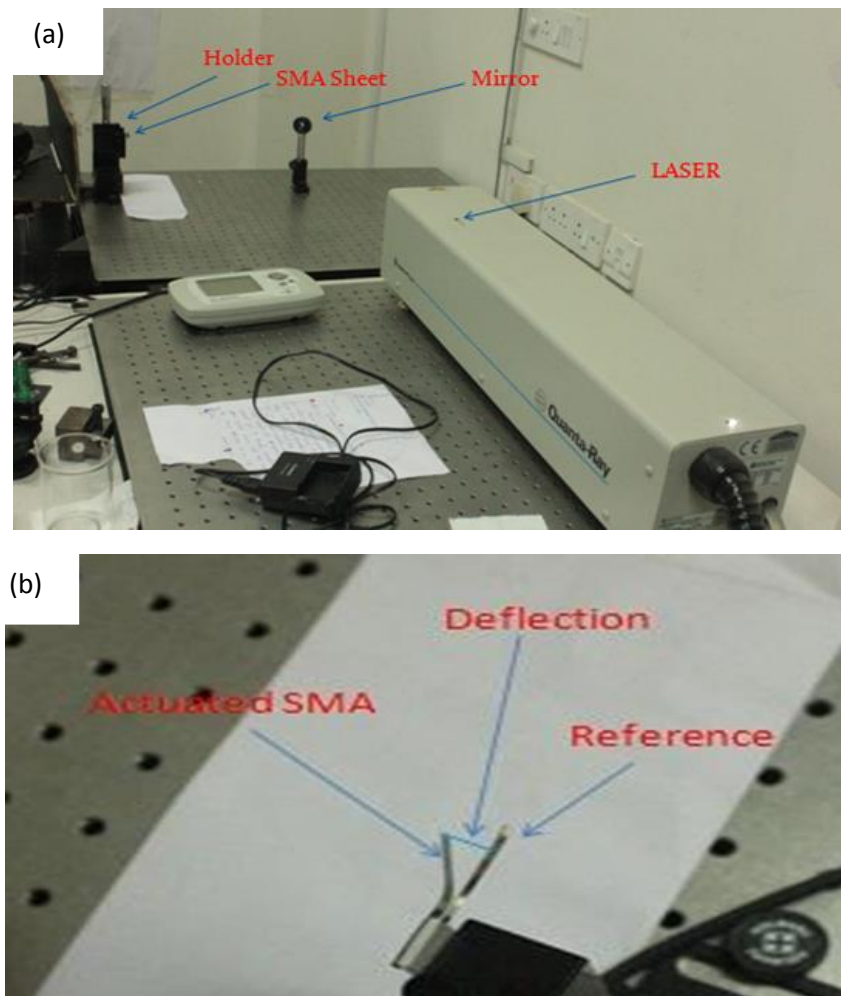


Figure 5.1 a) Setup for actuation of laser, b) Movement in SMA sheet due to laser power

5.2.1 Laser Fluence: Laser energy per unit area on the work material is measured in terms of the energy fluence. It is given algebraically as,

$$\text{Fluence} = \frac{\text{Energy}}{\text{Spot Area}}$$

Where, diameter of spot area = 2.0 mm

Therefore, Area of the spot $A = \frac{\pi d^2}{4}$

Energy = Avg. Power/ Frequency

Hence, Power = Fluence x Spot Area x Frequency repetition rate;

Frequency of the Laser is 10 Hertz

Based on power fluence was calculated and measured deflection of SMA NiTi Power was measured through energy meter.

Table. 5.1 Fluence values and their corresponding power values

Power (mW)	Fluence (mJ/cm²)
219.8	700
188.4	600
157	500
125.6	400
94.2	300
62.8	200
31.4	100

Two important things to be considered during laser actuation (especially for laser fluence):

a) Sufficient fluence: Laser should be able to provide the minimum energy, which would actuate the SMA i.e. it, should be able to raise the temperature at which the phase change occurs from martensite to austenite.

b) Fluence which would not cause ablation: Too much of laser fluence will erode the material from the surface of the SMA. This is undesirable. Hence the fluence level should be controlled to avoid the ablation.

In order to optimize the fluence levels, laser with different fluence levels were impinged on the SMA and the effect was studied.

The laser has a regulator which controls the power of the laser. There is not a regulator which directly controls the fluence since the area of impingement is also a governing factor. Hence, we need a relation between power and fluence which can be used to minimize the ablation. The ablation spots can be seen in the Fig 5.2

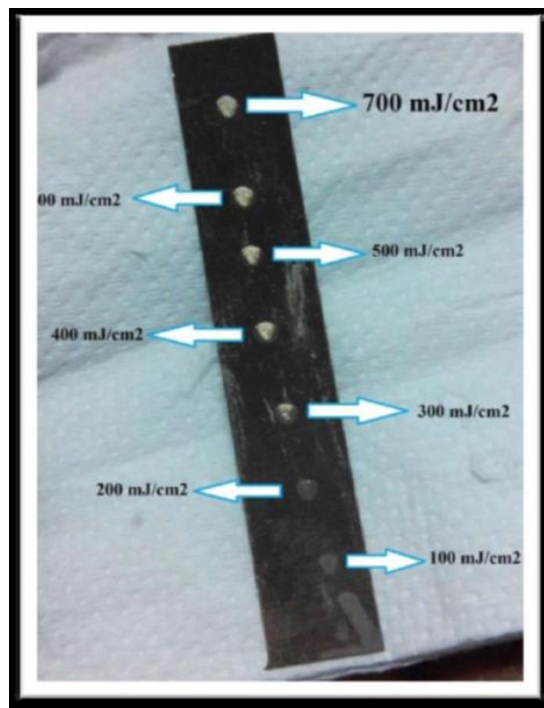
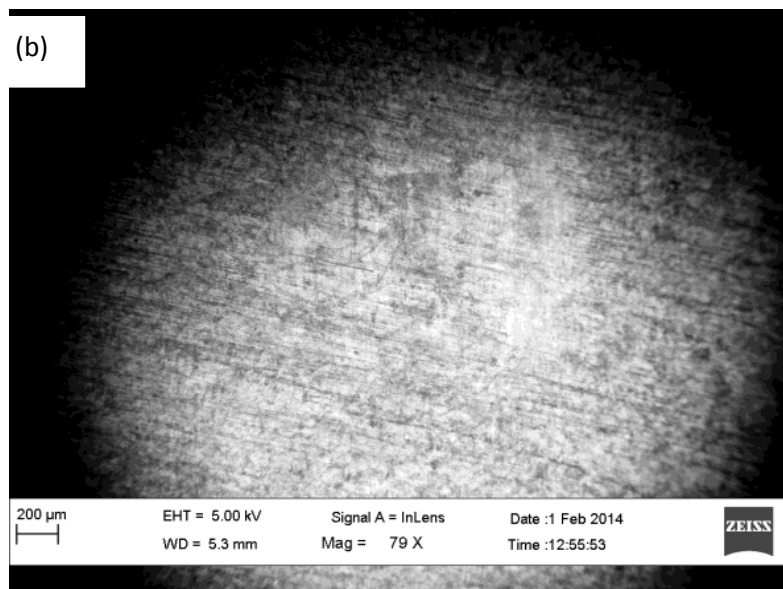
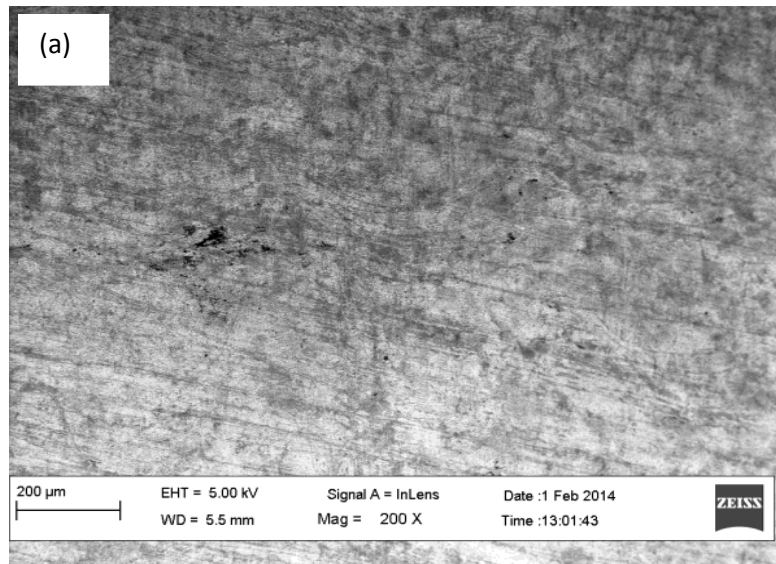


Fig. 5.2 Ablation Spots at different fluence levels

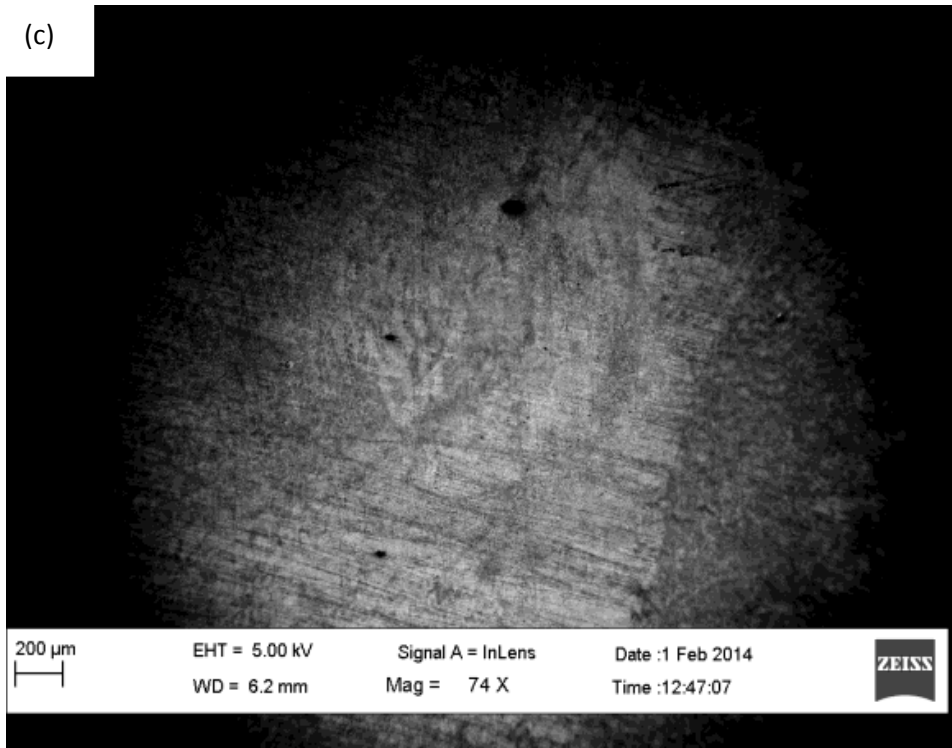
5.2.2 Characterization:

a) Scanning Electron Microscope Images: The SEM images have been helpful in the study of the ablation spots. It can be quite clearly observed in the images that as the fluence is increased, the scale of wear on the surface also increases.

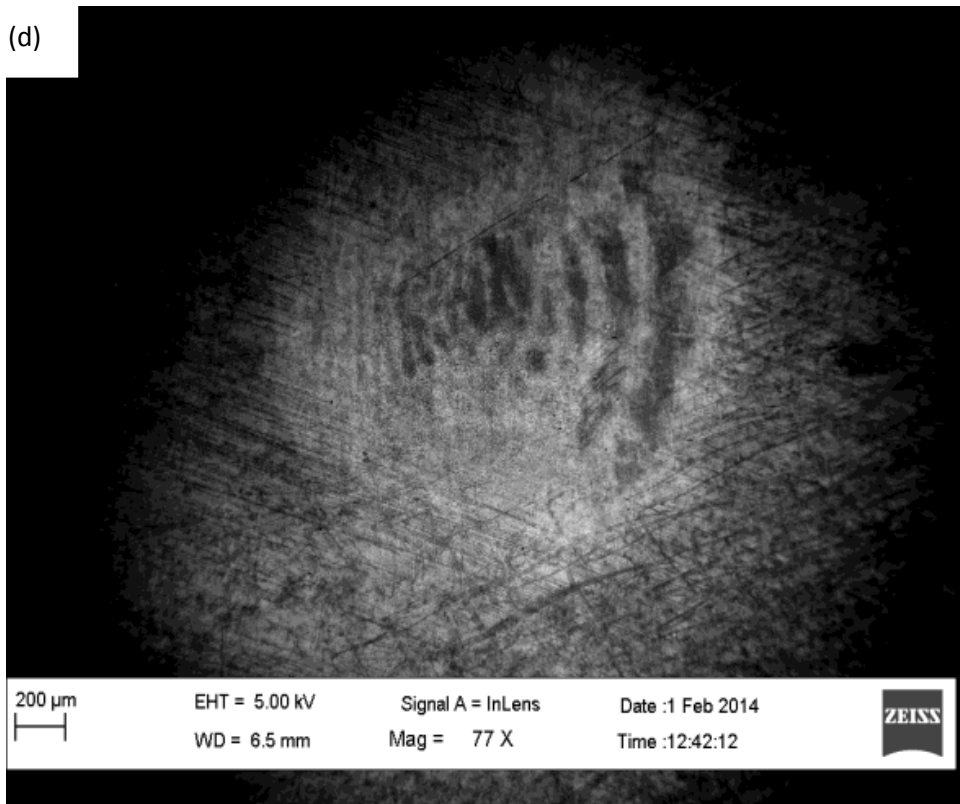
At a fluence value of $100\text{mJ}/\text{cm}^2$ (Fig 5.3 a), minimal ablation can be seen. At $200\text{mJ}/\text{cm}^2$ (Fig 5.3 b), a slight increase in the removal of the material is seen without any significant signs of ablation. At $300\text{ mJ}/\text{cm}^2$ (Fig 5.3 c), this is the fluence where the ablation really starts. The ripples have been formed inside the spot, which indicates a heavy flow of material in the outward direction. These ripples become more prominent as the fluence goes on increasing. Ablation at $700\text{ mJ}/\text{cm}^2$ (Fig 5.3 h) is observed to be maximum with a very high amount of material removal.



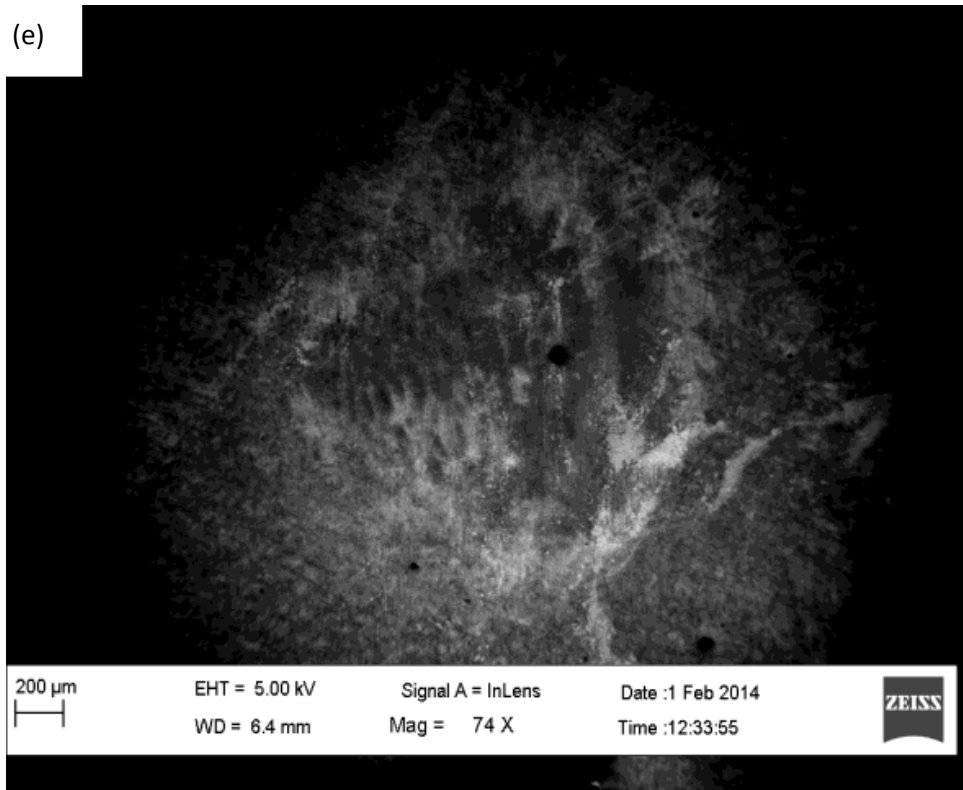
(c)



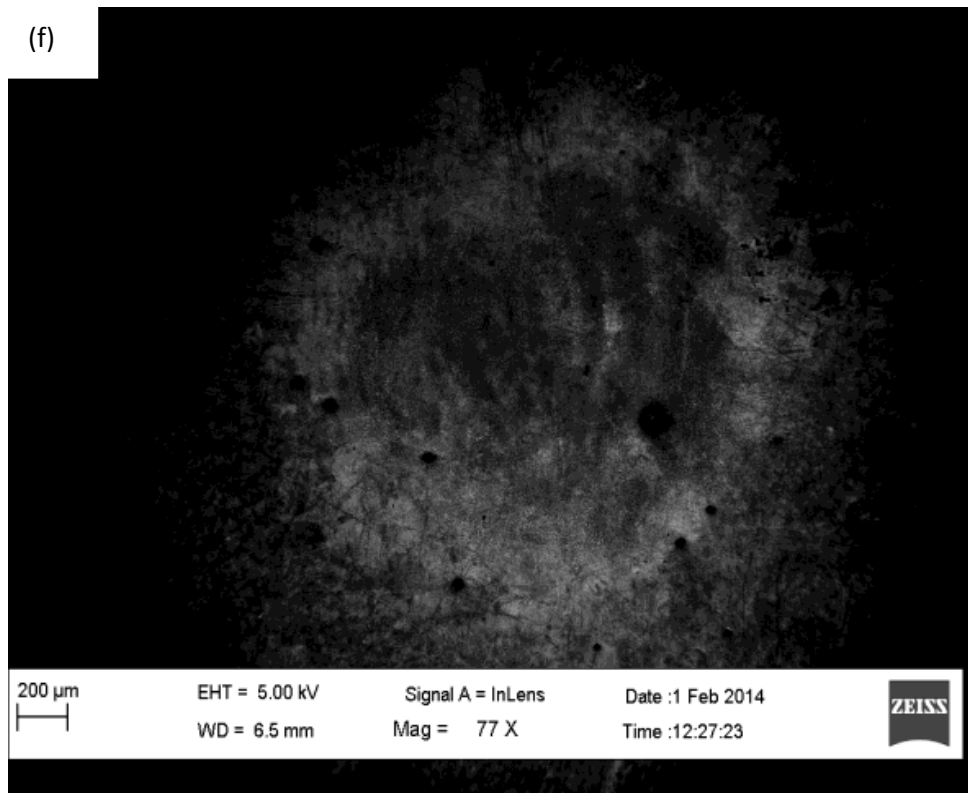
(d)



(e)



(f)



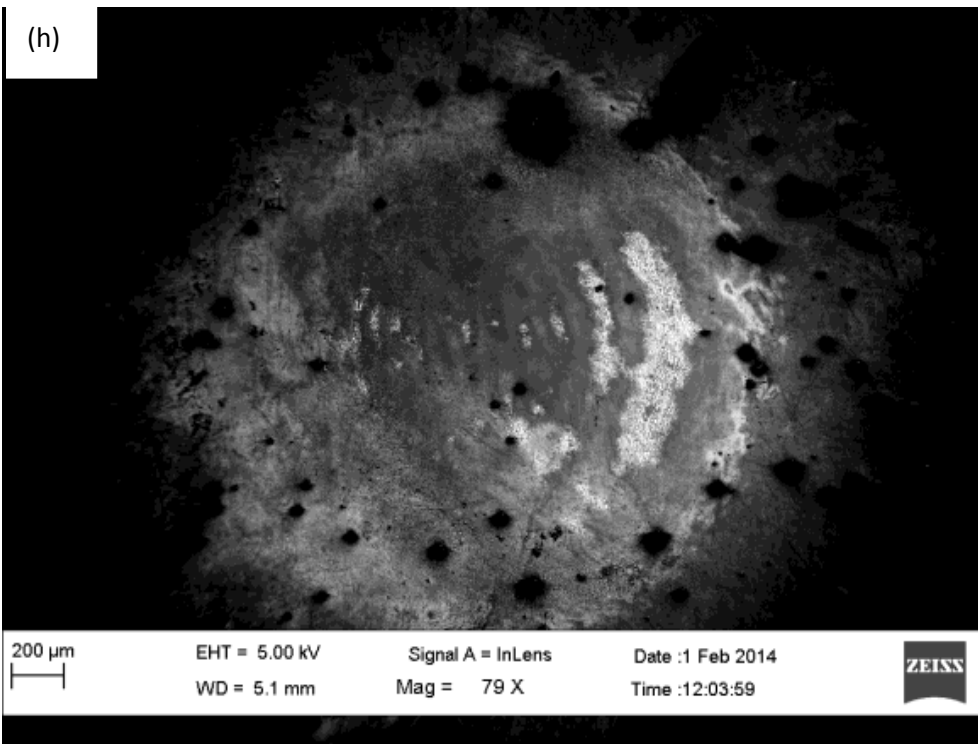
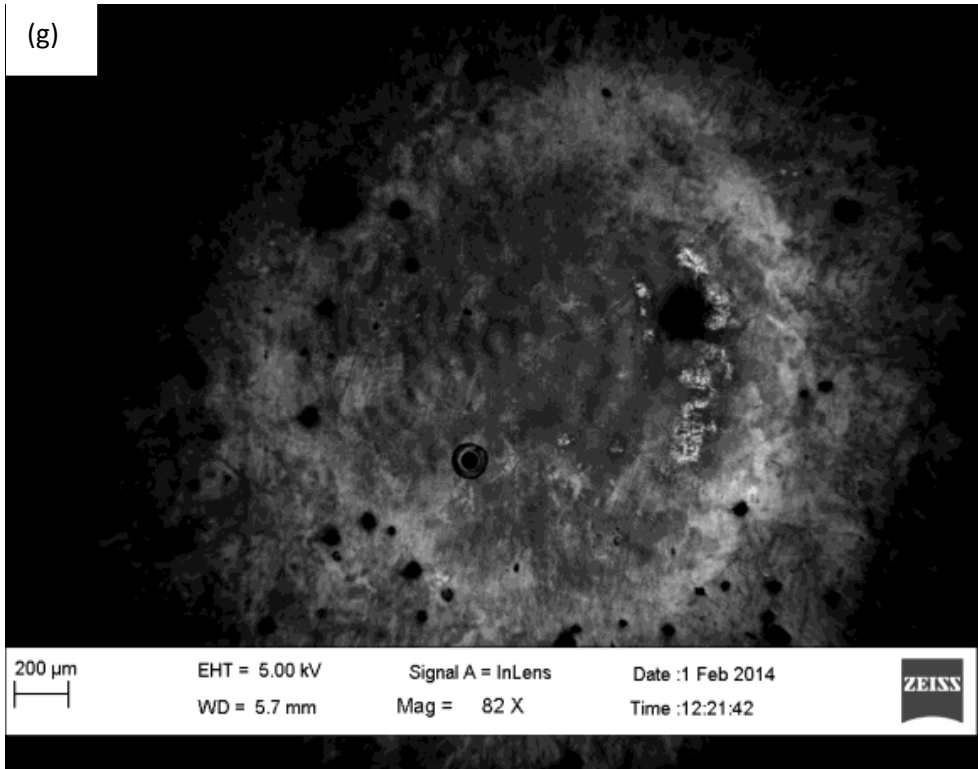


Fig 5.3 Laser with a fluence of a) Non-Treated SMA, b) $100\text{mJ}/\text{cm}^2$, c) $200\text{mJ}/\text{cm}^2$, d) $300\text{mJ}/\text{cm}^2$, e) $400\text{mJ}/\text{cm}^2$, f) $500\text{mJ}/\text{cm}^2$, g) $600\text{mJ}/\text{cm}^2$, h) $700\text{mJ}/\text{cm}^2$

b) Energy-dispersive X-ray spectroscopy is an analytical technique used for the elemental analysis or chemical characterization of a sample. It relies on an interaction of some source of X-ray excitation and a sample

The EDS analysis is done on the laser ablated sample and the results obtained are given in Table 5.2:

Table 5.2: Effect of the laser fluence on the composition of the Nitinol alloy

Fluence (mJ/cm ²)	Weight percent of Ti	Weight percent of Ni	Atomic percent of Ti	Atomic percent of Ni
0	52.35	47.65	57.39	42.61
100	53.23	46.77	58.24	41.76
200	52.54	47.46	57.57	42.43
300	51.72	48.28	56.77	43.23
400	51.9	48.1	56.95	43.05
500	52.04	47.96	57.08	42.92
600	51.5	48.5	56.55	43.45
700	51.19	48.81	56.24	43.76

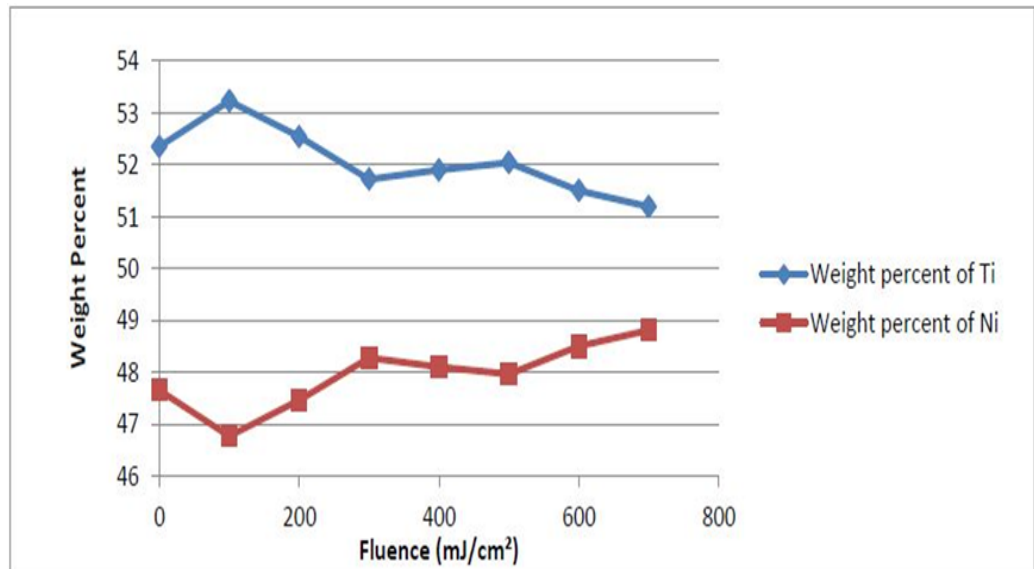


Fig. 5.4: Weight percentage of Ni and Ti with varying fluence values

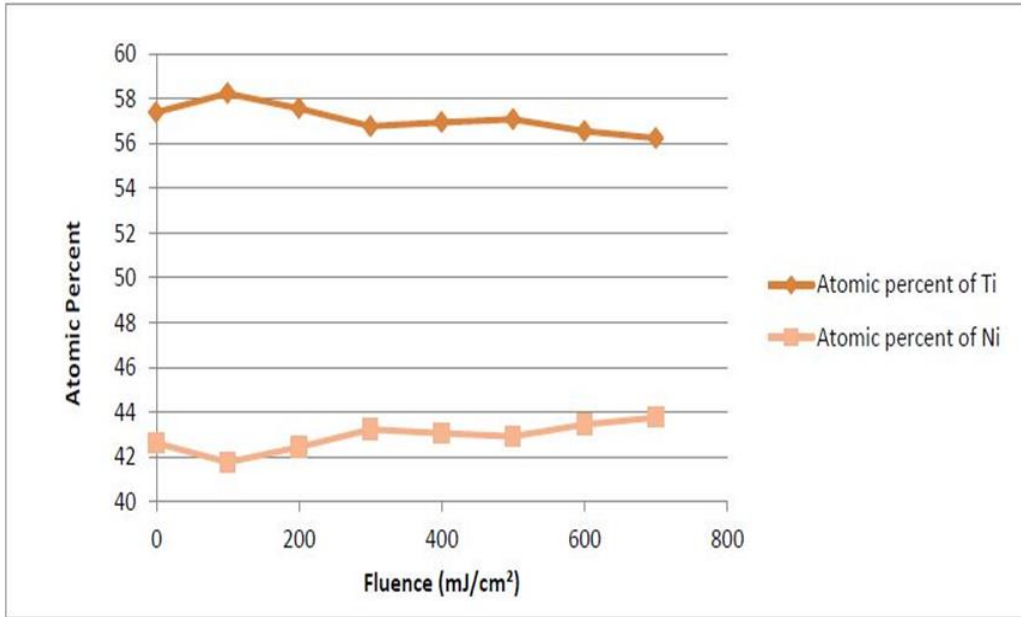


Fig 5.5 Atomic percentage of Ni and Ti with varying fluence values

Ablation is the removal of material because of the incident light. In most metals and glasses/crystals the removal is by vaporization of the material due to heat. It is believed that material is removed in the sample ablated by different fluence values. It is clear that the weight percentage of Ti decreases with the increasing fluence value and the weight percentage of Ni increases with the increasing fluence value (Fig 5.4). Similarly, the atomic percentage of Ti decreases with the increasing fluence value and the atomic percentage of Ni increases with the increasing fluence value.

Now, with laser ablation, both the Ti and Ni are vaporized and removed. The weight and atomic percent increase in the graph only shows that more of Ni is being vaporized than Ti. This is better represented by the bar graph below (Fig 5.5-5.6).

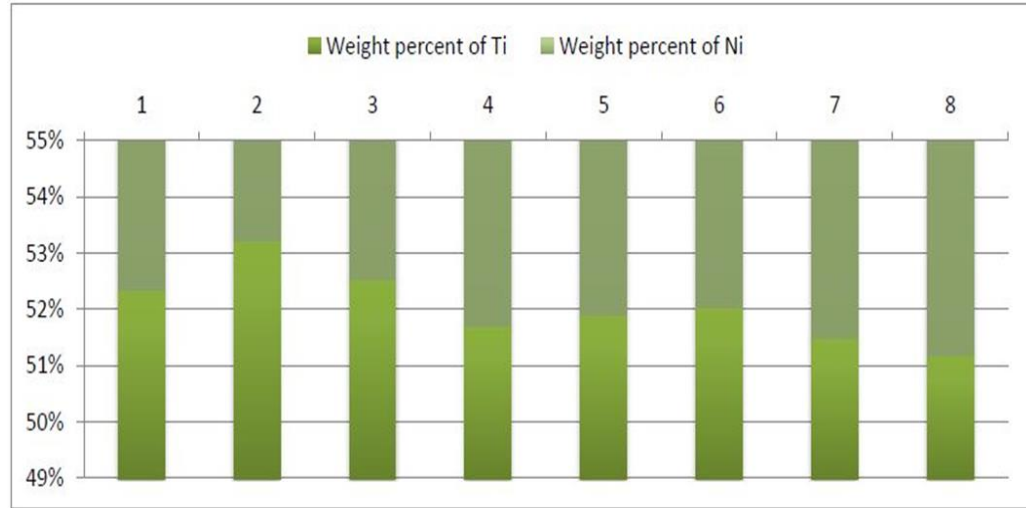


Fig 5.6 Comparison of weight percentage of Ni and Ti at different fluence values

5.3: Development of Micro devices: This section presents laser assisted actuation of micro devices which is more suitable for precision point of view as compared to the previous two sources. Since light has been used to manipulate MEMS devices for some years using a variety of different mechanisms. The earliest literature found on the subject used beams of light to heat various structures or membranes, causing thermal actuation. Some designed and developed micro devices are explained in the upcoming sections:

5.3.1 Tripod

5.3.1.1 Tripod: Using Sheet: SMA actuated Tripod have their own application in Opto-Mechatronics system design. The main objective of this research is to develop pulsed laser actuated SMA based tripod. In this regard, training and actuation of shape memory are of major interest to reach the particular application. The required shape was trained by developing a fixture. The actuation studies were with the help of a pulsed laser that is explained here, The technique of Michelson interferometer has been used to investigate the deflection in detail since the deflection is in few microns. Finally, an SMA based tripod was fabricated, and the deflection of the SMA based tripod was studied in detail.

5.3.1.2 Fabrication: The first step involves the training of SMA NiTi thin sheets. Fixture as shown in Fig 5.7 (a) was developed to train the SMAs sheets to get an (ω - Ω) Shape. Ni-Ti sheets of 0.25 mm thickness were mounted on the fixture, and it was heated for 30 min in a muffle furnace (Model-BTI 36) which has a capability of 0-230V and 15A, at a temperature of 550°C after 30 minutes, it was made to cool in the atmospheric condition. Fig 5.7 (b) shows the final shape of the SMA sheet, which is in the form of omega shape. In this train, SMA sheet heat flow is getting reduced whereas the temperature is the same means it will give more actuation after training the sheet [116].





Fig 5.7: Single way Training of SMA sheets a) Fixture used for training of SMA, b) Ni-Ti sheet trained in omega shape, c) Fabricated Tripod

5.3.1.3 Experimentation: In this section actuation of NiTi has been done through laser. Nd-YAG Laser (Model No: INDI: HG:10 S) is used for actuating the sheet. As the absorption coefficient of NiTi is higher at 355 nm wavelength, so the intensity of absorption will be higher than 532 and 1064 nm wavelength, so it is not chosen. In the case of 532nm Wavelength ablation of NiTi will be nominal at respective fluence whereas ablation of material in the case of 1064nm wavelength is more as compared to others so this was optimum. Since the sheet is trained (Fig.5.7 b) as an omega shape so when it is actuated through the laser, it will come to its omega shape and can be used for micro machining applications.

To investigate the laser-assisted actuation of SMA NiTi sheets in detail, the trained sheets, which was in the shape of Omega was made flat. The total length of the NiTi sheets after becoming flat was 50 mm length. The actuation was performed with a laser of 532 nm wavelength. It was observed NiTi sheet deflected 7.25 mm within 120 sec, without any damage to the surface. It is

actuated with various fluence, but best of one was chosen which is not affecting material behavior as well as property. Detail investigation of surface morphological analysis has been explained in the result section.

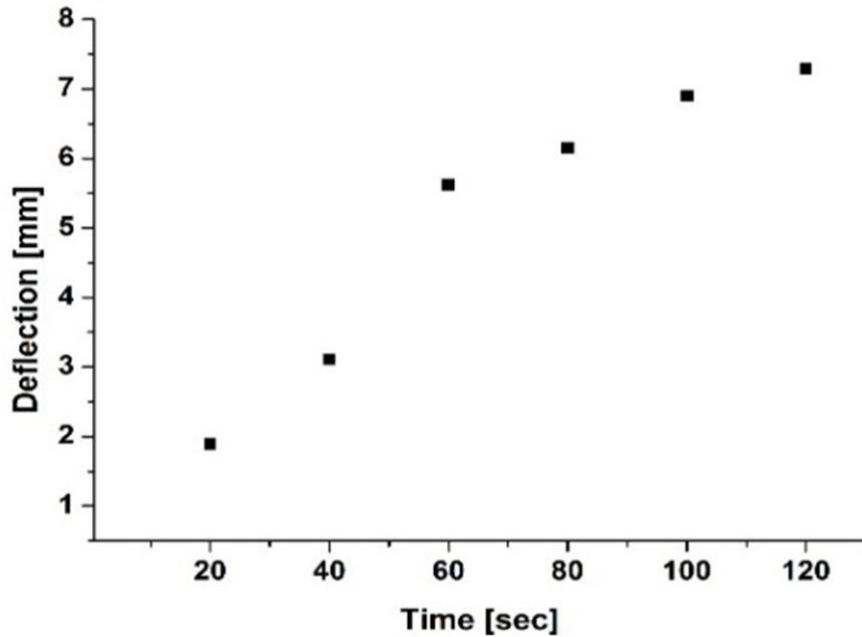


Fig 5.8: Deflection vs time for actuated SMA NiTi

It was observed that beyond 100 mJ/cm^2 ablation on the surface was observed below, with 100 mJ/cm^2 there was no trace of ablation, but mild actuation was observed. At 700 mJ/cm^2 and 500 mJ/cm^2 cracks, the formation was there, so 100 mJ/cm^2 was optimum. Hence studies were performed at different time scale with 100 mJ/cm^2 as shown in Fig 6.19, and at 120 sec a deflection of 7.25 mm (Fig 5.8) was observed.

5.3.1.4 Result and discussion: A three sets of NiTi thin sheet of 0.25 mm thickness were trained (Fig 5.7 c) to the shape of omega. The trained NiTi sheets were actuated using Nd-YAG laser. The deflections were experimentally analyzed using a Michelson's interferometer. In the case of laser-based actuation with laser fluence of 100 mJ/cm^2 , the morphology of the laser interacted surfaces was also evaluated and verified using characterization technique, i.e. SEM Micrograph,

TGA analysis, etc. Thus by increasing the laser interaction time by 120 sec a deflection of around 7.25 mm was achieved without any damage on the surface.

5.3.2 Micro valve:

5.3.2.1 Microvalve- using sheet: Since microvalves typically operate under high pressures and controlled flow rates are desired, a strong and robust actuator that can generate required displacements is required. SMA's are excellent candidates for satisfying these criteria, and their use in microvalves will be discussed in detail here. The microvalve is designed and fabricated to control small amounts of fluid flow of the order of $\mu\text{L}/\text{sec}$. Single way trained NiTi SMA is used in this micro-valve. In this work, laser-assisted actuation of SMA based micro valve is investigated designed, fabricated, and tested. Such devices exhibit a linear scalable valve function over a wide range of flow rates. Since the mode of heating here is a laser, there is a possibility that if high fluence is used then the incident area of SMA sheet may vaporize due to absorption of energy hence a maximum value of fluence must be known below which there is no damage to SMA.

To validate its model and the cause for depletion in its actuation property, morphological analysis has been done.

5.3.2.2 Objective: For achieving given objectives, experimentation has been done:

1. To designing and fabrication of micro valve for controlling the fluid flow.
2. To Train the SMA sheet and its actuation through Laser.
3. To validate the data's using results of the diagnostic tests (SEM, EDX, DSC, and TGA).
4. To develop an experimental set up for estimating Flow rate and leak rate.

5.3.2.3 Fabrication and working: Design of Micro valve is already shown in Fig. 5.9. The fabrication of micro valve (Fabricated Micro valve as shown in the Fig. 5.10) consists of Acrylic sheet and NiTi SMA sheet. SMA sheet dimension is $50 * 10 * 0.25\text{mm}^3$, which is attached to a gate for fluid passage.

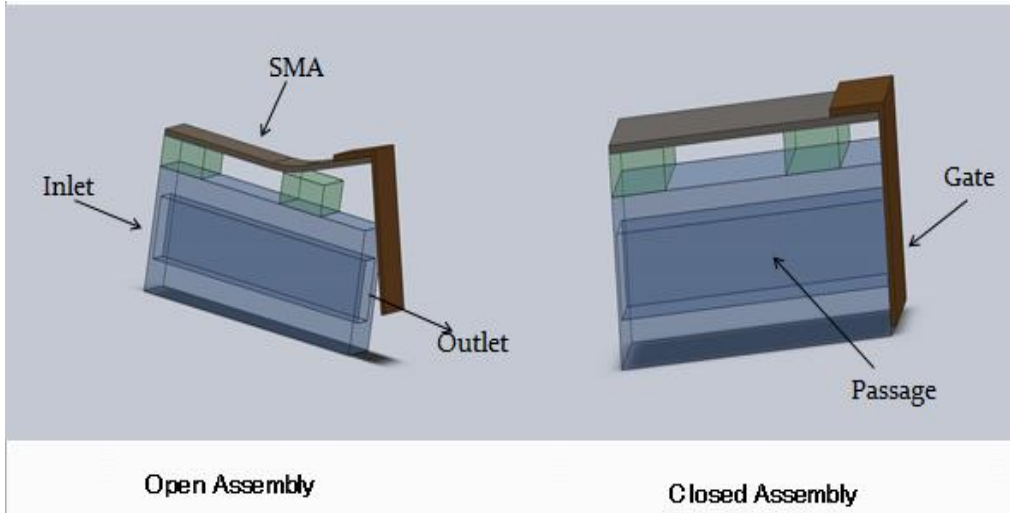
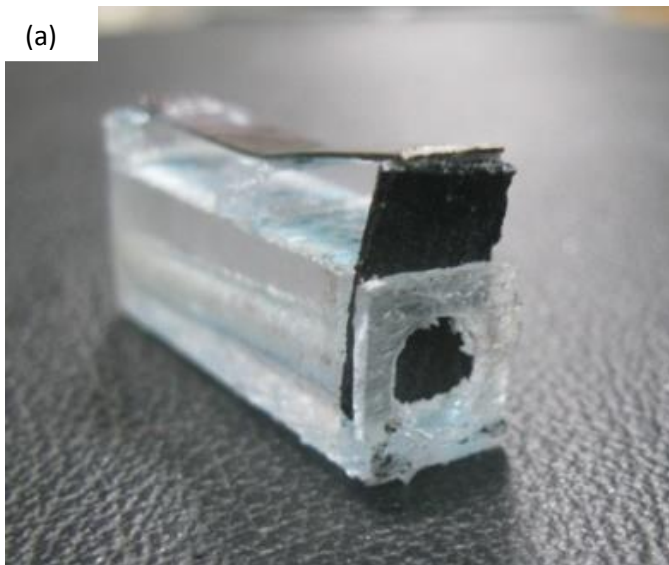


Fig. 5.9: Design of Micro valve open and closed assembly

Initially, the gate is in the closed position then as soon as heat is provided to SMA through Laser, it bends and results in an upward motion of gate because of which fluid passage opens and fluid start flowing. For fluid passage a plastic tube with an inner diameter of 1.5 mm and the outer diameter of 5mm is inserted in cubical case of dimension 10 mm x 10 mm x 50 mm, made by the acrylic sheet.



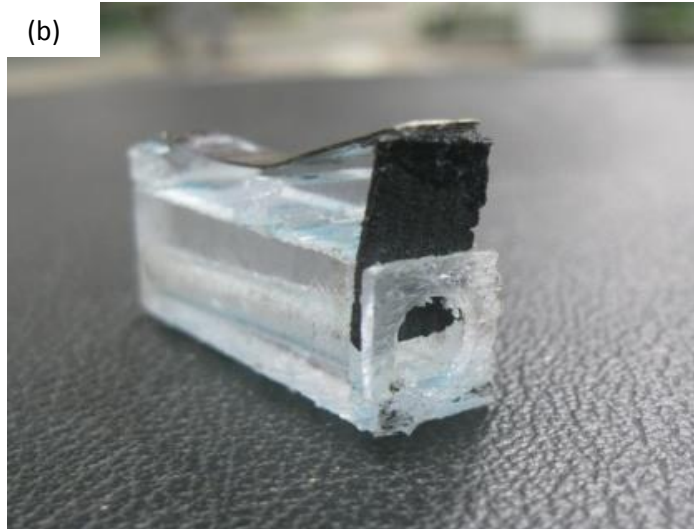


Fig 5.10: fabricated micro valve in a) open position, b) open position

5.3.2.4 Experimentation: Experimentation on the fabricated micro valve is done in two *steps*:

a) *Single way training of SMA sheet:* The first step involves the training of SMA NiTi thin sheets. A fixture as shown in Fig 5.11 (a) was developed to train the SMAs sheets to get a bent Shape. The NiTi sheets of 0.25 mm thickness were mounted on the fixture, and it was heated for 30 min in a muffle furnace (Model-BTI 36) as shown in Fig. 5.11 (b), which has a capability of 0-230V and 15A, at a temperature of 550°C after 30 minutes, it was made to cool in the atmospheric condition. Fig 5.11 (c) shows the final shape of the SMA sheet, which is in the bent form.





Fig 5.11 : Apparatus used in Training a) Fixture, b) Muffle furnace, c) bent sheet

b) Specification of Laser actuation: For laser actuation study, the trained SMA sheets were mounted on a stand. Fig. 5.12 a shows the laser actuated experimental setup and 5.12 b shown actuation of NiTi sheet. To investigate the laser actuation Nd: Yag Laser (Model: INDI-HG-10S) with the second harmonic frequency of 532 nm was used with 10Hz frequency. For actuation, optimum laser fluence and spot diameter were determined by studying the behavior of SMA sheet for various fluence and spot diameter.

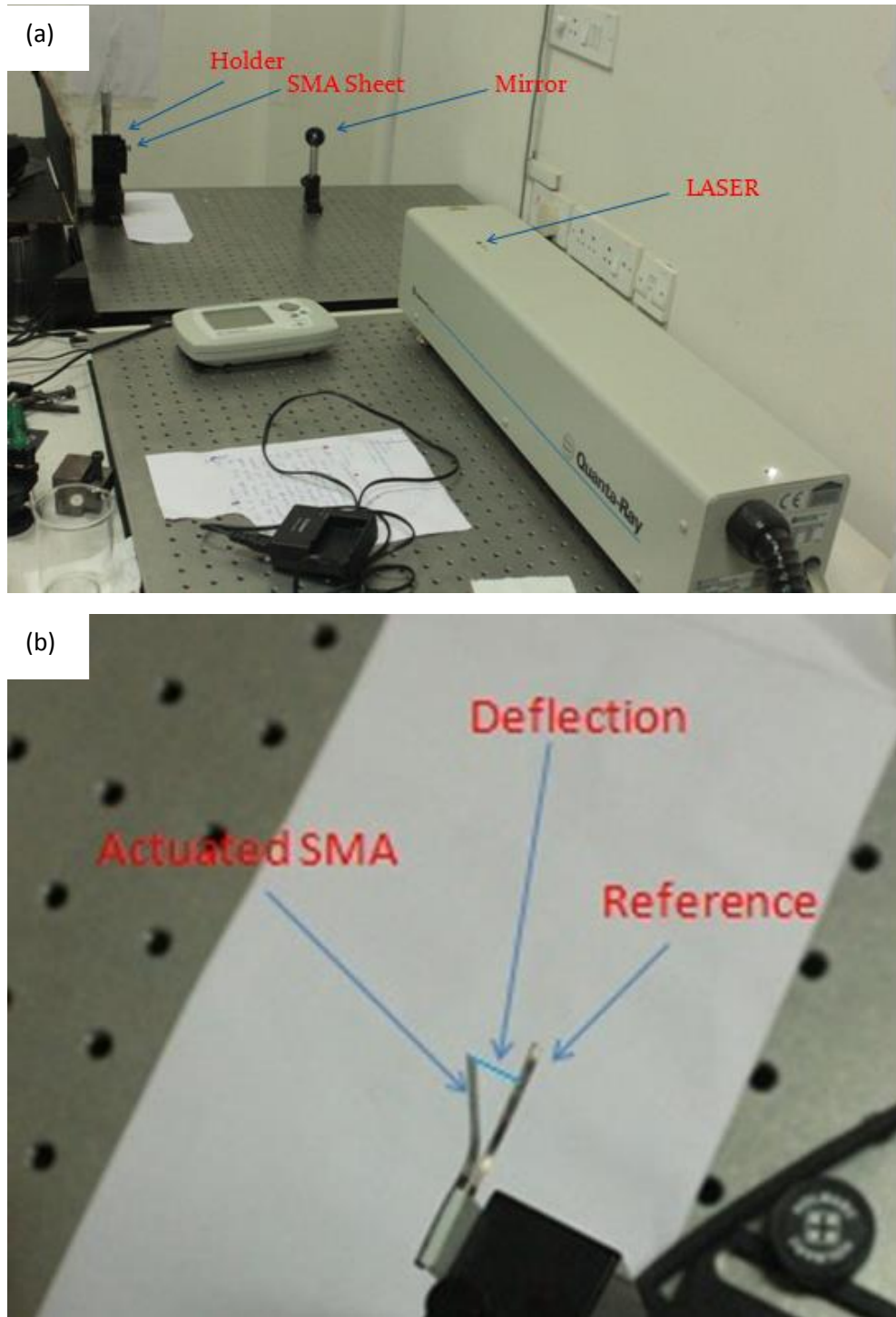


Fig 5.12 a) Laser actuation set up, b) deflection of SMA

Table 5.3 Deflection at given power

Power (mW)	Fluence (mJ/cm ²)	Time (s)	Deflection (mm)
20	10.19	4	0
30	15.28	4	2.3
40	20.38	4	5.2
50	25.48	4	7.29

5.3.2.5 Result and discussion: Deflection increases as actuation time increases. Deflection at given power is mentioned at different fluence for a constant time which is mentioned in Table 5.3. Deflection of SMA was observed as a function as laser intensity was kept constant which is useful for controlling the opening of the valve. With the help of following data desired value of flow rate can be obtained. Maximum deflection (Fig. 5.13) obtained for optimum laser fluence of 25.48mJ/cm² is 7.29 mm.

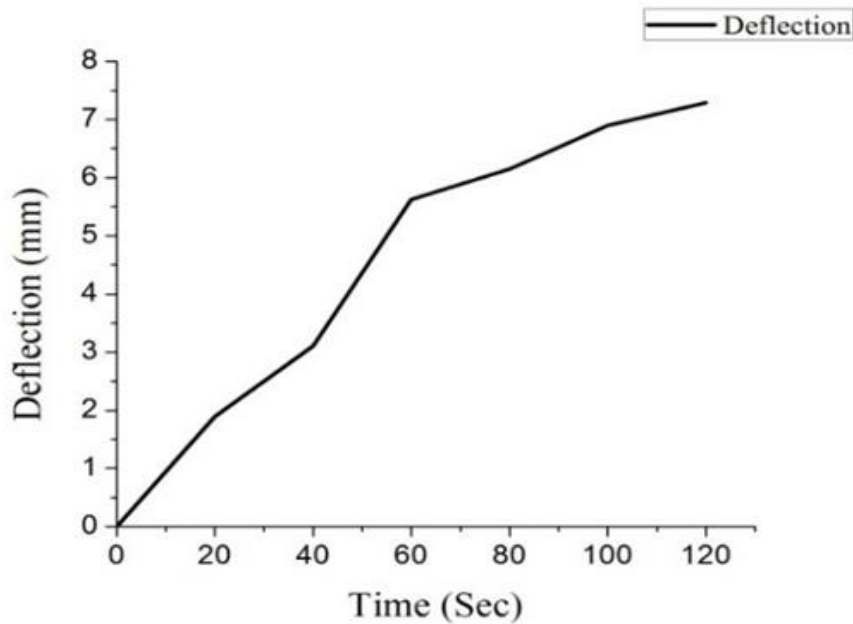
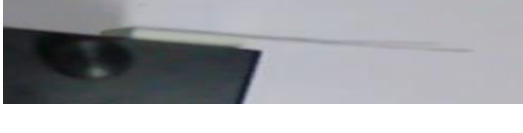
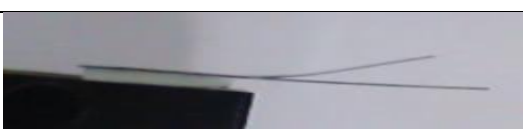
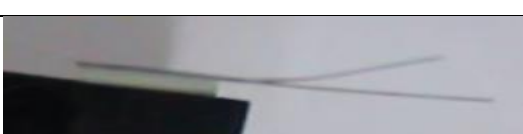


Fig 5.13: Deflection versus time plot

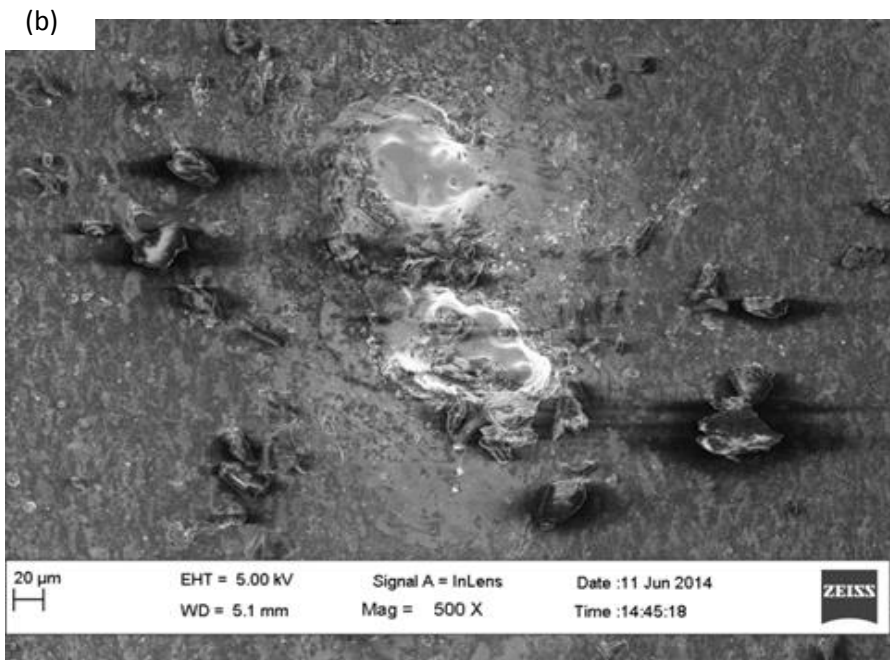
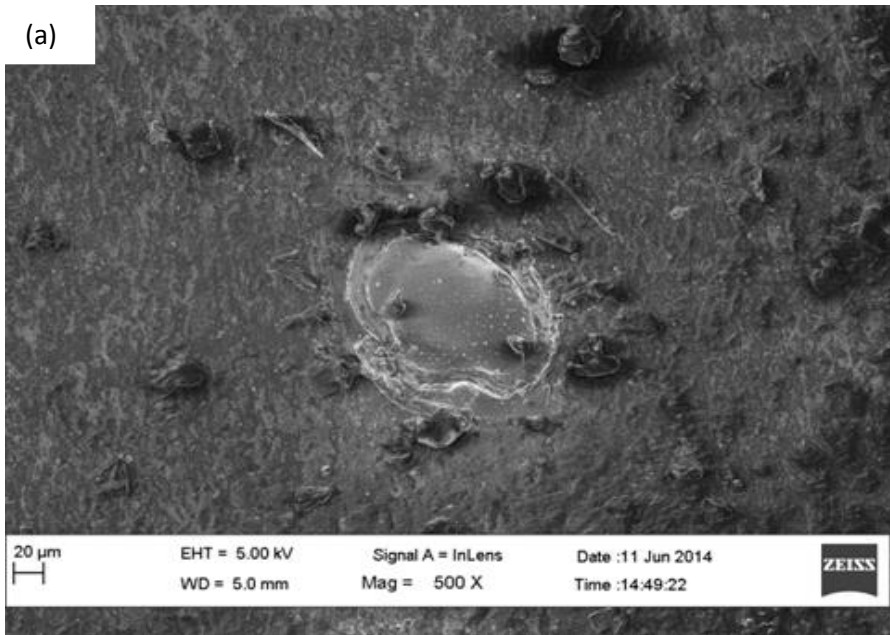
- *Deflection of SMA with time at a fluence of 25.48 mJ/cm²*: Deflection of SMA is tabulated in 5.4 at a fluence of 25.48 mJ/cm²

Table 5.4 Orientation at respective deflection

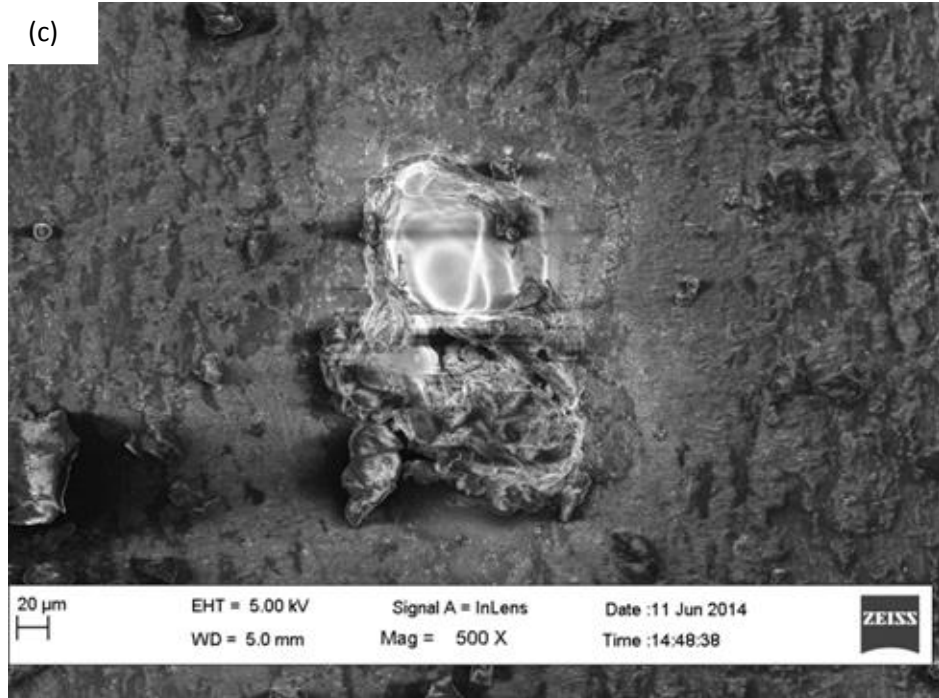
Time (s)	Deflection (mm)/ Angle (°)	Image
0	0 (0°)	
20	1.89 (4.3°)	
40	3.11 (7°)	
60	5.62 (12.7°)	
80	6.15 (13.8°)	
100	6.9 (15.4°)	
120	7.29 (16.2°)	

5.3.2.6 Characterization:

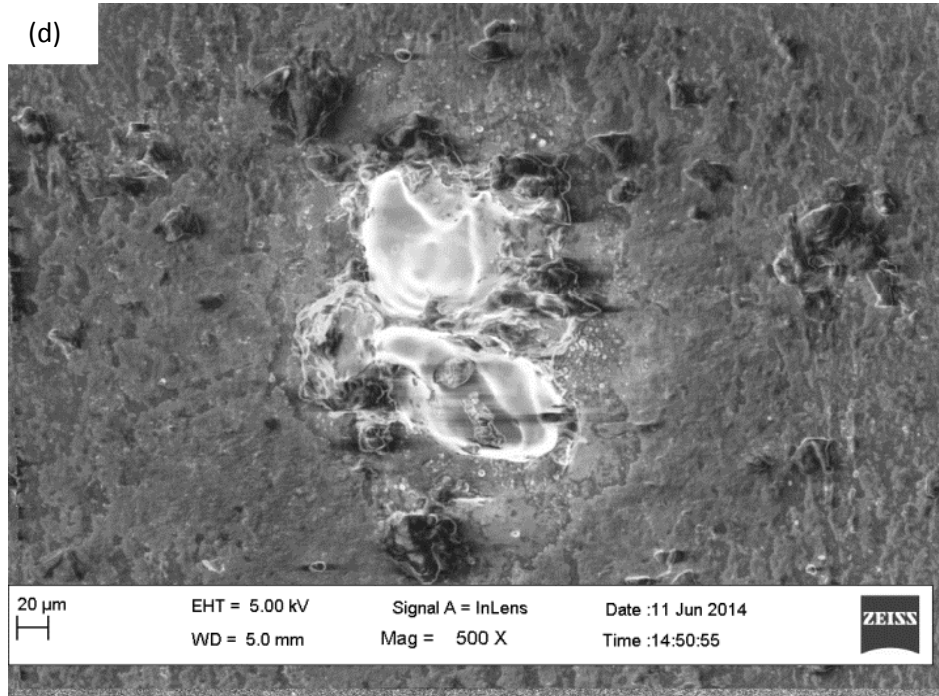
a) *SEM image at 0.5 mm:* For optimum fluence value LASER with spot diameter 0.5mm spot diameter was incident on the SMA sheet for a period of 5 min, and Scanning electron microscope images of the incident area were taken. Images 5.14 (a-f) are for fluence value of 100 mJ/cm^2 , 110 mJ/cm^2 , 120 mJ/cm^2 , 130 mJ/cm^2 , 140 mJ/cm^2 and 150 mJ/cm^2 respectively.



(c)



(d)



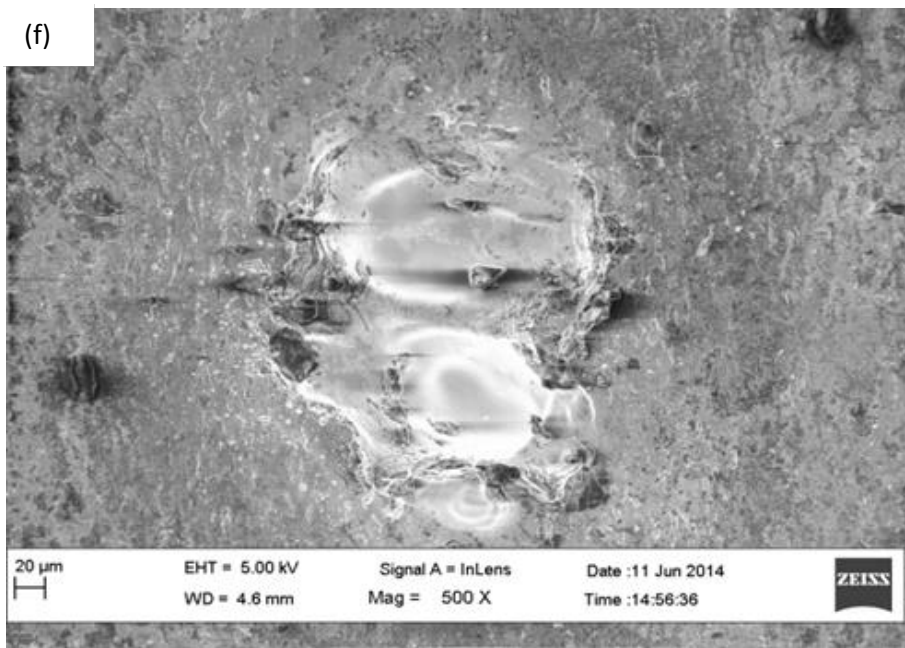
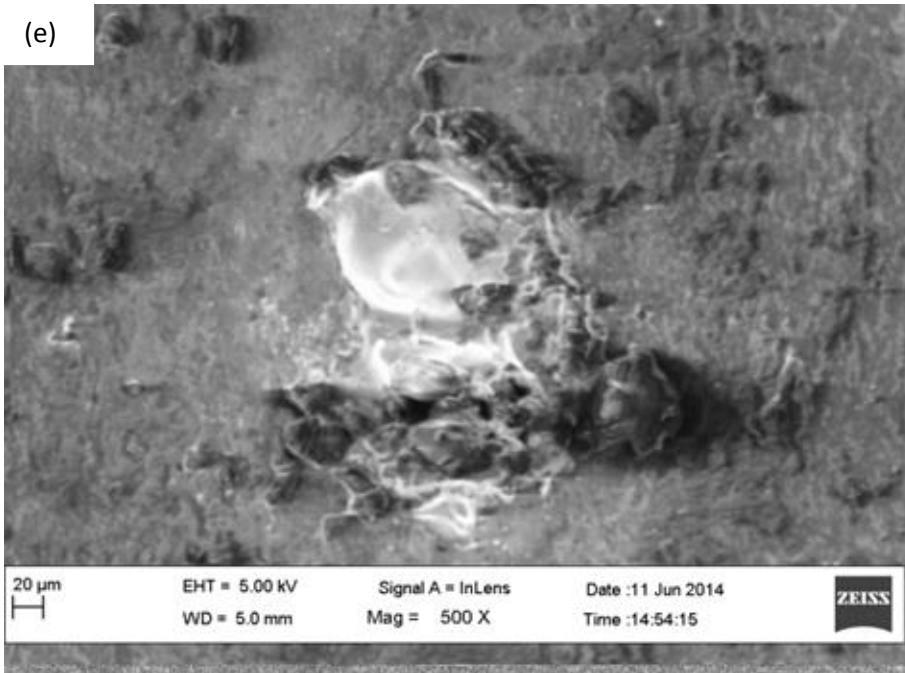
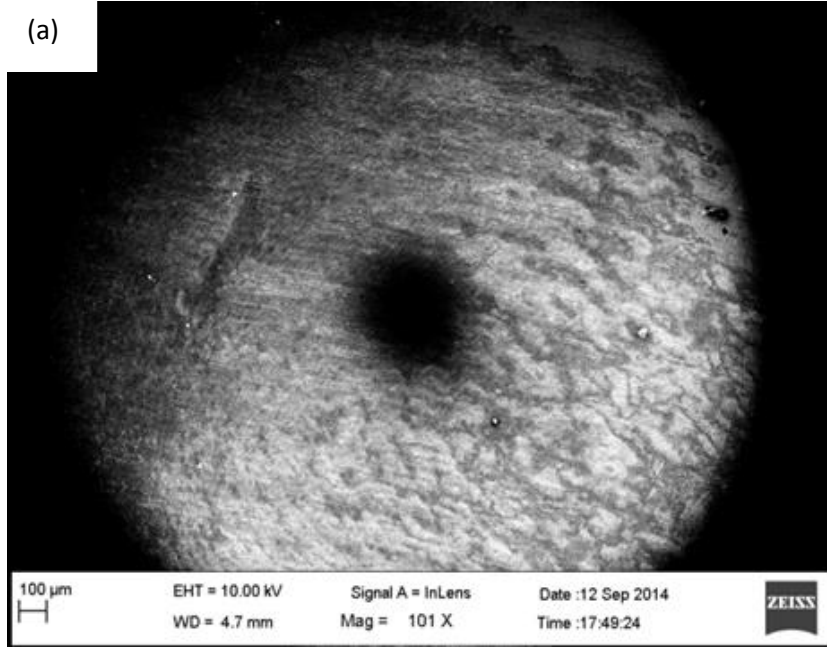


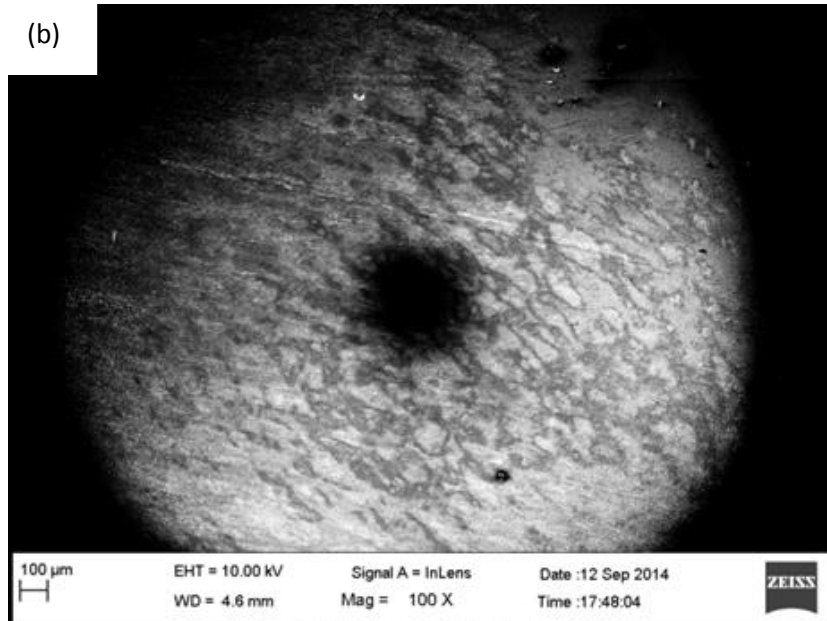
Fig 5.14 SEM image at a) 100 mJ/cm^2 , b) 110 mJ/cm^2 , c) 120 mJ/cm^2 ,
d) 130 mJ/cm^2 , e) 140 mJ/cm^2 and f) 150 mJ/cm^2

b) SEM image at 3.0 mm: Below are SEM images of SMA after incidence of LASER of spot diameter 3.0 mm for different values of fluence for 5 minutes. Images 5.15 (a-e) and are for fluence value of 70 mJ/cm^2 , 100 mJ/cm^2 , 130 mJ/cm^2 , 140 mJ/cm^2 and 155 mJ/cm^2 respectively.

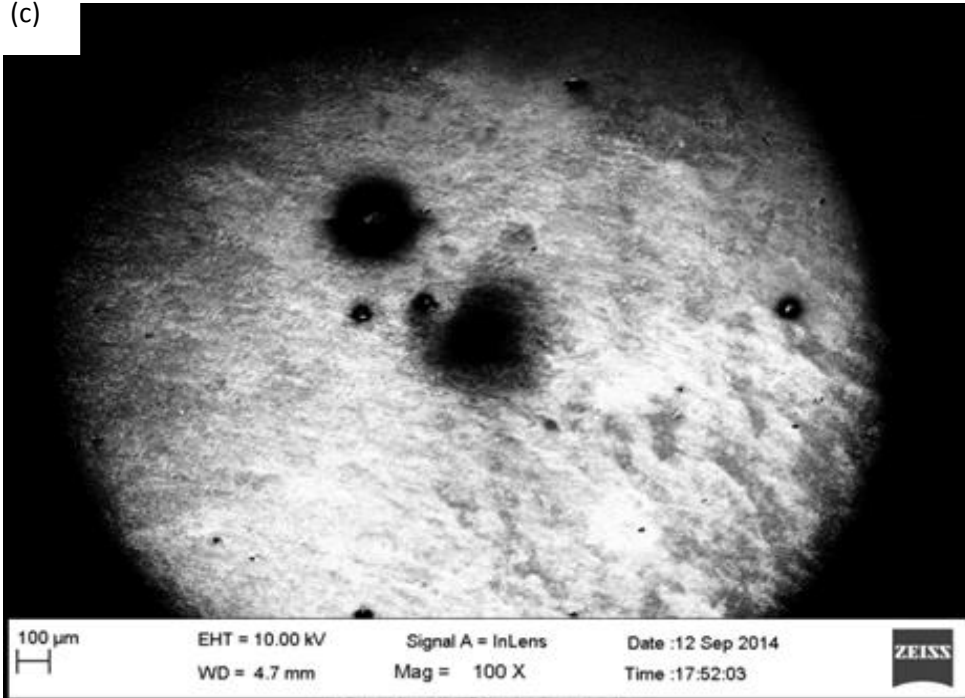
(a)



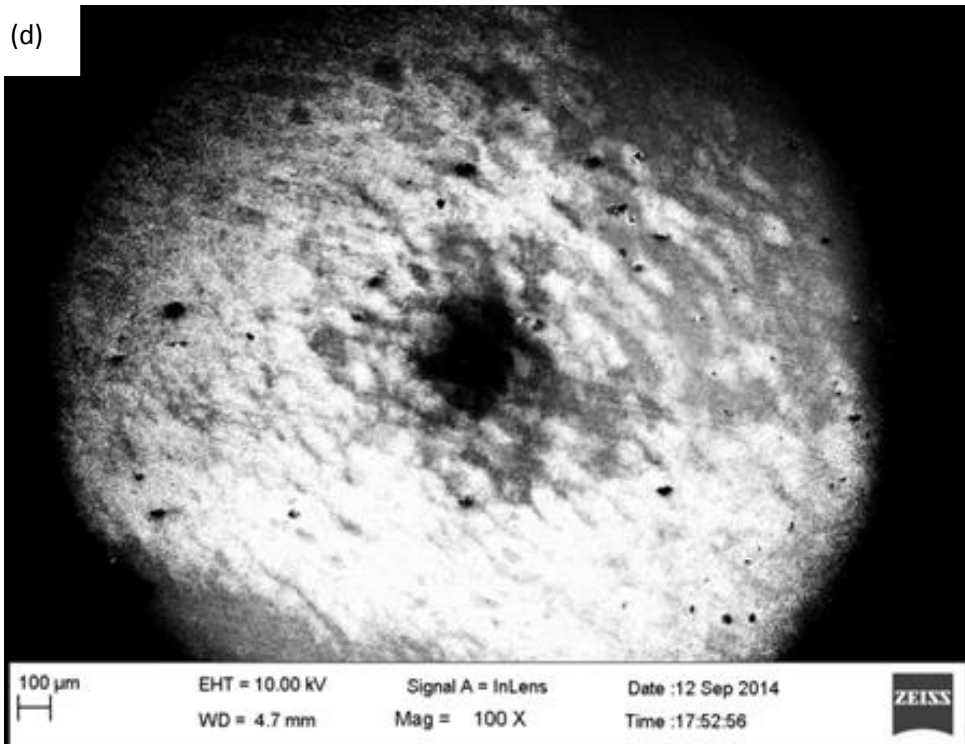
(b)



(c)



(d)



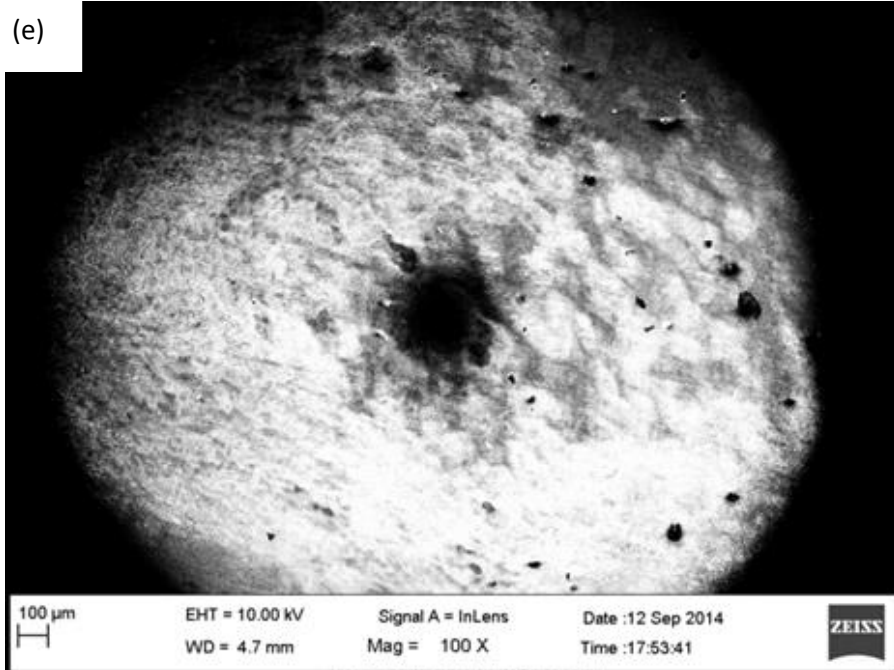


Fig 5.15 SEM image at a fluence level of a) 70 mJ/cm², b) 100 mJ/cm², c) 130 mJ/cm², d) 140 mJ/cm² and e) 155 mJ/cm²

Table 5.5 : Result of SMA actuation

Parameters	Lens (spot diameter 0.5 mm)	Lens (spot diameter 3.0 mm)	Lens (spot diameter 5.0 mm)
Actuation	No	Yes	Yes
Ablation	Yes	No	No
Disadvantage	No Actuation		May also strike at undesired location
		Best suited for our application	

It is clear from Table 5.5 that 3.0 mm diameter was good and suited for our application

c) **EDX images:** Composition of SMA has been revealed by Energy-dispersive X-ray spectroscopy test which gives atomic and the weight percent of Ni and Ti. Atomic percent of Ni and Ti is found to be 42.43% and 57.5% respectively, and Weight Percent is 47.46% and 52.54 % respectively (Fig 5.16)

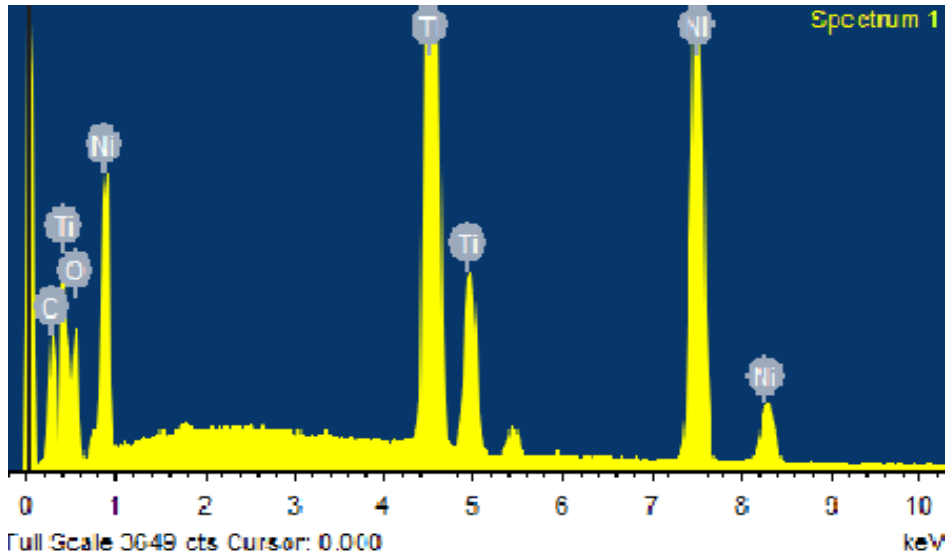


Fig 5.16: EDX image of SMA sheet

d) **DSC images:** DSC is a technique which gives a requirement of heat for increasing the temperature, both the sample and reference are maintained at nearly the same temperature throughout the experiment. DSC reveals (Fig 5.17) the transformation temperatures of SMA.

Martensite finish temperature (M_f): -13°C

Martensite start temperature (M_s): 11°C

Austenite start temperature (A_s): -11°C

Austenite finish temperature (A_f): 15°C

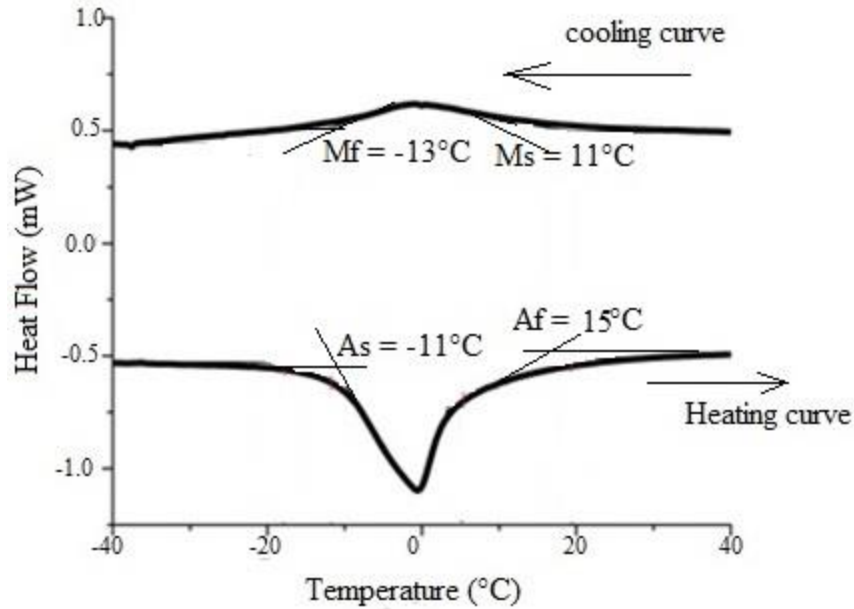


Fig 5.17: DSC curve of NiTi sheet

e) **TGA image:** Thermo Gravimetric Analysis is commonly used to determine selected characteristics of materials that exhibit either mass loss or gain due to decomposition, oxidation, or loss of volatiles (such as moisture). With the help of TGA we can measure the changes in physical and chemical properties of the material as a function of increasing temperature (with constant heating rate), or as a function of time (with constant temperature and constant mass loss) which is shown in Fig 5.18.

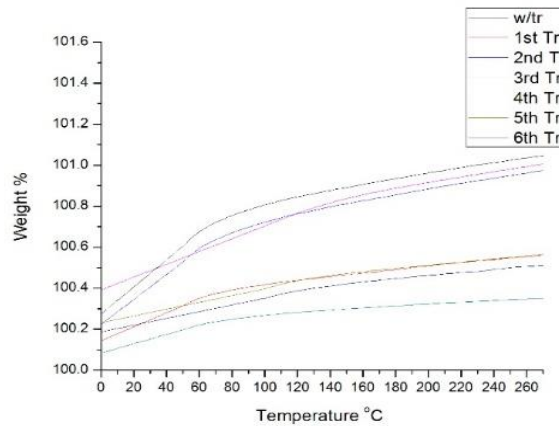


Fig 5.18: TGA image of NiTi sheet

d) Hardness Test: Micro- harness testing has been completed. For this, we preferred Vicker's Hardness test over Knoop hardness test because NiTi sheet is ductile. Since SMA sheet thickness was 0.25 mm; so, applied load for conducting microhardness testing was quite low as it was 300 gram. It is clear from Fig 5.19 that there is no effect of training on the sample .

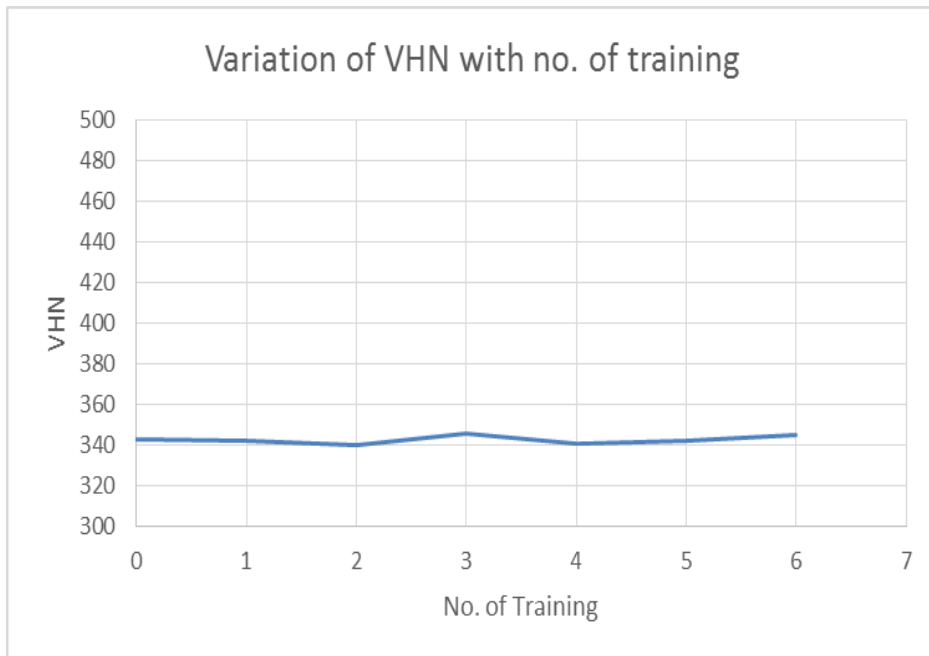


Fig. 5.19: variation of VHN with number of training

5.3.3 Micro valve Array: Microvalve arrays differ fundamentally in performance from single-channel-micro machined flow control valves for which the flow rate is controlled by varying the size of a single flow channel. The flow rate through a microvalve array scales linearly with the number of microvalves open, whereas flow rate through a single-channel valve varies, in low Reynolds number flows, with the height of gate open.

Moreover, array systems achieve precise flow control by relying on a multiplicity of simple low-precision elements rather than angle more complex high-precision element. This offers an advantage in fabrication since in micromachining multiplicity has a relatively low cost while complexity has a relatively high cost.

5.3.3.1 Design: Design for microvalve array for fluid flow control is described in Fig 5.20. The device consists of an array of microvalves working cooperatively to achieve precision flow control on a macroscopic level. Flow rate across the microvalve array is proportional to the number of microvalves open, yielding a scalable high-precision fluidic control system. To achieve precision flow control on a macroscopic level, a set of microvalves can be used. The flow rate through a microvalve array scales linearly with the number of microvalves open, whereas flow rate through a single-channel valve varies with the deflection of SMA and height of gate open. Each microvalve is independently controlled either by laser using optical fiber.

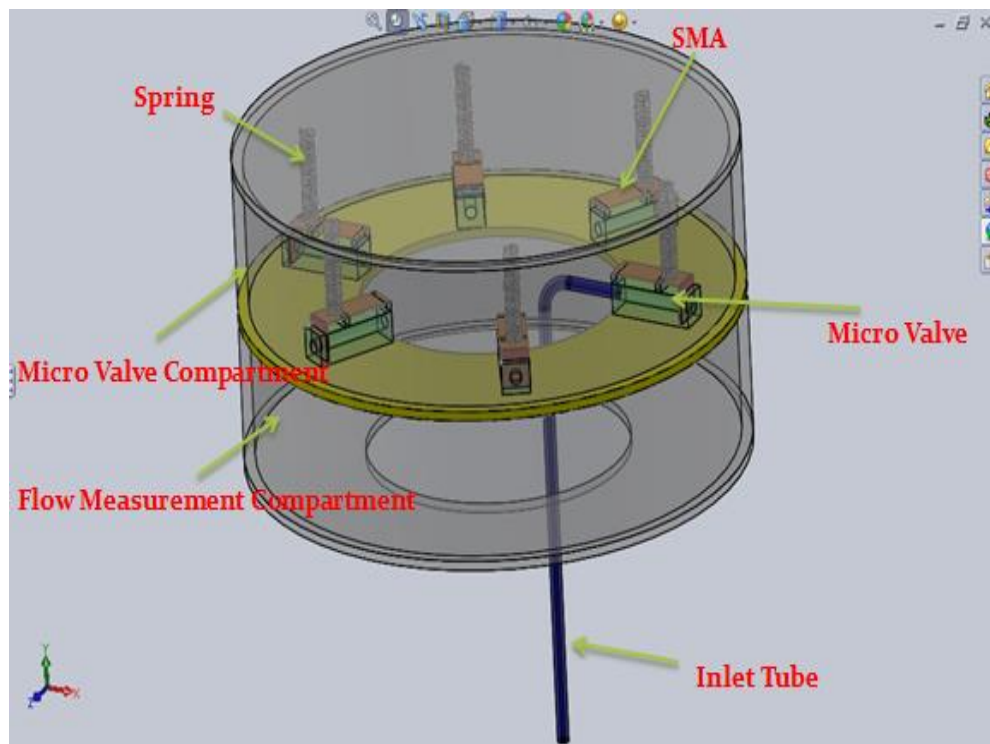


Fig 5.20 SOLIDWORK model showing design for Micro valve Array

5.3.3.2 Fabrication: Fabricated microvalve array for fluid flow control is shown in Fig 5.21. In this design, each microvalve is independently controlled, and the actuation method is the same as for a single microvalve. Since SMA is trained in one way, there must help me an arrangement for the counter force which brings

SMA back to straight position, here spring is attached at the end of each SMA sheet to provide deformation force when valve needs to be closed. With the help of microvalve, array flow rate of macro-level can be controlled in micro levels precision. Also, this can be used as micro mixing device in which different fluids can be mixed in a desired proportion.

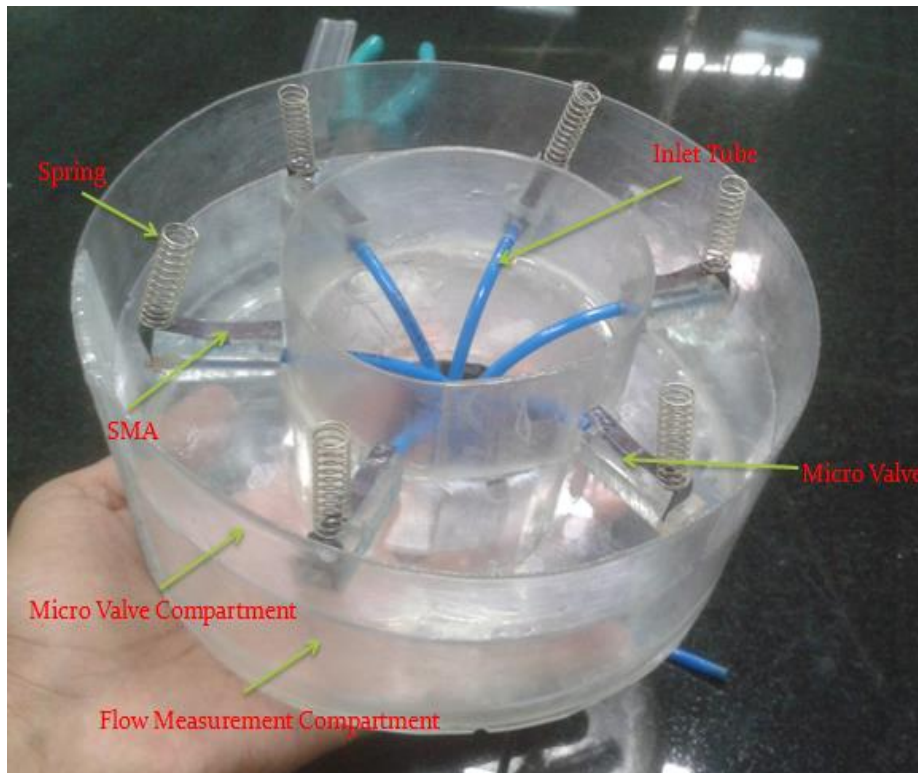


Fig 5.21 Fabricated Micro valve array

5.3.3.3 Result and discussion: SMA micro valve has been presented, which are actuated by a thin film microdevice of SMA NiTi. The experimental study and has been carried out to investigate the rate of flow. The following information can be drawn from the present results:

- a)* The pictorial view of Micro valve which is designed through Solid-works software is represented in Fig.5.9.
- b)* As per design ($50*10*0.25\text{mm}^3$), Micro valve is fabricated with acrylic SMA NiTi sheet for getting the flow rate in order of $\mu\text{L}/\text{sec}$, for flowing the liquid front

inside of valve 1.5 mm diameter as a hole is kept open along with the valve, which is shown in Fig. 5.10.

c) SMA Ni-Ti sheet whose thickness is 0.25mm is Trained in its predesigned shape for which Fixture and Muffle furnace is required, i.e. shown in Fig.5.11 (a, b and c)

d) For actuating the SMA sheet, Laser whose wavelength is 532 nm and frequency is 10 Hz is better because of its non-contact type and low power energy density source. (Fig 5.12)

e) The advantage of the Laser medium is to get maximum deflection 7.29 mm for an optimum fluence of 25.48 mJ/cm^2 as shown in Fig. 5.13

f) For checking the validation of NiTi, various characterizations has done like SEM, DSC, EDX, TGA, Hardness test, i.e., depicted in Figs 5.14 to 5.19 and 5.28. From which it is clear that for Composition of nitinol is 42.43% Ni and 57.5% Ti. laser fluence is optimum at 130 mJ/cm^2

g) Finally, Array of micro valve has been fabricated (Fig 5.21). It can be used as a micromixer also.

The research reviews the use of microvalve, and in the design using a material with SMA, Ni-Ti sheet passed the feasibility, executive design stages, as well as experimental tests on prototypes made using rapid prototyping techniques and development of Micro-mixer for the Bio-medical application.

5.3.3.4 Application of Microvalve Array as a Micromixer

Microvalve array has a potential application in Micromixer. Micromixer technologies applications are broadly categorised as:

(1) Chemical applications, including chemical synthesis, polymerization, and extraction;

(2) Biological applications, including DNA analysis, biological screening enzyme assays, protein folding;

(3) Detection/analysis of chemical or biochemical content combined with NMR, FTIR, or Raman spectroscopies.

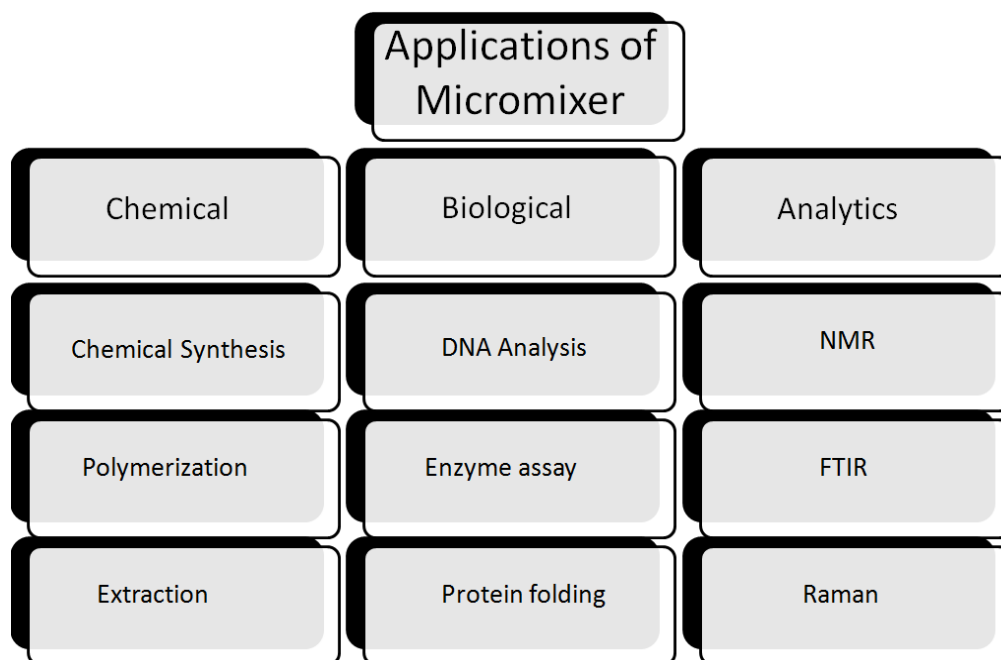


Fig 5.22 Application of Micro valve Array- Micromixer

In the chemical application, crystallization, extraction, polymerization, and organic synthesis have been reported, not only for laboratory studies but also for industrial applications. Microscale techniques are used in chemical synthesis to develop microreactors. In clinical medicine and biological studies, microfluidic systems have been widely applied to the identification of biochemical products, diagnosis, drug discovery, and investigation of disease symptoms. The biological and biochemical applications also include enzyme assays, biological screening assays, protein folding, and biological analytical assays. Non-destructive analytical/detection methods have yielded some benefits to chemical and biochemical processes.

5.4 Benefits of using Line beam in place of Spot Beam: In most of the literature, the laser is used as actuation medium but the laser used is a spot laser which is effective over the area it is falling, i.e. rest of the sample remains ineffective of the heat. Laser follows Gaussian curve: In a Gaussian beam, 86.5%

of the energy gets concentrated at the center and rest 13.5% lost at the edges leads to inhomogeneous intensity distribution. Lack of thermo-mechanical properties: No analysis is done on thermo-mechanical behavior, i.e., reliability, the surface characterization in the spring. No work is available to identify operating condition and spring parameters for life prediction models.

Spot beams are more concentrated in power than a wide beam, so the receiving end get a stronger signal. Since the coverage area is smaller, there is also a reduced risk of interference with another end i.e. NiTi using the same frequencies. So, line beam is preferred for uniform heating:

5.4.1 Preliminary Experimentation: The test setup is developed to perform experiments based on the medium used. It comprises an actuation unit and a displacement sensing unit with a load pulley arrangement. Two ways of actuation have been used here that includes Laser-based and hot water actuation. Nitinol SMA Spring which is equiatomic (50%Ni-50%Ti) in nature is used with specifications as described in Table 3.1. Heating-cooling cycle is defined for both processes based on the time when steady state is achieved which is different for both processes.

For the first time actuation of an SMA spring with a remotely controlled contactless source like a laser beam is reported in this project. Laser (Light amplification by stimulated emission of radiations) is used as one of the media to gain displacement in the NiTi spring. Nd: YAG pulsed laser (Quanta-Ray) with different wavelengths is used to perform the experiments. The first task for this work is to get an actuation with the help of a laser. The laser source is capable of focusing a point beam of diameter range between 1.5-2.5 mm depending upon the stand-off distance (distance between workpiece and laser source). However, with a point laser, the actuation attained is decidedly less, so the next task is to increase the area of the beam. Comparison between point spot actuation and a line spot actuation is also studied in Table 5.5.

5.4.2 Comparison on Point and Line actuation: Comparison analysis has been done for point and lines laser actuation which is tabulated below:

Table 5.6: Output Line and Point heating comparison

With Point laser actuation gained (mm)	With line laser actuation gained (mm)
0.38	7.14
2.68	6.92
4.37	6.80
4.59	6.54
4.64	5.65

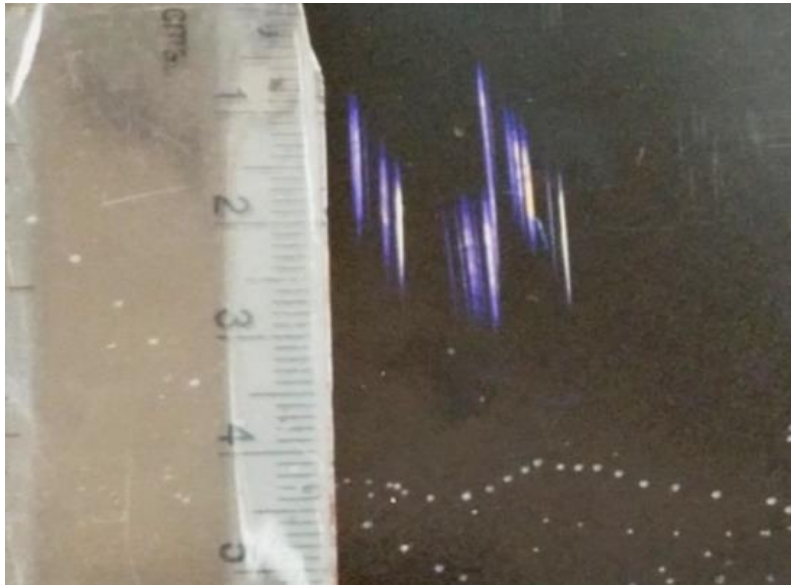


Fig 5.23: Output line gained when passed through Quartz tube with a scale as reference

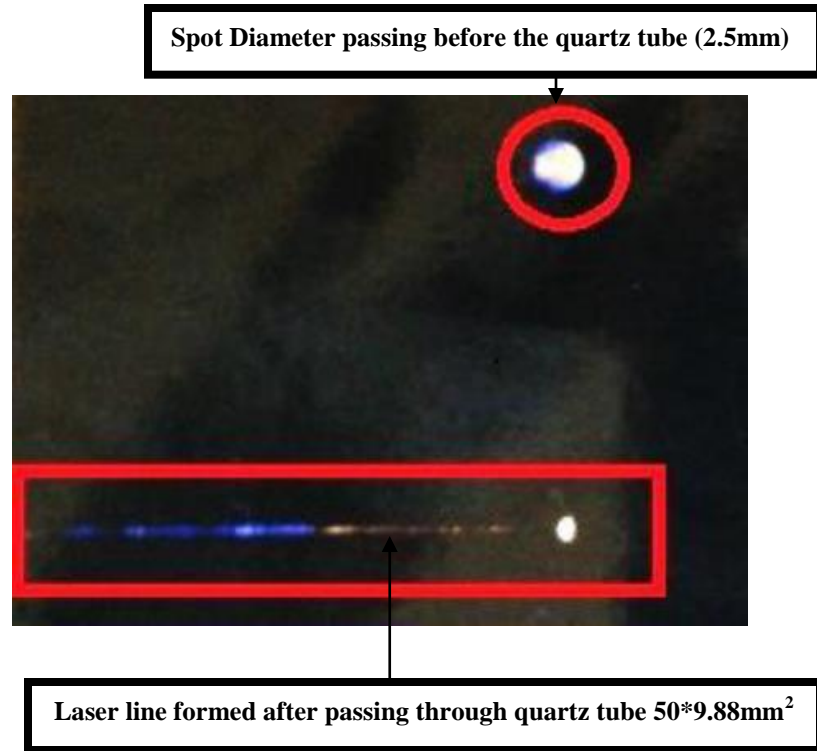


Fig 5.24: Image captured on a photographic sheet

At first, all the experiments were conducted using quartz tubes (Fig 5.25) to confirm the actuation through the laser, but it is then replaced by a planoconcave cylindrical lens that will increase the efficiency which is discussed in the result section. Hence, the slightest modifications can make drastic changes that can be exploited to enhance component functionality.



Fig 5.25: Quartz tubes used with varying diameters

5.4.3 Experimental Set up: The experimental setup consists of a cylindrical lens and an SMA spring (Fig 5.26). Laser actuation is performed using an Nd-YAG pulsed laser system with varying spot diameter at 532nm. Laser parameters (i.e., peak power, frequency, laser fluence) are altered to control the actuation. The laser is allowed to strike onto the cylindrical lens and then passes to the spring. Spring is fixed at one end, and the other end is connected to a varying load through a frictionless pulley.

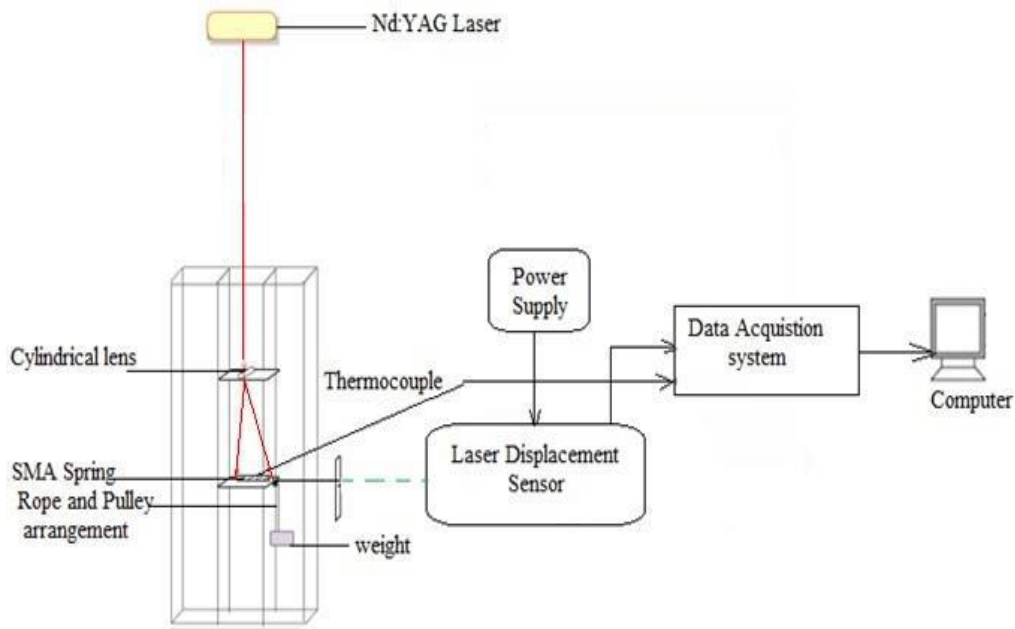


Fig. 5.26: Schematic for laser based actuation setup

To generate a displacement, Laser is made to strike where spring is held fixed at one end and then cooling is done through natural convection (Fig 5.27).

During the heating cycle, spring compresses pulling the mass in an upward direction against the gravity. This occurs because of martensite to austenite transformation. During the cooling cycle, spring elongates, and the mass moves in the downward direction. This occurs because of austenite changes to the martensite phase.

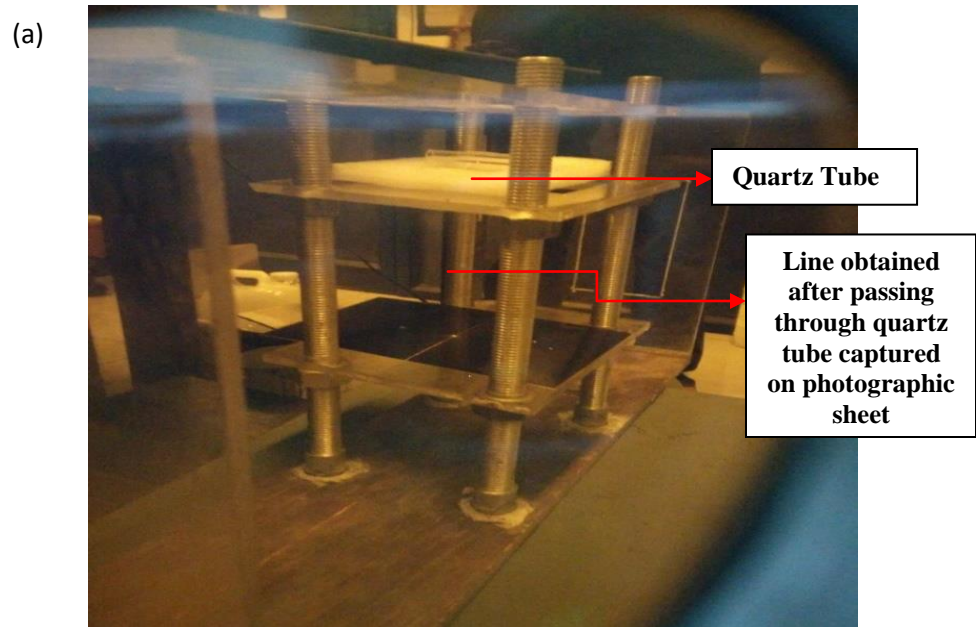


Fig 5.27 a) Line beam generation by using quartz tube b) Displacement calculation using LDS and flapper arrangement

The proposed system can investigate the behavior of SMA springs at varying temperature conditions, load, actuation and displacement conditions. This can be highly helpful in investigating the life cycle in detail.

5.4.4 Framing of the work: Three major changes that have been done in this work:

1.) In the preliminary stages, actuation is tried using a cylindrical quartz tube. However, the losses associated with quartz tubes are very high, need a cylindrical lens for this purpose.

2.) In the second trial, the quartz tube is replaced by a Plano concave cylindrical lens (Focal length f_1 100mm), which gave better results than the previous one. However, in order to further increase the output line, work is done on changing the lens arrangement.

3.) A Plano concave lens (f_1 100mm) along with a convex lens (f_2 100mm) is used to get the required actuation. Comparison between both the arrangements is shown in table 5.5.

- **Lens Arrangement Used:** The Cylindrical lens is used in place of the quartz tube. Spring is compressed on a particular area and not too much significant (Fig 5.28 a).



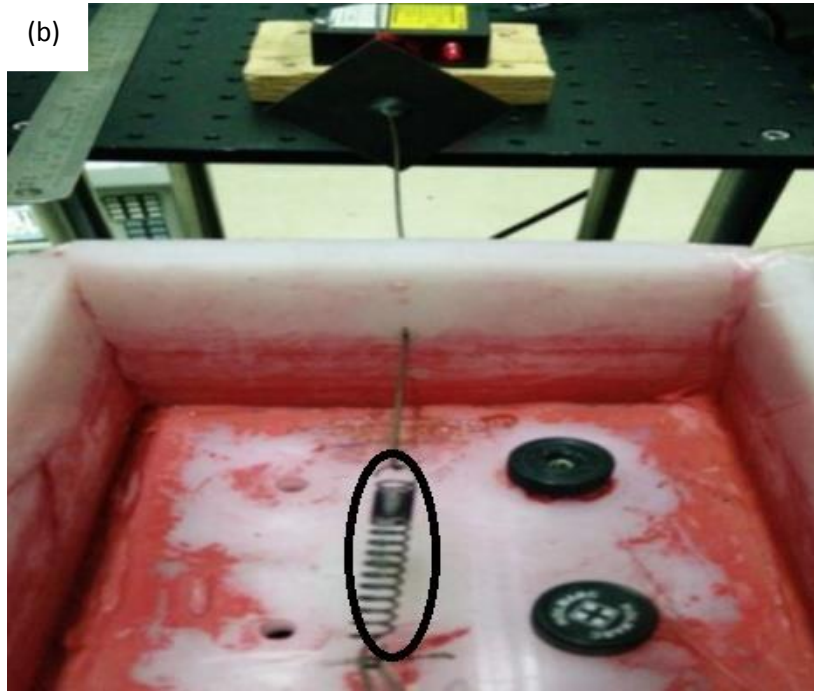


Fig 5.28 Lens arrangement used for conversion of point beam into line beam a) only cylindrical lens used, b) cylindrical + convex lens used

To mark a significant change combination of cylindrical lens and a convex lens is used (Fig 6.6 b).

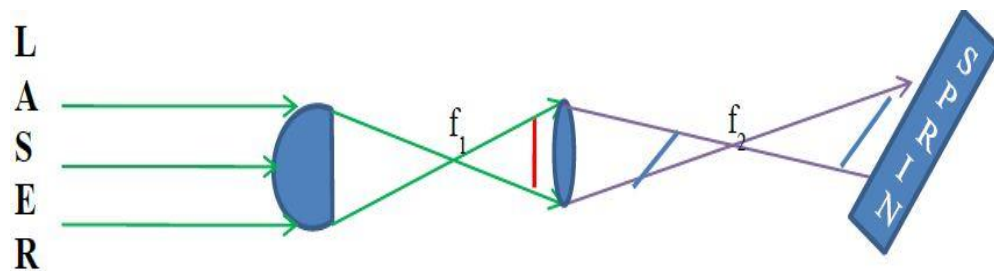


Fig 5.29: Schematic of combination of lens arrangement using their focal point

Table 5.7 Output and input values for both lens arrangements

Parameters	Cylindrical Lens	Cylindrical Lens + Convex Lens
Focal length	100 mm	100 mm
Laser beam diameter	3 mm	3 mm
Laser wavelength	532 nm	532 nm
Output laser line	7-8 mm	13-15 mm

5.4.5 Results and Discussion: Various changes have been done while performing the experiments based on the results found. At the preliminary stages, work was started with cylindrical quartz tubes. These tubes generated a line length of about 5-7 mm as shown in Fig 5.30 captured over a photographic sheet. Though it was found that the laser when passed through this quartz, it incurs heavy loss in the efficiency of the power.

Results can be seen in Table 5.8 below when experiments were performed using a quartz tube of diameter 5mm with varying spot diameter.

Fluence calculation is done based on the area of output line (assumed as rectangular spot) at different power values. Fig 5.30 shows a microscopic view of the line formed with the help of portable USB microscope at a magnification of 4X.

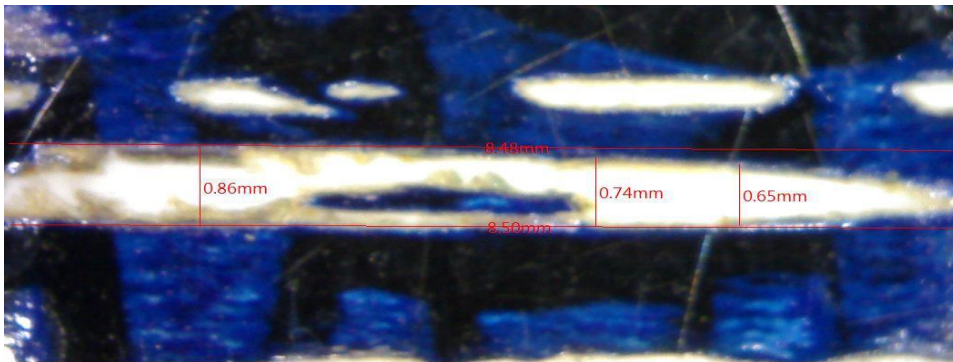


Fig 5.30: Microscopic image captured over photographic sheet

Table 5.8: Results using quartz tubes with varying diameter

Laser Spot Diameter	Power (mW)	Converted Length	Fluence (mJ/cm²)
2.5 mm	0.15	30 mm	306
	0.30	35 mm	612
	0.55	40 mm	1122
2.0 mm	0.15	10 mm	477
	0.30	15 mm	955
	0.55	17 mm	1751

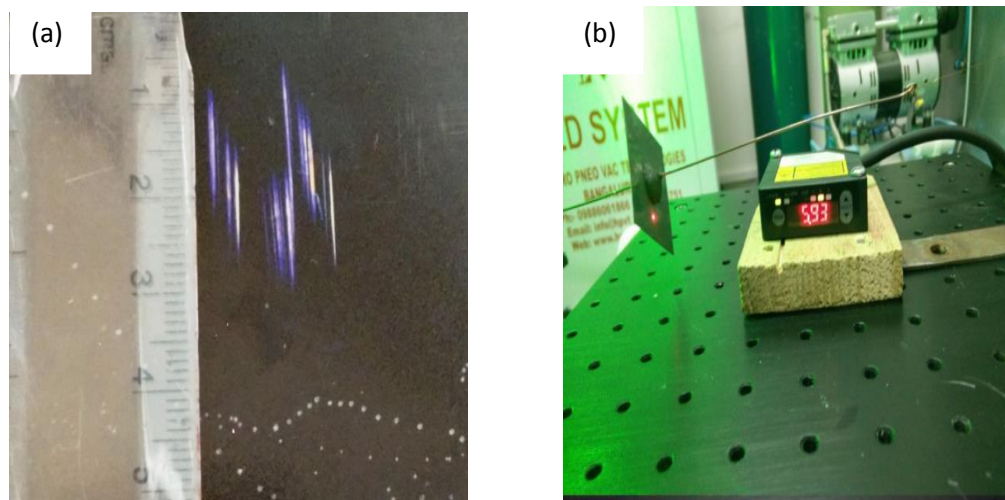


Fig. 5.31: a) Effect of laser on photographic sheet, b) Location of LDS in front of flapper

Above Fig 5.31 shows the line obtained with quartz tube captured in a photographic sheet in standard view with a centimeter scale kept parallel to it as a reference.

5.4.5.1 Effect of the cylindrical lens:

The losses with quartz tube are very high, so next set of experiments is performed with a Plano concave cylindrical lens. These lenses will convert the point beam to a rectangular beam with fewer losses when compared with the quartz tube.

The cylindrical lens is a Plano concave type lens with a focal length of 100 mm and curvature diameter 25mm. SMA spring is kept after the focal point because at focal point the intensity is very high which may ablate the spring at higher powers.

Table 5.9: Displacement gain in heating-cooling cycles

Cycle	Medium	Time (mins)	Displacement
1	Heating	4.90	7.93
	Cooling	2.00	0.64
2	Heating	4.80	4.56
	Cooling	1.36	0.42
3	Heating	3.90	4.20
	Cooling	1.49	0.40

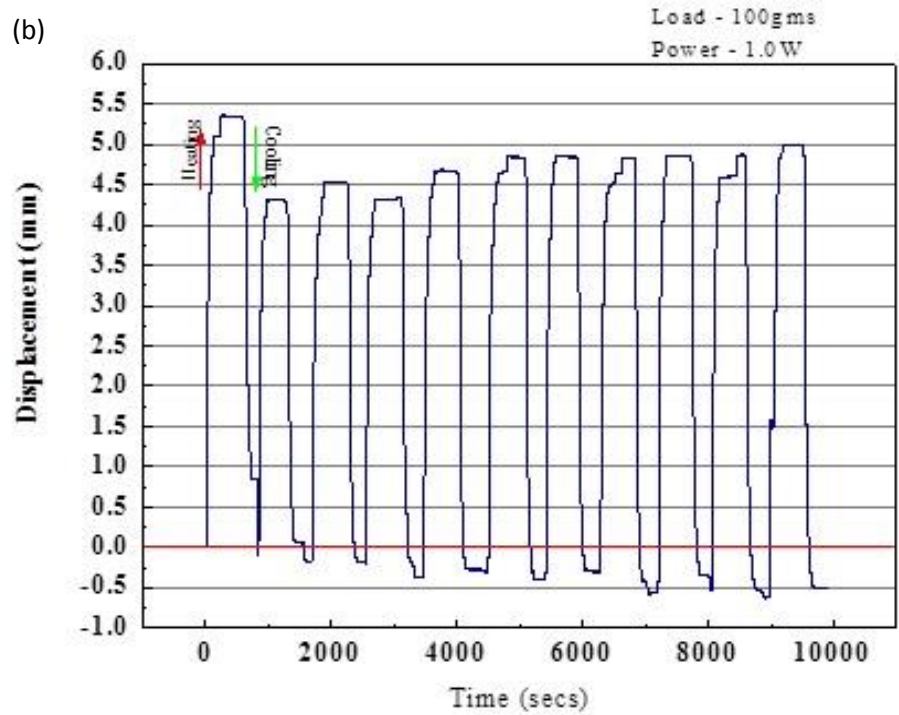
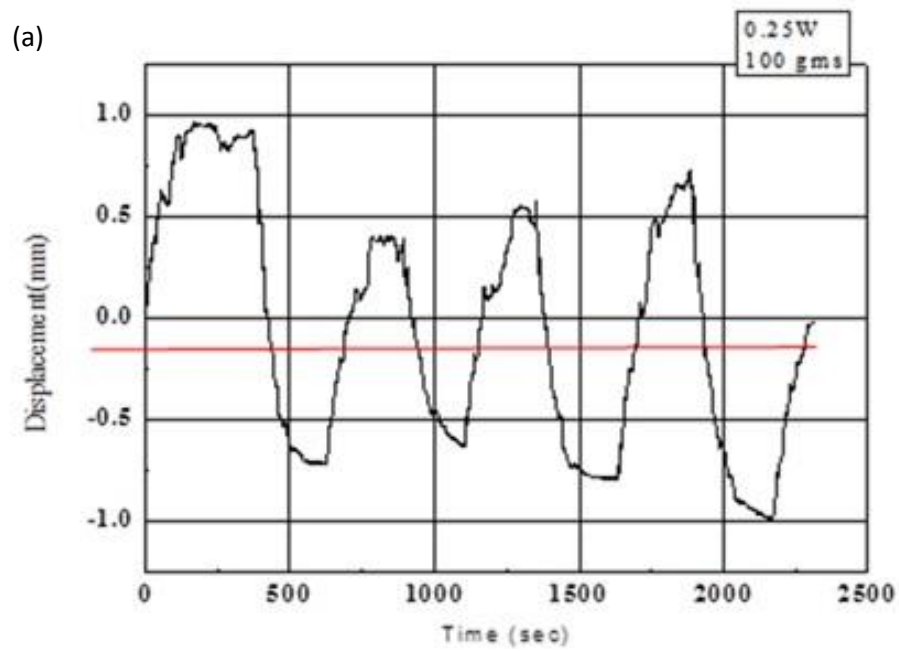
As it can be seen from the above table 5.9 where experiments for the first three cycles were performed using a cylindrical lens. Heating time required is more than the cooling time because of the inhomogeneous heating due to the Gaussian beam.

Displacement for the first cycle is very high which is approx. 8mm and it decreases further. This depends on the length of the line falling and the area over which it is affecting the spring. Even though the line length formed is more, but the intensity distribution varies as per the Gaussian beam profile.

5.4.5.2 Effect of combination Lens: After performing experiments with a cylindrical lens, it is found that the line obtained can further be increased if the combination of the lens is used. Therefore, a cylindrical lens plus a convex lens is used that increases the output length to 50% than it was before.

All the experiments were then done with this arrangement, and different characterization was performed to check the effects of heat over the SMA spring.

A minimum load of 100gms is required to enlarge a fully compressed NiTi spring (original 13.86mm) to about 20 mm. Different experiments were carried out by changing power, and the results are noted for every heating and cooling cycle.



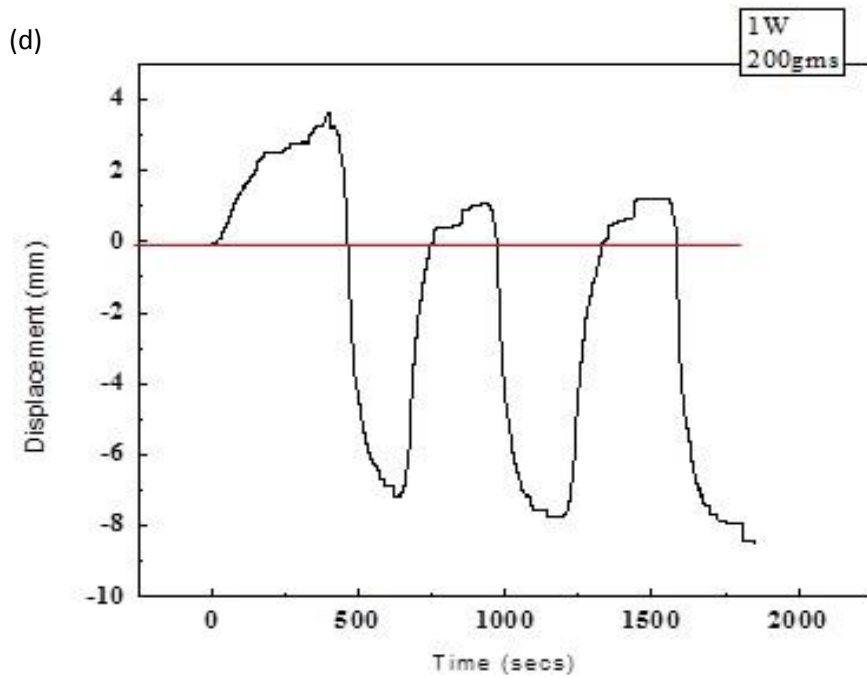
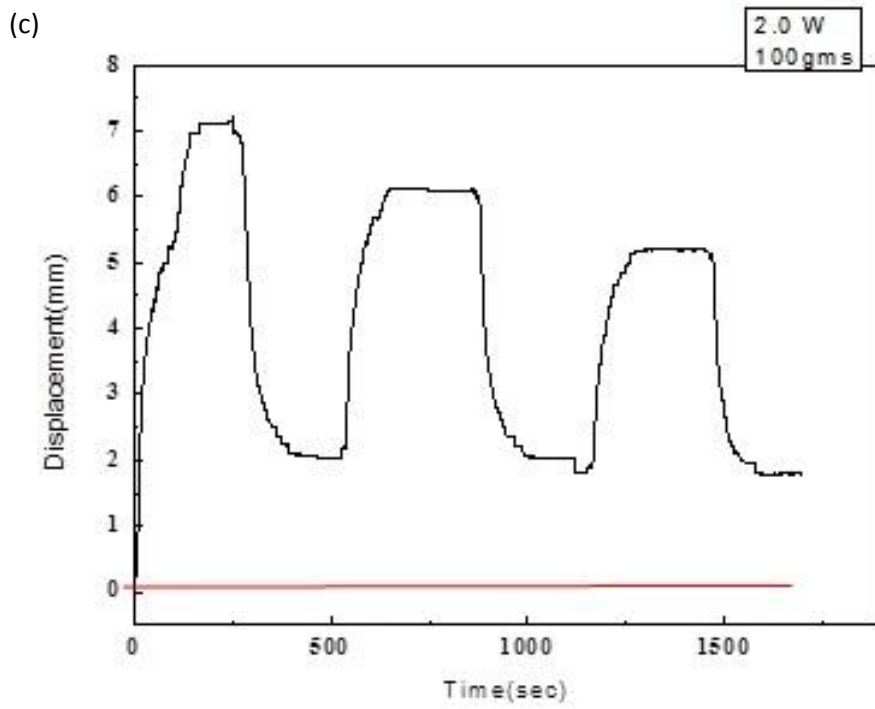


Fig 5.32: Displacement-Time relationship at a) 0.25 W, 100 grams and b) 1.0W, 100 grams c) 2 W and 200 grams, d) 1 W and 200 grams

Fig 5.32 above shows heating-cooling cycle for displacement-time relationship. Experiment was conducted for NiTi spring at different powers with an applied load of 100 grams. Heating time was set as 600 s (threshold for heating displacement) and cooling time as 300 s (threshold).

The LDS reference is taken as zero i.e. when the spring is extended because of applied weight and no thermal energy is provided. Also it can be observed that as the power value increases, displacement gained also increases. As we can see from the above Fig, the maximum actuation (compression) when heating is done is about 5.9 mm. Running for 10cycles, it can be seen that the actuation is getting stabilized except for the first few cycles (where it decreases). The reading going below zero is because of the load applied which extends the spring more than its compression. One cycle (Heating-cooling) is around 900 s and DAS captures this data in the terms of voltage.

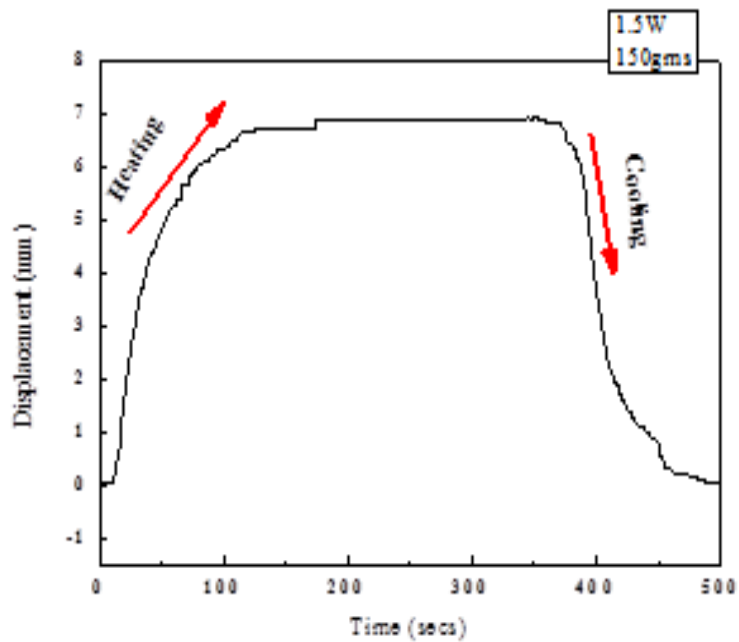


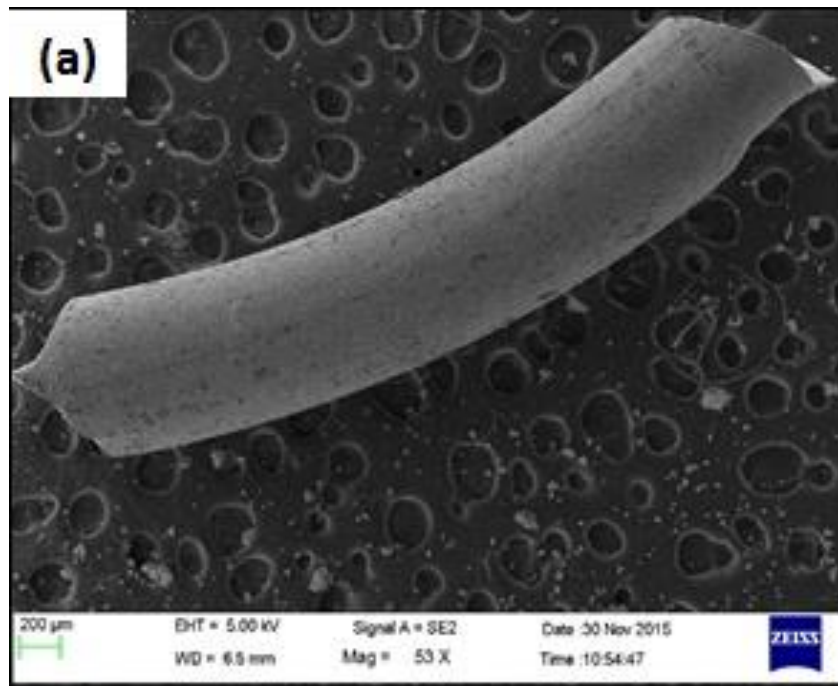
Fig 5.33: Single Heating-cooling cycle

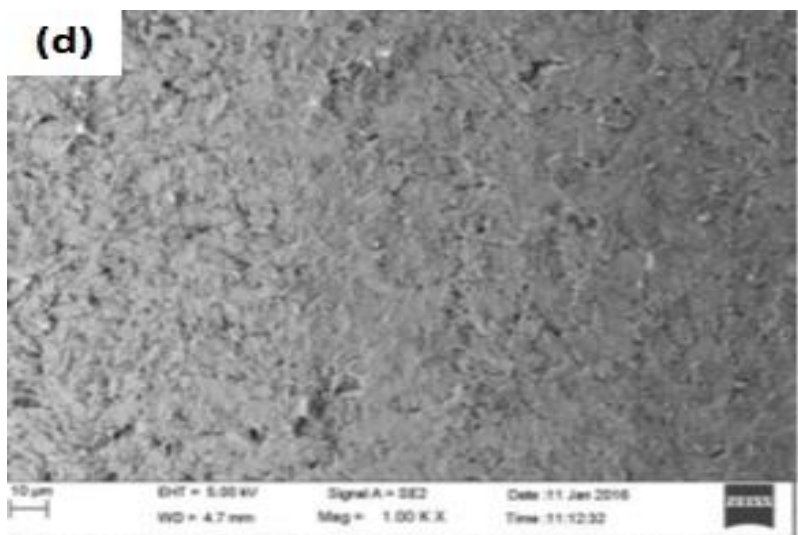
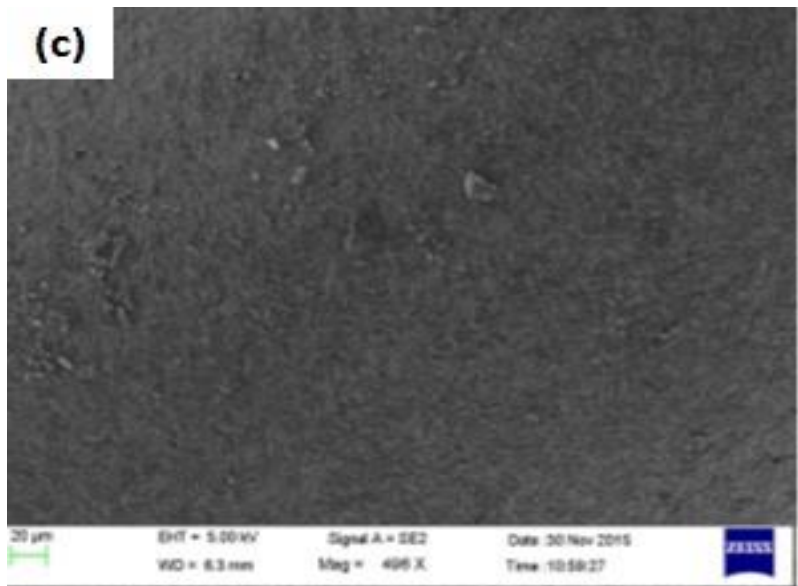
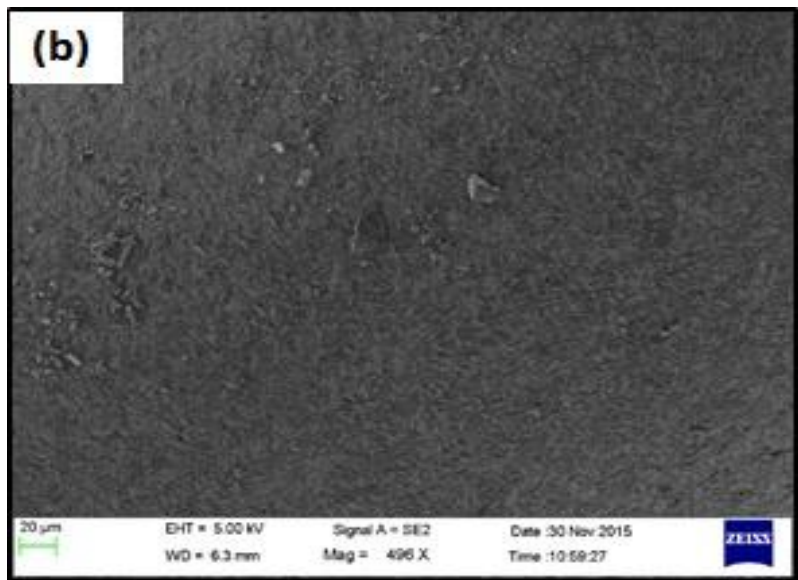
One heating-cooling cycle is taken for better clarification. In the Fig 5.33, it can be seen that the maximum displacement it is gaining is near to 7mm. Also,

it can be observed that the actuation is gained very fast and it went on increasing till 100s and the then steady state continues for the next 300 s. The heating time here is around 400 s. This time depends upon the sample to achieve a steady state and then cooling is done. This particular cycle is taken at 1.5 W and at a load of 150grams.

5.4.6 Morphological Analysis:

a) *Scanning Electron microscopy (SEM):* Surface morphology is studied through SEM images. Fig 5.34 shows scanning electron microscopy done on NiTi SMA Spring took for different powers and at different magnifications. A 10mm sample is cut from the spring and is analyzed over the region where the laser has influenced. The SEM images show that at low power (0.25W) the grains are not deteriorating, but some debris can be seen over the structure. Further in the morphology of NiTi spring shows some tearing feature with downside peaks and valleys clearly visible in the images. Depth in Fig 6.14 e shows that at higher powers the laser is ablating the spring. Though even after this, actuation of spring can be seen but the strength of spring decreases drastically.





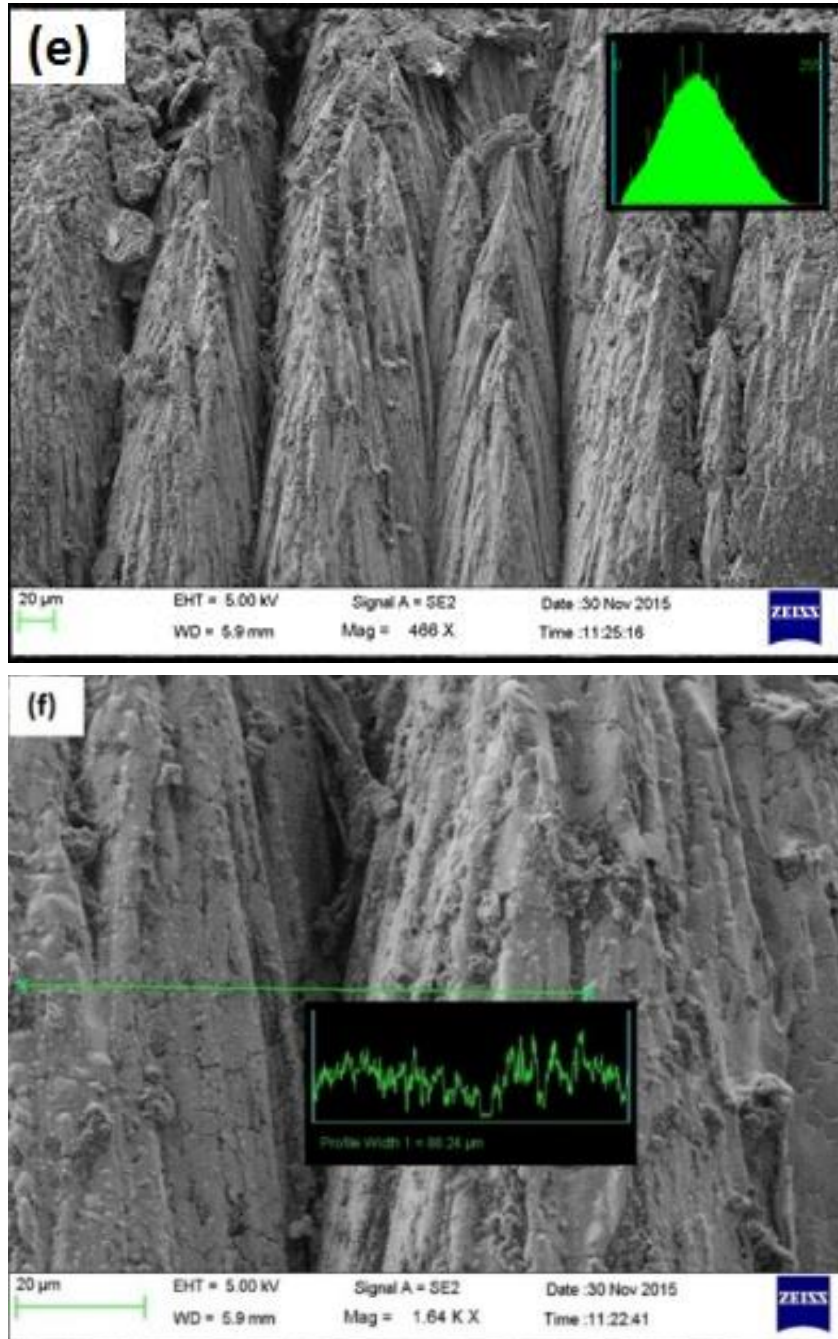


Fig 5.34: Scanning Electron microscopy done at (a) Sample cut out length (10mm), (b) Original sample, (c) 0.25W, (d) 1.0W, (e) 1.5 W, (f) 2.0W showing depth created due to laser ablation at higher power

b) Electro Dispersive analysis (EDX): Spring composition was determined using EDX. The composition of heat treated spring obtained through EDX is as follows: Ti: 22.62 at. %, Ni: 23.20 at. % and O: 54.18 at. %. It is necessary to do the

experiments in an inert atmosphere as the NiTi is easily oxidized due to the heat treatment at an open atmosphere. Alternatively, the oxide formation of NiTi spring which prevents Ni element to release from its alloy surface is beneficial for corrosion resistance and bio-compatibility. However, it was reported that this passivation layer on NiTi alloy was relatively fragile. The brittle and thin oxide layer may be destroyed during significant deformation or during complex interaction involving wear [149].

Table 5.10: EDX analysis after laser interaction

Element	Weight %	Atomic %
O	11.81	54.81
Ti	14.76	22.62
Ni	18.56	23.20

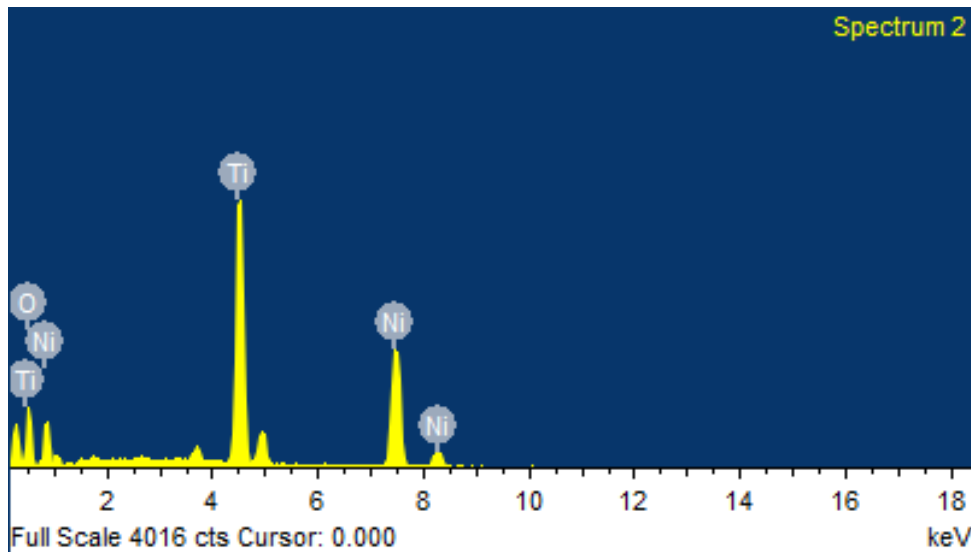
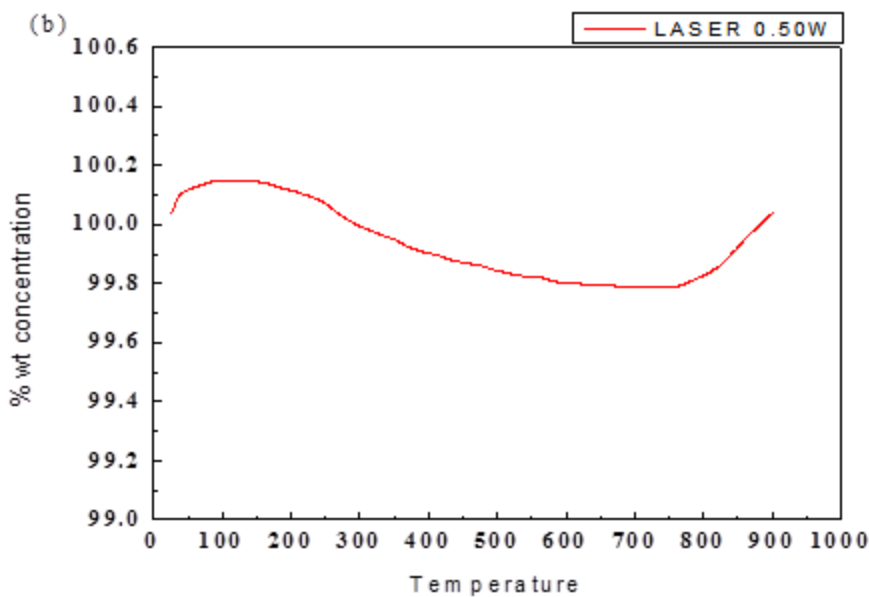
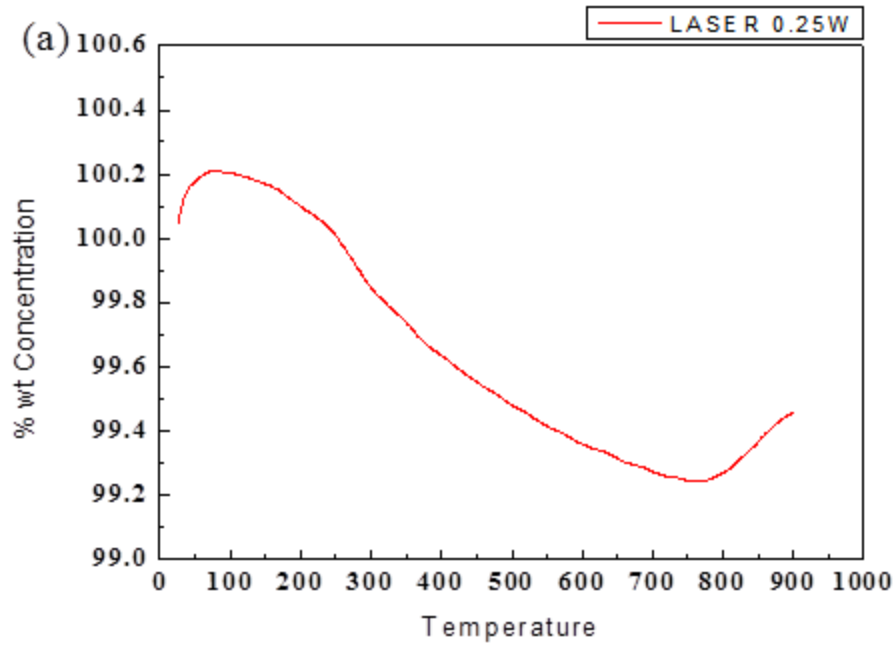


Fig 5.35: EDX representation showing peaks for particular components

Thermogravimetric analysis (TGA) was carried out to investigate the kinetics of oxidation. Thus the thermal stability of this SMA can be revealed by TGA. The test was carried out with a specimen weighing around 20 mJ at constant heating of 5 °C/min purged with nitrogen gas.

Fig 5.36 (a, b, c) shows the laser actuated spring at average powers, and the amount of weight gain goes on increasing with increased fluence. At a low

power of 0.25W (Fig 5.36 a), decomposition is seen after 100°C whereas, at high powers (i.e., at 0.50 W and 1.0 W), NiTi is severely oxidized. The presence of oxides is then confirmed by Energy Dispersive X-ray spectroscopy. Also, it can be seen that in all the graphs, reading again increases after 800°C. Nitridation occurs in NiTi at this temperature limit. As the TGA environment is purged with nitrogen gas, so there are high chances of nitride formation. Typically, titanium is prone to nitridation and forms Titanium nitrides and higher stoichiometric structures.



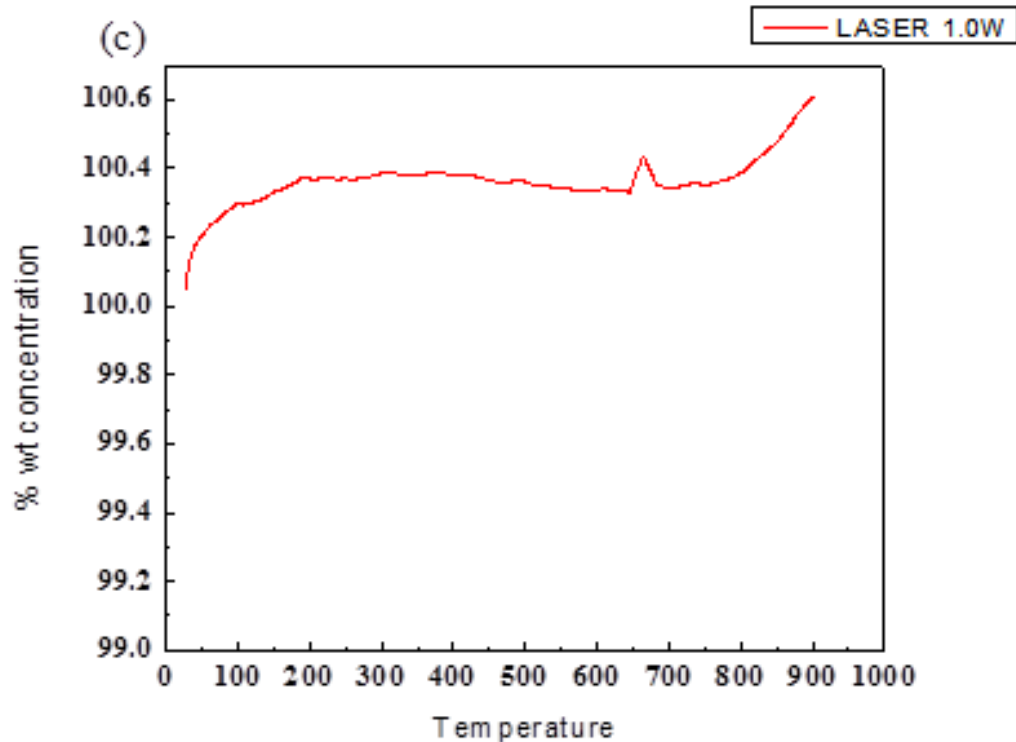


Fig 5.36: TGA analysis performed for springs undergoes heating at different laser powers (a) 0.25W, (b) 0.50W, (c) 1.0W

5.5 Drawback of pulsed Laser: Aside from their various applications, lasers are classified according to how they emit light, which includes “continuous and “pulsed” lasers. Since pulsed laser is beneficial for thin materials (quicker processing, high power capabilities, great for such types of applications that need high power density and can be Q switched which allows minor laser ablation. But there are some disadvantages also. It is not ideal for materials that have moderate thickness. It gives slower production for thicker materials. Lower absorption of radiation for lighter materials is major drawback. Although engraving resolutions can be high, it wouldn't allow for larger scan gap making it slower.

Main drawback is that for actuation of SMA, It required more time to achieve deflection. So continuous laser is preferred than pulsed laser which is discussed in next chapter.

5.6 Summary: In this study, the cyclical behavior of NiTi, a binary shape memory alloy is achieved by using pulsed Nd-YAG laser. It can be summarized as follows:

- It has been found that actuation gained by laser medium is good enough to use in practical applications.
- Laser at 532nm is used, and optimum power of about 1.0W is analyzed which gives fluence of 49mJ/mm².
- Thermogravimetric results show weight gain, i.e. oxidation till 100^oc, and then decomposition starts. Oxygen content is further validated with EDX. Also, weight gain after can be because of NiTi nitridation phenomenon.
- Different powers are also used in this chapter for comparative analysis.

Chapter 6

Continuous Fiber Laser Assisted Actuation of SMA spring

In this chapter, a novel approach is developed to handle the actuation of shape memory alloy (SMA) using continuous fiber laser, which will be responsiveness for next-generation MEMS devices. The thermo-mechanical and morphological analysis is also investigated and verified.

6.1 Introduction:

Laser actuation is a contactless energy transfer (CET) process where there is no physical contact between the laser source and the actuating component. The absence of intricate connections, eliminates additional element requirements such as wiring, connectors, etc. thus favors MEMS applications. The contactless feature also facilitates long distant actuation, improves actuator mobility and degree of freedom over other actuation methods. With this laser actuation, selective actuation on the SMA element is possible, i.e., in the case of springs only the selective coils can be actuated. This distinct selective actuation enables different stroke lengths of SMA actuators at different actuation speeds by controlling laser process parameters.

However, to the best of authors' knowledge, there is no detailed study on the laser actuation until the failure of the SMA component. A thorough experimental and numerical study wholly focusing on the attribute deeds of the SMA actuation of spring was carried out to understand the actuation behavior of SMA. Displacement analysis, thermogravimetric analysis, scanning electron microscopy (SEM) of laser interaction during as well as post-actuation studies are analyzed.

One option to amplify the stroke is to shape a set SMA wire into compressed helical springs. These springs can be made using straight wire with heat treatment techniques and do not require any amplification mechanisms. Although there are dynamic setups in the literature to explain a

helical SMA actuator's behavior, there are few publications that present experimental results for validation.

SMA's are of particular interest in actuation applications due to their high stress, high actuation strain, and high energy density. Further improvement to their actuation frequency and the number of transformation properties per NiTi component is desired to increase the range of applications for these materials [5]. In this chapter, NiTi SMA Spring is actuated through a laser beam (using continuous fiber laser) then its effect on the morphology of structure is analyzed. SMA exhibits different properties like one-way effect, two-way shape memory, and pseudo-elasticity, high damping capacity, good chemical resistance, and biocompatibility. All these properties made it suitable for that particular application required.

Here, the Laser source is used to heat the spring and actuation is gained. This chapter investigates the laser processing of NiTi SMA springs. The limitation of having one transformation property for a NiTi component has resulted in the development of numerous methods to increase the number of transformations possible. Previous methods explored to achieve multiple properties in a single component include antagonistically positioning SMA's, local heat treatment techniques, the two-way shape memory effect, welding, and local alteration of SMA properties of these methods, the local property modification methods are the most flexible and can be used on a wide scale and range of applications [144]. The range of temperature is 45-90 degree centigrade.

6.2: Details of Experimental Apparatus:

Apparatus consists of six major sub-parts such as (i) Continuous fiber laser equipped with PC; (ii) SMA NiTi spring; (iii) DC power supply unit; (iv) Laser displacement sensor; and (v) Data acquisition system and (vi) wire and pulley arrangement.

(i) Continuous fiber laser equipped with PC: 'LASER' stands for light amplification by stimulated emission of radiation. Each word of this sentence which more or less describes a process leading to the generation of laser. The laser is explained as a tool which generates highly directional, monochromatic, powerful beam, which can be focused to the spot diameters of the order of its

wavelength, where power densities of the full laser beam are concentrated can exceed $1\text{GW}/\text{cm}^2$ very easily.

This system consists of some components, i.e. Laser source (from a Yb doped fiber laser), Galvo-scanner, software, and PC. The advantage of using fiber laser is as follows:

- Light is already coupled into flexible fiber.
- High optical quality
- Compact size
- Higher wall plug efficiency
- The higher surface area to volume ratio allows efficient cooling of the laser.
- Fiber lasers exhibit high temperature and vibrational stability, extended lifetime, and maintenance-free turnkey operation
- No mass, No wear, Non-contact, Rapid on/off control
- Fiber laser can also refer to the machine tool that includes the fiber resonator. Applications of fiber lasers include material processing (marking, engraving, cutting), spectroscopy, Telecommunications, , medicine, and directed energy weapons.
- Fiber lasers are now being used to make high-performance surface-acoustic-wave (SAW) devices

Its subsystems are:

a) *Laser Source:* It is of 50 W fiber laser with beam delivery system. Fiber laser is a laser in which an active medium is an optical fiber doped with rare earth element such as erbium, ytterbium, and neodymium, etc. wavelength of the laser is 1064 nm.

b) *Galvo scanner:* The galvo consists of a galvanometer-based scanning motor with an optical mirror mounted on the shaft and a detector that provides positional feedback to the control board. The Galvo scanner which deflects the beam in X and Y direction is having a focal length of 160 mm. Inside there are two mirrors (X and Y) which deflect in the beam as per the user requirement. The scanning area is $100*100$ mm.

c) **Beam Delivery system:** The laser beam once centrally entering into Galvo head input aperture will be following two mirrors in the Galvo head. If the mounting of the Galvo head is not disturbed or loose, then the beam will exit from the output lens of Galvo centrally. Keep the object on the stand, and then one can adjust Galvo up or down with the arrangement provided. Galvo power supply is a linear power supply giving 15 V regulated voltage, and current rating is 5 Ampere.

d) **Control panel:** Fiber laser can be controlled by this panel only. The laser can be switched on/off, and X-Y stage can be moved by this.

e) **Software:** The actuation is controlled by software (HPGL slab). It comes along with Galvo scanner. HPGL software runs on PC with 900 Mhz CPU and 256 MB RAM at least.

ii) **SMA Ni-Ti spring:** Due to the spring action, one-way trained SMA springs are widely used as micro-actuators. Therefore, this setup incorporated spring as an SMA component. Spring specifications are given in Table 3.1

iii) **DC power supply unit (PS):** It is required to glow the laser displacement sensor (LDS). (Model: GWINSTEC GPD4303 S)

iv) **Laser displacement sensor (LDS):** As the study involved micro-actuation, LDS was chosen over other displacement measuring devices which gave the resolution of 2.5 μ m. (Model: Panasonic HLG108-A-C5).

v) **Data Acquisition System (DAS):** Measurements provided by LDS were recorded using a DAQ and were directly saved into a computer for further study (Agilent 34970A).

vi) **Load and Pulley arrangement:** External force was needed to keep the spring extended as the spring was trained to contract upon actuation, which is done automatically with the help of a pulley.

6.2.1: Procedure of Experimentation: All the experiments were conducted using the following procedure:

a) Three SMA Ni-Ti spring was chosen for actuation at different wattage, i.e. 15 W to 50 W.

b) Three different weights i.e. 1.5 N, 2.5 N and 3.5 N were used during experimentation.

c) Some passes (Pass means laser in the form of the line will go in a forward direction from one end to other end and then follow the reverse path up to starting point) were varying according to its full recovery, i.e. 1 to 8.

d) To trace the profile of the laser beam, photographic sheets were used which is also explained in the upcoming section.

e) Characterization of SMA is also done, i.e. SEM, TGA, and DSC, etc.

6.2.1.1: Experimentation: A SMA NiTi (Nitinol) spring, supplied by Dynalloy Inc, with the specifications mentioned in table 3.1 is used for actuation studies.

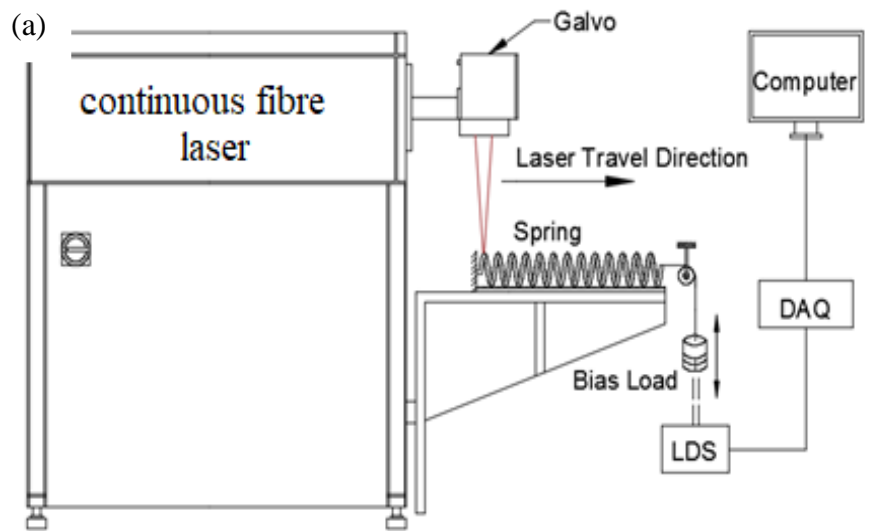


Fig. 6.1 a) schematic of laser assisted actuation and b) on line location of continuous laser assisted actuation

In order to deform the spring for actuation studies, one end of the closed coil spring is fixed, and the free end is loaded with 1.5 N, 2.5 N and 3.5 N loads. Figs. 6.1 (a and b) shows the experimental setup for the laser actuation of the SMA. Due to the applied load, deformation begins in the spring at a temperature of 17⁰C. Once the deformation due to the applied load terminates, the laser is switched on. Laser from the fiber laser source, doped with Yb active gain medium of 1064 nm wavelength is used for irradiating the SMA spring. To move this laser beam along the length of the spring for heat distribution, a dynamic reflecting mirrors or simply galvo mirrors are used. Laser guided through the optical fiber cable is made to fall on the galvo mirrors. These mirrors reflect the laser beam on the top surface of the spring.

A Laser beam width of 0.2mm traveling along the length of the spring was used for the experimental study. The Laser travel provides the necessary heat to attain the phase transformation temperature. Due to the shape memory effect, the spring displaces and returns to its initial closed coil position partially or completely. An LDS of the 2.5 μm resolution was used to measure this load displacement. The data from the LDS is acquired in the Ni-DAS interfaced with the computer for further data processing. Once the actuation was accomplished, the spring was allowed to cool to the room temperature. During cooling, the applied bias load brings the spring to the initial deformed state. After complete cooling, the next actuation cycle was carried out. A Laser power sweep of 15 W to 50W was used for the investigation of the thermomechanical behavior of the SMA spring.

6.2.1.2 Theory of Actuation: A SMA spring in a closed coil configuration is fixed at one end, and a deforming load is hung at the other end. The closed coil position is the trained shape of the SMA spring. The minimum and maximum stress required to deform the material is called de-twinning start stress σ_s and de-twinning finish stress σ_f respectively. Due to the applied load, de-twinning of the martensite structure takes place. This de-twinning induces a deformation coaxially on the spring up to a certain limit depending on the load.

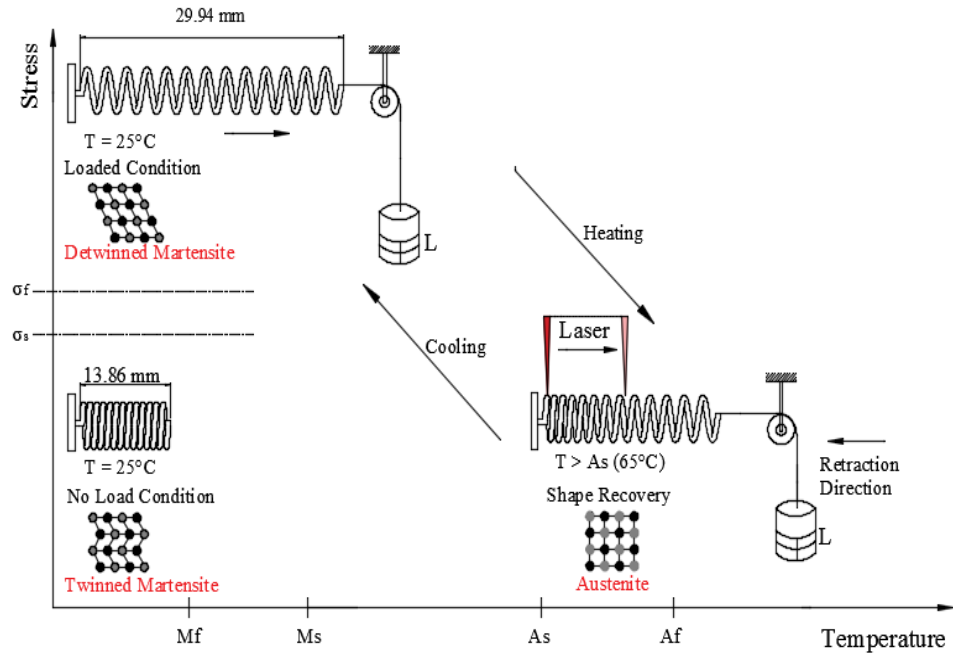
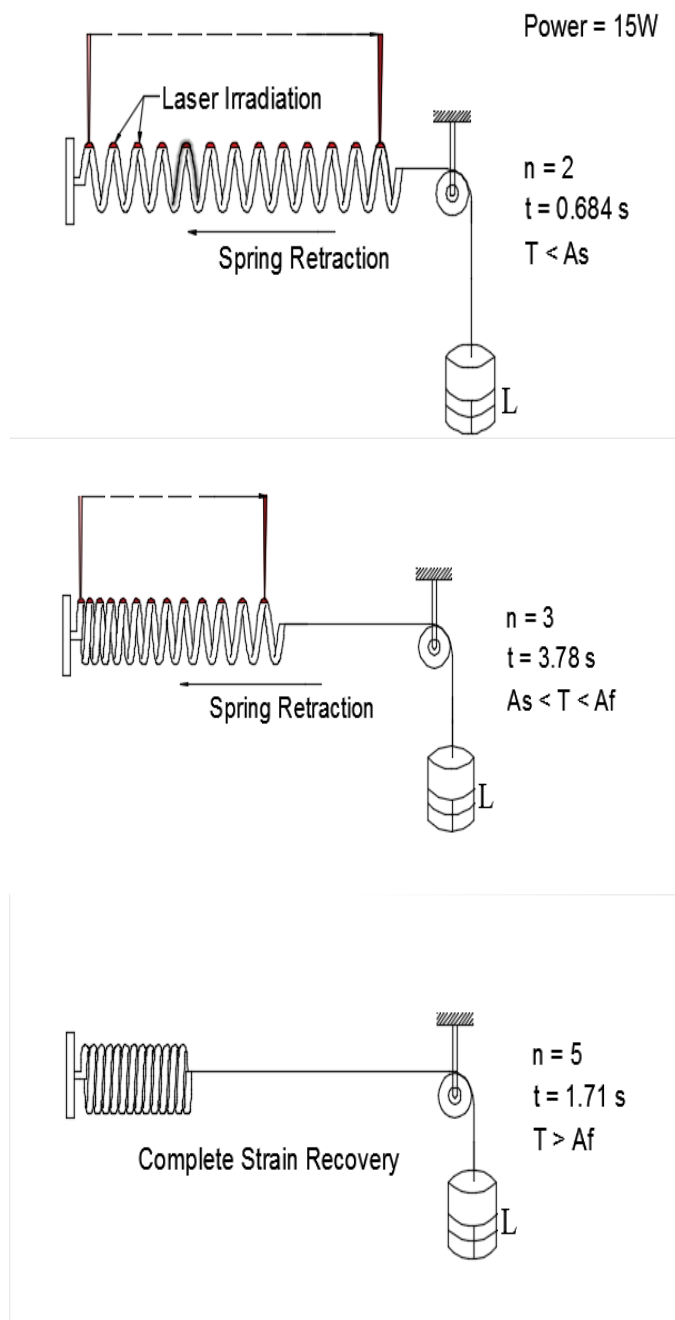


Fig.6.2: Schematic diagram for laser actuation of SMA spring

Fig. 6.2 shows the schematic diagram of Laser actuation of SMA spring. The laser is switched on, and it is made to irradiate on the top surface of the spring for thermal activation of shape memory effect. The energy irradiation from the laser causes a light-matter interaction, which is absorbed by the spring. This energy absorption increases the temperature of the spring at the localized irradiation points. An average increase in the temperature of the spring takes place due to the conduction of this localized high temperature to the entire volume of the spring. In order to achieve heating throughout the spring, the laser is scanned throughout the length of the spring. This laser scanning from one end and returning to the same end after traveling throughout the spring is called Pass.

Fig. 6.3 shows the schematic diagram of laser actuation of SMA spring at periodic time interval. When the temperature increases beyond austenite start temperature, the spring starts to actuate at discrete points. On the further rise in spring temperature beyond the austenite finish temperature, complete actuation takes place. Thus, the spring comes to its initial closed coil position along with the load. When the laser is switched off, heat losses

to the surrounding due to natural convection from the spring, thus cooling of the spring takes place. Due to cooling, the crystal structure begins to change from austenite to twinned martensite at Martensite start temperature (M_s), but this austenite to twinned martensite transformation cannot be observed, because the twinned martensite is immediately brought to de-twinned martensite by the bias load hung. The complete deformation due to the hung load occurs at Martensite finish temperature (M_f). This antagonist bias load helps in bringing back the spring to martensite state from austenite state, thus imitating the two-way effect for cyclic actuation of the spring.



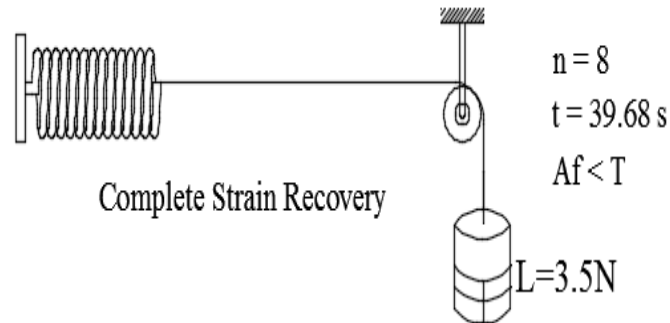


Fig 6.3: Actuation of SMA for complete strain recovery

6.3 Result and discussion: This section is divided into the following subdivision:

6.3.1: Thermomechanical Behavior: The thermomechanical behavior of SMA spring was studied for three different loads, i.e., 1.5 N, 2.5 N and 3.5N at different laser powers. Only with a load of 1.5 N, a sufficiently observable deformation was obtained. Hence a start load of 1.5 N was chosen. Whereas beyond 3.5 N, though a higher laser power was irradiated on the top surface of the spring, the SMA spring was unable to regain its original closed coil shape completely because of the heaviness. Since this study is concerned only on the complete shape memory recovery of the SMA spring, 3.5 N was considered as the maximum load because of its maximum capacity.

For the experimental simplicity, the laser power was irradiated in steps of 5 from 5.0 W to a maximum capacity of the laser system 50 W. It was observed that the minimum laser powers of 5.0 W and 10 W were not sufficient to increase the temperature of the spring near to or beyond A_s . Even though the number of passes was increased, the temperature of the spring increased up to the steady state level which was well below the required actuation temperature of the SMA spring. Hence the powers 5.0 W and 10 W was neglected for the actuation studies.

For a constant laser power, increasing the number of passes increases the temperature of the spring. This is because the irradiation time of the laser over the spring surface is more. However, the increase in temperature is observed only until the spring reaches a steady state with the environment, i.e. when the heat absorbed equals the heat emitted by the spring to the surrounding. Beyond that steady state, despite increasing the number of passes no change was observed in displacement. Fig. 6.4 shows that for a laser power of 15 W and a load of 3.5 N, by increasing the number of passes from 6 to 8, a slight increase in the displacement was observed.

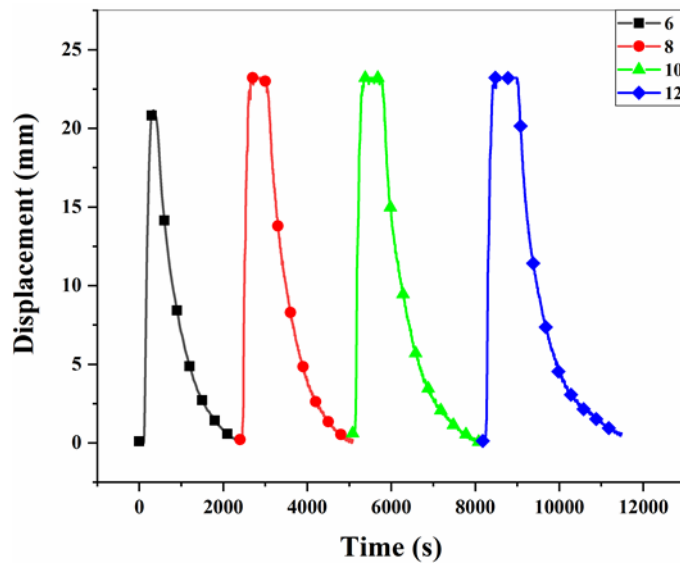


Fig 6.4: Actuation of SMA spring at 15 W with varying passes

Whereas on further increasing the number of passes to 10 and 12, no change in the displacement was observed. From Fig. 6.4, it could also be deduced that the heating curve of 6 passes has a sharp peak whereas for 8, 10 and 12 passes, the saturation was reached and only an increase in dwell time was observed. Supplying any heat surplus to this saturation will result only in the local damage to the spring with deterioration in the shape memory property of the spring over time. Hence, for particular laser power, the sufficient number of passes required for the actuation was fixed depending on the above procedure.

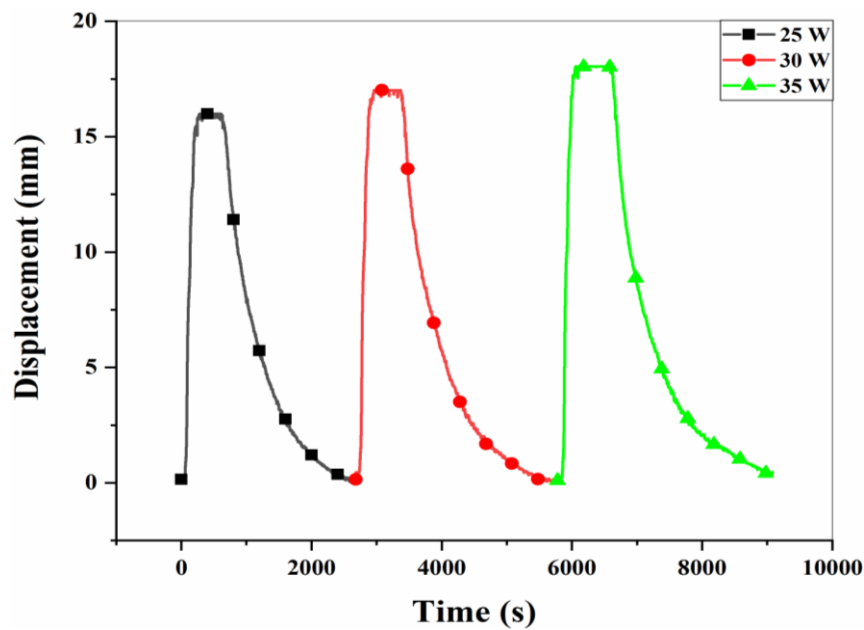


Fig 6.5: Actuation of SMA spring at varying power till full recovery

Laser power of 15W was irradiated on the top surface of the spring, initially for 2 to 3 passes there was no actuation observed in the spring. Furthermore, a gradual response due to the increase in passes was observed

Different Laser powers were used for the actuation of the SMA spring for loads of 1.5 N, 2.5 N and 3.5 N. Laser with a power from 15 W to 50 W were impinged on SMA NiTi when it was loaded with 1.5 N, 2.5 N and 3.5 N. It is tabulated below (Table 6.1)

For 15W laser power, at least seven passes are required to heat the spring to the actuation temperature. Increasing the number of passes results in increasing the temperature but not up to the austenite finish temperature. Thus for the power of 15W, the maximum displacement achieved was 10.3 mm for a load of 1.5 N. The same experiment was repeated for 2.5 N and 3.5 N. Due to the load, the spring extends to a greater distance. To cover the whole length with laser, the laser travel distance is increased. Thus there is a slight increase in heating time for the 1.5 N, 2.5 N and 3.5 N observed. Though there was a slight increase in heating time observed, the cooling time remained approximately equal. Hence, the experiment was conducted by increasing the laser power from 15 W to 50 W, and the corresponding number of passes were fixed accordingly. Increase in laser power causes

exposure to high temperature. Hence an increased cooling time is required for complete deflection of the spring.

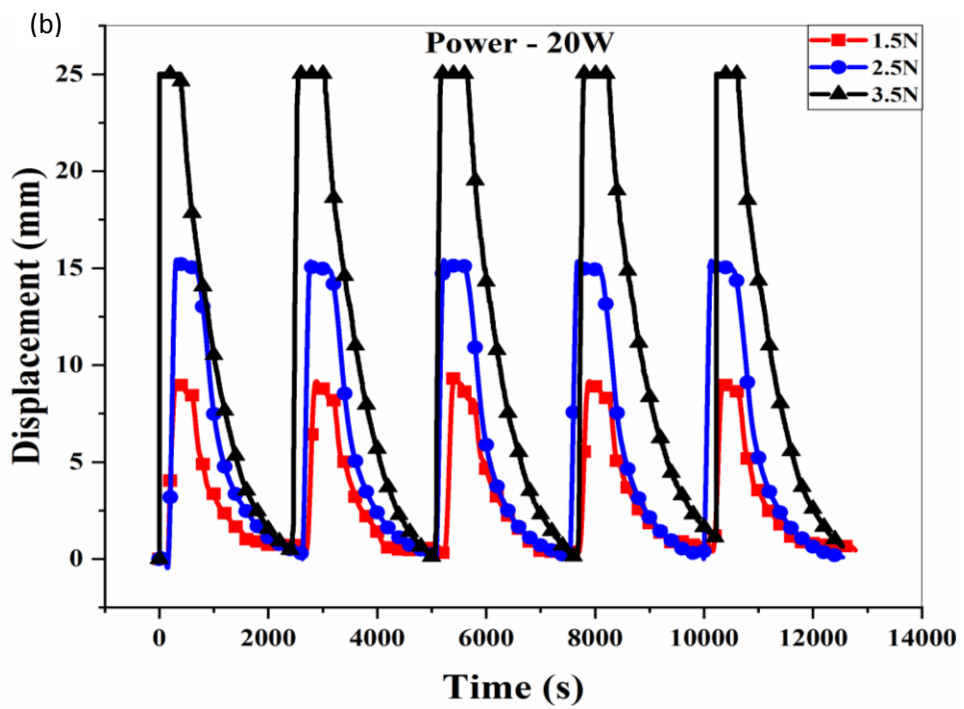
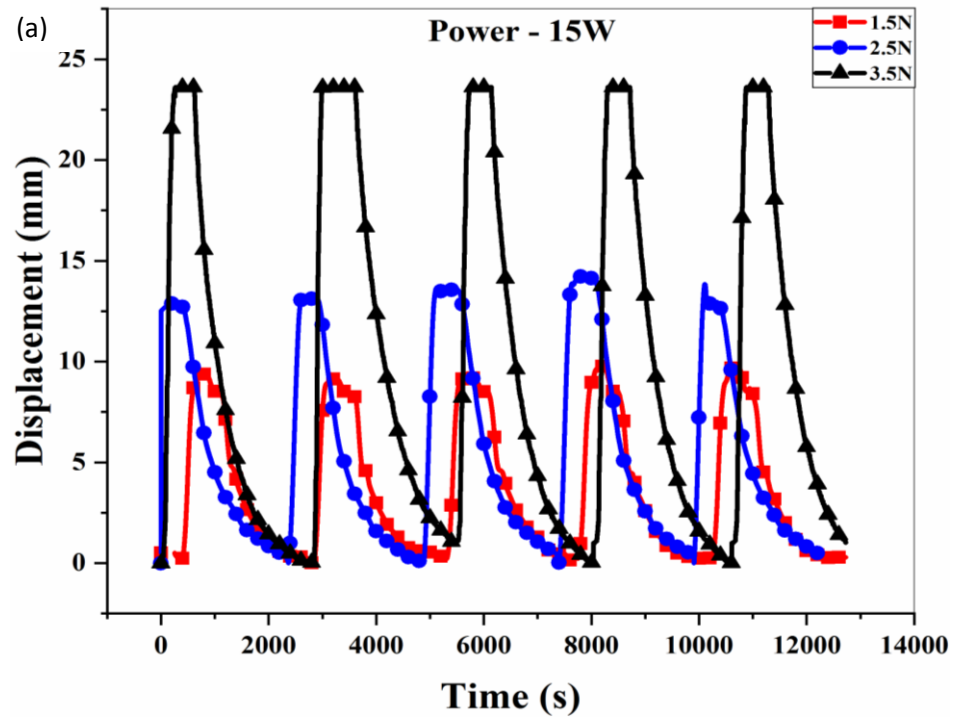
Note: Heating time was dependent on some passes but cooling time was operated manually (up to initial position or full recovery) using a stopwatch.

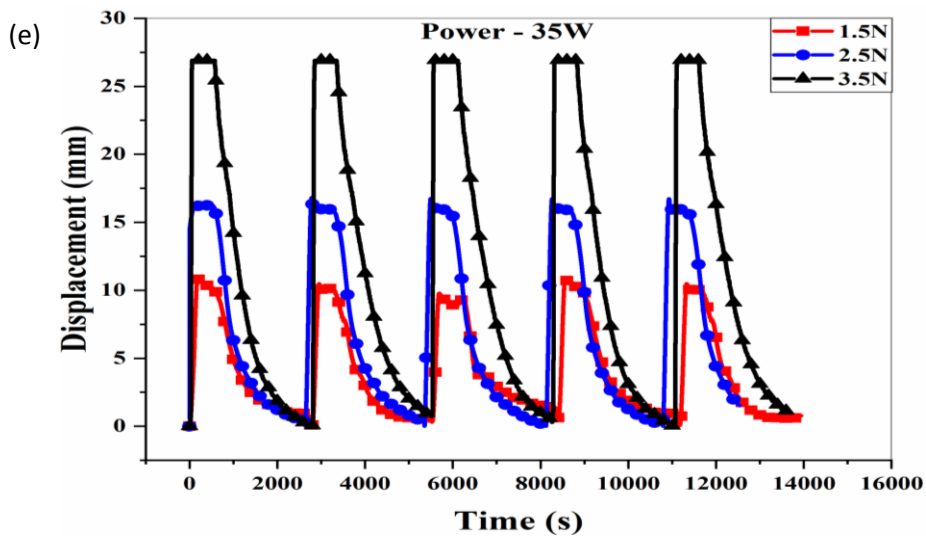
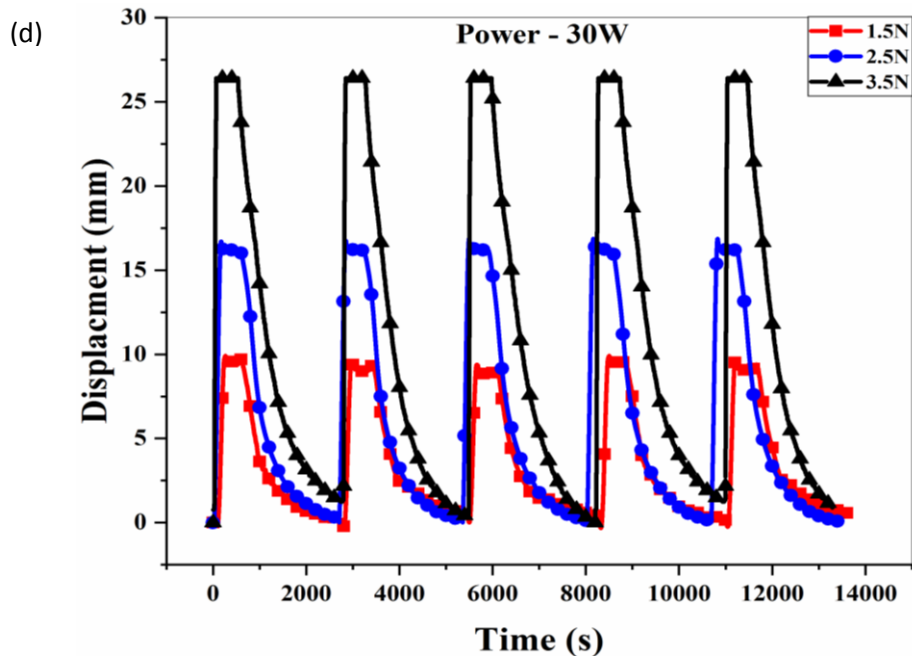
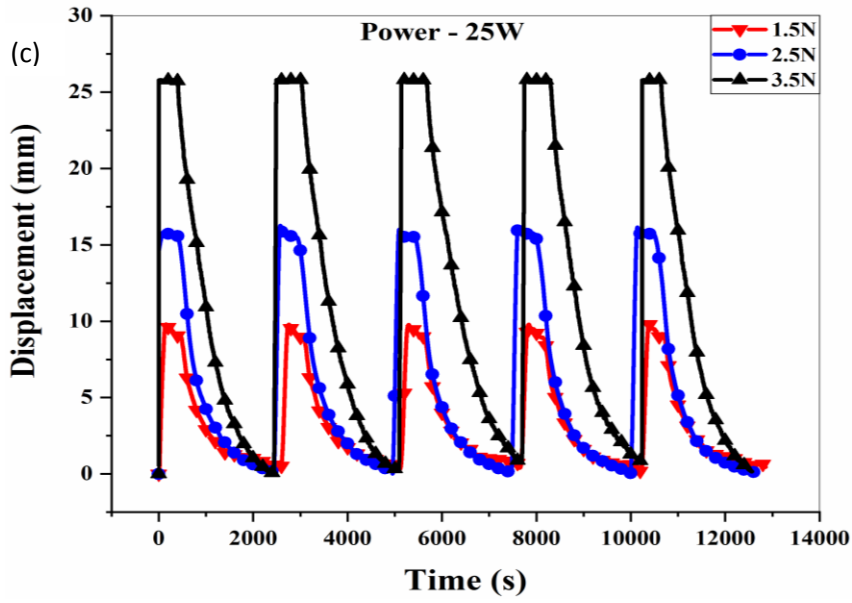
Table 6.1: Parameters for Laser actuation of SMA NiTi

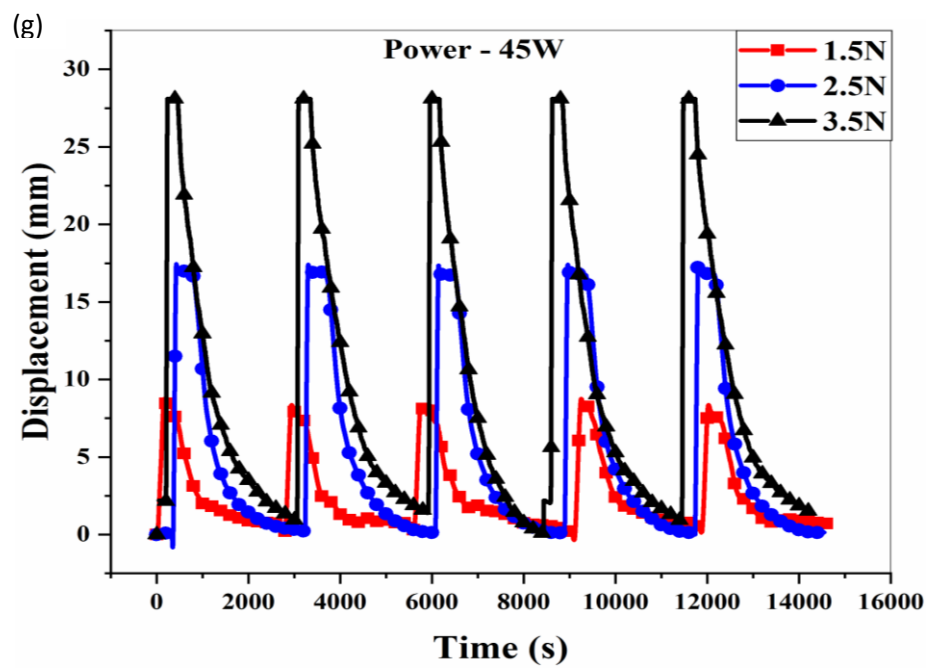
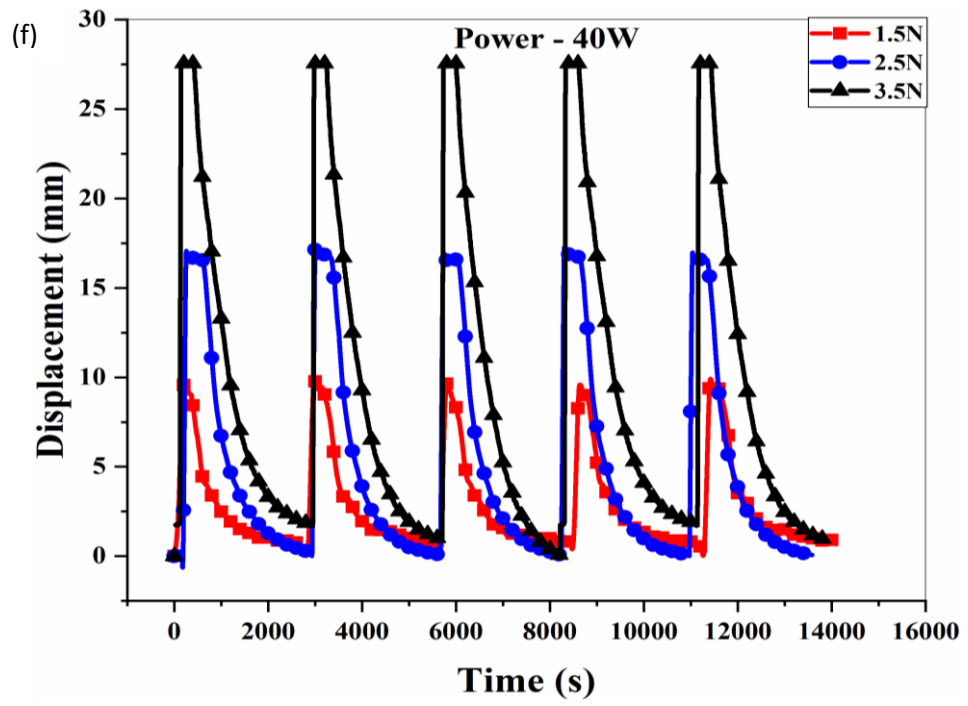
S.No	P (W)	W (N)	n	δ (mm)	HT (s)	CT (s)
1.	15	1.5	7	10.3	29.32	210
		2.5	8	14.8	30.89	
		3.5	8	23.7	35.27	
2.	20	1.5	3	10.1	12.57	230
		2.5	3	15.5	13.22	
		3.5	5	24.8	26.22	
3	25	1.5	2	10.5	8.37	240
		2.5	2	16.1	8.88	
		3.5	3	25.8	14.89	
4.	30	1.5	2	10.7	8.37	253
		2.5	2	16.8	8.88	
		3.5	2	26.4	9.92	
5.	35	1.5	2	11.2	8.37	260
		2.5	2	17	8.88	
		3.5	2	27.1	9.92	
6.	40	1.5	1	11.2	4.18	265
		2.5	1	17	4.44	
		3.5	1	27.7	4.96	
7.	45	1.5	1	11.3	4.18	270
		2.5	1	17.1	4.44	
		3.5	1	28.4	4.96	
8.	50	1.5	1	11.5	4.18	275
		2.5	1	17.1	4.44	
		3.5	1	28.9	4.96	

HT: Heating Time (s), CT: Cooling Time (s), δ : Displacement (mm), n: Number of Passes

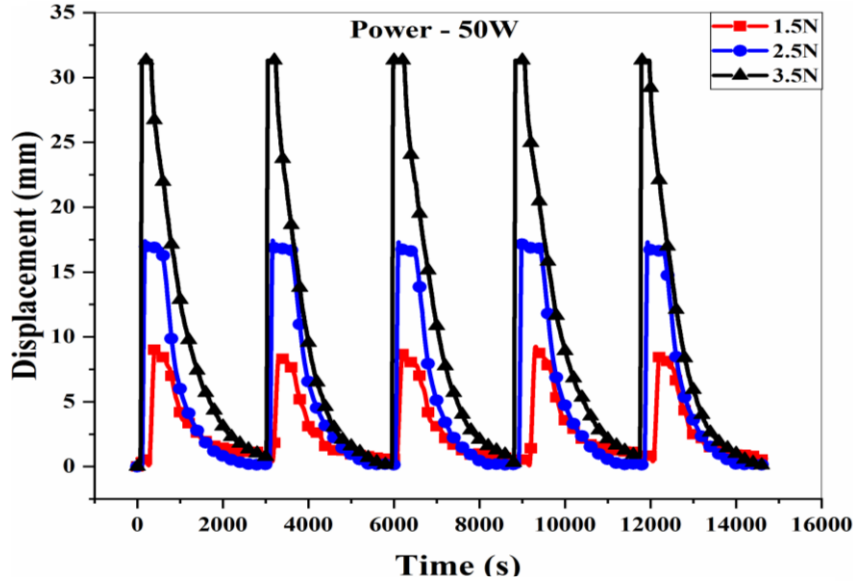
P: Power (w), W: Weight (N), As per Table 6.1, graphs are plotted. All graphs are shown in Figs 6.6 (a-h):







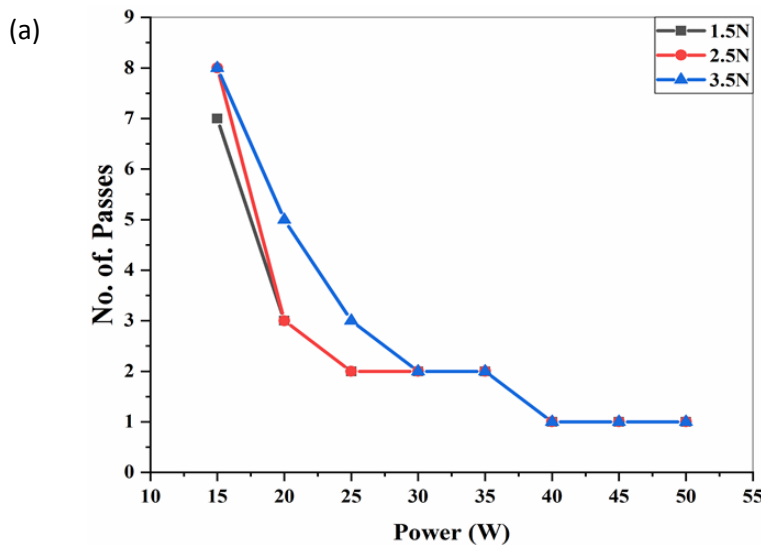
(h)

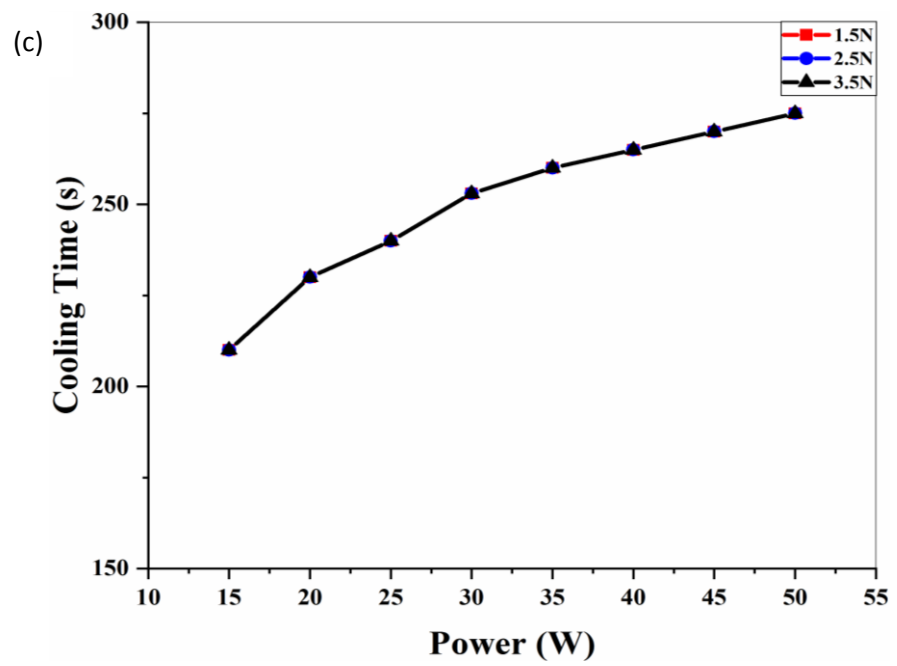
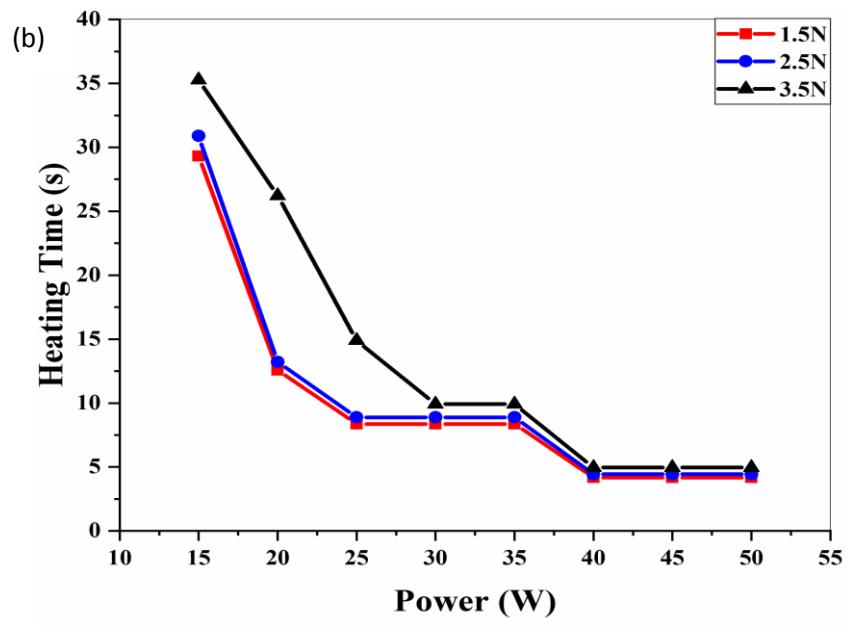


Figs 6.6 Thermo-mechanical behavior of NiTi SMA for its full recovery with a load of 1.5 N, 2.5 N and 3.5 N at a) 15 W, b) 20 W, c) 25 W, d) 30 W, e) 35 W, f) 40 W, g) 45 W, h) 50 W

6.3.2 : Effect of parameters on actuation: SMA actuation depends on power. Besides than power, some passes, heating time, cooling time, etc. Played important role. It is discussed in the upcoming section:

a) *The relationship between power and number of passes:* Since actuation of SMA depends on power and number of passes also. Pictorial representation between these parameters is shown in Fig 6.7 (a). It is inversely proportional to each other. If power decreases then some passes will be more. If maximum power is used then one pass is sufficient for full recovery. After 40 W only one pass is required for full recovery.





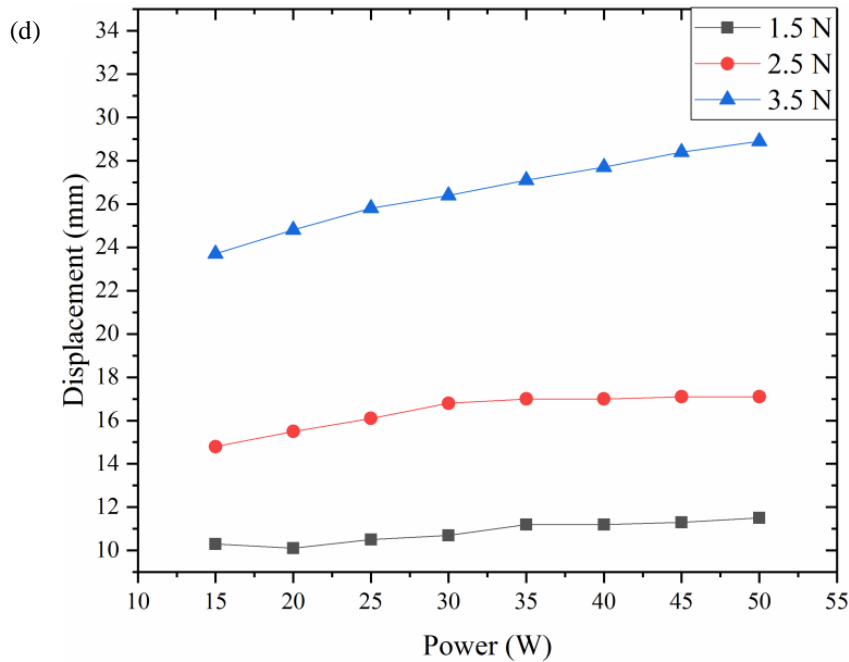


Fig 6.7 Relationship between a) Power and no of passes, b) Power and heating time, c) power and cooling time, d) power and displacement

b) The relationship between power and heating time: As power increases heating time will be less for complete recovery. According to Table 6.1, the requirement of heating time will be more for less power. Its relationship is shown in Fig 6.7 (b)

c) The relationship between power and cooling time: Power is directly proportional to cooling time. As power increases from 15 W to 50 W, its respective cooling time will also increase from 210 s to 275 s. It is shown in Fig 6.7 (c).

d) The relationship between power and displacement: Since displacement mainly depends on load only, i.e., 1.5 N, 2.5 N and 3.5 N. As weight increases, displacement will also increase, and reduction will occur due to the increment of power. Hence there is a small effect on displacement (Fig 6.7 d) due to power.

6.3.3: Mathematical Modelling: To examine the heat distribution in the spring due to the laser irradiation, COMSOL Multiphysics, a finite element package capable of solving coupled physics was used. The time-dependent differential heat flow equation must be solved, to determine the temperature.

$$\rho C_p \frac{\partial T}{\partial t} - \nabla(k \cdot \nabla T) = Q \dots \dots \dots \text{Eq 6.1}$$

Where ρ is the material density, C_p is the specific heat capacity, T is the temperature, t is the time, k is the thermal conductivity and Q is the volumetric heat source. This volumetric heat source is due to the heat absorbed by the spring from laser power irradiation, according to Beer-lambert law. The volumetric heat source along the radial and axial direction as a Gaussian beam profile can be written as follows:

$$Q(r,z) = Q_0(1-R_C) \frac{A_C}{\pi a^2} e^{-\left[\left(\frac{r}{a}\right)^2\right]} \cdot e^{-A_C Z} \dots \dots \dots \text{Eq 6.2}$$

where Q_0 is the incident laser power, R_C is the surface reflectivity, A_C is the absorption coefficient, a is the 1/e beam radius, $e^{-A_C Z}$ is the exponential decay due to absorption. The absorption coefficient and surface reflectivity can be calculated from

$$A_C = \frac{4\pi k}{\lambda} \dots \dots \dots \text{Eq 6.3}$$

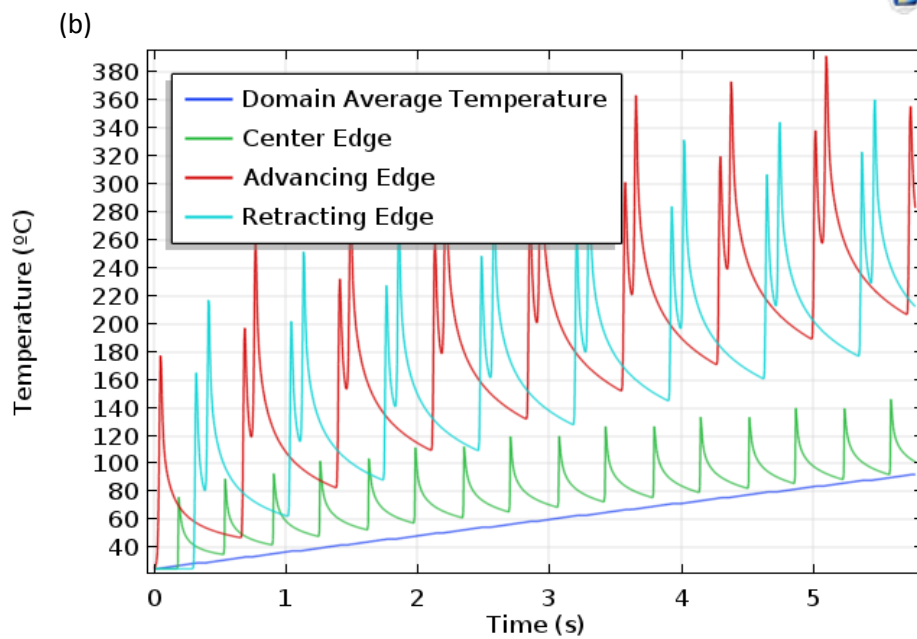
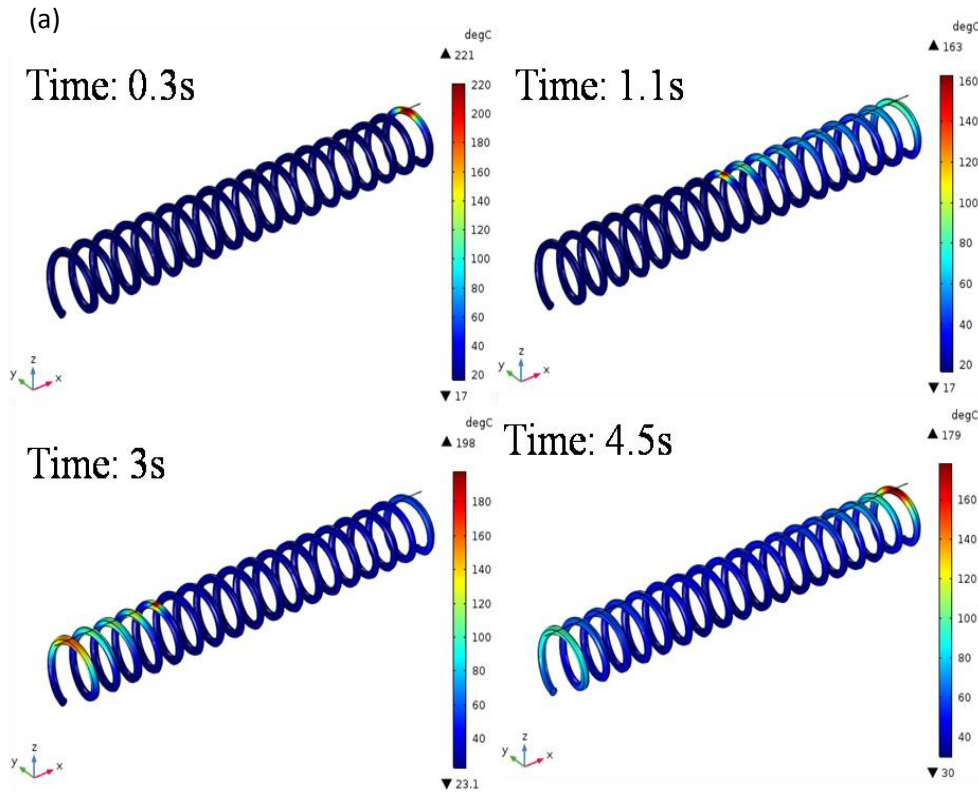
$$R_C = \frac{(n-1)^2}{(n+1)^2} \dots \dots \dots \text{Eq 6.4}$$

where λ is the laser wavelength and n is the refractive index [145-146].

6.3.4: Simulation: Since the spring comes in direct contact with the laser beam traveling the across the spring, it was difficult to make temperature measurements accurately. Hence, using COMSOL Multiphysics, a finite element tool, the heat distribution and the temperature reached by the spring during actuation was simulated.

As discussed in the mathematical modeling section, a volumetric heat source was made to travel throughout the length of the spring. Figs 6.8 a- b shows the travel of 15 W laser power along the length of the spring for eight passes over a period. It is clear from Fig 6.8 c that temperature will increase with increase the number of passes. Actuation of SMA also depends on spot

size. If power, as well as spot size of laser, will increase, the material will be ablated.



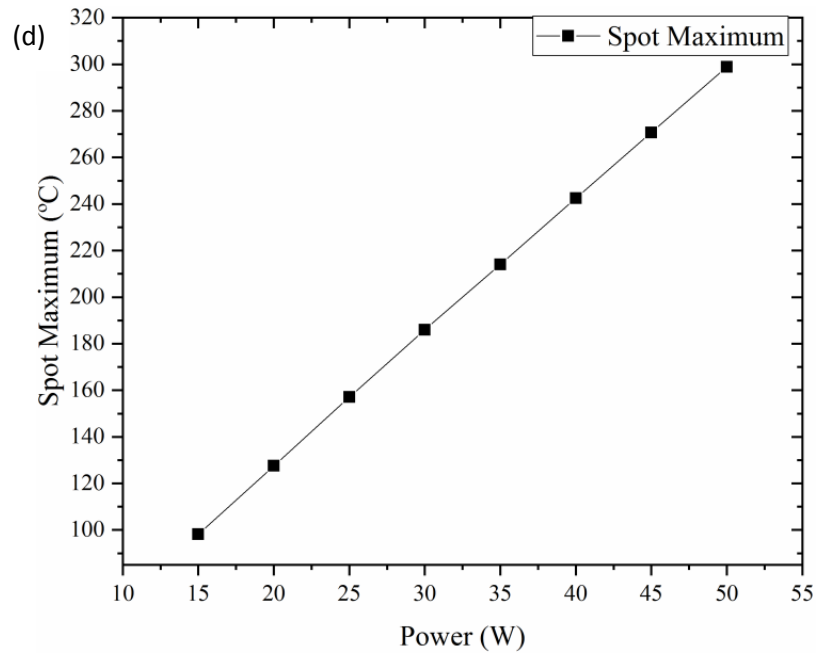
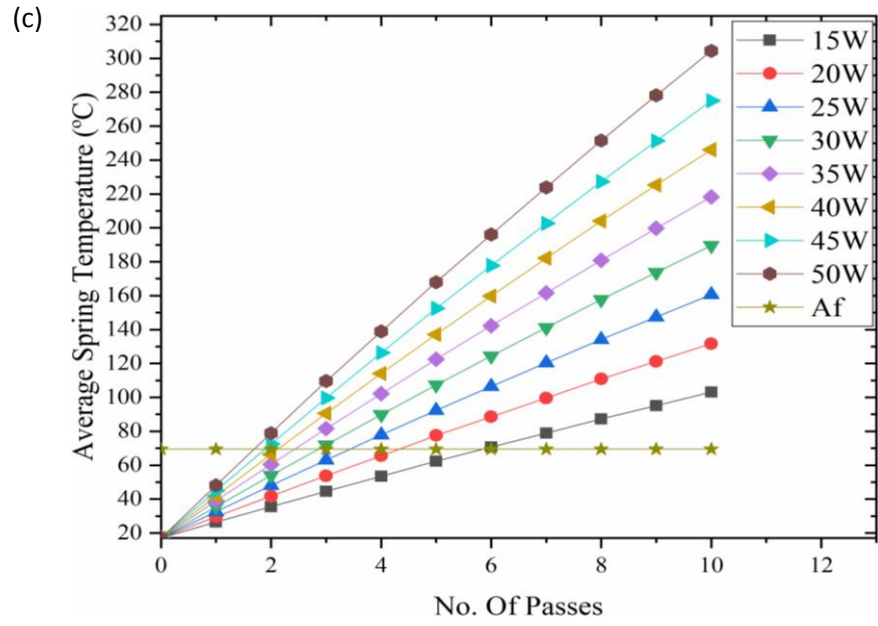


Fig 6.8: a) Simulation study of laser actuated SMA at 15 W, b) thermal behavior for 8 passes, c) comparison analysis of temperature for experimental and FLIR camera, d) effect of spot size on heat transfer

6.3.5: Characterization

6.3.5.1 Stereo Images: only one pass was enough to actuate the SMA with 50 W. If more than one pass was used then spring was failed. Fig 6.9 shows the stereo image.

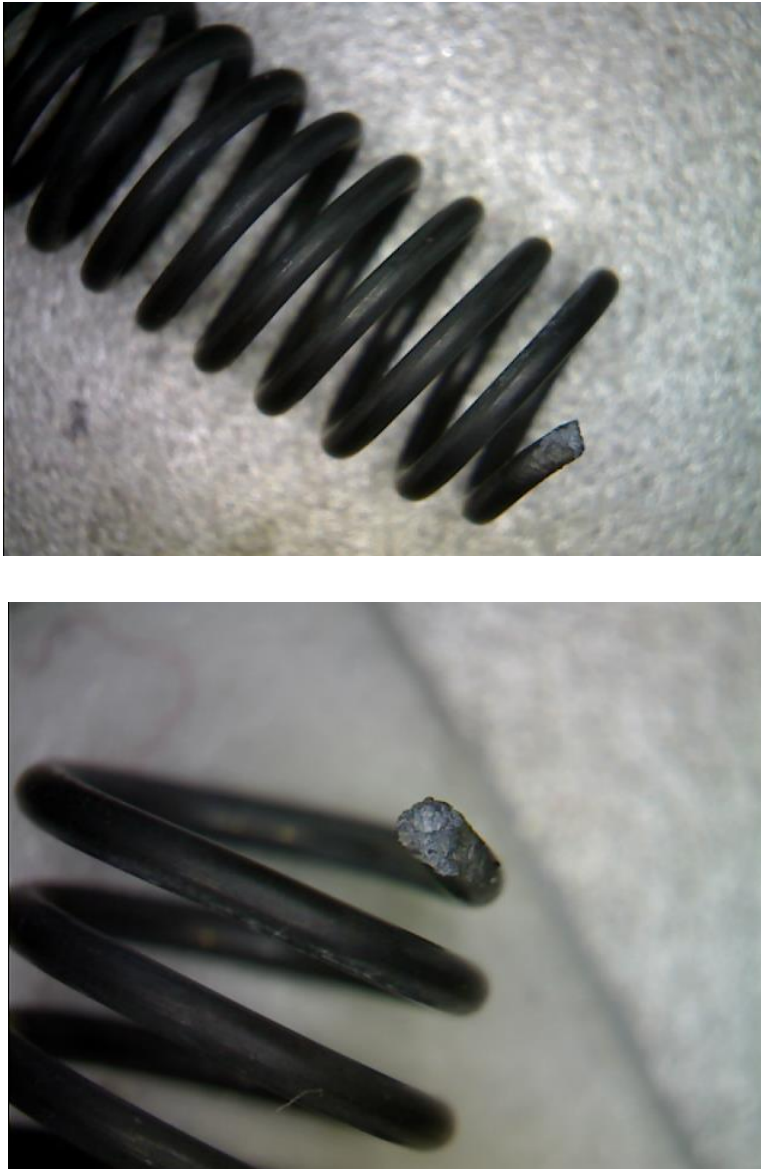
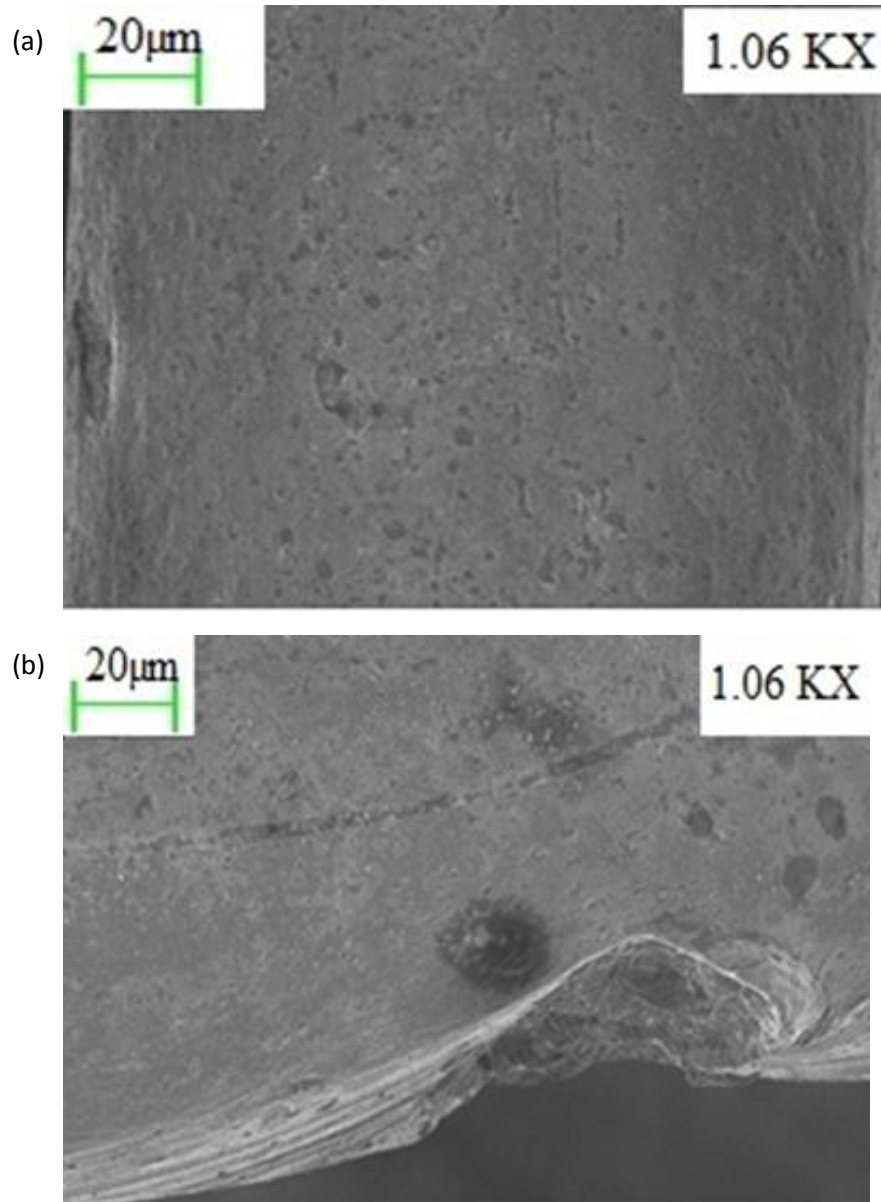


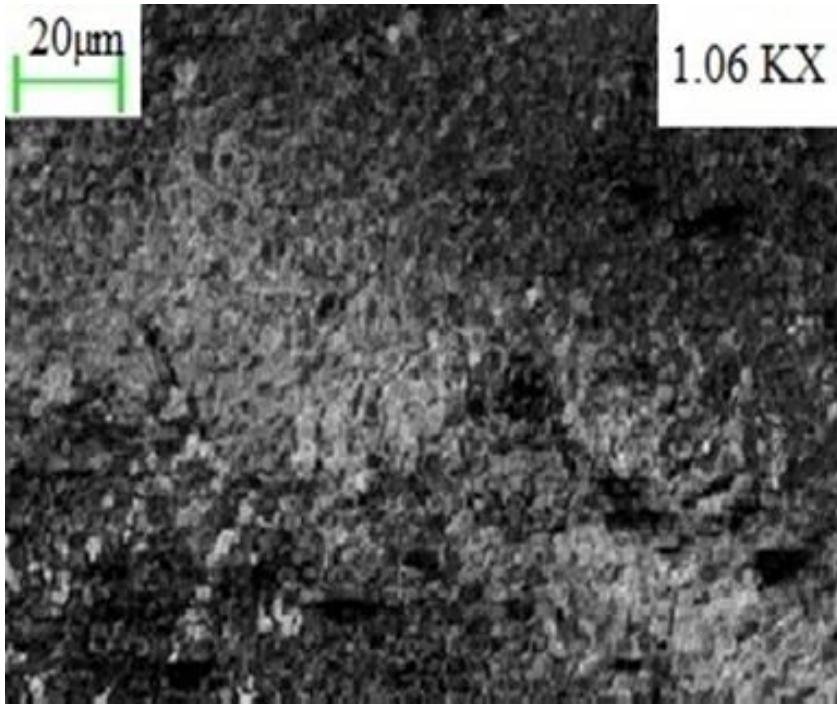
Fig 6.9 Stereo image of failed spring

6.3.5.2 Scanning Electron Microscope (SEM) images: SEM image reveals the information about the sample including external morphology (texture), chemical composition, and crystalline structure and orientation of materials

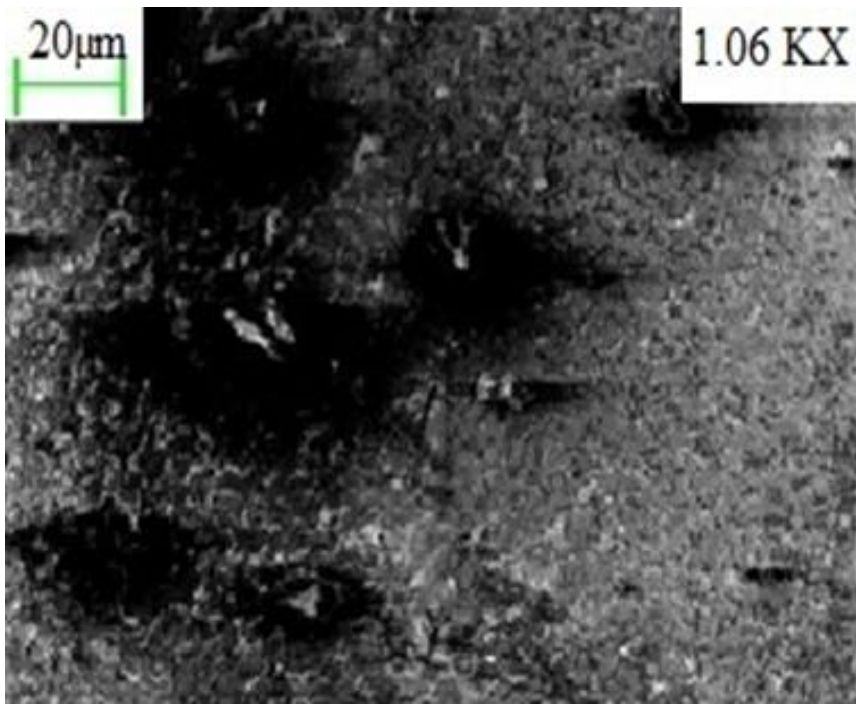
making up the sample. For different parameters, SEM images are shown below. It is clear from the images that as weight and power increased with the thermo-mechanical cycle, from scratches to crack formation occurs, which depicts its failure. Fig 6.10 (a) shows the SEM image of non-treated SMA spring which shows a smooth surface, Fig 6.10 (b) depicts the image for treatment of 5 W with 1.5 N load. One sharp mark is present which shows that treatment is in a particular area, means that is not uniform. When it is loaded with 2.5 N and laser is passed over the spring by ten times (Fig 6.10 c), small spots are available, and whereas for 3.5 N with the same wattage, its burrs are coming out depicted in Fig 6.10 (d). As the load and power increase, more cracks are visible, so it is concluded that failure of SMA spring is directly proportional to power and weight.

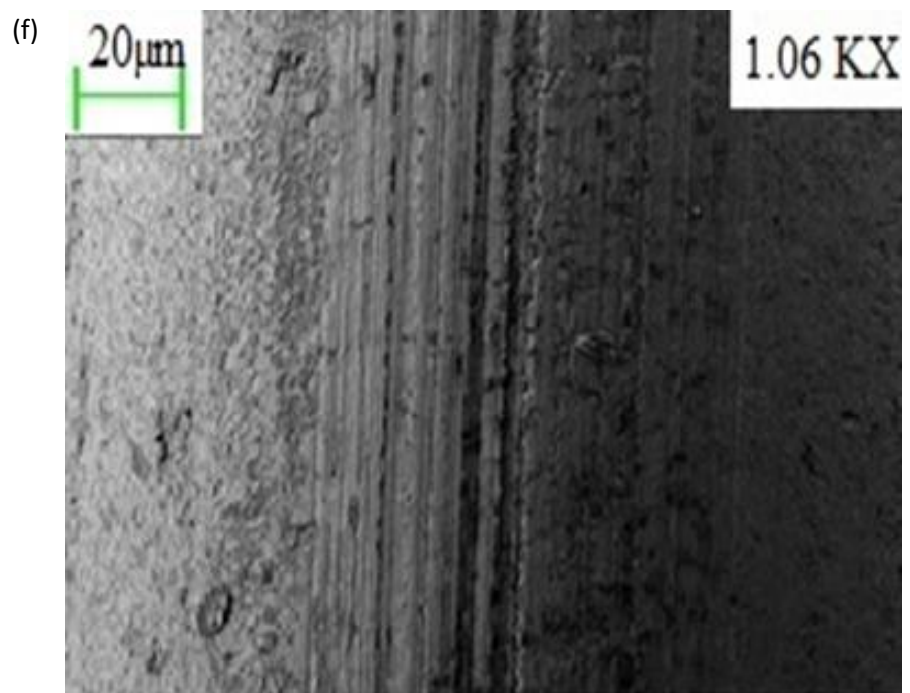
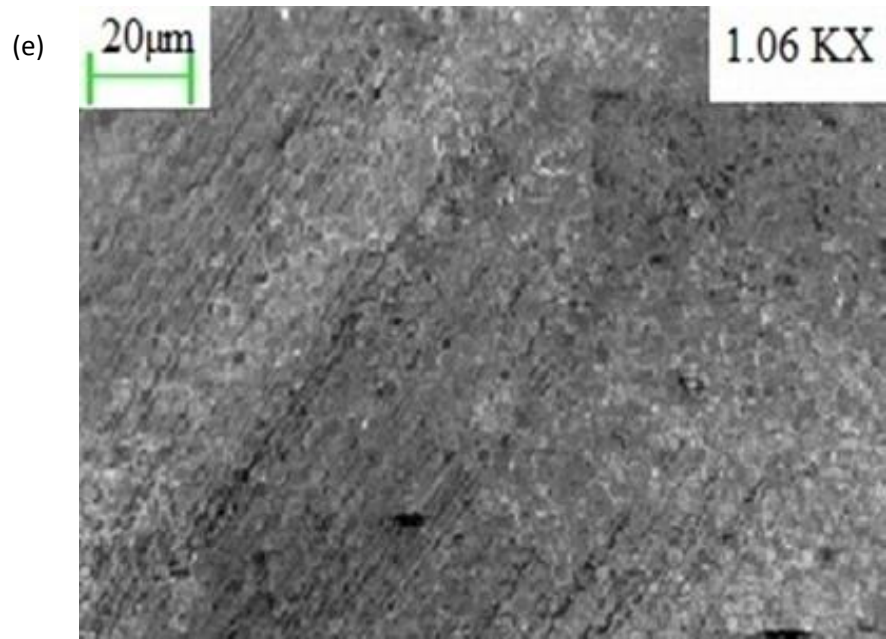


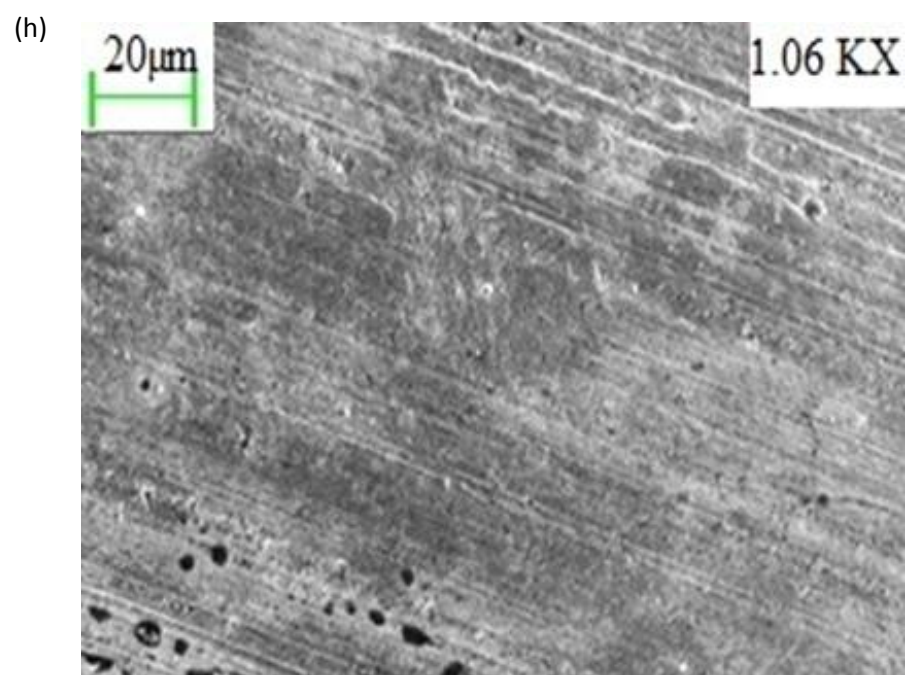
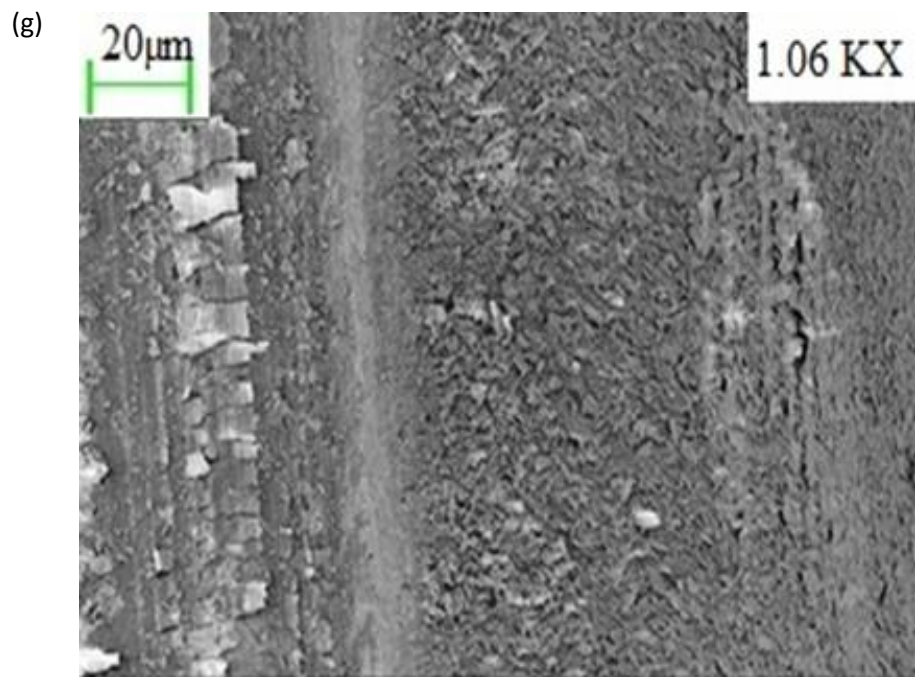
(c)



(d)







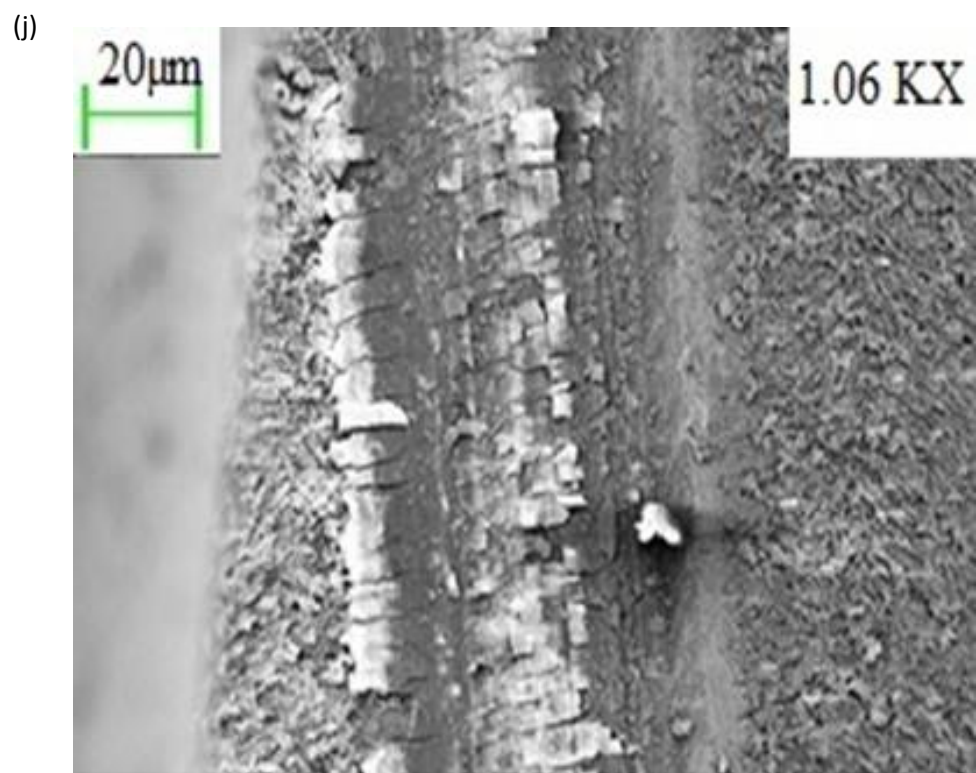
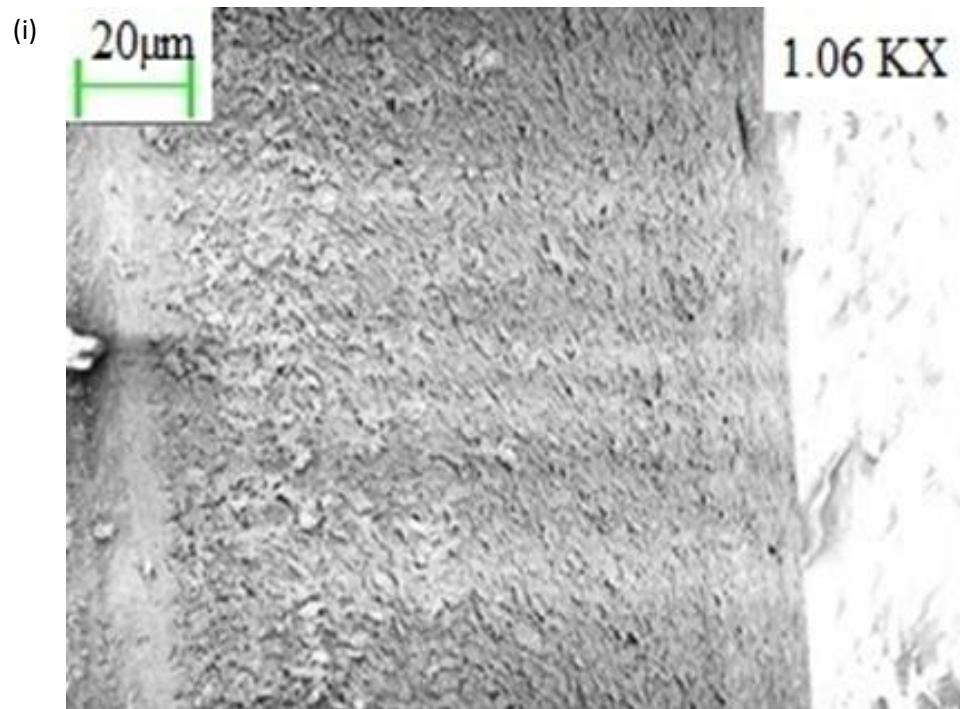


Fig 6.10: SEM images a) for Non Treated Spring, b) for 5 W, 1.5 N, c) for 5 W, 2.5 N, d) for 5 W, 3.5 N, e) for 10 W, 1.5 N, f) 10 W. 2.5 N, g) 10W, 3.5 N, h) 15 W, 1.5 N, i) 15 W, 2.5 N, j) 15 W, 3.5 N

6.3.6 Beam Profile: The significance of the beam profile is that the energy density, the concentration, and the collimation of the light are all affected by it. Also the propagation of the beam through space is significantly affected by the beam profile. The photographic sheet is used for measuring beam profile which is shown in Fig 6.11. The width of the laser beam was 2 mm (to make it visible) in place of 0.2 mm. Effect of load and its corresponding temperature and various morphological analysis has been reported in result and discussion section.

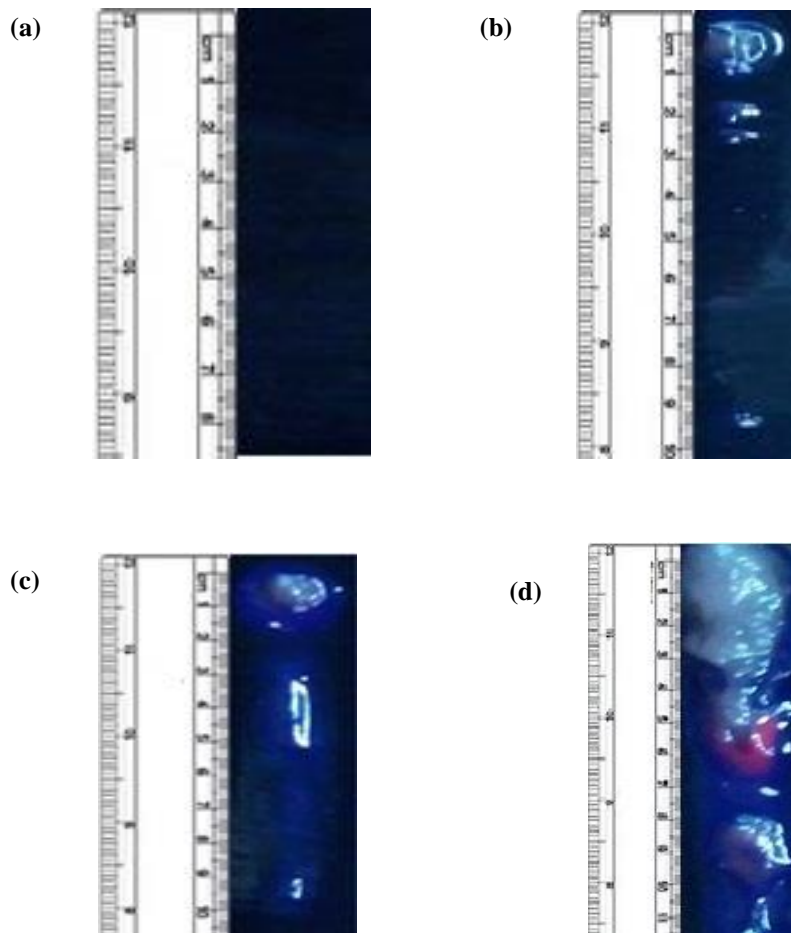


Fig 6.11: Effect of laser on Photographic sheet a) at 0.2 mm (invisible), 2 mm at 2 N b) 5 W, c) 10 W, d) 15W [for 5 passes]

6.4 Application:

6.4.1 Directional control valve (DCV): DCVs are one of the most fundamental parts of hydraulic machinery as well as the pneumatic machinery. They allow fluid flow into different paths from one or more sources. They usually consist of a spool inside a cylinder which is mechanically or

electrically controlled. The movement of the spool delimitate or permits the flow; thus it allows the Regimentation of fluid flow.

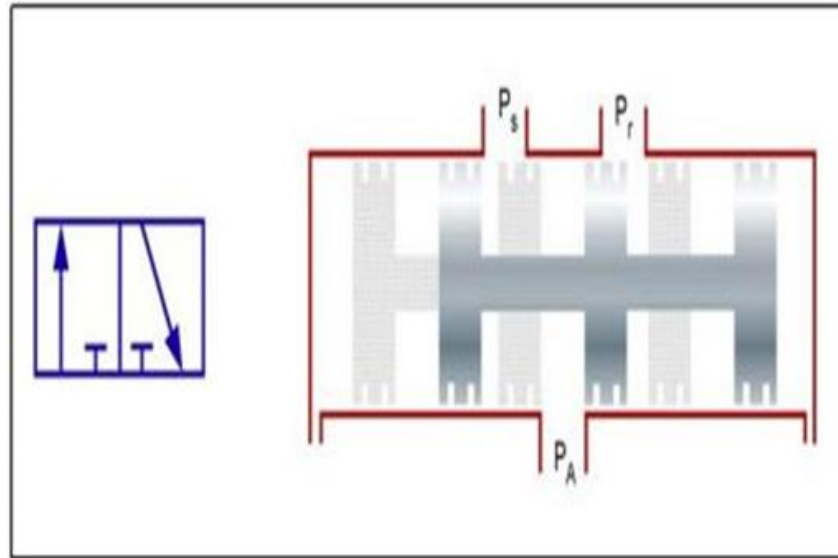


Fig. 6.12 Schematic of a 3/2 DCV

There are two axiological positions of directional control valve namely normal position where valve returns on the removal of actuating force and other are the working position which is the position of a valve when actuating force is applied. There is another class of valves with three or more position that can be spring centered with two working position and a normal position. Normal working of DCV is shown in Fig 6.12

There are many types of Directional Control Valve (DCVs) for example 3/2 DCV, 5/2 DCV and many more. 3/2 means that it has three ports and two spool position.

The codification of the Directional Control Valve can be made upon various parameters, and the driving one is the actuation method. DCVs can be actuated by various methods such as:

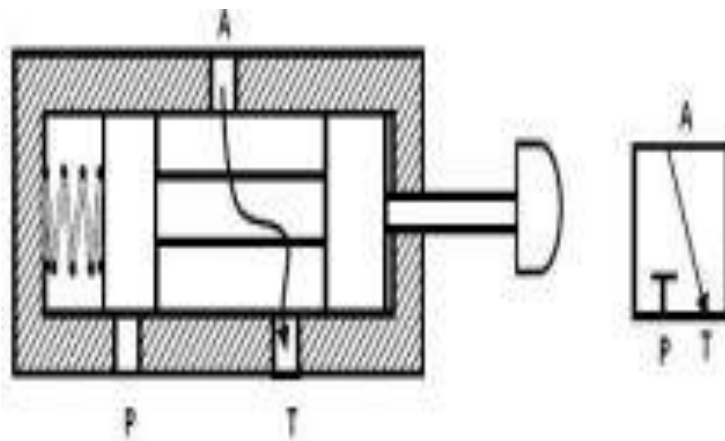
6.4.1.1 Manually Operated: Manually operated valves work with simple levers or paddles where the operator applies force to operate the valve. Spring force is sometimes used to recover the position of the valve. Some manual valves utilize either a lever or an external pneumatic or hydraulic signal to return the spool.

6.4.1.2 Hydraulically Operated: A hydraulically operated DCV works at much higher pressures than its pneumatic equivalent. They must, therefore, be

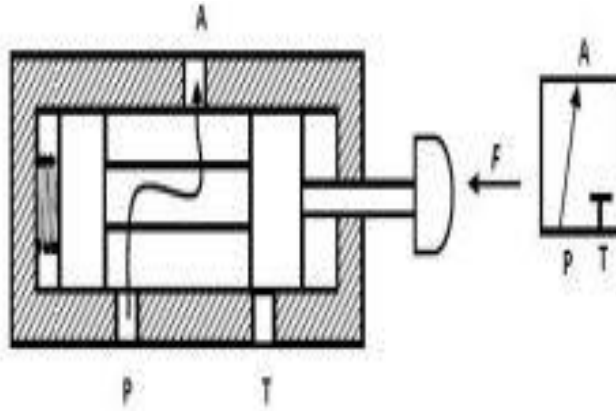
far more robust so are precision machined from higher quality and strength materials.

6.4.1.3 Solenoid Operated: They are widely used in the hydraulics industry. These valves make use of electromechanical solenoids for sliding of the spool. Because the simple application of electrical power provides control, these valves are used extensively. However, electrical solenoids cannot generate large forces unless supplied with large amounts of electrical power. Heat generation poses a threat to extended use of these valves when energized over time. Many have a limited duty cycle. This makes their direct acting use commonly limited to low actuating forces.

6.4.2 Working of a 3/2 Directional Control Valve: Three-way valves either block or allow flow from an inlet to an outlet. They also allow the outlet to flow back to the tank when the pump is blocked, while a two-way valve does not. A three-way valve has three ports, namely, a pressure inlet (P), an outlet to the system (A) and a return to the tank (T). The operation of a 3/2-way valve normally closed. In its normal position, the valve is held in position by a spring. In the normal position, the pressure port P is blocked, and outlet A is connected to the tank. In the actuated position, the pressure port is connected to the tank, and the tank port is blocked.



(a)



(b)

Fig 6.13: (a) Ports A and T are connected when force is not applied (valve un actuated). (b) Ports A and P are connected when force is applied (valve

6.4.2.1 Drawbacks of the current designs of the DCVs: Demerits of current DCV's are given below:

a) Lever-Spring Operated

- i) Automation is not possible.
- ii) The frequency of operation is limited.

b) Solenoid operated

Use of electrical components in the direct vicinity of the valve is unavoidable which is a threat to the safety of some sensitive areas like a nuclear power plant. Design problems mentioned above in current DCVs were tackled by using SMA based actuators in the DCV design. This was the motivation behind this project.

6.4.3 Conceptual model Design: After it was decided to use the SMA tension springs, conceptual CAD model was made using designing software Pro-Engineer (Fig 6.14)

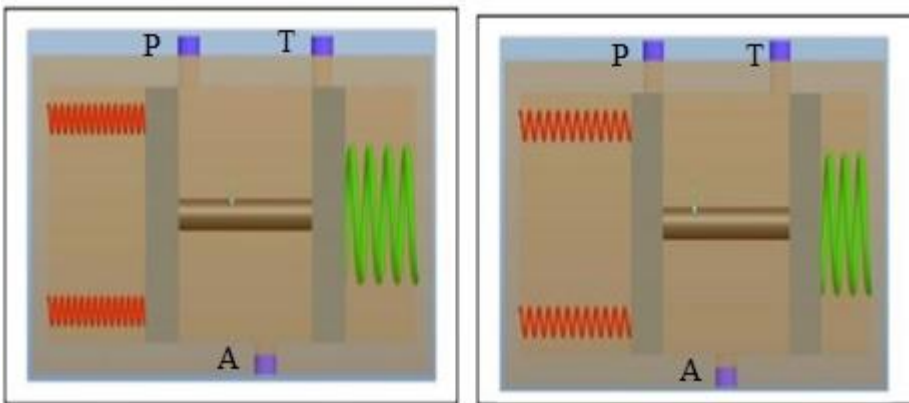
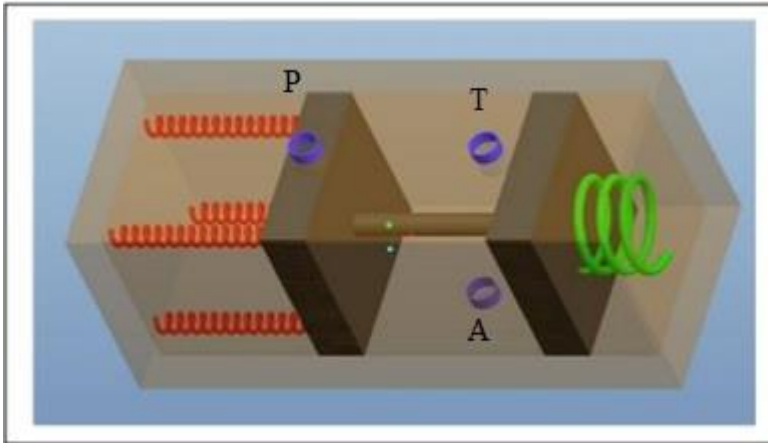


Fig 6.14: a) Spool position 1 (SMA heated), b) Spool position 1 (SMA cooled)

- **Fabrication:** Fabricated directional control valve is shown in the Fig 6.15 a and b.

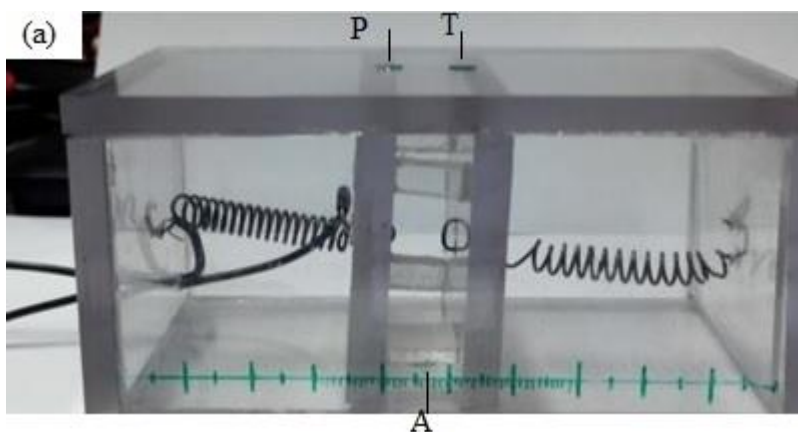




Fig 6.15: a) A working model of Directional Control Valve, b) Top view of Directional Control Valve

6.4.3.1 Working: SMA tension springs which we procured were trained to come into their original shape, i.e., at the free length of the spring after heating to about 55°C , and they were one-way trained. Hence another tension spring (of any suitable material) was required on the opposite side of the spool to keep the SMA springs in tension. So, initially (when SMA spring is not heated or “actuated”) port P is blocked by the piston and port T is connected to A. When the SMA spring is given heat energy (via any method), it contracts doing work against the tensile force of the other spring due to SME and previous training, thus moves spool to position 1 which opens port B and blocks port C at the same time connecting port A to port B.

6.4.3.2: Actuation of DCV: DCV is actuated using a continuous laser. For actuating this following parameter have been used:

Power: 10 W, Number of passes: 05

Total six cycles have been used for this actuation. One cycle is of approximately 500 s. Based on the previous experimentation its life cycle can also be estimated at different power (Fig 6.16).

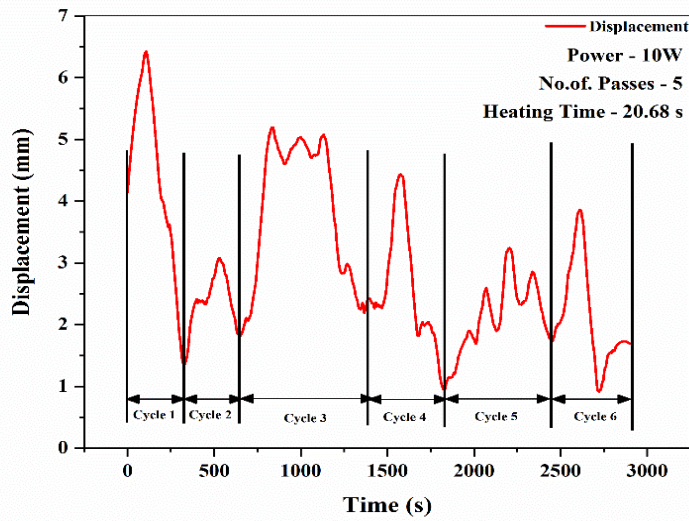


Fig 6.16: Actuation of DCV

6.5 Summary: Finally, SMA NiTi spring is actuated using continuous fiber laser. It is summarized as:

- It has been found that actuation is fast in this case and gained by laser medium is good enough to use in practical applications.
- Laser at 1064 nm is used, and the optimum power of about 15.0 W to 50 W is analyzed. To measure beam profile photographic sheets are used.
- DSC analysis is also done to measure its transformation temperature for different wattage. For an application point of view, the directional flow control valve is developed.
- It is faster than pulsed laser actuation which took less time.

Chapter 7

Conclusion and Future scope

The objective of this chapter is to provide a summary of the work reported in this thesis regarding research contributions and utility of the research. In the end, limitation and future scope of the present work are given.

7.1 Conclusions:

The current thesis has detailed the effects of Thermomechanical behavior on the binary Nitinol alloy under the influence of different medium. More specifically, the effects on mechanical performance, microstructure and phase transformation temperatures were analyzed. The following sections contain the conclusions of this work and recommendations for future research. The conclusions are grouped by the research objectives

7.1.1 Research Contributions:

➤ **Contact-based actuation strategy:** It is categorized in two way, i.e., Joule heating and hot fluid actuation. Thermomechanical behavior and life cycle analysis of SMA has been reported with different parameters.

• **Electrical Actuation:** Thermomechanical behavior and life cycle of SMA are measured regarding displacement, and detailed analysis is also done which is given below:

- 1) Actuation behavior is analysed through a developed test bench with various parameters.
- 2) On-off controlled, and PID controller is implemented to control the displacement, i.e., 10 mm, 15 mm and 20 mm.
- 3) Actuation behavior is analyzed through heat transfer analysis also.

- 4) In the view of application Stewart platform ($50*50*8 \text{ mm}^3$) is designed and developed and its precision of measuring capability is verified through Talbot interferometry. Stewart platform is helpful for positioning of tools with three degrees of freedom, i.e., 4 mm along the X and Y plane and 3 mm in the Z direction.
- **Hot fluid Actuation:** In this thesis actuation behavior of SMA is investigated under hot fluid medium and life cycle is also explained.
 1. Hot fluid (Water and gas) is used for actuating the SMA and analyzed for practical application.
 2. A heat engine is fabricated and analyzed with the medium of hot fluid.
 3. Through simulation, heat transfer analysis is done which supports better results of experiments.
 4. The life cycle of spring is also measured through which its useful life can be predicted.
 - **Non- contact-based actuation strategy:** It is classified in two way, i.e., Pulsed laser and continuous laser actuation. Thermomechanical behavior and life cycle analysis of SMA has been reported:
 - 1. Tripod is fabricated and actuated by using a pulsed laser with a laser. During maximum actuation, deflection was 7.25 mm within 120 s without any damage on the surface.
 - 2. Micro-valve is also fabricated, and used spot size was 0.5 mm for actuation, which gave a maximum deflection of 7.29 mm at an optimum fluence of 25.48 mJ/cm^2 (No-Ablation)
 - **Pulsed laser-assisted actuation:** Thermomechanical behavior of SMA is analyzed by using pulsed mode of Nd-YAG laser.
 1. Tripod is fabricated and actuated by using a pulsed laser with a laser. During maximum actuation, deflection was 7.25 mm within 120 s without any damage on the surface.
 2. Micro-valve is also fabricated, and used spot size was 0.5 mm for actuation, which gave a maximum deflection of 7.29 mm at an optimum fluence of 25.48 mJ/cm^2 (No-Ablation)
 - **Continuous laser assisted actuation:** For a quick response, it is preferred over the pulsed laser.

1. By using a continuous laser, a range of power is used for actuation of SMA.
2. On the application point of view, the directional control valve is fabricated and actuated by a continuous fibre laser. The required parameter is Power: 10 W and number of passes: 5.

The potential for use in engineering structures is limited by the range of temperatures within which phase change may take place and the rapidity with which these changes occur. The area of thermal shape change that perhaps has the greatest potential is that of actuation.

7.1.2 Utility and industrial implications of the research work:

The outcomes of the present research will help manufacturing industries in the following manner:

- i) World over industries is looking forward to the adaption of SMA based micro-devices or smart manufacturing. In such a situation, to the least, research presented in this thesis gives raise to a new dimension of SMA actuation strategies. It strongly advocates exploring novel setups and system to optimize and manage shop-floor operations.
- ii) The successful implementation of the present approaches will help in integrating various methodologies aspects at the decision-making stage itself thereby reducing human intervention in coordinating and implementing various operations plans.
- iii) All methodologies may not result into same performance improvement for all the manufacturing industries.
- iv) Lastly, the research equips the developed applications for an industrial purpose that allows high-level responsiveness to the dynamic conditions for various real-world manufacturing environments.

7.2 Future scope

The advanced integrated approaches developed in this research have a good potential for application in the manufacturing industry. This research is also not

an exception. Moreover, the limitations of the present research offer excellent scope for future research. Extending the current research by considering the failure and repair characteristics of each of the components will help in making the investigation more realistic, especially from the maintenance point of view. From dependency point of view, it will be interesting to model the effect of the failure of various components on process quality. Eventually, the core domain of MEMS-based research, which increasingly focuses on developing microdevices for machine-to-machine communications, can be utilized to build up more advanced intelligent operations for next-generation manufacturing.

REFERENCES

- [1] Ener S., Neuhaus J., Petry, W., Mole, R., Hradil, K., Siewert M., Gruner, M.E., Entel, P., Titov, I., Acet, M., (2012) “Effect of temperature and compositional changes on the phonon properties of Ni-Mn-Ga shape memory alloys” , *Physical Review B*, 86 (14), 14305 (1-9)
- [2] Mavroidis, C., Pfeiffer, C., Mosley, M., (1999) “Conventional Actuators, Shape Memory Alloys, and Electrorheological Fluids,” *Automation, Miniature Robotics and Sensors for Non-Destructive Testing and Evaluation*, Y., 1–26.
- [3] Kohl, M., (2004). *Shape Memory Microactuators*, Springer-Verlag Berlin Heidelberg, doi: 10.1007/978-3-662-09875-2
- [4] Mavroidis, C., (2002) “Development of Advanced Actuators Using Shape Memory Alloys and Electro rheological Fluids,” 14, 1–32.
- [5] Jani J. Mohd., Leary, M., Subic A., Gibson, M. A., (2014) “A review of shape memory alloy research, applications and opportunities,” *Material Design*, 56, 1078–1113, doi: /10.1016/j.matdes.2013.11.084
- [6] Henderson, E., Nash, D. H., Dempster, W. M.,(2011) “On the experimental testing of fine Nitinol wires for medical devices,” *Journal of Mechanical Behavior of Biomedical Materials*, 4 (3) 261–268, doi: 10.1016/j.jmbbm.2010.10.004
- [7] Anadón, J. R. Santiago, (2002), M.Sc Thesis“ Large force shape memory alloy linear actuator.
- [8] Shaw, J.A., Kyriakides, S., (1995). Thermo mechanical aspects of NiTi. *J Journal of Mechanical Physics Solid*, 43 (8), 1243–1281
- [9] Carlos, A. N. O., Cezar H. G., Carlos José de Araújo; Oscar O. A. Filho I, (2010)” Thermoelastic properties on Cu-Zn-Al shape memory springs” *Material Research*, 13(2), doi:: 10.1590/S1516-14392010000200016
- [10] Kheirikhah, M. M., Rabiee S., Edalat M. E., (2011) “A review of shape memory alloy actuators in robotics,” *Lecture Notes in Artificial Intelligence and Lecture Notes in Bioinformatics 6556 LNAI*, 206–217.
- [11] Yates, S. J., Kalamkarov, A. L., (2013) “Experimental Study of Helical Shape Memory Alloy Actuators: Effects of Design and Operating Parameters

- on Thermal Transients and Stroke,” *Metals* (Basel), 3, 123–149, doi:10.3390/met3010123
- [12] Wang, Z., Zu, X., Fu, Y., (2011), “Review on the temperature memory effect in shape memory alloys,” *International Journal of Smart and Nano Materials*, 2 (3), 101–119, doi: 10.1080/19475411.2011.592866
- [13] Yoo, Y. I., Lee, J. J.(2011)“Two-way shape memory effect of NiTi under compressive loading cycles,” *Physics Procedia*, , 22, 449–454, doi:10.1016/j.phpro.2011.11.070
- [14] Otsuka, K., Kakeshita, T., (2002) “Science and Technology of Shape-Memory Alloys: New Developments,” *MRS Bulletin.*, 27 (2), 91–100
- [15] Ostertag, O., Ostertagova E., (2015), “Shape Memory Alloy Actuator (SMA)” *Applied Mechanics and Materials*, 816, 9-15, doi:10.4028/www.scientific.net/AMM.816.
- [16] Liu Y., (2015), “The superelastic anisotropy in a NiTi shape memory alloy thin sheet” *Acta Materialia*, 1-17, doi: 10.1016/j.actamat.2015.03.022
- [17] Kim, H., Han, Y., young Lee, D., Ha, J.-I., Cho, K.J.,(2013) “Sensor less displacement estimation of a shape memory alloy coil spring actuator using inductance,” *Smart Material and Structures.*, 22(2), doi:10.1088/0964-1726/22/2/025001
- [18] Yang, K., (2010), “Research and Application of New Inserted Shape Memory Alloy Actuators, *IEEE Transactions on Industrial Electronics*” 57 (8), 2845–2850, doi: 10.1109/TIE.2010.2043034
- [19] Paik, J. K., Wood, R. J., (2012) “A bidirectional shape memory alloy folding actuator,” *Smart Materials and Structure.*, 21 (6), doi:10.1088/0964-1726/21/6/065013
- [20] Wang, L. X, Melnik, R. V. N., (2007), “Thermo-mechanical wave propagations in shape memory alloy rod with phase transformations,” *Mechanics of Advanced Materials and Structures*, 14(8), 665–676, doi: 10.1080/15376490701673227

- [21] Mishra, S. C., (2015), “Applications of Shape Memory Alloys : A Review,” Journal of Thin Films, Coating Science Technology, and Application, 2 (2), 1–7.
- [22] Wei, Z. G., Sandström, R., and Miyazaki, S.,(1998), “Shape memory materials and hybrid composites for smart systems Part II Shape-memory hybrid composites,” Journal of Material Science, 33(15), 3763–3783
- [23] Naresh, C., Bose, P. S. C., Rao, C. S. P., (2016), “Shape memory alloys: a state of art review,” IOP Conf. Series Material. Science and Engineering,149, 12054, 2016
- [24] Wu, M. H., Schetky, L. M.,(2000) “Industrial Applications for Shape Memory Alloys,” Int. Conf. Shape Memory and Super elastic Technologies, 182, 171–182.
- [25] Petrini, L. Migliavacca, F., (2011) “Biomedical Applications of Shape Memory Alloys,” Journal of Metallurgy, 2011
- [26] Fan, C., and Lin, C, (2009) “A Shape Memory Alloy Actuated Microgripper with Wide Handling Ranges,” Proceeding of International Conference on Advanced Intelligent Mechatronics, 12-17.
- [27] Benard, W. L., Kahn, H., Heuer, H.A., Huff, M. A. (1997) “A titanium-nickel shape-memory alloy actuated micropump *,” Proceeding of International Conference on Solid-state Sensors and Actuators, 361-364
- [28] Sagar, S. N. K., Sreekumar, M., (2013), “Miniaturized flexible flow pump using SMA actuator,” Procedia Engineering, 64, 896–906, doi: 10.1016/j.proeng.2013.09.166
- [29] Yoneyama T., Kobayashi, C., (2009), “12 - Endodontic instruments for root canal treatment using TiNi shape memory alloys”, Shape Memory Alloys for Biomedical Applications, 297-305, doi: 10.1533/9781845695248.2.297
- [30] Sanders, J. O., Sanders, A. E., More, R., Ashman, R. B., (1993), “A preliminary investigation of shape memory alloys in the surgical correction of scoliosis,” SPINE (Phila. Pa. 1976).,18(12), 1640–1646.

- [31] Wever, D., Elstrodt, J., Veldhuizen, A., Horn, J., (2002) “Scoliosis correction with shape-memory metal: Results of an experimental study,” *European Spine Journal*, 11(2), 100–106
- [32] Aguiar, R. A. A., Savi, M. A., Pacheco, P. M. C. L., (2010), Experimental and numerical investigations of shape memory alloy helical springs,” *Smart Materials and Structures*, 19(2), 1-9, doi:10.1088/0964-1726/19/2/025008
- [33] Lara-Quintanilla, A., Hulskamp A. W., Bersee H. E., (2013), “A high-rate shape memory alloy actuator for aerodynamic load control on wind turbines” *Journal of Intelligent Material Systems and Structures*, DOI: 10.1177/1045389X13478271
- [34] Kauffman G. B. and Mayo I., (1997), “The Story of Nitinol: The Serendipitous Discovery of the Memory Metal and Its Applications,” *Chem. Educ.*, 2(2), 1–21, doi: 10.1007/s00897970111a
- [35] Lagoudas D.C., BO Z., Qidwai A.M., (2015), “A Unified Thermodynamic Constitutive Model for SMA And Finite Element Analysis of Active Metal Matrix Composites” *Mechanics of Composite Materials and Structures*, 3, 153-179, DOI: 10.1080/10759419608945861
- [36] Webb., V.G., Lagoudas, D.C., Kudrila, A.J., (1998), “Hysteresis modeling of SMA actuators for control Applications” *Journal of Intelligent Material systems and structures*, 432-448.
- [37] Massad, J.E., Smith, R.C., Carman, Greg P, (2003), “A Free Energy Model for Thin- μ m Shape Memory Alloys” 1-11
- [38] Darling, T. W. Chu F., Migliori, Thoma A. D. J., Lopez M., (2002)“Elastic and thermodynamic properties of the shape-memory alloy AuZn,” 1-25.
- [39] Hu, L., Jiang, S.,Liu, S., Zhang Y., I, Y, Zhao C., (2016) “Transformation twinning and deformation twinning of NiTi shape memory alloy” *Materials Science and Engineering: A*, 660, 1-10, doi: 10.1016/j.msea.2016.02.066
- [40] Baron, M.-P. Morin, M., (1997), “Stress-Induced Transformation and Temperature-Induced Transformation in Cu-Zn-Al Single Crystals” *Journal of Physics IV France*, C5 (525-530)

- [41] Wang, J., Sehitoglu, H., Maier, H.J., (2013), “Dislocation slip stress prediction in shape memory alloys” *International Journal of Plasticity*, doi: 10.1016/j.ijplas.2013.08.017
- [42] Karaman, I., Kulkarni, A.V., Luo, Z.P., (2005)“Transformation behavior and unusual twinning in a NiTi shape memory alloy ausformed using equal channel angular extrusion,” *Philosophical Magazine*, 85 (16), doi: 10.1080/14786430412331331961
- [43] Wang, J., Sehitoglu, H.,(2013), “Twinning stress in shape memory alloys: Theory and experiments” *Acta Materialia*, doi: 10.1016/j.actamat.2013.07.053, 1-12
- [44] Birk T., Biswas, S., Frenzel J., Eggeler G., (2016) “Twinning-Induced Elasticity in NiTi Shape Memory Alloys” *Shape Memory and Super elasticity*, 145-159, doi: 10.1007/s40830-016-0064-1
- [45] Yoo, Y., Jin Kim Y., Shin, D., Lee J.,(2015), “Development of martensite transformation kinetics of NiTi shape memory alloys under compression” *International Journal of Solids and Structures*, doi: 10.1016/j.ijsolstr.2015.03.013, 51–61
- [46] Kok, M., Dağdelen F., Aydoğdu A., Aydoğdu Y., (2016), “The change of transformation temperature on NiTi shape memory alloy by pressure and thermal aging” *9th International Conference on Magnetic and Superconducting Materials*, 667, 1-7, doi:10.1088/1742-6596/667/1/012011
- [47] Dye D., (2012)“Microstructure and Properties of Materials” Book Chapter.
- [48] Pai Mizar, S., (2005), Ph.D.Thesis “Thermomechanical characterization of NiTiNOL and NiTiNOL based structures using ACES methodology”, 1-236
- [49] Daniel Mutter* and Peter Nielaba,(2010), “Simulation of structural phase transitions in NiTi” 1-12.
- [50] Abdul Wadood, (2016), “Brief overview on Nitinol as Biomaterial”, *Advances in Materials Science and Engineering*, 9 pages, doi:10.1155/2016/4173138

- [51] Wayman, C. M., (1983), Phase transformations, nondiffusive Physical ed R W Cahn and P Hansen (New York: North-Holland) pp 1031–75, doi: 10.1016/B978-0-444-53770-6.00009-5
- [52] Miyazaki, S., Imai, T., Igo Y., Otsuka, K., (1986), “Effect of cyclic deformation on the pseudo-elasticity characteristic of TiNi alloy”, *Metallurgical Transactions A*, 17A, 115-120.
- [53] Cormick Mc P G and Liu Y (1994), “Thermodynamic analysis of the martensitic transformation in TiNi—II. Effect of transformation cycling” *Acta Metallurgica et Materialia*, 42(7), 2407–13
- [54] Einarsson S. O., (2016), “Degradation of NiTi springs through electronic actuation” B.Sc Thesis. 1-48
- [55] Hebda D. and White S. R. (1995), “Effect of training conditions and extended thermal cycling on nitinol two-way shape memory behavior *Smart Material and structure*, 4 298–304
- [56] Tanaka K, Nishimura F, Hayashi T, Tobushi H and LExcellent C (1995) Phenomenological analysis on sub-loops and cyclic behavior in shape memory alloys under mechanical and thermal loads *Mechanics of Material*, 19, 281–92
- [57] Lagoudas D C and Bo Z (1999), “Thermomechanical modeling of polycrystalline SMAs under cyclic loading, part II: material characterization and experimental results for a stable transformation cycle *International Journal of Engineering science*, 37 1141–73
- [58] Melton K N and Mercier O (1979) Fatigue of NiTi thermoelastic martensites *Acta Materialia* **27** 137–44
- [59] Hornbogen, E. (2004), Review of Thermo-mechanical fatigue of shape memory alloys, 39, 385-399
- [60] Kang G, Song D., (2015), Review on structural fatigue of NiTi shape memory alloys: Pure mechanical and thermo-mechanical ones” *Theoretical and Applied Mechanics Letters* 5, 245–254
- [61] Qian H, Li H, Song G, G Wi, (2013), A Constitutive Model for Superelastic Shape Memory Alloys Considering the Influence of Strain Rate”, Hindawi Publishing corporation, doi: 10.1155/2013/248671

- [62] Mammano G., Dragon E., (2013)“, Functional fatigue of NiTi Shape memory wires for a range of end loading and constraints, Engineering Procedia, Italian research on Smart Materials and MEMS 23, 23-33
- [63] Auricchio F., Constantinescu A. Menna C, Scalet G. (2016), A shakedown analysis of high cycle fatigue of shape memory alloys”, International Journal of Fatigue 87 112–123
- [64] Colin J . , Fatemi A.,(2010) “Variable amplitude cyclic deformation and fatigue behavior of stainless steel 304L including the step, periodic, and random loadings” Fatigue & Fracture of Engineering Materials & Structures, 33, 205-220, doi: 10.1111/j.1460-2695.2009.01429.x
- [65] Jaka Tušek, Andrej Zerovnik, Matjaž Cebon, Miha Brojan, Borut Žužek, Kurt Engelbrecht, Andrea Cadelli, (2018) “Elastocaloric effect vs. fatigue life: Exploring the durability limits of NiTi plates under pre-strain conditions for elastocaloric cooling” Acta Materialia, 150 295-307
- [66] Phung N, Marti N, Blanche A, Ranc N, Favier V, (2013)“Very High Cycle Fatigue for single phase ductile materials: slip band appearance criterion.”Procedia Engineering, 66, 615-625
- [67] G. Eggeler, E. Hornbogen, A. Yawny, A. Heckmann and M. Wagner (2004,)“Structural-functional fatigue of NiTi shape memory alloys,” Material science and Engineering A, 378, 24-33.
- [68] Kazymyrovych, V ., (2009), Very high cycle fatigue of engineering materials – A Literature report” 1-33
- [69] Amengual, A., (1992), “partial cycling effects on the martensitic transformation of CuZnAl SMA” Scripta Materialia, 26, 1795-1798.
- [70] Bertacchini, Lagoudas, Dimitris C., Patoor, E., “Fatigue life characterization of shape memory alloys undergoing thermomechanical cyclic loading.” 36 (3), 314-318
- [71] H. Matsumoto, (1993) Transformation behavior of NiTi in relation to thermal cycling and deformation *Physica B* 190, 115-120.

- [72] Batalu D., Guouiu H., A., Aloman, G., (2014) “A review on TiNi shape memory alloys (SMA) used for medical applications Recycling aspects.”1-10.
- [73] Abdy, A., Sadiq, H., “Effect of heat treatment on the recovery stresses generated by super-elastic NiTi shape memory alloy wires.” 23rd Australasian Conference on the Mechanics of Structures and Materials, 211-216
- [74] F.M. Braz Fernandes, K.K. Mahesh and Andersan dos Santos Paula, “Thermomechanical Treatments for Ni-Ti Alloys.” Chapter 1, Shape Memory Alloys – Processing, Characterization, and Applications doi: /10.5772/56087
- [75] Gianni Rondelli, (1996), Corrosion resistance tests on NiTi shape memory alloy, *Biomaterials*, 17 (20)
- [76] Liu Y., , Zhenqing Li Hao, W., Chen B., (2018), Influence of Embedding SMA Fibres and SMA Fibre Surface Modification on the Mechanical Performance of BFRP Composite Laminates, *Materials*, 11(70)
- [77] Christopher B. Churchill and John A. Shaw, “Shakedown Response of Conditioned Shape Memory Alloy Wire” *Proc. of SPIE Vol. 6929 69291F-1-12*, doi: 10.1117/12.778726
- [78] Saikrishna, C.N, Ramaiah, K V, S , Pprabhu A, Bhaumik, S K, (2009)“ On stability of NiTi wire during thermo-mechanical cycling” 343-352, *Material science bulletin*, 32 (3), 343–352
- [79] G. Scirè Mammano, E. Dragoni (2013), “Functional fatigue of NiTi Shape Memory wires for a range of end loadings and constraints.” 23, 25-33; doi:: 10.3221/IGF-ESIS.23.03

- [80] S. Miyazaki, K. Otsuka, and Y. Suzuki, 1981 Transformation Pseudoelasticity and Deformation Behavior in a Ti 50.6at%Ni Alloy Scripta Materillia, . 15, 287-292.
- [81] Zanotti, C. Giuliani P., Tuissi, A. , Arnaboldi, S. , Casati R. (2009), Response of NiTi SMA wire electrically heated, 1-7, doi:10.1051/esomat/200906037
- [82] G. Costanza, M.E. Tata, C. Calisti (2010), “Nitinol one-way shape memory springs: Thermomechanical characterization and actuator design” Sensors and Actuators A: Physical, 157, 113-117.
- [83] Shu-Hung Liu, Tse-Shih Huang and Jia-Yush Yen (2010), “ Tracking Control of Shape-Memory-Alloy Actuators Based on Self-Sensing Feedback and Inverse Hysteresis Compensation” Sensors 10, 112-127; doi:10.3390/s100100112
- [84] Hunter Song, Eric Kubica, Rob Gorbet (2011), “Resistance Modelling of SMA wire actuators” CANSMART CINDE IZFP.
- [85] Suzuki, A. (2011), “Applications of shape memory alloys (SMAs) in hot water supplies.” 102-109.
- [86] Matthew D. Pierce (2011), “design and optimization of a shape memory alloy actuated pump with thermofluidic feedback” 1-89,.
- [87] Stephen A. Mascaró and H. Harry Asada, (2003), “Wet Shape Memory Alloy Actuators for Active Vasculated Robotic Flesh” IEEE International Conference on Robotics & Automation
- [88] Flemming L., (2005)“Control of Scalable Wet SMA Actuator Arrays” International Conference on Robotics and Automation 1350-1355
- [89] Dalia A. Abd El daym1 & Mostafa E. Gheith & Nadia A. Abbas & Laila A. Rashed4 & Zeinab A. Abd El Aziz, (2018), Corrosion behavior of erbium chromium-doped yttrium-scandium-gallium-garnet (Er,Cr:YSGG 2780 nm)

laser-treated titanium alloy used for dental applications at different pH conditions (in vitro study), *Laser in Dental science* DOI: /10.1007/s41547-018-0030-7

- [90] Castleman L.S., (1976), “Biocompatibility of Nitinol Alloy as an Implant Material” *Journal of Biomedical. Material Research*, 10, 695-731
- [91] Ronny Pfeifer *, Dirk Herzog, Michael Hustedt, Stephan Barcikowski (2010), Pulsed Nd: YAG laser cutting of NiTi shape memory alloys— Influence of process parameters, *Journal of Materials Processing Technology*, 1918-1925, doi:: 10.1016/j.jmatprotec.2010.07.004
- [92] Corneliu C,(2010) “Shape memory alloy”, Sciyo, ISBN 978-953-307-106-0
- [93] Bellouard Y, (2008), “Shape memory alloys for microsystems: A review from a material research perspective”, *Materials Science and Engineering A* 481–482 (2008) 582–589
- [94] Jeremy E. Schaffer and David L. Plumley (2009), Fatigue Performance of Nitinol Round Wire with Varying Cold Work Reductions, *JMEPEG* (2009) 18:563–568, DOI: 10.1007/s11665-009-9363-4
- [95] Adam W. Martinez¹ and Elliot L. Chaikof (2011), “ Microfabrication and nanotechnology in stent design” 256-268
- [96] Yung K.C. (2005), “Theoretical and experimental study on the kerf profile of the laser micro-cutting NiTi shape memory alloy using 355 nm Nd:YAG” *Smart Materials and Structure*. 14 337–342, doi:10.1088/0964-1726/14/2/006
- [97] Ahamed, S., Gurucharan N, Meyappan, R, Kulandaivelu, A., Deepa V Kumar, Sreenadh, B. (2012) “A comparative analysis between Nd: YAG and CO₂ lasers for their sealing ability of dentinal tubules with and without fluoride varnish: An in vitro study.” *Journal of Dental Lasers*, 6 (2), 51-56

- [98] L. C Chang and T A Read, (1951), “Plastic Deformation and Diffusionless Phase Changes In Metals - The Gold-Cadmium Beta Phase” 189, 47-48
- [99] Wei-hong GAO, Xiang-long MENG, Wei CAI, Lian-cheng ZHAO, “Effects of Co and Al addition on martensitic transformation and microstructure in ZrCu-based shape memory alloys” Transaction of Non-Ferrous metals, a society of China. 25, 850-855
- [100] Torra V, Isalgue, A., Ferran M, Francisco C. “From physical time dependent properties to guaranteed SMA dampers” 13th World Conference on Earthquake Engineering
- [101] Joachim, S. (2002) Phase change behavior of Nitinol shape memory alloy, 4 (7).
- [102] M. Karhu, T. Lindroos (2012), Microstructure analysis and damage patterns of thermally cycled Ti-49.7 Ni (at.%) wires, Smart Materials, and Structures 21
- [103] Wayman C M 1983 Phase transformations, nondiffusive Physical ed R W Cahn and P Haasen (New York: North-Holland) 1031-75
- [104] X. Peng *, W. Pi, J. Fan, (2008), A microstructure-based constitutive model for the pseudoelastic behavior of NiTi SMAs, International Journal of Plasticity 24, 966-990
- [105] Bigoni, D., Piccolroaz, A., (2004). Yield criteria for quasibrittle and frictional materials. Int. J. Sol. Struct. 41 (11-12), 2855-2878.
- [106] Zaki, W., Moumni, Z., (2007), A three-dimensional model of the thermomechanical behavior of shape memory alloys. Journal of mechanical physics solid 55, 2455-2490.
- [107] Lexcelent, C., Blanc, P., (2004). Phase transformation yield surface determination for some shape memory alloys. Acta Mater. 52 (8), 2317-2324.

- [108] Paiva, A., Savi, M.A., (2006). An overview of constitutive models for shape memory alloys. *Mathematical Problems in Engineering* 2006, 1–30 (article ID56876).
- [109] Kang, G.Z., Kan, Q.H., Qian, L.M., Liu, Y.J., (2009). Ratcheting deformation of superelastic and shape memory NiTi alloys. *Mech. Mater.* 41, 139–153.
- [110] Zaki, W., Moumni, Z., 2007. A 3D model of the cyclic thermomechanical behavior of shape memory alloys. *J. Mech. Phys. Solids* 55, 2427–2454.
- [111] Saleeb, A.F., Padula II, S.A., Kumar, A., (2011). A multi-axial, multi-mechanism based constitutive model for the comprehensive representation of the evolutionary response of SMAs under general thermomechanical loading conditions. *Int. J. Plast.* 27, 655–687.
- [112] Moiseev VN. Titanium in Russia (2005). *Metal Sci Heat Treat.* 2005;47:23-9.
- [113] Teh, Y. H., (2008), [Fast, Accurate Force and Position Control of Shape Memory Alloy Actuators], Australian National University
- [114] Steven G Shuy, Dimitris C Lagoudasz, Declan Hughesx and John T Wenx (1997), “Modeling of a flexible beam actuated by shape memory alloy wires” *Smart Mater. Struct.* 6 265–277.
- [115] Pathak, A., Brei, D. and Luntz, J., 2010. “Transformation Strain Based Method for Convective Heat Transfer Characterization from Shape Memory Alloy Wires” *Smart Material and Structures*, 19(3), 5005_5015.
- [116] J van Humbeeck: *Materials Science and Engineering A*. Vol. 275 (1999), pp.134-148. [http://dx.doi.org/10.1016/S0921-5093\(99\)00293-2](http://dx.doi.org/10.1016/S0921-5093(99)00293-2)
- [117] L.J. Garner, L.N. Wilson, D.C. Lagoudas and O. K Rediniotis (2001): *Smart Materials and Structures*, 9.673-683

- [118] W. Huang (2002) On the selection of shape memory alloys for actuators, *Materials and Design* 23 (2002) 11–19.
- [119] S.Hirose, K.Ikuta, K.Sato,(1986) Development of Shape Memory Alloy Actuator (Improvement of Output Performance by this Introduction of A sigma-mechanism), *Journal of the Robotics Society of Japan (JRSJ)* , Vo1.4-6, pp.28138 (in Japanese)
- [120] Kjell J. G^oasvik (2002) *Optical Metrology*, Book, ISBN 0-470-84300-4
- [121] Kreis T 1996 *Holographic Interferometry* (Berlin: Akademie), 138–49
- [122] Schirripa, G., Spagnolo¹, D Ambrosini² and D Paoletti (2002), *Journal of Applied Optics*, 4, S376–S380
- [123] M. Takeda and S. Kobayashi ((1984).), “Lateral aberration measurement with a digital Talbot interferometer,” *Applied Optics*. 23, 1760–1764
- [124] D.S. Mehta, S. Saito, H. Hinosugi, M. Takeda (2003), T. Kurokawa, *Applied Optics*. 42 1296
- [125] M.-H. Chiu and D.-C. Su (1997) “Angle measurement using total internal-reflection heterodyne interferometry,” *Opt. Eng.* 36, 1750–1753 (1997).
- [126] D. Malacara, M. Servin, and Z. Malacara (1998), “Interferogram Analysis for Optical Testing” (Marcel Dekker)
- [127] Shashi Prakash, Sumitra Singh and Santosh Rana (2006) Setting sensitivity in collimation testing using Lau interferometry” *Journal of Applied optics A- Pure and Applied Optics*, 8, 290–294, doi:10.1088/1464-4258/8/3/010
- [128] D. Pristinski, V.Kozlovskaya, S.Sukhishvili (2006), “Determination of film thickness, and refractive index in one measurement of phase modulated ellipsometry”, *JOSAA*23, 2639–2644.
- [129] D. blood (1998).. *Displays-Echnol. Appl.* 18(3):125-128

- [130] P. Gao, S.-M. Swei, and Z. Yuan,(1999) “A new piezo-driven precision micropositioning stage is utilizing flexure hinges,” *Nanotechnology*, vol. 10, pp. 394–398,
- [131] M. Gogola and M. Goldfarb (1999), “Design of a PZT-actuated proportional drum brake,” *IEEE/ASME Trans. Mechatron.*, vol. 4, pp. 409–416, Apr..
- [132] A. G. Erdman and G. N. Sandor (1991), *Mechanical Design: Analysis and synthesis*, 2nd ed. Englewood Cliffs, NJ: Prentice-Hall, 1991, vol. 1.
- [133] R. S. Stoughton and T. Arai, “Modified Stewart platform manipulator with improved dexterity,” *IEEE Transactions on Robotics and Automation*, vol. 9, no. 2, pp. 166–172, 1993.
- [134] R. Boian, H. Kourtev, K. Erickson, J. Deutsch, J. Lewis, and G. Burdea, “Dual Stewart-platform gait rehabilitation system for individuals post-stroke,” in *Proceedings of the 2nd International Workshop on Virtual Rehabilitation*, Piscataway, NJ, USA, 2003.
- [135] N. Ando, P. Korondi, and H. Hashimoto, “Development of micromanipulator and haptic interface for networked micromanipulation,” *IEEE/ASME Transactions on Mechatronics*, vol. 6, no. 4, pp. 417–427, 2001.
- [136] T. Raparelli, P. B. Zobel, and F. Durante, “Design of a parallel robot actuated by shape memory alloy wires,” *Materials Transactions*, vol. 43, no. 5, pp. 1015–1022, 2002.
- [137] R. Abiri, M. Kabganian, and R. Nadafi, “Fabrication, modeling and set-point control of a new flexible microrobot module (FMM) by using SMA actuators,” in *Proceedings of the 1st RSI/ISM International Conference on Robotics and Mechatronics (ICRoM '13)*, pp. 141–146, February 2013.

- [138] M. B. S. Roslan, V. Amirtham, T. Nagarajan, and F. M. Hashim, “SMA actuator technology application in Stewart Platform construction,” *Journal of Applied Sciences*, vol. 11, no. 23, pp. 3783–3790, 2011.
- [139] A. Lundbladh, D.S. Hennigson, and A.V. Johansson (1992). An efficient spectral integration method for the solution of the Navier-Stokes equations. Technical Report FFA-TN 1992-28, Aeronautical Research Institute of Sweden, 1992.
- [140] S. Degeratu (2008), “Practical Aspects Regarding the Design of Intelligent Systems Using the SMA Spring”, *Wseas EMESEG*, 2008, Heraclion, Crete. Greece, July, pp. 226-231
- [141] Villanueva, A., C. Smith, and S. Priya. 2011. “A Biomimetic Robotic Jellyfish (Robojelly) Actuated by Shape Memory Alloy
- [142] Ean H. Schiller, (2002), Heat Engine Driven by Shape Memory Alloys: Prototyping and Design, M.Sc Thesis
- [143] A. Tuissi , S. Besseghini (1999), Effect of Nd-YAG laser welding on the functional properties of the Ni–49.6at.%Ti[J]. *Materials Science and Engineering* , A 273–275 813-817.
- [144] Y. Li, L. Cui, P. Shi, and D. Yang, (2001) “Phase transformation behaviors of prestrained TiNi shape memory alloy fibers under the constraint of a hard substrate,” *Material Structures.*, vol. 49, no. 3, pp. 224–227,
- [145] M. D. Feit and A. M. Rubenchik, (2003), “Mechanisms of CO₂ laser mitigation of laser damage growth in fused silica,” *Proc. SPIE* 4932, 91–102
- [146] J.R. Köhler, S. Eisele (2010), Influence of precursor layer ablation on laser doping of silicon, *Progress in Photovoltaics: Research and Applications*. 18, 334-339.